Adsorption and Ion Exchange

M. Douglas LeVan, Ph.D., *Centennial Professor, Department of Chemical Engineering, Vanderbilt University; Member, American Institute of Chemical Engineers, American Chemical Society, International Adsorption Society. (Section Editor)*

Giorgio Carta, Ph.D., *Professor, Department of Chemical Engineering, University of Virginia; Member, American Institute of Chemical Engineers, American Chemical Society, International Adsorption Society.*

Carmen M. Yon, M.S., *Development Associate, UOP, Des Plaines, IL; Member, American Institute of Chemical Engineers. (Process Cycles, Equipment)*

Nomenclature and Units

a	specific external surface area per unit bed volume, m²/m³
a_v	surface area per unit particle volume, m²/m³ particle
A	surface area of solid, m²/kg
A_s	chromatography peak asymmetry factor
b	correction factor for resistances in series
c	fluid-phase concentration, mol/m³ fluid
c_p	pore fluid-phase concentration, mol/m³
c^s	fluid-phase concentration at particle surface, mol/m³
C_{pf}°	ideal gas heat capacity, J/(mol K)
C_s	heat capacity of sorbent solid, J/(kg K)
d_p	particle diameter, m
D	fluid-phase diffusion coefficient, m²/s
D_e	equivalent diffusion coefficient, m²/s
D_L	axial dispersion coefficient, m²/s
D_p	pore diffusion coefficient, m²/s
D_s	adsorbed-phase (solid, surface, particle, or micropore) diffusion coefficient, m²/s
$\underline{D_0}$	diffusion coefficient corrected for thermodynamic driving force, m²/s
$\bar{D}$	ionic self-diffusion coefficient, m²/s
F	fractional approach to equilibrium
F_v	volumetric flow rate, m³/s
h	enthalpy, J/mol; reduced height equivalent to theoretical plate
htu	reduced height equivalent to a transfer unit
HETP	height equivalent to theoretical plate, m
HTU	height equivalent to a transfer unit, m
J	mass-transfer flux relative to molar average velocity, mol/(m²·s); J function
k	rate coefficient, s⁻¹
k_a	forward rate constant for reaction kinetics, m³/(mol s)
k_c	rate coefficient based on fluid-phase concentration driving force, m³/(kg·s)
k_f	external mass-transfer coefficient, m/s
k_n	rate coefficient based on adsorbed-phase concentration driving force, s⁻¹
k'	retention factor
K	isotherm parameter
K^e	molar selectivity coefficient
K'	rational selectivity coefficient
L	bed length, m
m	isotherm exponent
M_r	molecular weight, kg/kmol
M_s	mass of adsorbent, kg
n	adsorbed-phase concentration, mol/kg adsorbent
n^s	ion-exchange capacity, g-equiv/kg
N	number of transfer or reaction units; $k_f a L/(\varepsilon v^{\rm ref})$ for external mass transfer; $15(1-\varepsilon)\varepsilon_p D_p L/(\varepsilon v^{\rm ref} R_p^2)$ for pore diffusion; $15 \Lambda D_s L/(\varepsilon v^{\rm ref} R_p^2)$ for solid diffusion; $k_n \Lambda L/(\varepsilon v^{\rm ref})$ for linear driving-force approximation; $k_a c_{\rm ref} \Lambda L/[(1-R)\varepsilon v^{\rm ref}]$ for reaction kinetics
N_p	number of theoretical plates
N_{Pe}	$v^{\rm ref} L/D_L$, bed Peclet number (number of dispersion units)
p	partial pressure, Pa
P	pressure, Pa
Pe	particle-based Peclet number, $d_p v/D_L$
q^{st}	isosteric heat of adsorption, J/mol
Q_i	amount of component i injected with feed, mol
r, R	separation factor; particle radial coordinate, m
r_c	column internal radius, m
r_m	hydrodynamic radius of molecule, m
r_p	particle radius, m
$r_{\rm pore}$	pore radius, m
r_s	radius of subparticles, m
$\Re$	gas constant, Pa·m³/(mol K)
Re	Reynolds number based on particle diameter, $d_p \varepsilon v/\nu$
s	UNILAN isotherm parameter
Sc	Schmidt number, ν/D
Sh	Sherwood number, $k_f d_p/D$

t	time, s
t_c	cycle time, s
t_f	feed time, s
t_r	chromatographic retention time, s
T	absolute temperature, K
u_f	fluid-phase internal energy, J/mol
$u_s, u_{\rm sol}$	stationary-phase and sorbent solid internal energy, J/kg
v	interstitial velocity, m/s
V_f	extraparticle fluid volume, m³
W	volume adsorbed as liquid, m³; baseline width of chromatographic peak, s
x	adsorbed-phase mole fraction; particle coordinate, m
y	fluid-phase mole fraction
z	bed axial coordinate, m; ionic valence

Greek letters

α	separation factor
β	scaling factor in Polanyi-based models; slope in gradient elution chromatography
Δ	peak width at half height, s
ε	void fraction of packing (extraparticle); adsorption potential in Polanyi model, J/mol
ε_p	particle porosity (intraparticle void fraction)
ε_b	total bed voidage (inside and outside particles)
γ	activity coefficient
Γ	surface excess, mol/m²
κ	Boltzmann constant
Λ	partition ratio
Λ^∞	ultimate fraction of solute adsorbed in batch
μ	fluid viscosity, kg/(m s)
μ_0	zero moment, mol s/m³
μ_1	first moment, s
ν	kinematic viscosity, m²/s
Ω	cycle-time dependent LDF coefficient
φ	volume fraction or mobile-phase modulator concentration, mol/m³
π	spreading pressure, N/m
ψ	LDF correction factor
Ψ	mechanism parameter for combined resistances
ρ	subparticle radial coordinate, m
ρ_b	bulk density of packing, kg/m³
ρ_p	particle density, kg/m³
ρ_s	skeletal particle density, kg/m³
σ^2	second central moment, s²
τ	dimensionless time
τ_1	throughput parameter
τ_p	tortuosity factor
ξ	particle dimensionless radial coordinate
ζ	dimensionless bed axial coordinate

Subscripts

a	adsorbed phase
f	fluid phase
i, j	component index
tot	total

Superscripts

−	an averaged concentration
^	a combination of averaged concentrations
°	dimensionless concentration variable
e	equilibrium
ref	reference
s	saturation
SM	service mark
TM	trademark
0	initial fluid concentration in batch
0′	initial adsorbed-phase concentration in batch
∞	final state approached in batch

GENERAL REFERENCES

1. Adamson, *Physical Chemistry of Surfaces,* Wiley, New York, 1990.
2. Barrer, *Zeolites and Clay Minerals as Adsorbents and Molecular Sieves,* Academic Press, New York, 1978.
3. Breck, D. W., *Zeolite Molecular Sieves,* Wiley, New York, 1974.
4. Cheremisinoff and Ellerbusch, *Carbon Adsorption Handbook,* Ann Arbor Science, Ann Arbor, 1978.
5. Dorfner (ed.), *Ion Exchangers,* W. deGruyter, Berlin, 1991.
6. Dyer, *An Introduction to Zeolite Molecular Sieves,* Wiley, New York, 1988.
7. EPA, *Process Design Manual for Carbon Adsorption,* U.S. Envir. Protect. Agency., Cincinnati, 1973.
8. Gembicki, Oroskar, and Johnson, "Adsorption, Liquid Separation" in *Kirk-Othmer Encyclopedia of Chemical Technology,* 4th ed., Wiley, 1991.
9. Guiochon, Golsham-Shirazi, and Katti, *Fundamentals of Preparative and Nonlinear Chromatography,* Academic Press, Boston, Massachusetts, 1994.
10. Gregg and Sing, *Adsorption, Surface Area and Porosity,* Academic Press, New York, 1982.
11. Helfferich, *Ion Exchange,* McGraw-Hill, New York, 1962; reprinted by University Microfilms International, Ann Arbor, Michigan.
12. Helfferich and Klein, *Multicomponent Chromatography,* Marcel Dekker, New York, 1970.
13. Jaroniec and Madey, *Physical Adsorption on Heterogeneous Solids,* Elsevier, New York, 1988.
14. Karge and Ruthven, *Diffusion in Zeolites and Other Microporous Solids,* Wiley, New York, 1992.
15. Keller, Anderson, and Yon, "Adsorption" in Rousseau (ed.), *Handbook of Separation Process Technology,* Wiley-Interscience, New York, 1987.
16. Rhee, Aris, and Amundson, *First-Order Partial Differential Equations: Volume 1. Theory and Application of Single Equations; Volume 2. Theory and Application of Hyperbolic Systems of Quasi-Linear Equations,* Prentice Hall, Englewood Cliffs, New Jersey, 1986, 1989.
17. Rodrigues, LeVan, and Tondeur (eds.), *Adsorption: Science and Technology,* Kluwer Academic Publishers, Dordrecht, The Netherlands, 1989.
18. Rudzinski and Everett, *Adsorption of Gases on Heterogeneous Surfaces,* Academic Press, San Diego, 1992.
19. Ruthven, *Principles of Adsorption and Adsorption Processes,* Wiley, New York, 1984.
20. Ruthven, Farooq, and Knaebel, *Pressure Swing Adsorption,* VCH Publishers, New York, 1994.
21. Sherman and Yon, "Adsorption, Gas Separation" in *Kirk-Othmer Encyclopedia of Chemical Technology,* 4th ed., Wiley, 1991.
22. Streat and Cloete, "Ion Exchange," in Rousseau (ed.), *Handbook of Separation Process Technology,* Wiley, New York, 1987.
23. Suzuki, *Adsorption Engineering,* Elsevier, Amsterdam, 1990.
24. Tien, *Adsorption Calculations and Modeling,* Butterworth-Heinemann, Newton, Massachusetts, 1994.
25. Valenzuela and Myers, *Adsorption Equilibrium Data Handbook,* Prentice Hall, Englewood Cliffs, New Jersey, 1989.
26. Vermeulen, LeVan, Hiester, and Klein, "Adsorption and Ion Exchange" in Perry, R. H. and Green, D. W. (eds.), *Perry's Chemical Engineers' Handbook* (6th ed.), McGraw-Hill, New York, 1984.
27. Wankat, *Large-Scale Adsorption and Chromatography,* CRC Press, Boca Raton, Florida, 1986.
28. Yang, *Gas Separation by Adsorption Processes,* Butterworth, Stoneham, Massachusetts, 1987.
29. Young and Crowell, *Physical Adsorption of Gases,* Butterworths, London, 1962.

DESIGN CONCEPTS

INTRODUCTION

Adsorption and ion exchange share so many common features in regard to application in batch and fixed-bed processes that they can be grouped together as sorption for a unified treatment. These processes involve the transfer and resulting equilibrium distribution of one or more solutes between a fluid phase and particles. The partitioning of a single solute between fluid and sorbed phases or the selectivity of a sorbent towards multiple solutes makes it possible to separate solutes from a bulk fluid phase or from one another.

This section treats batch and fixed-bed operations and reviews process cycles and equipment. As the processes indicate, fixed-bed operation with the sorbent in granule, bead, or pellet form is the predominant way of conducting sorption separations and purifications. Although the fixed-bed mode is highly useful, its analysis is complex. Therefore, fixed beds including chromatographic separations are given primary attention here with respect to both interpretation and prediction.

Adsorption involves, in general, the accumulation (or depletion) of solute molecules at an interface (including gas-liquid interfaces, as in foam fractionation, and liquid-liquid interfaces, as in detergency). Here we consider only gas-solid and liquid-solid interfaces, with solute distributed selectively between the fluid and solid phases. The accumulation per unit surface area is small; thus, highly porous solids with very large internal area per unit volume are preferred. Adsorbent surfaces are often physically and/or chemically heterogeneous, and bonding energies may vary widely from one site to another. We seek to promote physical adsorption or *physisorption,* which involves van der Waals forces (as in vapor condensation), and retard chemical adsorption or *chemisorption,* which involves chemical bonding (and often dissociation, as in catalysis). The former is well suited for a regenera-ble process, while the latter generally destroys the capacity of the adsorbent.

Adsorbents are natural or synthetic materials of amorphous or microcrystalline structure. Those used on a large scale, in order of sales volume, are activated carbon, molecular sieves, silica gel, and activated alumina [Keller et al., gen. refs.].

Ion exchange usually occurs throughout a polymeric solid, the solid being of gel-type, which dissolves some fluid-phase solvent, or truly porous. In ion exchange, ions of positive charge in some cases (cations) and negative charge in others (anions) from the fluid (usually an aqueous solution) replace dissimilar ions of the same charge initially in the solid. The ion exchanger contains permanently bound functional groups of opposite charge-type (or, in special cases, notably weak-base exchangers act as if they do). Cation-exchange resins generally contain bound sulfonic acid groups; less commonly, these groups are carboxylic, phosphonic, phosphinic, and so on. Anionic resins involve quaternary ammonium groups (strongly basic) or other amino groups (weakly basic).

Most ion exchangers in large-scale use are based on synthetic resins—either preformed and then chemically reacted, as for polystyrene, or formed from active monomers (olefinic acids, amines, or phenols). Natural zeolites were the first ion exchangers, and both natural and synthetic zeolites are in use today.

Ion exchange may be thought of as a reversible reaction involving chemically equivalent quantities. A common example for cation exchange is the familiar water-softening reaction

$$Ca^{++} + 2NaR \rightleftharpoons CaR_2 + 2Na^+$$
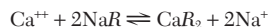
where R represents a stationary univalent anionic site in the polyelectrolyte network of the exchanger phase.

TABLE 16-1   Classification of Sorptive Separations

Type of interaction	Basis for separation	Examples
Adsorption	Equilibrium	Numerous purification and recovery processes for gases and liquids
		Activated carbon-based applications
		Desiccation using silica gels, aluminas, and zeolites
		Oxygen from air by PSA using 5A zeolite
	Rate	Nitrogen from air by PSA using carbon molecular sieve
	Molecular sieving	Separation on *n*- and *iso*-parafins using 5A zeolite
		Separation of xylenes using zeolite
Ion exchange (electrostatic)	Equilibrium	Deionization
		Water softening
		Rare earth separations
		Recovery and separation of pharmaceuticals (e.g., amino acids, proteins)
Ligand exchange	Equilibrium	Chromatographic separation of glucose-fructose mixtures with Ca-form resins
		Removal of heavy metals with chelating resins
		Affinity chromatography
Solubility	Equilibrium	Partition chromatography
None (purely steric)	Equilibrium partitioning in pores	Size exclusion or gel permeation chromatography

Table 16-1 classifies sorption operations by the type of interaction and the basis for the separation. In addition to the normal sorption operations of adsorption and ion exchange, some other similar separations are included. Applications are discussed in this section in "Process Cycles."

Example 1: Surface Area and Pore Volume of Adsorbent   A simple example will show the extent of internal area in a typical granular adsorbent. A fixed bed is packed with particles of a porous adsorbent material. The bulk density of the packing is 500 kg/m^3, and the interparticle void fraction is 0.40. The intraparticle porosity is 0.50, with two-thirds of this in cylindrical pores of diameter 1.4 nm and the rest in much larger pores. Find the surface area of the adsorbent and, if solute has formed a complete monomolecular layer 0.3 nm thick inside the pores, determine the percent of the particle volume and the percent of the total bed volume filled with adsorbate.

From surface area to volume ratio considerations, the internal area is practically all in the small pores. One gram of the adsorbent occupies 2 cm^3 as packed and has 0.4 cm^3 in small pores, which gives a surface area of 1150 m^2/g (or about 1 mi^2 per 5 lb or 6.3 mi^2/ft^3 of packing). Based on the area of the annular region filled with adsorbate, the solute occupies 22.5 percent of the internal pore volume and 13.5 percent of the total packed-bed volume.

DESIGN STRATEGY

The design of sorption systems is based on a few underlying principles. First, knowledge of *sorption equilibrium* is required. This equilibrium, between solutes in the fluid phase and the solute-enriched phase of the solid, supplants what in most chemical engineering separations is a fluid-fluid equilibrium. The selection of the sorbent material with an understanding of its equilibrium properties (i.e., capacity and selectivity as a function of temperature and component concentrations) is of primary importance. Second, because sorption operations take place in batch, in fixed beds, or in simulated moving beds, the processes have *dynamical character.* Such operations generally do not run at steady state, although such operation may be approached in a simulated moving bed. Fixed-bed processes often approach a periodic condition called a periodic state or cyclic steady state, with several different feed steps constituting a cycle. Thus, some knowledge of how transitions travel through a bed is required. This introduces both time and space into the analysis, in contrast to many chemical engineering operations that can be analyzed at steady state with only a spatial dependence. For good design, it is crucial to understand fixed-bed performance in relation to adsorption equilibrium and rate behavior. Finally, many *practical aspects* must be included in design so that a process starts up and continues to perform well, and that it is not so overdesigned that it is wasteful. While these aspects are process-specific, they include an understanding of dispersive phenomena at the bed scale and, for regenerative processes, knowledge of aging characteristics of the sorbent material, with consequent changes in sorption equilibrium.

Characterization of Equilibria   Phase equilibrium between fluid and sorbed phases for one or many components in adsorption or two or more species in ion exchange is usually the single most important factor affecting process performance. In most processes, it is much more important than mass and heat transfer rates; a doubling of the stoichiometric capacity of a sorbent or a significant change in the shape of an isotherm would almost always have a greater impact on process performance than a doubling of transfer rates.

A difference between adsorption and ion exchange with completely ionized resins is indicated in the *variance* of the systems. In adsorption, part of the solid surface or pore volume is vacant. This diminishes as the fluid-phase concentration of solute increases. In contrast, for ion exchange the sorbent has a fixed total capacity and merely exchanges solutes while conserving charge. Variance is defined as the number of independent concentration variables in a sorption system at equilibrium—that is, variables that one can change separately and thereby control the values of all others. Thus, it also equals the difference between the total number of concentration variables and the number of independent relations connecting them. Numerous cases arise in which ion exchange is accompanied by chemical reaction (neutralization or precipitation, in particular), or adsorption is accompanied by evolution of sensible heat. The concept of variance helps greatly to assure correct interpretations and predictions.

The working capacity of a sorbent depends on fluid concentrations and temperatures. Graphical depiction of sorption equilibrium for single component adsorption or binary ion exchange (monovariance) is usually in the form of isotherms [$n_i = n_i(c_i)$ or $n_i(p_i)$ at constant T] or isosteres [$p_i = p_i(T)$ at constant n_i]. Representative forms are shown in Fig. 16-1. An important dimensionless group dependent on adsorption equilibrium is the **partition ratio** (see Eq. 16-125), which is a measure of the relative affinities of the sorbed and fluid phases for solute.

Historically, isotherms have been classified as *favorable* (concave downward) or *unfavorable* (concave upward). These terms refer to the spreading tendencies of transitions in fixed beds. A favorable isotherm gives a compact transition, whereas an unfavorable isotherm leads to a broad one.

Example 2: Calculation of Variance   In mixed-bed deionization of a solution of a single salt, there are 8 concentration variables: 2 each for cation, anion, hydrogen, and hydroxide. There are 6 connecting relations: 2 for ion exchange and 1 for neutralization equilibrium, and 2 ion-exchanger and 1 solution electroneutrality relations. The variance is therefore 8 − 6 = 2.

Adsorbent/Ion Exchanger Selection   Guidelines for sorbent selection are different for regenerative and nonregenerative systems. For a nonregenerative system, one generally wants a high capacity and a strongly favorable isotherm for a purification and additionally high selectivity for a separation. For a regenerative system, high overall capacity and selectivity are again desired, but needs for cost-effective
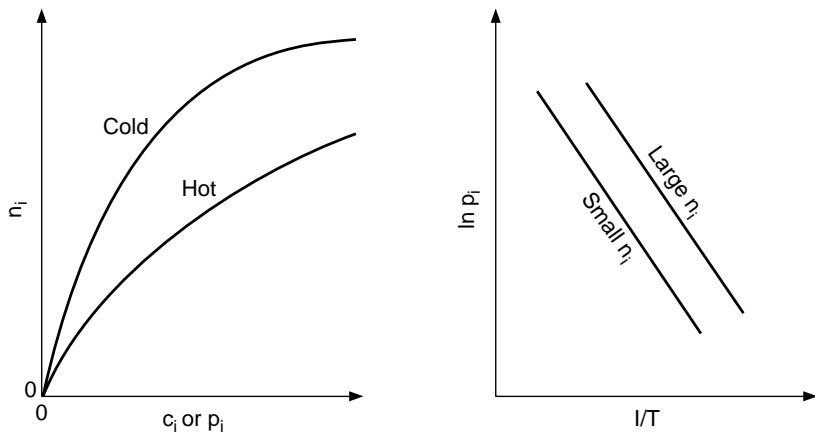
FIG. 16-1   Isotherms (left) and isosteres (right). Isosteres plotted using these coordinates are nearly straight parallel lines, with deviations caused by the dependence of the isosteric heat of adsorption on temperature and loading.

regeneration leading to a reasonable working capacity influence what is sought after in terms of isotherm shape. For separations by pressure swing adsorption (or vacuum pressure swing adsorption), generally one wants a linear to slightly favorable isotherm (although purifications can operate economically with more strongly favorable isotherms). Temperature-swing adsorption usually operates with moderately to strongly favorable isotherms, in part because one is typically dealing with heavier solutes and these are adsorbed fairly strongly (e.g., organic solvents on activated carbon and water vapor on zeolites). Exceptions exist, however; for example, water is adsorbed on silica gel and activated alumina only moderately favorably, with some isotherms showing unfavorable sections. Equilibria for ion exchange separations generally vary from moderately favorable to moderately unfavorable; depending on feed concentrations, the alternates often exist for the different steps of a regenerative cycle. Other factors in sorbent selection are mechanical and chemical stability, mass transfer characteristics, and cost.

Fixed-Bed Behavior   The number of transitions occurring in a fixed bed of initially uniform composition before it becomes saturated by a constant composition feed stream is generally equal to the variance of the system. This introductory discussion will be limited to single transition systems.

Methods for analysis of fixed-bed transitions are shown in Table 16-2. Local equilibrium theory is based solely of stoichiometric concerns and system nonlinearities. A transition becomes a "simple wave" (a gradual transition), a "shock" (an abrupt transition), or a combination of the two. In other methods, mass-transfer resistances are incorporated.

The asymptotic behavior of transitions under the influence of mass-transfer resistances in long, "deep" beds is important. The three basic asymptotic forms are shown in Fig. 16-2. With an unfavorable isotherm, the breadth of the transition becomes proportional to the depth of bed it has passed through. For the linear isotherm, the breadth becomes proportional to the square root of the depth. For the favorable isotherm, the transition approaches a constant breadth called a *constant pattern*.

Design of nonregenerative sorption systems and many regenerative ones often relies on the concept of the mass-transfer zone or MTZ, which closely resembles the constant pattern [Collins, *Chem. Eng. Prog. Symp. Ser. No. 74*, **63**, 31 (1974); Keller et al., gen. refs.]. The length of this zone (depicted in Fig. 16-3) together with stoichiometry can be used to predict accurately how long a bed can be utilized prior to breakthrough. Upstream of the mass-transfer zone, the adsorbent is in equilibrium with the feed. Downstream, the adsorbent is in its initial state. Within the mass-transfer zone, the fluid-phase concentration drops from the feed value to the initial, presaturation state. Equilibrium with the feed is not attained in this region. As a result, because an adsorption bed must typically be removed from service shortly after breakthrough begins, the full capacity of the bed is not utilized. Obviously, the broader that the mass-transfer zone is, the greater will be the extent of unused capacity. Also shown in the figure is the length of the equivalent equilibrium section (LES) and the length of equivalent unused bed (LUB). The length of the MTZ is divided between these two.

Adsorption with strongly favorable isotherms and ion exchange between strong electrolytes can usually be carried out until most of the stoichiometric capacity of the sorbent has been utilized, corresponding to a thin MTZ. Consequently, the total capacity of the bed is

TABLE 16-2   Methods of Analysis of Fixed-Bed Transitions

| Method	Purpose	Approximations
Local equilibrium theory	Shows wave character—simple waves and shocks Usually indicates best possible performance Better understanding	Mass and heat transfer very rapid Dispersion usually neglected If nonisothermal, then adiabatic
Mass-transfer zone	Design based on stoichiometry and experience	Isothermal MTZ length largely empirical Regeneration often empirical
Constant pattern and related analyses	Gives asymptotic transition shapes and upper bound on MTZ	Deep bed with fully developed transition
Full rate modeling	Accurate description of transitions Appropriate for shallow beds, with incomplete wave development General numerical solutions by finite difference or collocation methods	Various to few
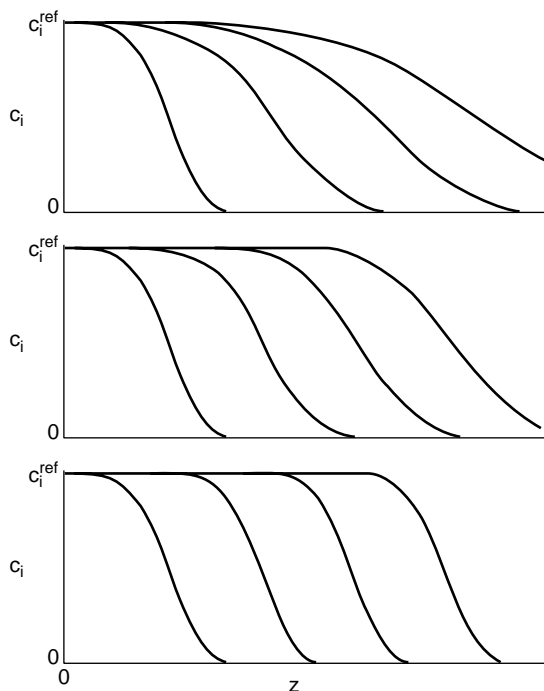
FIG. 16-2   Limiting fixed-bed behavior: simple wave for unfavorable isotherm (top), square-root spreading for linear isotherm (middle), and constant pattern for favorable isotherm (bottom). [*From LeVan in Rodrigues et al. (eds.),* Adsorption: Science and Technology, *Kluwer Academic Publishers, Dordrecht, The Netherlands, 1989; reprinted with permission.*]

FIG. 16-3   Bed profiles (top and middle) and breakthrough curve (bottom). The bed profiles show the mass-transfer zone (MTZ) and equilibrium section at breakthrough. The stoichiometric front divides the MTZ into two parts with contributions to the length of equivalent equilibrium section (LES) and the length of equivalent unused bed (LUB).

practically constant regardless of the composition of the solution being treated.

The effluent concentration history is the breakthrough curve, also shown in Fig. 16-3. The effluent concentration stays at or near zero or a low residual concentration until the transition reaches the column outlet. The effluent concentration then rises until it becomes unacceptable, this time being called the breakthrough time. The feed step must stop and, for a regenerative system, the regeneration step begins.

Two dimensionless variables play key roles in the analysis of single transition systems (and some multiple transition systems). These are the **throughput parameter** [see Eq. (16-129)] and the **number of transfer units** (see Table 16-13). The former is time made dimensionless so that it is equal to unity at the stoichiometric center of a breakthrough curve. The latter is, as in packed tower calculations, a measure of mass-transfer resistance.

Cycles   Design methods for cycles rely on mathematical modeling (or empiricism) and often extensive pilot plant experiments. Many cycles can be easily analyzed using the methods described above applied to the collection of steps. In some cycles, however, especially those operated with short cycle times or in shallow beds, transitions may not be very fully developed, even at a periodic state, and the complexity may be compounded by multiple sorbates.

A wide variety of complex process cycles have been developed. Systems with many beds incorporating multiple sorbents, possibly in layered beds, are in use. Mathematical models constructed to analyze such cycles can be complex. With a large number of variables and nonlinear equilibria involved, it is usually not beneficial to make all
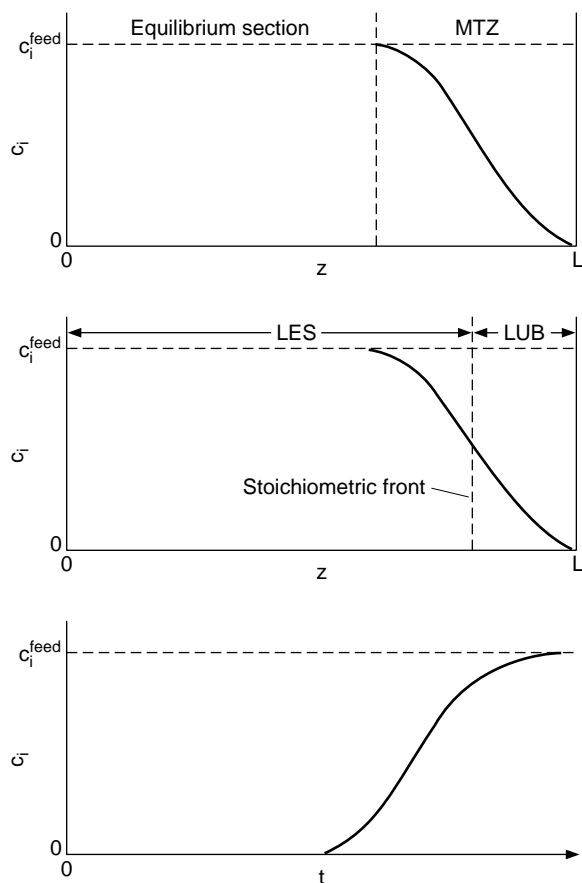
variables in such models dimensionless; doing so does not help appreciably in making comparisons with other largely dissimilar systems. If dimensionless variables are used, these usually begin with a dimensionless bed length and a dimensionless time, which is often different from the throughput parameter.

Practical Aspects   There are a number of process-specific concerns that are accounted for in good design. In regenerable systems, sorbents age, losing capacity because of fouling by heavy contaminants, loss of surface area or crystallinity, oxidation, and the like. Mass-transfer resistances may increase over time. Because of particle shape, size distribution, or column packing method, dispersion may be more pronounced than would normally be expected. The humidity of an entering stream will usually impact a solvent recovery application. Safety, including the possibility of a fire, may be a concern. For gas-phase adsorption, scale-up from an isothermal laboratory column to a nonisothermal pilot plant column to a largely adiabatic process column requires careful judgment. If the MTZ concept is utilized, the length of the MTZ cannot be reliably determined solely from knowledge on other systems. Experience plays the key role in accounting for these and other such factors.

ADSORBENTS AND ION EXCHANGERS

CLASSIFICATIONS AND CHARACTERIZATIONS

Adsorbents   Table 16-3 classifies common adsorbents by structure type and water adsorption characteristics. Structured adsorbents take advantage of their crystalline structure (zeolites and silicalite) and/or their molecular sieving properties. The hydrophobic (nonpolar surface) or hydrophilic (polar surface) character may vary depending on the competing adsorbate. A large number of zeolites have been identified, and these include both synthetic and naturally occurring (e.g., mordenite and chabazite) varieties.

TABLE 16-3   Classification of Common Adsorbents

	Amorphous	Structured
Hydrophobic	Activated carbon Polymers	Carbon molecular sieves Silicalite
Hydrophilic	Silica gel Activated alumina	Common zeolites: 3A (KA), 4A (NaA), 5A (CaA), 13X (NaX), Mordenite, Chabazite, etc.

The classifications in Table 16-3 are intended only as a rough guide. For example, a carbon molecular sieve is truly amorphous but has been manufactured to have certain structural, rate-selective properties. Similarly, the extent of hydrophobicity of an activated carbon will depend on its ash content and its level of surface oxidation.

Zeolites are crystalline aluminosilicates. Zeolitic adsorbents have had their water of hydration removed by calcination to create a structure with well-defined openings into crystalline cages. The molecular sieving properties of zeolites are based on the size of these openings. Two crystal types are common: type A (with openings formed by 4 sodalite cages) and type X or Y (with openings formed by 6 sodalite cages). Cations balancing charge and their locations determine the size of opening into a crystal unit cell. Nominal openings sizes for the most common synthetic zeolites are 0.3 nm for KA, 0.4 nm for NaA, 0.5 nm for CaA, and 1.0 nm for NaX. Further details, including effective molecular diameters, are widely available [Barrer; Breck; Ruthven; Yang, gen. refs.].

Many adsorbents, particularly the amorphous adsorbents, are characterized by their pore size distribution. The distribution of small pores is usually determined by analysis, using one of several available methods, of a cryogenic nitrogen adsorption isotherm, although other probe molecules are also used. Russell and LeVan [*Carbon,* **32,** 845 (1994)] compare popular methods using a single nitrogen isotherm measured on activated carbon and provide numerous references. The distribution of large pores is usually determined by mercury porisimetry [Gregg and Sing, gen. refs.].

Table 16-4 shows the IUPAC classification of pores by size. Micropores are small enough that a molecule is attracted to both of the opposing walls forming the pore. The potential energy functions for these walls superimpose to create a deep well, and strong adsorption results. Hysteresis is generally not observed. (However, water vapor adsorbed in the micropores of activated carbon shows a large hysteresis loop, and the desorption branch is sometimes used with the Kelvin equation to determine the pore size distribution.) Capillary condensation occurs in mesopores and a hysteresis loop is typically found. Macropores form important paths for molecules to diffuse into a particle; for gas-phase adsorption, they do not fill with adsorbate until the gas phase becomes saturated.

TABLE 16-4   Classification of Pore Sizes

Type	Slit Width° (w)	Characteristic
Micropore†	$w < 2$ nm	Superimposed wall potentials
Mesopore	2 nm $< w < 50$ nm	Capillary condensation
Macropore	$w > 50$ nm	Effectively flat walled until $p \rightarrow P^s$

°Or pore diameter.
†Further subdivided into ultramicropores and supermicropores (Gregg and Sing, gen. refs.).

Ion Exchangers   Ion exchangers are classified according to (1) their functionality and (2) the physical properties of the support matrix. Cation and anion exchangers are classified in terms of their ability to exchange positively or negatively charged species. Strongly acidic and strongly basic ion exchangers are ionized and thus are effective at nearly all pH values (pH 0–14). Weakly acidic exchangers are typically effective in the range of pH 5–14. Weakly basic resins are effective in the range of pH 0–9. Weakly acidic and weakly basic exchangers are often easier to regenerate, but leakage due to incomplete exchange may occur. Chelating resins containing iminodiacetic acid form specific metal complexes with metal ions with complex stability constants that follow the same order as those for EDTA. However, depending on pH, they also function as weak cation exchangers. The achievable ion-exchange capacity depends on the concentration of ionogenic groups and their availability as an exchange site. The latter is a function of the support matrix.

Polymer-based, synthetic ion-exchangers known as resins are available commercially in gel type or truly porous forms. Gel-type resins are not porous in the usual sense of the word, since their structure depends upon swelling in the solvent in which they are immersed. Removal of the solvent usually results in a collapse of the three-dimensional structure, and no significant surface area or pore diameter can be defined by the ordinary techniques available for truly porous materials. In their swollen state, gel-type resins approximate a true molecular-scale solution. Thus, we can identify an internal porosity ε_p only in terms of the equilibrium uptake of water or other liquid. When crosslinked polymers are used as the support matrix, the internal porosity so defined varies in inverse proportion to the degree of crosslinking, with swelling and therefore porosity typically being more pronounced in solvents with a high dielectric constant. The ion held by the exchanger also influences the resin swelling. Thus, the size of the resin particles changes during the ion-exchange process as the resin is changed from one form to another, and this effect is more dramatic for resins with a lower degree of crosslinking. The choice of degree of crosslinking is dependent on several factors including: the extent of swelling, the exchange capacity, the intraparticle diffusivity, the ease of regeneration, and the physical and chemical stability of the exchanger under chosen operating conditions. The concentration of ionogenic groups determines the capacity of the resin. Although the capacity per unit mass of dry resin is insensitive to the degree of crosslinking, except for very highly crosslinked resins, the exchange capacity per unit volume of swollen resin increases significantly with degree of crosslinking, so long as the mesh size of the polymer network allows the ions free access to functional groups within the interior of the resin. The degree of crosslinking also affects the rate of ion exchange. The intraparticle diffusivity decreases nearly exponentially with the mesh size of the matrix. As a result, resins with a lower degree of crosslinking are normally required for the exchange of bulky species, such as organic ions with molecular weight in excess of 100. The regeneration efficiency is typically greater for resins with a lower degree of crosslinking. Finally, the degree of crosslinking also affects the long-term stability of the resin. Strongly acidic and strongly basic resins are subject to irreversible oxidative degradation of the polymer and thermal and oxidative decomposition of functional groups. Generally, more highly crosslinked resins are less prone to irreversible chemical degradation but they may be subject to osmotic breakage caused by volume changes that occur during cyclic operations. In general, experience shows that an intermediate degree of crosslinking is often preferred. However, readers are referred to manufacturers' specifications for resin stability data at different operating conditions.

Truly porous, synthetic ion exchangers are also available. These materials retain their porosity even after removal of the solvent and have measurable surface areas and pore size. The term macroreticular is commonly used for resins prepared from a phase separation technique, where the polymer matrix is prepared with the addition of a liquid that is a good solvent for the monomers, but in which the polymer is insoluble. Matrices prepared in this way usually have the appearance of a conglomerate of gel-type microspheres held together to

form an interconnected porous network. Macroporous resins possessing a more continuous gellular structure interlaced with a pore network have also been obtained with different techniques and are commercially available. Since higher degrees of crosslinking are typically used to produce truly porous ion-exchange resins, these materials tend to be more stable under highly oxidative conditions, more attrition-resistant, and more resistant to breakage due to osmotic shock than their gel-type counterparts. Moreover, since their porosity does not depend entirely on swelling, they can be used in solvents with low dielectric constant where gel-type resins can be ineffective. Porous ion-exchange resins are also useful for the recovery and separation of high-molecular-weight substances such as proteins or colloidal particles. Specialty resins with very large pore sizes (from 30 nm to larger than 1000 nm) are available for these applications. In general, compared to gel-type resins, truly porous resins typically have somewhat lower capacities and can be more expensive. Thus, for ordinary ion-exchange applications involving small ions under nonharsh conditions, gel-type resins are usually preferred.

PHYSICAL PROPERTIES

Selected data on commercially available adsorbents and ion exchangers are given in Tables 16-5 and 16-6. The purpose of the tables is twofold: to assist the engineer or scientist in identifying materials suitable for a needed application, and to supply typical physical property values.

Excellent sources of information on the characteristics of adsorbents or ion exchange products for specific applications are the manufacturers themselves. The names, addresses, and phone numbers of suppliers may be readily found in most libraries in sources such as the *Thomas Register* and *Dun & Bradstreet*. Additional information on adsorbents and ion exchangers is available in many of the general references and in several articles in *Kirk-Othmer Encyclopedia of Chemical Technology*. A recent comprehensive summary of commercial ion-exchangers, including manufacturing methods, properties, and applications, is given by Dorfner (*Ion Exchangers,* de Gruyter, New York, 1991).

TABLE 16-5   Physical Properties of Adsorbents

Material and uses	Shape[*] of particles	Size range, U.S. standard mesh[†]	Internal porosity, %	Bulk dry density, kg/L	Average pore diameter, nm	Surface area, km²/kg	Sorptive capacity, kg/kg (dry)
Aluminas							
Low-porosity (fluoride sorbent)	G, S	8–14, etc.	40	0.70	~7	0.32	0.20
High-porosity (drying, separations)	G	Various	57	0.85	4–14	0.25–0.36	0.25–0.33
Desiccant, CaCl₂-coated	G	3–8, etc.	30	0.91	4.5	0.2	0.22
Activated bauxite	G	8–20, etc.	35	0.85	5		0.1–0.2
Chromatographic alumina	G, P, S	80–200, etc.	30	0.93			~0.14
Silicates and aluminosilicates							
Molecular sieves	S, C, P	Various					
Type 3A (dehydration)			~30	0.62–0.68	0.3	~0.7	0.21–0.23
Type 4A (dehydration)			~32	0.61–0.67	0.4	~0.7	0.22–0.26
Type 5A (separations)			~34	0.60–0.66	0.5	~0.7	0.23–0.28
Type 13X (purification)			~38	0.58–0.64	1.0	~0.6	0.25–0.36
Silicalite (hydrocarbons)	S, C, P	Various		0.64–0.70	0.6	~0.4	0.12–0.16
Dealumininated Y (hydrocarbons)	S, C, P	Various		0.48–0.53	0.8	0.5–0.8	0.28–0.42
Mordenite (acid drying)				0.88	0.3–0.8		0.12
Chabazite (acid drying)				0.72	0.4–0.5		0.20
Silica gel (drying, separations)	G, P	Various	38–48	0.70–0.82	2–5	0.6–0.8	0.35–0.50
Magnesium silicate (decoloring)	G, P	Various	~33	~0.50		0.18–0.30	
Calcium silicate (fatty-acid removal)	P		75–80	~0.20		~0.1	
Clay, acid-treated (refining of petroleum, food products)	G	4–8		0.85			
Fuller's earth (same)	G, P	<200		0.80			
Diatomaceous earth	G	Various		0.44–0.50		~0.002	
Carbons							
Shell-based	G	Various	60	0.45–0.55	2	0.8–1.6	0.40
Wood-based	G	Various	~80	0.25–0.30		0.8–1.8	~0.70
Petroleum-based	G, C	Various	~80	0.45–0.55	2	0.9–1.3	0.3–0.4
Peat-based	G, C, P	Various	~55	0.30–0.50	1–4	0.8–1.6	0.5
Lignite-based	G, P	Various	70–85	0.40–0.70	3	0.4–0.7	0.3
Bituminous-coal-based	G, P	8–30, 12–40	60–80	0.40–0.60	2–4	0.9–1.2	0.4
Synthetic polymer based (pyrolized)	S	20–100	40–70	0.49–0.60		0.1–1.1	
Carbon molecular sieve (air separation)		Various	35–50	0.5–0.7	0.3–0.6		0.5–0.20
Organic polymers							
Polystyrene (removal of organics, e.g., phenol; antibiotics recovery)	S	20–60	40–60	0.64	4–20	0.3–0.7	
Polyacrylic ester (purification of pulping wastewaters; antibiotics recovery)	G, S	20–60	50–55	0.65–0.70	10–25	0.15–0.4	
Phenolic (also phenolic amine) resin (decolorizing and deodorizing of solutions)	G	16–50	45	0.42		0.08–0.12	0.45–0.55

[*]Shapes: C, cylindrical pellets; F, fibrous flakes; G, granules; P, powder; S, spheres.
[†]U.S. Standard sieve sizes (given in parentheses) correspond to the following diameters in millimeters: (3) 6.73, (4) 4.76, (8) 2.98, (12) 1.68, (14) 1.41, (16) 1.19, (20) 0.841, (30) 0.595, (40) 0.420, (50) 0.297, (60) 0.250, (80) 0.177, (200) 0.074.

TABLE 16-6 Physical Properties of Ion-Exchange Materials

Material	Shape[a] of particles	Bulk wet density (drained), kg/L	Moisture content (drained), % by weight	Swelling due to exchange, %	Maximum operating temperature,[b] °C	Operating pH range	Exchange capacity Dry, equivalent/kg	Exchange capacity Wet, equivalent/L
Cation exchangers: strongly acidic								
Polystyrene sulfonate								
Homogeneous (gel) resin	S				120–150	0–14		
4% cross-linked		0.75–0.85	64–70	10–12			5.0–5.5	1.2–1.6
6% cross-linked		0.76–0.86	58–65	8–10			4.8–5.4	1.3–1.8
8–10% cross-linked		0.77–0.87	48–60	6–8			4.6–5.2	1.4–1.9
12% cross-linked		0.78–0.88	44–48	5			4.4–4.9	1.5–2.0
16% cross-linked		0.79–0.89	42–46	4			4.2–4.6	1.7–2.1
20% cross-linked		0.80–0.90	40–45	3			3.9–4.2	1.8–2.0
Porous structure								
12–20% cross-linked	S	0.81	50–55	4–6	120–150	0–14	4.5–5.0	1.5–1.9
Sulfonated phenolic resin	G	0.74–0.85	50–60	7	50–90	0–14	2.0–2.5	0.7–0.9
Sulfonated coal	G							
Cation exchangers: weakly acidic								
Acrylic (pK 5) or methacrylic (pK 6)								
Homogeneous (gel) resin	S	0.70–0.75	45–50	20–80	120	4–14	8.3–10	3.3–4.0
Macroporous	S	0.67–0.74	50–55	10–100	120		~8.0	2.5–3.5
Phenolic resin	G	0.70–0.80	~50	10–25	45–65	0–14	2.5	1.0–1.4
Polystyrene phosphonate	G, S	0.74	50–70	<40	120	3–14	6.6	3.0
Polystyrene iminodiacetate	S	0.75	68–75	<100	75	3–14	2.9	0.7
Polystyrene amidoxime	S	~0.75	58	10	50	1–11	2.8	0.8–0.9
Polystyrene thiol	S	~0.75	45–50		60	1–13	~5	2.0
Cellulose								
Phosphonate	F						~7.0	
Methylene carboxylate	F, P, G						~0.7	
Greensand (Fe silicate)	G	1.3	1–5	0	60	6–8	0.14	0.18
Zeolite (Al silicate)	G	0.85–0.95	40–45	0	60	6–8	1.4	0.75
Zirconium tungstate	G	1.15–1.25	~5	0	>150	2–10	1.2	1.0
Anion exchangers: strongly basic								
Polystyrene-based								
Trimethyl benzyl ammonium (type I)								
Homogeneous, 8% CL	S	0.70	46–50	~20	60–80	0–14	3.4–3.8	1.3–1.5
Porous, 11% CL	S	0.67	57–60	15–20	60–80	0–14	3.4	1.0
Dimethyl hydroxyethyl ammonium (type II)								
Homogeneous, 8% CL	S	0.71	~42	15–20	40–80	0–14	3.8–4.0	1.2
Porous, 10% CL	S	0.67	~55	12–15	40–80	0–14	3.8	1.1
Acrylic-based								
Homogeneous (gel)	S	0.72	~70	~15	40–80	0–14	~5.0	1.0–1.2
Porous	S	0.67	~60	~12	40–80	0–14	3.0–3.3	0.8–0.9
Cellulose-based								
Ethyl trimethyl ammonium	F				100	4–10	0.62	
Triethyl hydroxypropyl ammonium					100	4–10	0.57	
Anion exchangers: intermediately basic (pK 11)								
Polystyrene-based	S	0.75	~50	15–25	65	0–10	4.8	1.8
Epoxy-polyamine	S	0.72	~64	8–10	75	0–7	6.5	1.7
Anion exchangers: weakly basic (pK 9)								
Aminopolystyrene								
Homogeneous (gel)	S	0.67	~45	8–12	100	0–7	5.5	1.8
Porous	S	0.61	55–60	~25	100	0–9	4.9	1.2
Acrylic-based amine								
Homogeneous (gel)	S	0.72	~63	8–10	80	0–7	6.5	1.7
Porous	S	0.72	~68	12–15	60	0–9	5.0	1.1
Cellulose-based								
Aminoethyl	P						1.0	
Diethyl aminoethyl	P						~0.9	

[a]Shapes: C, cylindrical pellets; G, granules; P, powder; S, spheres.
[b]When two temperatures are shown, the first applies to H form for cation, or OH form for anion, exchanger; the second, to salt ion.

Several densities and void fractions are commonly used. For adsorbents, usually the **bulk density** ρ_b, the weight of clean material per unit bulk volume as packed in a column, is reported. The dry **particle density** ρ_p is related to the (external) **void fraction of packing** ε by

$$\rho_p = \frac{\rho_b}{1-\varepsilon} \qquad (16\text{-}1)$$

The **skeletal density** ρ_s of a particle (or crystalline density for a pure chemical compound) is given in terms of **internal porosity** ε_p by

$$\rho_s = \frac{\rho_p}{1-\varepsilon_p} \qquad (16\text{-}2)$$

For an adsorbent or ion exchanger, the **wet density** ρ_w of a particle is related to these factors and to the liquid density ρ_f by

$$\rho_w = \rho_p + \varepsilon_p \rho_f \qquad (16\text{-}3)$$

The **total voidage** ε_b in a packed bed (outside and inside particles) is

$$\varepsilon_b = \varepsilon + (1-\varepsilon)\varepsilon_p \qquad (16\text{-}4)$$

SORPTION EQUILIBRIUM

The quantity of a solute adsorbed can be given conveniently in terms of moles or volume (for adsorption) or ion-equivalents (for ion exchange) per unit mass or volume (dry or wet) of sorbent. Common units for adsorption are mol/(m³ of fluid) for the fluid-phase concentration c_i and mol/(kg of clean adsorbent) for adsorbed-phase concentration n_i. For gases, partial pressure may replace concentration.

Many models have been proposed for adsorption and ion exchange equilibria. The most important factor in selecting a model from an engineering standpoint is to have an accurate mathematical description over the entire range of process conditions. It is usually fairly easy to obtain correct capacities at selected points, but isotherm shape over the entire range is often a critical concern for a regenerable process.

GENERAL CONSIDERATIONS

Forces   Molecules are attracted to surfaces as the result of two types of forces: dispersion-repulsion forces (also called London or van der Waals forces) such as described by the Lennard-Jones potential for molecule-molecule interactions; and electrostatic forces, which exist as the result of a molecule or surface group having a permanent electric dipole or quadrupole moment or net electric charge.

Dispersion forces are always present and in the absence of any stronger force will determine equilibrium behavior, as with adsorption of molecules with no dipole or quadrupole moment on nonoxidized carbons and silicalite.

If a surface is polar, its resulting electric field will induce a dipole moment in a molecule with no permanent dipole and, through this polarization, increase the extent of adsorption. Similarly, a molecule with a permanent dipole moment will polarize an otherwise nonpolar surface, thereby increasing the attraction.

For a polar surface and molecules with permanent dipole moments, attraction is strong, as for water adsorption on a hydrophilic adsorbent. Similarly, for a polar surface, a molecule with a permanent quadrupole moment will be attracted more strongly than a similar molecule with a weaker moment; for example, nitrogen is adsorbed more strongly than oxygen on zeolites (Sherman and Yon, gen. refs.).

Surface Excess   With a Gibbs dividing surface placed at the surface of the solid, the surface excess of component i, Γ_i (mol/m²), is the amount per unit area of solid contained in the region near the surface, above that contained at the fluid-phase concentration far from the surface. This is depicted in two ways in Fig. 16-4. The quantity adsorbed per unit mass of adsorbent is

$$n_i = \Gamma_i A \qquad (16\text{-}6)$$

where A (m²/kg) is the surface area of the solid.

For a porous adsorbent, the amount adsorbed in the pore structure per unit mass of adsorbent, based on surface excess, is obtained by the difference

$$n_i = n_i^{tot} - V_p c_i^\infty \qquad (16\text{-}6)$$

where n_i^{tot} (mol/kg) is the total amount of component i contained within the particle's pore volume V_p (m³/kg), and c_i^∞ is the concentration outside of the particle. If thermodynamics is a concern and n_i differs significantly from n_i^{tot} (as it will for weakly adsorbed species), then

it is important to consider adsorbed-phase quantities in terms of surface excesses.

A second convention is the placement of an imaginary envelope around the outermost boundary of a porous particle, so that all solute and nonadsorbing fluid contained within the pores of the particle is considered adsorbed.

Classification of Isotherms by Shape   Representative isotherms are shown in Fig. 16-5, as classified by Brunauer and coworkers.
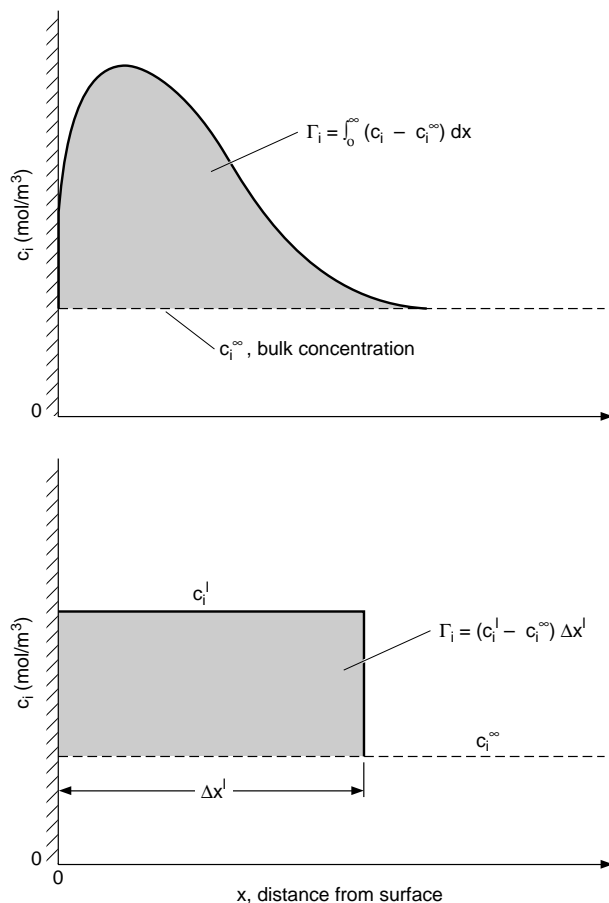

FIG. 16-4   Depictions of surface excess Γ_i. *Top:* The force field of the solid concentrates component i near the surface; the concentration c_i is low at the surface because of short-range repulsive forces between adsorbate and surface. *Bottom:* Surface excess for an imagined homogeneous surface layer of thickness Δx^l.
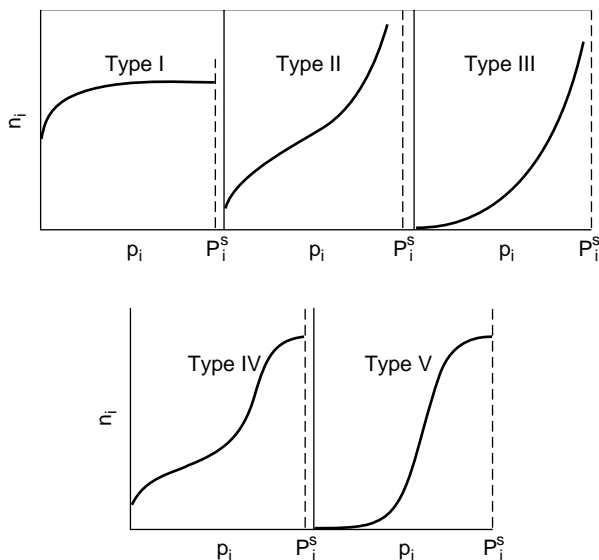
FIG. 16-5   Representative isotherm types. p_i and P_i^s are pressure and vapor pressure of the solute. [*Brunauer,* J. Am. Chem. Soc., **62**, 1723 (1940); reprinted with permission.]

Curves that are concave downward throughout (type I) have historically been designated as "favorable," while those that are concave upward throughout (type III) are "unfavorable." Other isotherms (types II, IV, and V) have one or more inflection points. The designations "favorable" and "unfavorable" refer to fixed-bed behavior for the uptake step, with a favorable isotherm maintaining a compact wave shape. A favorable isotherm for uptake is unfavorable for the discharge step. This becomes particularly important for a regenerative process, in which a favorable isotherm may be too favorable for regeneration to occur effectively.

Categorization of Equilibrium Models   Historically, sorption equilibrium has been approached from different viewpoints. For adsorption, many models for flat surfaces have been used to develop explicit equations and equations of state for pure components and mixtures, and many of the resulting equations are routinely applied to porous materials. Explicit equations for pore filling have also been proposed, generally based on the Polanyi potential theory. Ion exchange adds to these approaches concepts of absorption or dissolution (absorption) and exchange reactions. Statistical mechanics and molecular dynamics contribute to our understanding of all of these approaches (Steele, *The Interaction of Gases with Solid Surfaces,* Pergamon, Oxford, 1974; Nicholson and Parsonage, *Computer Simulation and the Statistical Mechanics of Adsorption,* Academic Press, New York, 1982). Mixture models are often based on the adsorbed solution theory, which uses thermodynamic equations from vapor-liquid equilibria with volume replaced by surface area and pressure replaced by a two-dimensional spreading pressure. Other approaches include lattice theories and mass-action exchange equilibrium.

Heterogeneity   Adsorbents and ion exchangers can be physically and chemically heterogeneous. Although exceptions exist, solutes generally compete for the same sites. Models for adsorbent heterogeneity have been developed for both discrete and continuous distributions of energies [Ross and Olivier, *On Physical Adsorption,* Interscience, New York, 1964; Jaroniec and Madey, Rudzinski and Everett, gen. refs.].

Isosteric Heat of Adsorption   The most useful heat of adsorption for fixed-bed calculations is the *isosteric heat of adsorption,* which is given by the Clausius-Clapeyron type relation

$$q_i^{st} = \Re T^2 \left.\frac{\partial \ln p_i}{\partial T}\right|_{n_i, n_j} \qquad (16\text{-}7)$$

where the n_j can be dropped for single-component adsorption. q_i^{st} is positive by convention. If isosteres are straight lines when plotted as $\ln p_i$ versus T^{-1} (see Fig. 16-1), then Eq. (16-7) can be integrated to give

$$\ln p_i = f(n_i) - \frac{q_i^{st}}{\Re T} \qquad (16\text{-}8)$$

where $f(n_i)$ is an arbitrary function dependent only on n_i. Many other heats of adsorption have been defined and their utility depends on the application (Ross and Olivier; Young and Crowell, gen. refs.).

From Eq. (16-8), if a single isotherm is known in the pressure explicit form $p_i = p_i(n_i, T)$ and if q_i^{st} is known at least approximately, then equilibria can be estimated over a narrow temperature range using

$$\ln \frac{p_i}{p_i^{ref}} = \frac{q_i^{st}}{\Re}\left(\frac{1}{T^{ref}} - \frac{1}{T}\right) \qquad (\text{const } n_i) \qquad (16\text{-}9)$$

Similarly, Eq. (16-9) is used to calculate the isosteric heat of adsorption from two isotherms.

Experiments   Sorption equilibria are measured using apparatuses and methods classified as volumetric, gravimetric, flow-through (frontal analysis), and chromatographic. Apparatuses are discussed by Yang (gen. refs.). Heats of adsorption can be determined from isotherms measured at different temperatures or measured independently by calorimetric methods.

Dimensionless Concentration Variables   Where appropriate, isotherms will be written here using the dimensionless system variables

$$c_i^\circ = \frac{c_i}{c_i^{ref}} \qquad n_i^\circ = \frac{n_i}{n_i^{ref}} \qquad (16\text{-}10)$$

where the best choice of reference values depends on the operation.

In some cases, to allow for some preloading of the adsorbent, it will be more convenient to use the dimensionless transition variables

$$c_i^\circ = \frac{(c_i - c_i')}{(c_i'' - c_i')} \qquad n_i^\circ = \frac{(n_i - n_i')}{(n_i'' - n_i')} \qquad (16\text{-}11)$$

where single and double primes indicate initial and final concentrations, respectively. Figure 16-6 shows n° plotted versus c° for a sample system. Superimposed are an upward transition (loading) and a downward transition (unloading), shown by the respective positions of (c_i', n_i') and (c_i'', n_i'').

SINGLE COMPONENT OR EXCHANGE

The simplest relationship between solid-phase and fluid-phase concentrations is the **linear isotherm**

$$n_i = K_i c_i \qquad \text{or} \qquad n_i = K_i' p_i \qquad (16\text{-}12)$$
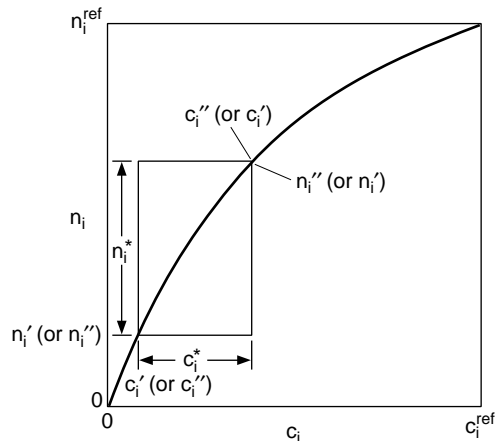

FIG. 16-6   Isotherm showing concentration variables for a transition from (c_i', n_i') to (c_i'', n_i'').

Thermodynamics requires that a linear limit be approached in the Henry's law region for all isotherm equations.

Flat Surface Isotherm Equations   The classification of isotherm equations into two broad categories for flat surfaces and pore filling reflects their origin. It does not restrict equations developed for flat surfaces from being applied successfully to describe data for porous adsorbents.

The classical isotherm for a homogeneous flat surface, and most popular of all nonlinear isotherms, is the **Langmuir isotherm**

$$n_i = \frac{n_i^s K_i c_i}{1 + K_i c_i} \tag{16-13}$$

where n_i^s is the monolayer capacity approached at large concentrations and K_i is an equilibrium constant. These parameters are often determined by plotting $1/n_i$ versus $1/c_i$. The derivation of the isotherm assumes negligible interaction between adsorbed molecules.

The classical isotherm for multilayer adsorption on a homogeneous, flat surface is the **BET isotherm** [Brunauer, Emmett, and Teller, *J. Am. Chem. Soc.*, **60,** 309 (1938)]

$$n_i = \frac{n_i^s K_i p_i}{[1 + K_i p_i - (p_i/P_i^s)][1 - (p_i/P_i^s)]} \tag{16-14}$$

where p_i is the pressure of the adsorbable component and P_i^s is its vapor pressure. It is useful for gas-solid systems in which condensation is approached, fitting type-II behavior.

For a heterogeneous flat surface, a classical isotherm is the **Freundlich isotherm**

$$n_i = K_i c_i^{m_i} \tag{16-15}$$

where m_i is positive and generally not an integer. The isotherm corresponds approximately to an exponential distribution of heats of adsorption. Although it lacks the required linear behavior in the Henry's law region, it can often be used to correlate data on heterogeneous adsorbents over wide ranges of concentration.

Several isotherms combine aspects of both the Langmuir and Freudlich equations. One that has been shown to be effective in describing data mathematically for heterogeneous adsorbents is the **Tóth isotherm** [*Acta Chim. Acad. Sci. Hung.,* **69,** 311 (1971)]

$$n_i = \frac{n_i^s p_i}{[(1/K_i) + p_i^{m_i}]^{1/m_i}} \tag{16-16}$$

This three-parameter equation behaves linearly in the Henry's law region and reduces to the Langmuir isotherm for $m = 1$. Other well-known isotherms include the **Radke-Prausnitz isotherm** [Radke and Prausnitz, *Ind. Eng. Chem. Fundam.,* **11,** 445 (1972); *AIChE J.,* **18,** 761 (1972)]

$$n_i = \frac{n_i^s K_i p_i}{(1 + K_i p_i)^m} \tag{16-17}$$

and the **Sips isotherm** [Sips, *J. Chem. Phys.,* **16,** 490 (1948); Koble and Corrigan, *Ind. Eng. Chem.,* **44,** 383 (1952)] or **loading ratio correlation** with prescribed temperature dependence [Yon and Turnock, *AIChE Symp. Ser.,* **67**(117), 75 (1971)]

$$n_i = \frac{n_i^s (K_i p_i)^m}{1 + (K_i p_i)^m} \tag{16-18}$$

Another three-parameter equation that often fits data well and is linear in the Henry's law region is the **UNILAN equation** [Honig and Reyerson, *J. Phys. Chem.,* **56,** 140 (1952)]

$$n_i = \frac{n_i^s}{2s_i} \ln \frac{1 + K_i e^{s_i} p_i}{1 + K_i e^{-s_i} p_i} \tag{16-19}$$

which reduces to the Langmuir equation as $s_i \to 0$.

Equations of state are also used for pure components. Given such an equation written in terms of the two-dimensional spreading pressure π, the corresponding isotherm is easily determined, as described later for mixtures [see Eq. (16-42)]. The two-dimensional equivalent of an ideal gas is an ideal surface gas, which is described by

$$\pi A = n_i \Re T \tag{16-20}$$

which readily gives the linear isotherm, Eq. (16-12). Many more complicated equations of state are available, including two-dimensional analogs of the virial equation and equations of van der Waals, Redlich-Kwong, Peng-Robinson, and so forth [Adamson, gen. refs.; Patrykiejewet et al., *Chem. Eng. J.,* **15,** 147 (1978); Haydel and Kobayashi, *Ind. Eng. Chem. Fundam.,* **6,** 546 (1967)].

Pore-Filling Isotherm Equations   Most pore-filling models are grounded in the **Polanyi potential theory.** In Polanyi's model, an attracting potential energy field is assumed to exist adjacent to the surface of the adsorbent and concentrates vapors there. Adsorption takes place whenever the strength of the field, independent of temperature, is great enough to compress the solute to a partial pressure greater than its vapor pressure. The last molecules to adsorb form an equipotential surface containing the adsorbed volume. The strength of this field, called the adsorption potential ε (J/mol), was defined by Polanyi to be equal to the work required to compress the solute from its partial pressure to its vapor pressure

$$\varepsilon = \Re T \ln \left(\frac{P_i^s}{p_i} \right) \tag{16-21}$$

The same result is obtained by considering the change in chemical potential. In the basic theory, W (m³/kg), the volume adsorbed as saturated liquid at the adsorption temperature, is plotted versus ε to give a characteristic curve. Data measured at different temperatures for the same solute-adsorbent pair should fall on this curve. Using the method, it is possible to use data measured at a single temperature to predict isotherms at other temperatures. Data for additional, homologous solutes can be collapsed into a single "correlation curve" by defining a scaling factor β, the most useful of which has been V/V^{ref}, the adsorbate molar volume as saturated liquid at the adsorption temperature divided by that for a reference compound. Thus, by plotting W versus ε/β or $\varepsilon/\dot{V}$ for data measured at various temperatures for various similar solutes and a single adsorbent, a single curve should be obtained. Variations of the theory are often used to evaluate properties for components near or above their critical points [Grant and Manes, *Ind. Eng. Chem. Fund.,* **5,** 490 (1966)].

The most popular equations used to describe the shape of a characteristic curve or a correlation curve are the two-parameter **Dubinin-Radushkevich** (DR) equation

$$\frac{W}{W_0} = \exp\left[-k \left(\frac{\varepsilon}{\beta} \right)^2 \right] \tag{16-22}$$

and the three-parameter **Dubinin-Astakhov** (DA) equation

$$\frac{W}{W_0} = \exp\left[-k \left(\frac{\varepsilon}{\beta} \right)^m \right] \tag{16-23}$$

where W_0 is micropore volume and m is related to the pore size distribution [Gregg and Sing, gen. refs.]. Neither of these equations has correct limiting behavior in the Henry's law regime.

Ion Exchange   A useful tool is provided by the **mass action law** for describing the general exchange equilibrium in fully ionized exchanger systems as

$$z_B A + z_A \overline{B} \rightleftharpoons z_B \overline{A} + z_A B$$
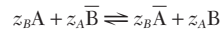
where overbars indicate the ionic species in the ion exchanger phase and z_A and z_B are the valences of ions A and B. The associated equilibrium relation is of the form

$$K_{A,B}^c = K_{A,B} \left(\frac{\gamma_A}{\overline{\gamma}_A} \right)^{z_B} \left(\frac{\overline{\gamma}_B}{\gamma_B} \right)^{z_A} = \left(\frac{n_A}{c_A} \right)^{z_B} \left(\frac{c_B}{n_B} \right)^{z_A} \tag{16-24}$$

where $K_{A,B}^c$ is the apparent equilibrium constant or molar selectivity coefficient, $K_{A,B}$ is the thermodynamic equilibrium constant based on activities, and the γs are activity coefficients. Often it is desirable to represent concentrations in terms of equivalent ionic fractions based on solution normality c_{tot} and fixed exchanger capacity n^s as $c_i^* = z_i c_i / c_{\mathrm{tot}}$ and $n_i^* = z_i n_i / n_{\mathrm{tot}}$, where $c_{\mathrm{tot}} = \sum z_j c_j$ and $n_{\mathrm{tot}} = \sum z_j n_j = n^s$ with the summations extended to all counter-ion species. A rational selectivity coefficient is then defined as

$$K_{A,B}' = K_{A,B}^c \left(\frac{n_{\mathrm{tot}}}{c_{\mathrm{tot}}} \right)^{z_A - z_B} = \left(\frac{n_A^*}{c_A^*} \right)^{z_B} \left(\frac{c_B^*}{n_B^*} \right)^{z_A} \tag{16-25}$$

For the exchange of ions of equal valence ($z_A = z_B$), $K_{A,B}^c$ and $K_{A,B}'$ are

coincident and, to a first approximation, independent of concentration. When $z_A > z_B$, $K'_{A,B}$ decreases with solution normality. This reflects the fact that ion exchangers exhibit an increasing affinity for ions of lower valence as the solution normality increases.

An alternate form of Eq. (16-25) is

$$n_A^\circ = K_{A,B}^c \left(\frac{n_{tot}}{c_{tot}}\right)^{(z_A - z_B)/z_B} \left(\frac{1 - n_A^\circ}{1 - c_A^\circ}\right)^{z_A/z_B} c_A^\circ \qquad (16\text{-}26)$$

When B is in excess $(c_A^\circ, n_A^\circ \to 0)$, this reduces to

$$n_A^\circ = K_{A,B}^c \left(\frac{n_{tot}}{c_{tot}}\right)^{(z_A - z_B)/z_B} c_A^\circ = K_A c_A^\circ \qquad (16\text{-}27)$$

where the linear equilibrium constant $K_A = K_{A,B}^c (n_{tot}/c_{tot})^{(z_A/z_B)-1}$ decreases with solution normality c_{tot} when $z_A > z_B$ or increases when $z_A < z_B$.

Table 16-7 gives equilibrium constants for crosslinked cation and anion exchangers for a variety of counterions. The values given for cation exchangers are based on ion A replacing Li^+, and those given for anion exchangers are based on ion A replacing Cl^-. The selectivity for a particular ion generally increases with decreasing hydrated ion size and increasing degree of crosslinking. The selectivity coefficient for any two ions A and D can be obtained from Table 16-7 from values of $K_{A,B}$ and $K_{D,B}$ as

$$K_{A,D} = K_{A,B}/K_{D,B} \qquad (16\text{-}28)$$

The values given in this table are only approximate, but they are adequate for process screening purposes with Eqs. (16-24) and (16-25). Rigorous calculations generally require that activity coefficients be accounted for. However, for the exchange between ions of the same valence at solution concentrations of 0.1 N or less, or between any ions at 0.01 N or less, the solution-phase activity coefficients prorated to unit valence will be similar enough that they can be omitted.

Models for ion exchange equilibria based on the mass-action law taking into account solution and exchanger-phase nonidealities with equations similar to those for liquid mixtures have been developed by several authors [see Smith and Woodburn, *AIChE J.*, **24**, 577 (1978); Mehablia et al., *Chem. Eng. Sci.*, **49**, 2277 (1994)]. Thermodynamics-based approaches are also available [Soldatov in Dorfner, gen. refs.; Novosad and Myers, *Can J. Chem. Eng.*, **60**, 500 (1982); Myers and Byington in Rodrigues, ed., *Ion Exchange Science and Technology*, NATO ASI Series, No. 107, Nijhoff, Dordrecht, 1986, pp. 119–145] as well as approaches for the exchange of macromolecules, taking into account steric-hindrance effects [Brooks and Cramer, *AIChE J.*, **38**, 12 (1992)].

Example 3: Calculation of Useful Ion-Exchange Capacity An 8 percent crosslinked sulfonated resin is used to remove calcium from a solution containing 0.0007 mol/l Ca^{+2} and 0.01 mol/l Na^+. The resin capacity is 2.0 equiv/l. Estimate the resin capacity for calcium removal.

From Table 16-7, we obtain $K_{Ca,Na} = 5.16/1.98 = 2.6$. Since $n_{tot} = 2$ equiv/l and $c_{tot} = 2 \times 0.0007 + 0.01 = 0.024$ equiv/l, $K'_{Ca,Na} = 2.6 \times 2/0.011 = 470$. Thus, with $c_{Ca}^\circ = 2 \times 0.0007/0.011 = 0.13$, Eq. (16-25) gives $470 = (n_{Ca}^\circ/0.13)[(1 - 0.13)/(1 - n_{Na}^\circ)]^2$ or $n_{Ca}^\circ = 0.9$. The available capacity for calcium is $n_{Ca} = 0.9 \times 2.0/2 = 0.9$ mol/l.

Donnan Uptake The uptake of an electrolyte as a neutral ion pair of a salt is called Donnan uptake. It is generally negligible at low ionic concentrations. Above 0.5 g·equiv/l with strongly ionized exchangers (or at lower concentrations with those more weakly ionized), the resin's fixed ion-exchange capacity is measurably exceeded as a result of electrolyte invasion. With only one coion species Y (matching the charge sign of the fixed groups in the resin), its uptake n_Y equals the total excess uptake of the counterion. Equilibrium is described by the mass-action law. For the case of a resin in A-form in equilibrium with a salt AY, the excess counterion uptake is given by [Helfferich, gen. refs., pp. 133–147]

$$z_Y n_Y = \left[\frac{n^{s2}}{4} + (z_Y c_Y)^2 \left(\frac{\gamma_{AY}}{\overline{\gamma}_{AY}}\right)^2 \left(\frac{\overline{a}_w}{a_w}\right)^{\overline{v}_{AY}/\overline{v}_w}\right]^{1/2} - \frac{n^s}{2} \qquad (16\text{-}29)$$

where γs are activity coefficients, as water activities, and vs partial molar volumes. For dilute conditions, Eq. (16-29) predicts a squared dependence of n_Y on c_Y. Thus, the electrolyte sorption isotherm has a strong positive curvature. Donnan uptake is more pronounced for resins of lower degree of crosslinking and for counterions of low valence.

Separation Factor By analogy with the mass-action case and appropriate for both adsorption and ion exchange, a **separation factor** r can be defined based on dimensionless system variables [Eq. (16-10)] by

$$r = \frac{c_i^\circ(1 - n_i^\circ)}{n_i^\circ(1 - c_i^\circ)} \quad \text{or} \quad r = \frac{n_B^\circ/c_B^\circ}{n_A^\circ/c_A^\circ} \qquad (16\text{-}30)$$

This term is analogous to relative volatility or its reciprocal (or to an equilibrium selectivity). Similarly, the assumption of a constant sepa-

TABLE 16-7 Equilibrium Constants for Polystyrene DVB Cation and Anion Exchangers

	Strong acid sulfonated cation exchangers (Li^+ reference ion)						
	Degree of crosslinking				Degree of crosslinking		
Counterion	4% DVB	8% DVB	16% DVB	Counterion	4% DVB	8% DVB	16% DVB
Li^+	1.00	1.00	1.00	Mg^{++}	2.95	3.29	3.51
H^+	1.32	1.27	1.47	Zn^{++}	3.13	3.47	3.78
Na^+	1.58	1.98	2.37	Co^{++}	3.23	3.74	3.81
NH_4^+	1.90	2.55	3.34	Cu^{++}	3.29	3.85	4.46
K^+	2.27	2.90	4.50	Cd^{++}	3.37	3.88	4.95
Rb^+	2.46	3.16	4.62	Ni^{++}	3.45	3.93	4.06
Cs^+	2.67	3.25	4.66	Ca^{++}	4.15	5.16	7.27
Ag^+	4.73	8.51	22.9	Pb^{++}	6.56	9.91	18.0
Tl^+	6.71	12.4	28.5	Ba^{++}	7.47	11.5	20.8

	Strong base anion exchangers, 8% DVB (Cl^- reference ion)					
Counterion	Type I resin°	Type II resin†	Counterion	Type I resin[a]	Type II resin[b]
Salicylate	32	28	Cyanide	1.6	1.3
Iodide	8.7	7.3	Chloride	1.0	1.0
Phenoxide	5.2	8.7	Hydroxide	0.05–0.07	0.65
Nitrate	3.8	3.3	Bicarbonate	0.3	0.5
Bromide	2.8	2.3	Formate	0.2	0.2
Nitrite	1.2	1.3	Acetate	0.2	0.2
Bisulfite	1.3	1.3	Fluoride	0.09	0.1
Cyanide	1.6	1.3	Sulfate	0.15	0.15

°Trimethylamine
†Dimethyl-hydroxyethylamine
Data from Bonner and Smith, *J. Phys. Chem.*, **61**, 326 (1957) and Wheaton and Bauman, *Ind. Eng. Chem.*, **45**, 1088 (1951).

ration factor is a useful assumption in many sorptive operations. [It is constant for the Langmuir isotherm, as described below, and for mass-action equilibrium with $m = 1$ in Eq. (16-24).] This gives the constant separation factor isotherm

$$n_i^\circ = \frac{c_i^\circ}{r + (1-r)c_i^\circ} \tag{16-31}$$

The separation factor r identifies the equilibrium increase in n_i° from 0 to 1, which accompanies an increase in c_i° from 0 to 1. For a concentration change over only part of the isotherm, a separation factor R can be defined for the dimensionless transition variables [Eq. (16-11)]. This separation factor is

$$R = \frac{n_i''/c_i''}{n_i'/c_i'} = \frac{c_i^\circ(1 - n_i^\circ)}{n_i^\circ(1 - c_i^\circ)} \tag{16-32}$$

and gives an equation identical to Eq. (16-31) with R replacing r.

Figure 16-7 shows constant separation factor isotherms for a range of r (or R) values. The isotherm is linear for $r = 1$, favorable for $r < 1$, rectangular (or irreversible) for $r = 0$, and unfavorable for $r > 1$. As a result of symmetry properties, if r is defined for adsorption of component i or exchange of ion A for B, then the reverse process is described by $1/r$.

The Langmuir isotherm, Eq. (16-13), corresponds to the constant separation factor isotherm with

$$r = 1/(1 + K_i c_i^{\text{ref}}) \tag{16-33}$$

for system variables Eq. (16-10) or

$$R = \frac{r + (1-r)(c_i'/c_i^{\text{ref}})}{r + (1-r)(c_i''/c_i^{\text{ref}})} \tag{16-34}$$

for transition variables [Eq. (16-11)]. Vermeulen et al. [gen. refs.] give additional properties of constant separation factor isotherms.

Example 4: Application of Isotherms Thomas [*Ann. N.Y. Acad. Sci.,* **49,** 161 (1948)] provides the following Langmuir isotherm for the adsorption of anthracene from cyclohexane onto alumina:

$$n_i = \frac{22c_i}{1 + 375c_i}$$

with n_i in mol anthracene/kg alumina and c_i in mol anthracene/l liquid.
a.   What are the values of K_i and n_i^s according to Eq. (16-13)?

$$K_i = 375 \text{ l/mol}$$

$$n_i^s = \frac{22}{K_i} = 0.0587 \text{ mol/kg}$$
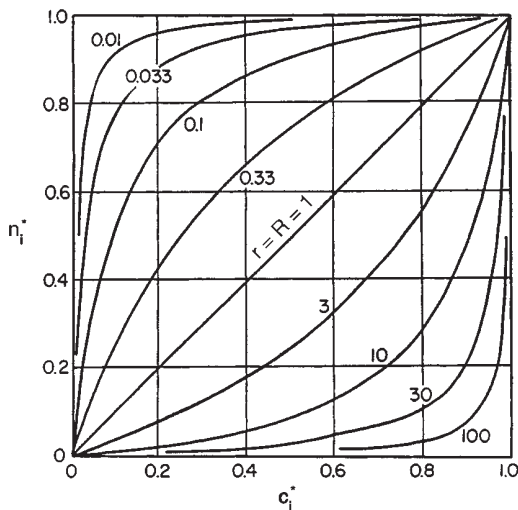
FIG. 16-7 Constant separation factor isotherm as a function of the separation factor r (or interchangeably R). Each isotherm is symmetric about the perpendicular line connecting (0,1) and (1,0). Isotherms for r and $1/r$ are symmetric about the 45° line.

b.   For a feed concentration of 8.11×10^{-4} mol/l, what is the value of r?

$$r = \frac{1}{1 + K_i(8.11 \times 10^{-4})} = 0.766 \qquad \text{[from Eq. (16-33)]}$$

c.   If the alumina is presaturated with liquid containing 2.35×10^{-4} mol/l and the feed concentration is 8.11×10^{-4} mol/l, what is the value of R?

$$R = 0.834 \qquad \text{[from Eq. (16-32) or (16-34)]}$$

MULTIPLE COMPONENTS OR EXCHANGES

When more than one adsorbed species or more than two ion-exchanged species interact in some manner, equilibrium becomes more complicated. Usually, thermodynamics provides a sound basis for prediction.

Adsorbed-Solution Theory The common thermodynamic approach to multicomponent adsorption treats adsorption equilibrium in a way analogous to fluid-fluid equilibrium. The theory has as its basis the Gibbs adsorption isotherm [Young and Crowell, gen. refs.], which is

$$A d\pi = \sum_i n_i \, d\mu_i \quad (\text{const } T) \tag{16-35}$$

where μ is chemical potential. For an ideal gas $(d\mu = \Re T d \ln p_i)$, if it is assumed that an adsorbed solution is defined with a pure-component standard state (as is common for a liquid solution), then Eq. (16-35) can be integrated to give [Rudisill and LeVan, *Chem. Eng. Sci.,* **47,** 1239 (1992)]

$$p_i = \gamma_i x_i P_i^{\text{ref}}(T, \pi) \tag{16-36}$$

where γ_i and x_i are the adsorbed-phase activity coefficient and mole fraction of component i and P_i^{ref} is the standard state, specified to be at the temperature and spreading pressure of the mixture.

Equation (16-36) with $\gamma_i = 1$ provides the basis for the ideal adsorbed-solution theory [Myers and Prausnitz, *AIChE J.,* **11,** 121 (1965)]. The spreading pressure for a pure component is determined by integrating Eq. (16-35) for a pure component to obtain

$$\frac{\pi A}{\Re T} = \int_0^{P_i^{\text{ref}}} \frac{n_i}{p_i} \, dp_i \tag{16-37}$$

where n_i is given by the pure-component isotherm. Also, since $\sum x_i = 1$, Eq. (16-36) with $\gamma_i = 1$ gives $\sum (p_i/P_i^{\text{ref}}) = 1$. With no area change on mixing for the ideal solution, the total number of moles adsorbed per unit weight of adsorbent is determined using a two-dimensional form of Amagat's law:

$$\frac{1}{n_{\text{tot}}} = \sum \frac{x_i}{n_i^{\text{ref}}} \tag{16-38}$$

where $n_{\text{tot}} = \sum n_i$ and n_i^{ref} is given by the pure-component isotherm at P_i^{ref}. Adsorbed-phase concentrations are calculated using $n_i = x_i n_{\text{tot}}$. Generally, different values of π [or $\pi A/(\Re T)$] must be tried until the one is found that satisfies Eqs. (16-37) and $\sum x_i = 1$.

Example 5: Application of Ideal Adsorbed-Solution Theory Consider a binary adsorbed mixture for which each pure component obeys the Langmuir equation, Eq. (16-13). Let $n_1^s = 4$ mol/kg, $n_2^s = 3$ mol/kg, $K_1 p_1 = K_2 p_2 = 1$. Use the ideal adsorbed-solution theory to determine n_1 and n_2.

Substituting the pure component Langmuir isotherm

$$n_i = \frac{n_i^s K_i p_i}{1 + K_i p_i}$$

into Eq. (16-37) and integrating gives

$$\frac{\pi A}{\Re T} = n_i^s \ln(1 + K_i P_i^{\text{ref}})$$

which can be solved explicitly for $K_i P_i^{\text{ref}}$. Values are guessed for $\pi A/(\Re T)$, values of $K_i P_i^{\text{ref}}$ are calculated from the equation above, and $\sum x_i = \sum K_i p_i/(K_i P_i^{\text{ref}}) = 1$ is checked to see if it is satisfied. Trial and error gives $\pi A/(\Re T) = 3.8530$ mol/kg, $K_1 P_1^{\text{ref}} = 1.6202$, $K_2 P_2^{\text{ref}} = 2.6123$, and $x_1 = 0.61720$. Evaluating the pure-component isotherms at the reference pressures and using Eq. (16-38) gives $n_{\text{tot}} = 2.3475$ mol/kg, and finally $n_i = x_i n_{\text{tot}}$ gives $n_1 = 1.4489$ mol/kg and $n_2 = 0.8986$ mol/kg.

Other approaches to account for various effects have been developed. Negative deviations from Raoult's law (i.e., $\gamma_i < 1$) are frequently

found due to adsorbent heterogeneity [e.g., Myers, *AIChE J.,* **29,** 691 (1983)]. Thus, contributions include accounting for adsorbent heterogeneity [Valenzuela et al., *AIChE J.,* **34,** 397 (1988)] and excluded pore-volume effects [Myers, in Rodrigues et al., gen. refs.]. Several activity coefficient models have been developed to account for non-ideal adsorbate-adsorbate interactions including a spreading pressure-dependent activity coefficient model [e.g., Talu and Zwiebel, *AIChE J.,* **32,** 1263 (1986)] and a vacancy solution theory [Suwanayuen and Danner, *AIChE J.,* **26,** 68, 76 (1980)].

Langmuir-Type Relations   For systems composed of solutes that individually follow Langmuir isotherms, the traditional multi-component Langmuir equation, obtained via a kinetic derivation, is

$$n_i = \frac{n_i^s K_i p_i}{1 + \sum K_i p_i} \qquad (16\text{-}39)$$

This equation has been criticized on thermodynamic grounds because it does not satisfy the Gibbs adsorption isotherm unless all monolayer capacities n_i^s are equal.

To satisfy the Gibbs adsorption isotherm for unequal monolayer capacities, explicit isotherms can be obtained in the form of a series expansion [LeVan and Vermeulen, *J. Phys. Chem.,* **85,** 3247 (1981)]. A two-term form is

$$n_1 = \frac{(n_1^s + n_2^s)K_1 p_1}{2(1 + K_1 p_1 + K_2 p_2)} + \frac{(n_1^s - n_2^s)K_1 p_1 K_2 p_2}{(K_1 p_1 + K_2 p_2)^2} \ln(1 + K_1 p_1 + K_2 p_2)$$

$$(16\text{-}40)$$

where the subscripts may be interchanged. Multicomponent forms are also available [Frey and Rodrigues, *AIChE J.,* **40,** 182 (1994)].

Example 6: Comparison of Binary Langmuir Isotherms   Use the numerical values in Example 5 to evaluate the binary Langmuir isotherms given by Eqs. (16-39) and (16-40) and compare results with the exact answers given in Example 5.

Equation (16-39) gives $n_1 = 1.3333$ mol/kg and $n_2 = 1.0000$ mol/kg for an average deviation from the exact values of approximately 10 percent. Equation (16-40) gives $n_1 = 1.4413$ mol/kg and $n_2 = 0.8990$ mol/kg for an average deviation of about 0.6 percent.

Freundlich-Type Relations   A binary Freundlich isotherm, obtained from the ideal adsorbed solution theory in loading-explicit closed form [Crittenden et al., *Environ. Sci. Technol.,* **19,** 1037 (1985)], is

$$c_i = \frac{n_i}{\sum_{j=1}^{N} n_j} \left(\frac{\sum_{j=1}^{N} (n_j/m_j)}{K_i/m_i} \right)^{1/m_i} \qquad (16\text{-}41)$$

Equations of State   If an equation of state is specified for a multicomponent adsorbed phase of the form $\pi A/(\Re T) = f(n_1, n_2, \dots)$, then the isotherms are determined using [Van Ness, *Ind. Eng. Chem. Fundam.,* **8,** 464–473 (1969)]

$$\ln \left(\frac{K_i p_i}{n_i/M_s} \right) = \int_A^\infty \left[\frac{\partial[\pi A/(\Re T)]}{\partial n_i} \bigg|_{T,A,n_j} - 1 \right] \frac{dA}{A} \qquad (16\text{-}42)$$

where, because integration is over A, M_s is mass of adsorbent, units for n and A are mol and m² (rather than mol/kg and m²/kg), and $K_i p_i/(n_i/M_s) = 1$ is the linear lower limit approached for the ideal surface gas [see Eqs. (16-12) and (16-20)].

Ion Exchange—Stoichiometry   In most applications, except for some weak-electrolyte and some concentrated-solution cases, the following summations apply:

$$\sum_i z_i c_i = c_{\text{tot}} = \text{const} \qquad \sum_i z_i n_i = n_{\text{tot}} = \text{const} \qquad (16\text{-}43)$$

In equivalent-fraction terms, the sums become

$$\sum_i c_i^* = 1 \qquad \sum_i n_i^* = 1 \qquad (16\text{-}44)$$

Mass Action   Here the equilibrium relations, consistent with Eq. (16-25), are

$$K'_{ij} = \left(\frac{n_i^*}{c_i^*} \right)^{z_j} \left(\frac{c_j^*}{n_j^*} \right)^{z_i} \qquad (16\text{-}45)$$
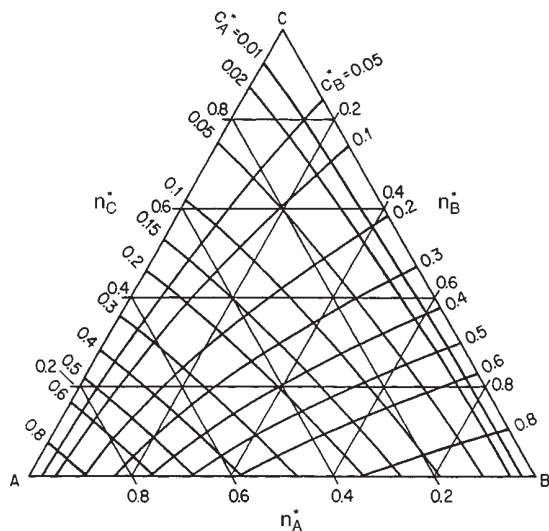
FIG. 16-8   Ideal mass-action equilibrium for three-component ion exchange with unequal valences. $K'_{A,C} = 8.06$; $K'_{B,C} = 3.87$. Duolite C-20 polystyrenesulfonate resin, with Ca as *A,* Mg as *B,* and Na as *C.* [*Klein et al.,* Ind. Eng. Chem. Fund., **6,** *339 (1967); reprinted with permission.*]

For an *N*-species system, with N c^*s (or n^*s) known, the N n^*s (or c^*s) can be found by simultaneous solution of the $N - 1$ independent i,j combinations for Eq. (16-45) using Eq. (16-43); one n_j^*/c_j^* is assumed, the other values can be calculated using Eq. (16-45), and the sum of the trial n^*s (or c^*s) is compared with Eq. (16-44).

Because an *N*-component system has $N - 1$ independent concentrations, a three-component equilibrium can be plotted in a plane and a four-component equilibrium in a three-dimensional space. Figure 16-8 shows a triangular plot of c^* contours in equilibrium with the corresponding n^* coordinates.

Improved models for ion-exchange equilibria based on the mass-action law that take into account solution and exchanger-phase non-idealities with equations similar to those for liquid mixtures have been developed by several authors including Smith and Woodburn [*AIChE J.,* **24,** 577 (1978)] and Mehablia et al. [*Chem. Eng. Sci.,* **49,** 2277 (1994)]. Thermodynamics-based approaches are also available [Soldatov in Dorfner, gen. refs.; Novosad and Myers, *Can J. Chem. Eng.,* **60,** 500 (1982); Myers and Byington in Rodrigues, ed., *Ion Exchange: Science and Technology,* NATO ASI Series, No. 107, Nijhoff, Dordrecht, 1986, pp. 119–145] as well as approaches for the exchange of macromolecules taking into account steric-hindrance effects [Brooks and Cramer, *AIChE J.,* **38,** 12 (1992)].

Constant Separation-Factor Treatment   If the valences of all species are equal, the separation factor α_{ij} applies, where

$$\alpha_{ij} = K_{ij} = \frac{n_i^* c_j^*}{c_i^* n_j^*} \qquad (16\text{-}46)$$

For a binary system, $r = \alpha_{BA} = 1/\alpha_{AB}$. The symbol r applies primarily to the process, while α is oriented toward interactions between pairs of solute species. For each binary pair, $r_{ij} = \alpha_{ji} = 1/\alpha_{ij}$.

Equilibrium then is given explicitly by

$$n_i^* = \frac{c_i^*}{\sum_j \alpha_{ji} c_j^*} = \frac{\alpha_{iN} c_i^*}{\sum_j \alpha_{jN} c_j^*} \qquad (16\text{-}47)$$

and

$$c_i^* = \frac{n_i^*}{\sum_j \alpha_{ij} n_j^*} = \frac{\alpha_{Ni} n_i^*}{\sum_j \alpha_{Nj} n_j^*} \qquad (16\text{-}48)$$

For the constant separation factor case, the c^* contours in a plot like Fig. 16-8 are linear.

CONSERVATION EQUATIONS

Material balances, often an energy balance, and occasionally a momentum balance are needed to describe an adsorption process. These are written in various forms depending on the specific application and desire for simplicity or rigor. Reasonably general material balances for various processes are given below. An energy balance is developed for a fixed bed for gas-phase application and simplified for liquid-phase application. Momentum balances for pressure drop in packed beds are given in Sec. 6.

MATERIAL BALANCES

At a microscale, a sorbable component exists at three locations—in a sorbed phase, in pore fluid, and in fluid outside particles. As a consequence, in material balances time derivatives must be included of terms involving n_i, c_{pi} (the pore concentration), and c_i (the extraparticle concentration). Let $\bar{n}_i$ represent n_i averaged over particle volume, and let $\bar{c}_{pi}$ represent c_{pi} averaged over pore fluid volume.

For batch or stirred tank processes, in terms of the mass of adsorbent M_s (kg), extraparticle volume of fluid V_f (m³), and volumetric flow rates F_v (m³/s) in and out of a tank, the material balance on component i is

$$M_s \frac{d\hat{n}_i}{dt} + \frac{d(V_f c_i)}{dt} = F_{v,\text{in}} c_{\text{in},i} - F_{v,\text{out}} c_i \qquad (16\text{-}49)$$

with
$$\hat{n}_i = \bar{n}_i + (\varepsilon_p/\rho_p)\bar{c}_{pi} = \bar{n}_i + [(1-\varepsilon)\varepsilon_p/\rho_b]\bar{c}_{pi} \qquad (16\text{-}50)$$

where ρ_p and ρ_b are particle and bulk densities, and ε and ε_p are void fraction (extra particle volume fraction) and particle porosity, respectively.

For a fixed-bed process, the material balance for component i is

$$\rho_b \frac{\partial \hat{n}_i}{\partial t} + \varepsilon \frac{\partial c_i}{\partial t} + \varepsilon \frac{\partial (vc_i)}{\partial z} = \varepsilon D_L \frac{\partial}{\partial z}\left(c\frac{\partial y_i}{\partial z}\right) \qquad (16\text{-}51)$$

where v is interstitial fluid velocity, D_L is a Fickian axial dispersion coefficient, and $y_i = c_i/c$ is the fluid-phase mole fraction of component i. An alternative form, grouping together fluid-phase concentrations rather than intraparticle concentrations, is

$$\rho_b \frac{\partial \bar{n}_i}{\partial t} + \varepsilon_b \frac{\partial \hat{c}_i}{\partial t} + \varepsilon \frac{\partial (vc_i)}{\partial z} = \varepsilon D_L \frac{\partial}{\partial z}\left(c\frac{\partial y_i}{\partial z}\right) \qquad (16\text{-}52)$$

where, noting Eq. (16-4), $\hat{c}_i$ is defined by

$$\varepsilon_b \hat{c}_i = \varepsilon c_i + (1-\varepsilon)\varepsilon_p \bar{c}_{pi} \qquad (16\text{-}53)$$

For moving-bed processes, we add a term to Eq. (16-51) to obtain

$$\rho_b\left[\frac{\partial \hat{n}_i}{\partial t} + v_s \frac{\partial \hat{n}_i}{\partial z}\right] + \varepsilon\left[\frac{\partial c_i}{\partial t} + \frac{\partial (vc_i)}{\partial z} - D_L \frac{\partial}{\partial z}\left(c\frac{\partial y_i}{\partial z}\right)\right] = 0 \quad (16\text{-}54)$$

where v_s is the solid-phase velocity (opposite in sign to v for a countercurrent process).

ENERGY BALANCE

Many different forms of the energy balance have been used in fixed-bed adsorption studies. The form chosen for a particular study depends on the process considered (e.g., temperature swing adsorption or pressure swing adsorption) and on the degree of approximation that is appropriate.

The energy balance for a general fixed-bed process, ignoring dispersion, is

$$\rho_b \frac{\partial u_s}{\partial t} + \frac{\partial(\varepsilon_b cu_f)}{\partial t} + \frac{\partial(\varepsilon vch_f)}{\partial z} = -\frac{2h_w(T-T_w)}{r_c} \qquad (16\text{-}55)$$

where h_w is a heat transfer coefficient for energy transfer with the column wall and r_c is the radius of the column. The second term of Eq. (16-55) combines contributions from both pore and extraparticle fluid.

Thermodynamic paths are necessary to evaluate the enthalpy (or internal energy) of the fluid phase and the internal energy of the stationary phase. For gas-phase processes at low and modest pressures, the enthalpy departure function for pressure changes can be ignored and a reference state for each pure component chosen to be ideal gas at temperature T^{ref}, and a reference state for the stationary phase (adsorbent plus adsorbate) chosen to be adsorbate-free solid at T^{ref}. Thus, for the gas phase we have

$$h_f = \sum_i y_i h_{fi} = \sum_i y_i\left[h_{fi}^{\text{ref}} + \int_{T^{\text{ref}}}^{T} C_{pfi}^{\circ}\, dT\right] \qquad (16\text{-}56)$$

$$u_f = h_f - P/c \qquad (16\text{-}57)$$

and for the stationary phase

$$u_s = u_{\text{sol}} + nu_a \approx u_{\text{sol}} + nh_a \qquad (16\text{-}58)$$

$$u_{\text{sol}} = u_{\text{sol}}^{\text{ref}} + \int_{T^{\text{ref}}}^{T} C_s\, dT \qquad (16\text{-}59)$$

The enthalpy of the adsorbed phase h_a is evaluated along a path for which the gas-phase components undergo temperature change from T_{ref} to T and then are adsorbed isothermally, giving

$$h_a = \sum_i x_i h_{fi} - \left(\frac{1}{n}\right)\sum_i \int_0^{n_i} q_i^{st}(n_i, n_j, T)\, dn_i \qquad (16\text{-}60)$$

The isoteric heat of adsorption q_i^{st} is composition-dependent, and the sum of integrals Eq. (16-60) is difficult to evaluate for multicomponent adsorption if the isosteric heats indeed depend on loading. Because each isosteric heat depends on the loadings of all components, the sum must be evaluated for a path beginning with clean adsorbent and ending with the proper loadings of all components. If the isosteric heat of adsorption is constant, as is commonly assumed, then the energy balance (Eq. 16-55) becomes

$$\left[\rho_b\left(C_s + \sum_i n_i C_{pfi}^{\circ}\right) + \varepsilon_b c C_{pf}^{\circ}\right]\frac{\partial T}{\partial t} - \rho_b \sum_i q_i^{st}\frac{\partial n_i}{\partial t} - \frac{\partial(\varepsilon_b P)}{\partial t}$$
$$+ \varepsilon v c C_{pf}^{\circ}\frac{\partial T}{\partial z} = -\frac{2h_w(T-T_w)}{r_c} \qquad (16\text{-}61)$$

where Eq. (16-51) with $D_L = 0$ has been used. Equation (16-61) is a popular form of the energy balance for fixed-bed adsorption calculations. Often the first summation on the left-hand side, which involves gas-phase heat capacities, is neglected, or the gas-phase heat capacities are replaced by adsorbed-phase heat capacities.

Nonisothermal liquid-phase processes may be driven by changes in feed temperature or heat addition or withdrawal through a column wall. For these, heats of adsorption and pressure effects are generally of less concern. For this case a suitable energy balance is

$$(\rho_b C_s + \varepsilon_b c C_{pf}^{\circ})\frac{\partial T}{\partial t} + \varepsilon v c C_{pf}^{\circ}\frac{\partial T}{\partial z} = -\frac{2h_w(T-T_w)}{r_c} \qquad (16\text{-}62)$$

RATE AND DISPERSION FACTORS

The performance of adsorption processes results in general from the combined effects of thermodynamic and rate factors. It is convenient to consider first thermodynamic factors. These determine the process performance in a limit where the system behaves ideally; i.e. without mass transfer and kinetic limitations and with the fluid phase in perfect piston flow. **Rate factors** determine the efficiency of the real process in relation to the ideal process performance. Rate factors include heat- and mass-transfer limitations, reaction kinetic limitations, and hydrodynamic dispersion resulting from the velocity distribution across the bed and from mixing and diffusion in the interparticle void space.

TRANSPORT AND DISPERSION MECHANISMS

Figure 16-9 depicts porous adsorbent particles in an adsorption bed with sufficient generality to illustrate the nature and location of individual transport and dispersion mechanisms. Each mechanism involves a different driving force and, in general, gives rise to a different form of mathematical result.

Intraparticle Transport Mechanisms Intraparticle transport may be limited by *pore diffusion, solid diffusion, reaction kinetics* at phase boundaries, or two or more of these mechanisms together.

1. *Pore diffusion in fluid-filled pores.* These pores are sufficiently large that the adsorbing molecule escapes the force field of the adsorbent surface. Thus, this process is often referred to as *macropore diffusion.* The driving force for such a diffusion process can be approximated by the gradient in mole fraction or, if the molar concentration is constant, by the gradient in concentration of the diffusing species within the pores.

2. *Solid diffusion in the adsorbed phase.* Diffusion in pores sufficiently small that the diffusing molecule never escapes the force field of the adsorbent surface. In this case, transport may occur by an activated process involving jumps between adsorption sites. Such a process is often called *surface diffusion* or, in the case of zeolites, *micropore* or *intracrystalline* diffusion. The driving force for the process can thus be approximated by the gradient in concentration of the species in its adsorbed state. Phenomenologically, the process is not distinguishable from that of homogeneous diffusion that occurs inside a sorbent gel or in a pore-filling fluid that is immiscible with the external fluid. The generic term *solid diffusion* is used here to encompass the general traits of these physically different systems.

3. *Reaction kinetics at phase boundaries.* Rates of adsorption and desorption in porous adsorbents are generally controlled by mass transfer within the pore network rather than by the kinetics of sorption at the surface. Exceptions are the cases of chemisorption and affinity-adsorption systems used for biological separations, where the kinetics of bond formation can be exceedingly slow.

Intraparticle convection can also occur in packed beds when the adsorbent particles have very large and well-connected pores. Although, in general, bulk flow through the pores of the adsorbent particles is only a small fraction of the total flow, intraparticle convection can affect the transport of very slowly diffusing species such as macromolecules. The driving force for convection, in this case, is the pressure drop across each particle that is generated by the frictional resistance to flow experienced by the fluid as this flows through the packed bed [Rodrigues et al., *Chem. Eng. Sci.*, **46**, 2765 (1991); Carta et al., *Sep. Technol.*, **2**, 62 (1992); Frey et al., *Biotechnol. Progr.*, **9**, 273 (1993); Liapis and McCoy, *J. Chromatogr.*, **599**, 87 (1992)]. Intraparticle convection can also be significant when there is a total pressure difference between the center of the particle and the outside, such as is experienced in pressurization and depressurization steps of pressure swing adsorption or when more gas is drawn into an adsorbent to equalize pressure as adsorption occurs from the gas phase within a porous particle [Lu et al., *AIChE J.*, **38**, 857 (1992); Lu et al., *Gas Sep. Purif.*, **6**, 89 (1992)].

Extraparticle Transport and Dispersion Mechanisms Extraparticle mechanisms are affected by the design of the contacting device and depend on the hydrodynamic conditions outside the particles.

4. *External mass transfer* between the external surfaces of the adsorbent particles and the surrounding fluid phase. The driving force is the concentration difference across the boundary layer that surrounds each particle, and the latter is affected by the hydrodynamic conditions outside the particles.

5. *Mixing,* or lack of mixing, between different parts of the contacting equipment. This may occur through the existence of a velocity distribution or dead zones in a packed bed or through inefficient mixing in an agitated contactor. In packed-bed adsorbers, mixing is often described in terms of an axial dispersion coefficient whereby all mechanisms contributing to axial mixing are lumped together in a single effective coefficient.

Heat Transfer Since adsorption is generally accompanied by the evolution of heat, the rate of heat transfer between the adsorbent particles and the fluid phase may be important. In addition, heat transfer can occur across the column wall in small diameter beds and is important in energy applications of adsorption. In gas adsorption systems, even with highly porous particles, the controlling heat transfer resistance is generally associated with extraparticle transport [Lee and Ruthven, *Can. J. Chem. Eng.*, **57**, 65 (1979)], so that the temperature within the particles is essentially uniform. In liquid-phase adsorption, intraparticle and extraparticle heat transfer resistances are generally comparable. However, in this case the heat capacity of the fluid phase is sufficiently high that temperature effects may be negligible except in extreme cases. General discussions of heat-transfer effects in adsorbents and adsorption beds are found in Suzuki (gen. refs., pp. 187–208 and pp. 275–290) and in Ruthven (gen. refs., pp. 189–198 and pp. 215–219).

INTRAPARTICLE MASS TRANSFER

The phenomenological aspects of diffusional mass transfer in adsorption systems can be described in terms of Fick's law:

$$J_i = -D_i(c_i)\,\frac{\partial c_i}{\partial x} \qquad (16\text{-}63)$$

This expression can be used to describe both pore and solid diffusion so long as the driving force is expressed in terms of the appropriate concentrations. Although the driving force should be more correctly expressed in terms of chemical potentials, Eq. (16-63) provides a qualitatively and quantitatively correct representation of adsorption systems so long as the diffusivity is allowed to be a function of the adsorbate concentration. The diffusivity will be constant only for a thermodynamically ideal system, which is only an adequate approximation for a limited number of adsorption systems.

Results for several individual mechanisms will now be considered. The equations that follow refer to local conditions within the contacting equipment that may apply to the average concentrations in the neighborhood of a single adsorbent particle. Generally, they apply to particles that can be approximated as spherical and of a uniform size and properties. An appropriately chosen mean particle size must be used in these equations when dealing with adsorbents having a broad particle size distribution. The appropriate average depends on the controlling mass-transfer mechanism. For intraparticle mass-transfer mechanisms, the volume or mass-average particle size usually provides the best prediction.
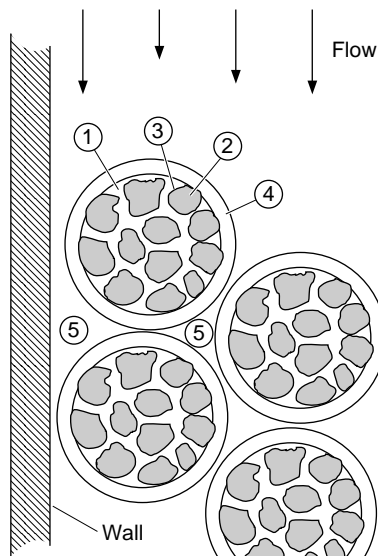

FIG. 16-9 General scheme of adsorbent particles in a packed bed showing the locations of mass transfer and dispersive mechanisms. Numerals correspond to numbered paragraphs in the text: 1, pore diffusion; 2, solid diffusion; 3, reaction kinetics at phase boundary; 4, external mass transfer; 5, fluid mixing.

Pore Diffusion   When fluid transport through a network of fluid-filled pores inside the particles provides access for solute adsorption sites, the diffusion flux can be expressed in terms of a pore diffusion coefficient D_{pi} as:

$$J_i = -\varepsilon_p D_{pi} \frac{\partial c_{pi}}{\partial r} \qquad (16\text{-}64)$$

D_{pi} is smaller than the diffusivity in a straight cylindrical pore as a result of the random orientation of the pores, which gives a longer diffusion path, and the variation in the pore diameter. Both effects are commonly accounted for by a tortuosity factor τ_p such that $D_{pi} = D_i / \tau_p$. In principle, predictions of the tortuosity factor can be made if the pore structure, pore size, and shape distributions are known (see Dullien, *Porous Media: Fluid Transport and Pore Structure*, Academic Press, NY, 1979). In some cases, approximate prediction can be obtained from the following equations.

Mackie and Meares, *Proc. Roy. Soc.*, **A232,** 498 (1955):

$$\tau_p = \frac{(2 - \varepsilon_p)^2}{\varepsilon_p} \qquad (16\text{-}65a)$$

Wakao and Smith, *Chem. Eng. Sci.*, **17,** 825 (1962):

$$\tau_p = \frac{1}{\varepsilon_p} \qquad (16\text{-}65b)$$

Suzuki and Smith, *Chem. Eng. J.*, **3,** 256 (1972):

$$\tau_p = \varepsilon_p + 1.5(1 - \varepsilon_p) \qquad (16\text{-}65c)$$

In practice, however, the predictive value of these equations is rather uncertain, and vastly different results are obtained from each. All of them, on the other hand, predict that τ_p increases as the porosity decreases.

For catalyst particles, Satterfield (*Heterogeneous Catalysis in Practice*, McGraw-Hill, 1980) recommends the use of a value of $\tau_p = 4$ when no other information is available, and this can be used for many adsorbents. In general, however, it is more reliable to treat the tortuosity as an empirical constant that is determined experimentally for any particular adsorbent.

For adsorbent materials, experimental tortuosity factors generally fall in the range 2–6 and generally decrease as the particle porosity is increased. Higher apparent values may be obtained when the experimental measurements are affected by other resistances, while values much lower than 2 generally indicate that surface or solid diffusion occurs in parallel to pore diffusion.

Ruthven (gen. refs.) summarizes methods for the measurement of effective pore diffusivities that can be used to obtain tortuosity factors by comparison with the estimated pore diffusion coefficient of the adsorbate. Molecular diffusivities can be estimated with the methods in Sec. 6.

For gas-phase diffusion in small pores at low pressure, the molecular mean free path may be larger than the pore diameter, giving rise to Knudsen diffusion. Satterfield (*Mass Transfer in Heterogeneous Catalysis,* MIT, Cambridge, MA, 1970, p. 43), gives the following expression for the pore diffusivity:

$$D_{pi} = \frac{1}{\tau_p} \left[\frac{3}{4r_{\text{pore}}} \left(\frac{\pi M_{ri}}{2RT} \right)^{1/2} + \frac{1}{D_i} \right]^{-1} \qquad (16\text{-}66)$$

where r_{pore} is the average pore radius, T the absolute temperature, and M_{ri} the molecular weight.

For liquid-phase diffusion of large adsorbate molecules, when the ratio $\lambda_m = r_m / r_{\text{pore}}$ of the molecule radius r_m to the pore radius is significantly greater than zero, the pore diffusivity is reduced by steric interactions with the pore wall and hydrodynamic resistance. When $\lambda_m < 0.2$, the following expressions derived by Brenner and Gaydos [*J. Coll. Int. Sci.*, **58,** 312 (1977)] for a hard sphere molecule (a particle) diffusing in a long cylindrical pore, can be used

$$D_{pi} = \frac{D_i}{\tau_p} (1 - \lambda_m)^{-2} \left[1 + \frac{9}{8} \lambda_m \ln \lambda_m - 1.539 \lambda_m \right] \qquad (16\text{-}67)$$

r_m is the Stokes-Einstein radius of the solute that can be determined from the free diffusivity as

$$r_m = \frac{\kappa T}{6 \pi \mu D_i} \qquad (16\text{-}68)$$

where κ is the Boltzmann constant. When $\lambda_m > 0.2$, the centerline approximation [Anderson and Quinn, *Biophys. J.*, **14,** 130, (1974)] can be used instead of Eq. (16-67)

$$D_{pi} = \frac{D_i}{\tau_p} (1 - 2.1044 \lambda_m + 2.089 \lambda_m^3 - 0.984 \lambda_m^5) \times 0.865 \qquad (16\text{-}69)$$

The 0.865 factor is used to match this equation to the Brenner and Gaydos expression for $\lambda_m = 0.2$. In these cases, the pore concentration C_{pi} is related to the external concentration C_i by the partition ratio $(1 - \lambda_m)^2$.

Solid Diffusion   In the case of pore diffusion discussed above, transport occurs within the fluid phase contained inside the particle; here the solute concentration is generally similar in magnitude to the external fluid concentration. A solute molecule transported by pore diffusion may attach to the sorbent and detach many times along its path. In other cases, attachment can be essentially permanent, but in both cases, only detached molecules undergo transport. In contrast, the following four instances illustrate cases where diffusion of adsorbate molecules occurs in their adsorbed state within phases that are distinct from the pore fluid:

1.   Movement of mobile adsorbed solute molecules along pore surfaces, without detaching
2.   Transport in a homogeneously dissolved state, as for a neutral molecule inside a sorbent gel or in a pore filled with a liquid which is immiscible with the external fluid
3.   Ion transport in charged ion-exchange resins
4.   Advance of an adsorbate molecule from one cage to another within a zeolite crystal

In these cases, the diffusion flux may be written in terms of the adsorbed solute concentration as

$$J_i = -\rho_p D_{si} \frac{\partial n_i}{\partial r} \qquad (16\text{-}70)$$

The diffusion coefficient in these phases D_{si} is usually considerably smaller than that in fluid-filled pores; however, the adsorbate concentration is often much larger. Thus, the diffusion rate can be smaller or larger than can be expected for pore diffusion, depending on the magnitude of the fluid/solid partition coefficient.

Numerical values for solid diffusivities D_{si} in adsorbents are sparse and disperse. Moreover, they may be strongly dependent on the adsorbed phase concentration of solute. Hence, locally conducted experiments and interpretation must be used to a great extent. Summaries of available data for surface diffusivities in activated carbon and other adsorbent materials and for micropore diffusivities in zeolites are given in Ruthven, Yang, Suzuki, and Karger and Ruthven (gen. refs.).

Surface diffusivities are generally strongly dependent on the fractional surface coverage and increase rapidly at surface coverage greater than 80 percent [see for example Yang et al., *AIChE J.*, **19,** 1052 (1973)]. For estimation purposes, the correlation of Sladek et al. [*Ind. Eng. Chem. Fundam.*, **13,** 100 (1974)] can be used to predict surface diffusivities for gas-phase adsorption on a variety of adsorbents.

Zeolite crystallite diffusivities for sorbed gases range from 10^{-7} to 10^{-14} cm²/s. These diffusivities generally show a strong increase with the adsorbate concentration that is accounted for by the Darken thermodynamic correction factor

$$D_{si} = D_{0i} \frac{d \ln a_i}{d \ln n_i} \qquad (16\text{-}71)$$

where D_{0i} is the corrected diffusivity, a_i the thermodynamic activity of the species in the adsorbed phase, and n_i the adsorbed phase solute concentration. Corrected diffusivities D_{0i} calculated according to this equation are often found to be essentially independent of concentration. If the adsorption equilibrium isotherm obeys the Langmuir equation [Eq. (16-13)], Eq. (16-71) yields:

$$D_{si} = D_{0i} \left(1 - \frac{n_i}{n_i^s} \right)^{-1} \qquad (16\text{-}72)$$

The effect of temperature on diffusivities in zeolite crystals can be expressed in terms of the Eyring equation (see Ruthven, gen. refs.).

In ion-exchange resins, diffusion is further complicated by electrical coupling effects. In a system with M counterions, diffusion rates are described by the Nernst-Planck equations (Helfferich, gen. refs.). Assuming complete Donnan exclusion, these equations can be written as:

$$J_i = -\rho_p \frac{1}{z_i} \sum_{j=1}^{M-1} \overline{D}_{i,j} \frac{\partial z_j n_j}{\partial r} \tag{16-73}$$

with

$$\overline{D}_{i,j} = -\frac{\overline{D}_i(\overline{D}_j - \overline{D}_M)z_i^2 n_i}{\sum_{k=1}^{M} \overline{D}_k z_k^2 n_k} \tag{16-74a}$$

$$\overline{D}_{i,i} = \overline{D}_i - \frac{\overline{D}_i(\overline{D}_i - \overline{D}_M)z_i^2 n_i}{\sum_{k=1}^{M} \overline{D}_k z_k^2 n_k} \tag{16-74b}$$

which are dependent on the **ionic self diffusivities** $\overline{D}_i$ of the individual species. As a qualitative rule, ionic diffusivities of inorganic species in crosslinked polystyrene-DVB ion-exchange resins compared with those in water are 1:10 for monovalent ions, 1:100 for divalent ions, and 1:1000 for trivalent ions. Table 16-8 shows typical ionic diffusivities of inorganic ions in cation and anion exchange resins; larger organic ions, however, can have ionic diffusivities much smaller than inorganic ions of the same valence [see, for example, Jones and Carta, *Ind. Eng. Chem. Research,* **32,** 117 (1993)].

For mixtures of unlike ions (the usual case), the apparent diffusivity will be intermediate between these values because of the electrical coupling effect. For a system with two counterions A and B, with charge z_A and z_B, Eqs. (16-73) and (16-74) reduce to:

$$J_A = -\rho_p \overline{D}_{A,B} \frac{\partial n_A}{\partial r} = -\rho_p \frac{\overline{D}_A \overline{D}_B [z_A^2 n_A + z_B^2 n_B]}{z_A^2 \overline{D}_A n_A + z_B^2 \overline{D}_B n_B} \frac{\partial n_A}{\partial r} \tag{16-75}$$

which shows that the apparent diffusivity $\overline{D}_{A,B}$ varies between $\overline{D}_A$ when the ionic fraction of species A in the resin is very small and $\overline{D}_B$ when the ionic fraction of A in the resin approaches unity, indicating that the ion present in smaller concentration has the stronger effect on the local interdiffusion rate.

Combined Pore and Solid Diffusion In porous adsorbents and ion-exchange resins, intraparticle transport can occur with pore and solid diffusion in parallel. The dominant transport process is the faster one, and this depends on the relative diffusivities and concentrations in the pore fluid and in the adsorbed phase. Often, equilibrium between the pore fluid and the solid phase can be assumed to exist locally at each point within a particle. In this case, the mass-transfer flux is expressed by:

$$J_i = -\left[\varepsilon_p D_{pi} + \rho_p D_{si} \frac{dn_i^e}{dc_i}\right] \frac{\partial c_{pi}}{\partial r} = -D_{ei}(c_{pi}) \frac{\partial c_{pi}}{\partial r} \tag{16-76}$$

where dn_i^e/dc_i is the derivative of the adsorption isotherm and it has been assumed that at equilibrium $c_{pi} = c_i$. This equation suggests that

in such an adsorbent, pore and solid diffusivities can be obtained by determining the apparent diffusivity D_{ei} for conditions of no adsorption ($dn_i^e/dc_i = 0$) and for conditions of strong adsorption, where dn_i^e/dc_i is large. If the adsorption isotherm is linear over the range of experimental measurement:

$$D_{ei} = \varepsilon_p D_{pi} + \rho_p K_i D_{si} \tag{16-77}$$

Thus, a plot of the apparent diffusivity versus the linear adsorption equilibrium constant should be linear so long as D_{pi} and D_{si} remain constant.

In a particle having a **bidispersed pore structure** comprising spherical adsorptive subparticles of radius r_s forming a macroporous aggregate, separate flux equations can be written for the macroporous network in terms of Eq. (16-64) and for the subparticles themselves in terms of Eq. (16-70) if solid diffusion occurs.

EXTERNAL MASS TRANSFER

Because of the complexities encountered with a rigorous treatment of the hydrodynamics around particles in industrial contactors, mass transfer to and from the adsorbent is described in terms of a mass-transfer coefficient k_f. The flux at the particle surface is:

$$N_i = k_f(c_i - c_i^s) \tag{16-78}$$

where c_i and c_i^s are the solute concentrations in the bulk fluid and at the particle surface, respectively. k_f can be estimated from available correlations in terms of the Sherwood number $Sh = k_f d_p/D_i$ and the Schmidt number $Sc = \nu/D_i$. For packed-bed operations, the correlations in Table 16-9 are recommended. A plot of these equations is given in Fig. 16-10 for representative ranges of Re and Sc with $\varepsilon = 0.4$.

External mass-transfer coefficients for particles suspended in agitated contactors can be estimated from equations in Levins and Glastonbury [*Trans. Instn. Chem. Eng.,* **50,** 132 (1972)] and Armenante and Kirwan [*Chem. Eng. Sci.,* **44,** 2871 (1989)].

AXIAL DISPERSION IN PACKED BEDS

The axial dispersion coefficient [cf. Eq. (16-51)] lumps together all mechanisms leading to axial mixing in packed beds. Thus, the axial dispersion coefficient must account not only for molecular diffusion and convective mixing but also for nonuniformities in the fluid velocity across the packed bed. As such, the axial dispersion coefficient is best determined experimentally for each specific contactor.

The effects of **flow nonuniformities,** in particular, can be severe in gas systems when the ratio of bed-to-particle diameters is small; in liquid systems when viscous fingering occurs as a result of large viscosity gradients in the adsorption bed; when very small particles (<50 μm) are used, such as in high performance liquid chromatography systems; and in large-diameter beds. A lower bound of the axial

TABLE 16-8 Self Diffusion Coefficients in Polystyrene-divinylbenzene Ion Exchangers (units of 10^{-7} cm^2/s)*

Temperature		0.3 °C					25 °C			
Crosslinking, %	4	6	8	12	16	4	6	8	12	16
Cation exchangers (sulfonated): Dowex 50										
Na$^+$	6.7		3.4	1.15	0.66	14.1		9.44		2.40
Cs$^+$			6.6		1.11			13.7		3.10
Ag$^+$			2.62		1.00			6.42		2.75
Zn^{2+}			0.21		0.03			0.63		0.14
La^{3+}		0.30	0.03		0.002			0.092		0.005
Anion exchangers (dimethyl hydroxyethylamine): Dowex 2										
Cl$^-$			1.25					3.54		
Br$^-$		(1.8)	1.50	0.63		0.06	(4.3)	3.87	2.04	0.26
I$^-$			0.35					1.33		
BrO$_3^-$			1.76					4.55		
WO$_4^{2-}$			0.60					1.80		
PO$_4^{3-}$			0.16					0.57		

*Data from Boyd and Soldano, *J. Am. Chem. Soc.,* **75,** 6091 (1953).

TABLE 16-9   Recommended Correlations for External Mass Transfer Coefficients in Adsorption Beds ($Re = \varepsilon v d_p/\nu$, $Sc = \nu/D$)

Equation	Re	Phase	Ref.
$Sh = 1.15\left(\dfrac{Re}{\varepsilon}\right)^{0.5} Sc^{0.33}$	$Re > 1$	Gas/liquid	Carberry, *AIChE J.*, **6**, 460 (1960)
$Sh = 2.0 + 1.1\, Re^{0.6} Sc^{0.33}$	$3 < Re < 10^4$	Gas/liquid	Wakao and Funazkri, *Chem. Eng. Sci.*, **33**, 1375 (1978)
$Sh = 1.85\left(\dfrac{1-\varepsilon}{\varepsilon}\right)^{0.33} Re^{0.33} Sc^{0.33}$	$Re < 40$	Liquid	Kataoka et al., *J. Chem. Eng. Japan*, **5**, 132 (1972)
$Sh = \dfrac{1.09}{\varepsilon} Re^{0.33} Sc^{0.33}$	$0.0015 < Re < 55$	Liquid	Wilson and Geankoplis, *Ind. Eng. Chem. Fundam.*, **5**, 9 (1966)
$Sh = \dfrac{0.25}{\varepsilon} Re^{0.69} Sc^{0.33}$	$55 < Re < 1050$	Liquid	Wilson and Geankoplis, *Ind. Eng. Chem. Fundam.*, **5**, 9 (1966)

dispersion coefficient can be estimated for well-packed beds from correlations that follow.

Neglecting flow nonuniformities, the contributions of molecular diffusion and turbulent mixing arising from stream splitting and recombination around the sorbent particles can be considered additive [Langer et al., *Int. J. Heat and Mass Transfer*, **21**, 751 (1978)]; thus, the axial dispersion coefficient D_L is given by:

$$\frac{D_L}{D_i} = \gamma_1 + \gamma_2 \frac{d_p v}{D_i} = \gamma_1 + \gamma_2 \frac{(Re)(Sc)}{\varepsilon} \tag{16-79}$$

or, in terms of a particle-based Peclet number ($Pe = d_p v/D_L$), by:

$$\frac{1}{Pe} = \frac{\gamma_1 \varepsilon}{(Re)(Sc)} + \gamma_2 \tag{16-80}$$

The first term in Eqs. (16-79) and (16-80) accounts for molecular diffusion, and the second term accounts for mixing. For the first term, Wicke [*Ber. Bunsenges.*, **77**, 160 (1973)] has suggested:

$$\gamma_1 = 0.45 + 0.55\varepsilon \tag{16-81}$$

which, for typical void fractions, $\varepsilon = 0.35 - 0.5$ gives $\gamma_1 = 0.64 - 0.73$ (Ruthven, gen. refs.). Expressions for the axial mixing term, γ_2 in Eq. (16-79) are given in Table 16-10. The expression of Wakao and Funazkri includes an axial diffusion term, γ_1, that varies from 0.7 for nonporous particles to $20/\varepsilon$, depending on the intraparticle mass-transfer mechanism. For strongly adsorbed species, Wakao and Funazkri suggest that the effective axial dispersion coefficient is much

larger than that predicted on the basis of nonporous, nonadsorbing particles. The Gunn expression includes a term σ_v^2 accounting for deviations from plug flow. σ_v^2 is defined as the dimensionless variance of the distribution of the ratio of velocity to average velocity over the cross section of the bed. The parameter values included in this equation are valid for spherical particles. Values for nonspherical particles can be found in the original reference.

Figure 16-11 compares predicted values of D_L/D_i for $\sigma_v = 0$ and $\varepsilon = 0.4$ with $Sc = 1$ (gases at low pressure), and $Sc = 1000$ (liquids), based on the equations in Table 16-10.

Correlations for axial dispersion in beds packed with very small particles (<50 μm) that take into account the holdup of liquid in a bed are discussed by Horvath and Lin [*J. Chromatogr.*, **126**, 401 (1976)].

RATE EQUATIONS

Rate equations are used to describe interphase mass transfer in batch systems, packed beds, and other contacting devices for sorptive processes and are formulated in terms of fundamental transport properties of adsorbent and adsorbate.

General Component Balance   For a spherical adsorbent particle:

$$\varepsilon_p \frac{\partial c_{pi}}{\partial t} + \rho_p \frac{\partial n_i}{\partial t} = \frac{1}{r^2} \frac{\partial}{\partial r}(-r^2 N_i) \tag{16-82}$$

For particles that have no macropores, such as gel-type ion-exchange resins, or when the solute holdup in the pore fluid is small, ε_p may be
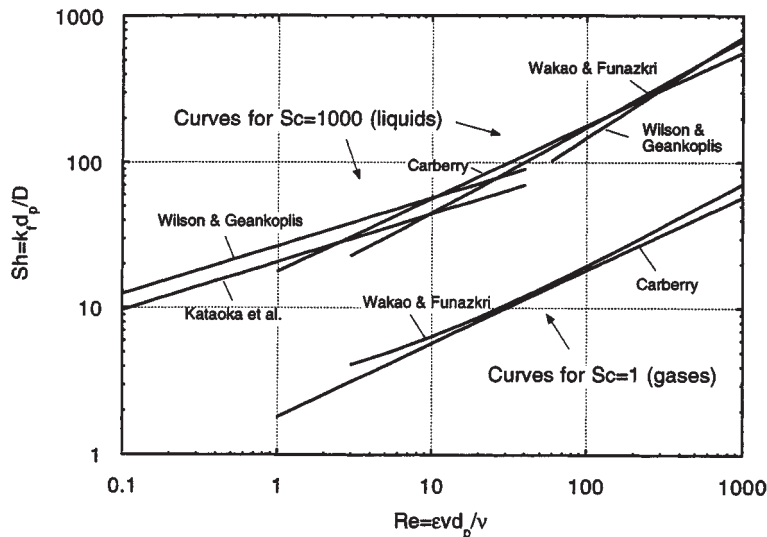
FIG. 16-10   Sherwood number correlations for external mass-transfer coefficients in packed beds for $\varepsilon = 0.4$ (adapted from Suzuki, gen. refs.).

TABLE 16-10 Coefficients for Axial Dispersion Correlations in Packed Beds Based on Eq. (16-79)

γ_1	γ_2	Ref.
0.73	$0.5\left(1 + \dfrac{13\gamma_1\varepsilon}{ReSc}\right)^{-1}$	Edwards and Richardson, *Chem. Eng. Sci.*, **23**, 109 (1968)
Nonporous particles: 0.7 Porous particles: $\leq 20/\varepsilon$	0.5	Wakao and Funazkri, *Chem. Eng. Sci.*, **33**, 1375 (1978)
1	$\dfrac{3}{4}\varepsilon + \dfrac{\pi^2\varepsilon(1-\varepsilon)}{6}\ln(ReSc)$	Koch and Brady, *J. Fluid Mech.*, **154**, 399 (1985)
0.714	$\dfrac{\sigma_v^2}{2} + (1+\sigma_v^2)\left\{\gamma(1-p)^2 + \gamma^2 p(1-p)^3\left[e^{-\frac{1}{\gamma p(1-p)}} - 1\right]\right\}$ with $\gamma = 0.043\,ReSc/(1-\varepsilon)$ $p = 0.33\exp(-24/Re) + 0.17$	Gunn, *Chem. Eng. Sci.*, **2**, 363 (1987)

taken as zero. Ignoring bulk flow terms, the fluxes N_i and J_i are equal. In this case, coupling the component balance with the flux expressions previously introduced gives the rate equations in Table 16-11. Typical boundary conditions are also included in this table.

Linear Driving Force Approximation   Simplified expressions can also be used for an approximate description of adsorption in terms of rate coefficients for both extraparticle and intraparticle mass transfer controlling. As an approximation, the rate of adsorption on a particle can be written as:

$$\frac{\partial \hat{n}_i}{\partial t} = kf(n_i, c_i) \qquad (16\text{-}83)$$

where k is a rate coefficient, and the function $f(n_i, c_i)$ is a driving force relationship. The variables k_c and k_n are used to denote rate coefficients based on fluid-phase and adsorbed-phase concentration driving forces, respectively.

Commonly used forms of this rate equation are given in Table 16-12. For adsorption bed calculations with constant separation factor systems, somewhat improved predictions are obtained using correction factors ψ_s and ψ_p defined in Table 16-12 is the partition ratio defined by Eq. (16-25).

The linear driving force (LDF) approximation is obtained when the driving force is expressed as a concentration difference. It was originally developed to describe packed-bed dynamics under linear equilibrium conditions [Glueckauf, *Trans. Far. Soc.*, **51**, 1540 (1955)]. This form is exact for a nonlinear isotherm only when external mass transfer is controlling. However, it can also be used for nonlinear sys-

tems with pore or solid diffusion mechanisms as an approximation, since it provides qualitatively correct results.

Alternate driving force approximations, item 2B in Table 16-12, for solid diffusion, and item 3B in Table 16-12, for pore diffusion, provide somewhat more accurate results in constant pattern packed-bed calculations with pore or solid diffusion controlling for constant separation factor systems.

The reaction kinetics approximation is mechanistically correct for systems where the reaction step at pore surfaces or other fluid-solid interfaces is controlling. This may occur in the case of chemisorption on porous catalysts and in affinity adsorbents that involve very slow binding steps. In these cases, the mass-transfer parameter k is replaced by a second-order reaction rate constant k_a. The driving force is written for a constant separation factor isotherm (column 4 in Table 16-12). When diffusion steps control the process, it is still possible to describe the system by its apparent second-order kinetic behavior, since it usually provides a good approximation to a more complex exact form for single transition systems (see "Fixed Bed Transitions").

Combined Intraparticle Resistances   When solid diffusion and pore diffusion operate in parallel, the effective rate is the sum of these two rates. When solid diffusion predominates, mass transfer can be represented approximately in terms of the LDF approximation, replacing k_n in column 2 of Table 16-12 with

$$k_n^c = \frac{15\psi_s D_{si}}{r_p^2} + \frac{15(1-\varepsilon)\psi_p\varepsilon_p D_{pi}}{\Lambda r_p^2} \qquad (16\text{-}84)$$
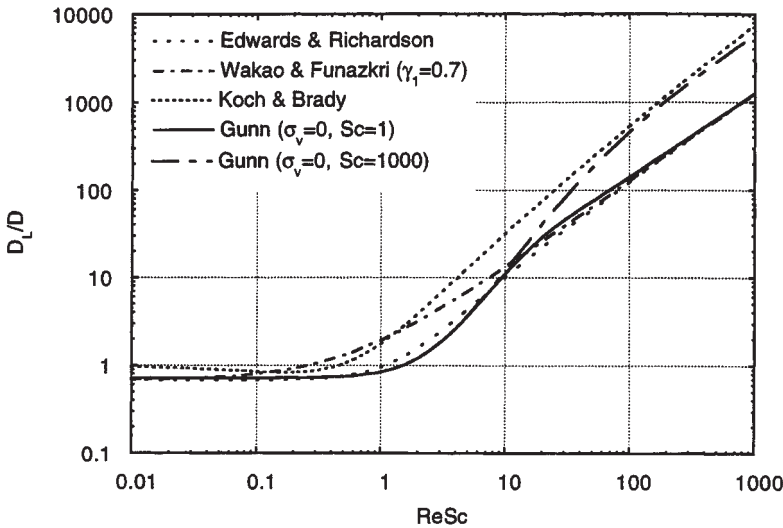
FIG. 16-11   Axial dispersion coefficient correlations for well-packed beds for $\varepsilon = 0.4$.

TABLE 16-11 Rate Equations for Description of Mass Transfer in Spherical Adsorbent Particles

Mechanism	Flux equation	Rate equation
A. Pore diffusion	16-64	$\varepsilon_p \dfrac{\partial c_{pi}}{\partial t} + \rho_p \dfrac{\partial n_i}{\partial t} = \dfrac{1}{r^2}\dfrac{\partial}{\partial r}\left(\varepsilon_p D_{pi} r^2 \dfrac{\partial c_{pi}}{\partial r}\right)$ $(\partial c_{pi}/\partial r)_{r=0}=0,\ (\varepsilon_p D_{pi}\partial c_{pi}/\partial r)_{r=r_p}=k_f(c_i-c_{pi|_{r=r_p}})$ or $(c_{pi})_{r=r_p}=c_i$ for no external resistance
B. Solid diffusion	16-70	$\dfrac{\partial n_i}{\partial t}=\dfrac{1}{r^2}\dfrac{\partial}{\partial r}\left(D_{si} r^2 \dfrac{\partial n_i}{\partial r}\right)$ $(\partial n_i/\partial r)_{r=0}=0,\ (\rho_p D_{si}\partial n_i/\partial r)_{r=r_p}=k_f(c_i-c_i^s)$ or $(n_i)_{r=r_p}=n_i^e(c_i)$ for no external resistance
C. Parallel pore and solid diffusion (local equilibrium between pore and adsorbed phase)	16-76	$\left(\varepsilon_p+\rho_p\dfrac{dn_i^e}{dc_i}\right)\dfrac{\partial c_{pi}}{\partial t}=\dfrac{1}{r^2}\dfrac{\partial}{\partial r}\left[r^2\left(\varepsilon_p D_{pi}+\rho_p D_{si}\dfrac{dn_i^e}{dc_i}\right)\dfrac{\partial c_{pi}}{\partial r}\right]$ $(\partial c_{pi}/\partial r)_{r=0}=0,\ [(\varepsilon_p D_{pi}+\rho_p D_{si}dn_i^e/dc_i)\partial c_{pi}/\partial r]_{r=r_p}=k_f(c_i-c_{pi|_{r=r_p}})$ or $(c_{pi})_{r=r_p}=c_i$ for no external resistance
D. Diffusion in bidispersed particles (no external resistance)	16-64 and 16-70	$\dfrac{\partial n_i}{\partial t}=\dfrac{1}{\rho^2}\dfrac{\partial}{\partial \rho}\left(D_{si}\rho^2\dfrac{\partial n_i}{\partial \rho}\right),\ (\partial n_i/\partial \rho)_{\rho=0}=0,\ (n_i)_{\rho=r_s}=n_i^e(c_{pi})$ $\bar{n}_i(r,t)=\dfrac{3}{r_s^3}\displaystyle\int_0^{r_s}\rho^2 n_i\,d\rho$ $\varepsilon_p\dfrac{\partial c_{pi}}{\partial t}+\rho_p\dfrac{\partial \bar{n}_i}{\partial t}=\dfrac{1}{r^2}\dfrac{\partial}{\partial r}\left(\varepsilon_p D_{pi}r^2\dfrac{\partial c_{pi}}{\partial r}\right),\ (\partial c_{pi}/\partial r)_{r=0}=0,\ (c_{pi})_{r=r_p}=c_i$

TABLE 16-12 Expressions for Rate Coefficient k and Driving Force Relationships for Eq. 16-83

Mechanism	1. External film	2. Solid diffusion	3. Pore diffusion	4. Reaction kinetics
Expression for rate coefficient, k	$k_c=\dfrac{k_f a}{\rho_b}=\dfrac{3(1-\varepsilon)k_f}{\rho_b r_p}$	$k_n=\dfrac{15\psi_s D_{si}}{r_p^2}$	$k_n=\dfrac{15\psi_p(1-\varepsilon)\varepsilon_p D_{pi}}{\Lambda r_p^2}$	k_a
A. Linear driving force (LDF)	$c-c_i^e$	$n_i^e-\bar{n}_i$	$n_i^e-\bar{n}_i$	—
LDF for constant R	$c_i-\dfrac{Rc^{ref}\bar{n}_i/n^{ref}}{1-(R-1)\bar{n}_i/n^{ref}}$	$\dfrac{n^{ref}c_i/c^{ref}}{R+(R-1)c_i/c^{ref}}-\bar{n}_i$	$\dfrac{n^{ref}c_i/c^{ref}}{R+(R-1)c_i/c^{ref}}-\bar{n}_i$	—
Correction factors ψ for constant R	—	$\dfrac{0.894}{1-0.106R^{0.5}}$	$\dfrac{0.775}{1-0.225R^{0.5}}$	—
B. Alternate driving force for constant R	—	$\dfrac{n_i^{e2}-\bar{n}_i^2}{2\bar{n}_i}$	$\dfrac{n_i^e-\bar{n}_i}{[1-(R-1)\bar{n}_i/n^{ref}]^{0.5}}$	—
Correction factors ψ for alternate driving force	—	$\dfrac{0.590}{1-0.410R^{0.5}}$	$\dfrac{0.548}{1-0.452R^{0.5}}$	—
C. Reaction kinetics for constant R	—	—	—	$\dfrac{c_i(n^{ref}-\bar{n}_i)-R\bar{n}_i(c^{ref}-c_i)}{1-R}$

References: 1A. Beaton and Furnas, *Ind. Eng. Chem.,* **33,** 1500 (1941); Michaels, *Ind. Eng. Chem.,* **44,** 1922 (1952);
2A,3A. Glueckauf and Coates, *J. Chem. Soc.,* 1315 (1947); *Trans. Faraday Soc.,* **51,** 1540 (1955); Hall et al., *Ind. Eng. Chem. Fundam.,* **5,** 212 (1966)
2B. Vermeulen, *Ind. Eng. Chem.,* **45,** 1664 (1953)
3B. Vermeulen and Quilici, *Ind. Eng. Chem. Fundam.,* **9,** 179 (1970)
4C. Hiester and Vermeulen, *Chem. Eng. Progr.,* **48,** 505 (1952)

When pore diffusion predominates, use of column 3 in Table 16-12 is preferable, with k_n^c replacing k_n.

For particles with a **bidispersed pore structure,** the mass-transfer parameter k_n in the LDF approximation (column 2 in Table 16-12) can be approximated by the series-combination of resistances as:

$$\frac{1}{k_n^c}=\frac{1}{b_s}\left[\frac{\Lambda r_p^2}{15(1-\varepsilon)\psi_p\varepsilon_p D_{pi}}+\frac{r_s^2}{15\psi_s D_{si}}\right] \tag{16-85}$$

where b_s is a correction to the driving force that is described below. In the limiting cases where the controlling resistance is diffusion through the particle pores or diffusion within the subparticles, the rate coefficients $k_n=15(1-\varepsilon)\psi_p\varepsilon_p D_{pi}/\Lambda r_p^2$ and $k_n=15\psi_s D_{si}/r_s^2$ are obtained.

Overall Resistance With a linear isotherm ($R=1$), the overall mass transfer resistance is the sum of intraparticle and extraparticle resistances. Thus, the overall LDF coefficient for use with a particle-side driving force (column 2 in Table 16-12) is:

$$\frac{1}{k_n^o}=\frac{\Lambda r_p}{3(1-\varepsilon)k_f}+\frac{1}{k_n^c} \tag{16-86}$$

or

$$\frac{1}{k_c^o}=\frac{\rho_b r_p}{3(1-\varepsilon)k_f}+\frac{\rho_b}{\Lambda k_n^c} \tag{16-87}$$

for use with a fluid-phase driving force (column 1 in Table 16-12).

In either equation, k_n^c is given by Eq. (16-84) for parallel pore and surface diffusion or by Eq. (16-85) for a bidispersed particle. For nearly linear isotherms $(0.7 < R < 1.5)$, the same linear addition of resistance can be used as a good approximation to predict the adsorption behavior of packed beds, since solutions for all mechanisms are nearly identical. With a highly favorable isotherm $(R \rightarrow 0)$, however, the rate at each point is controlled by the resistance that is locally greater, and the principle of additivity of resistances breaks down. For approximate calculations with intermediate values of R, an overall transport parameter for use with the LDF approximation can be calculated from the following relationship for solid diffusion and film resistance in series

$$\frac{\Lambda r_p}{3(1-\varepsilon)k_f} + \frac{r_p^2}{15\psi_s D_{si}} = \frac{b_s}{k_n^c}$$

$$= \frac{b_f \Lambda}{\rho_b k_c^o} \tag{16-88}$$

b_s and b_f are correction factors that are given by Fig. 16-12 as a function of the separation factor R and the mechanism parameter

$$\Psi = \frac{10\psi_s D_{si}\Lambda}{D_i} \frac{1}{Sh} \tag{16-89}$$

Axial Dispersion Effects   In adsorption bed calculations, axial dispersion effects are typically accounted for by the axial diffusionlike term in the bed conservation equations [Eqs. (16-51) and (16-52)]. For nearly linear isotherms $(0.5 < R < 1.5)$, the combined effects of axial dispersion and mass-transfer resistances on the adsorption behavior of packed beds can be expressed approximately in terms of an apparent rate coefficient k_c for use with a fluid-phase driving force (column 1, Table 16-12):

$$\frac{1}{k_c} = \frac{\rho_b}{\varepsilon} \frac{D_L}{v^2} + \frac{1}{k_c^o} \tag{16-90}$$

which extends the linear addition principle to combined axial dispersion and mass-transfer resistances. Even for a highly nonlinear isotherm $(R = 0.33)$, the linear addition principle expressed by this equation provides a useful approximation except in the extreme case of low mass-transfer resistance and large axial dispersion, when $D_L\rho_p k_c^o/v^2\varepsilon \gg 5$ [Garg and Ruthven, *Chem. Eng. Sci.*, **30**, 1192 (1975)]. However, when the isotherm is irreversible $(R \rightarrow 0)$, the linear addition principle breaks down and axial dispersion has to be taken into account by explicit models (see "Fixed Bed Transitions").

Rapid Adsorption-Desorption Cycles   For rapid cycles with particle diffusion controlling, when the cycle time t_c is much smaller than the time constant for intraparticle transport, the LDF approximation becomes inaccurate. The generalized expression

$$\frac{\partial \hat{n}_i}{\partial t} = \Omega k_n (n_i^e - \bar{n}_i) \tag{16-91}$$

can be used for packed-bed calculations when the parameter Ω is defined to be a function of the cycle time such that the amount of solute adsorbed and desorbed during a cycle is equal to that obtained by solution of the complete particle diffusion equations. Graphical and analytical expressions for Ω in the case of a single particle, usable for very short beds, are given by Nakao and Suzuki [*J. Chem. Eng. Japan*, **16**, 114 (1983)] and Carta [*Chem. Eng. Sci.*, **48**, 622 (1993)]. With equal adsorption and desorption times, $t_a = t_d = t_c/2$, Ω approaches the value $\pi^2/15$ for long cycle times and the asymptote $\Omega = 1.877/\sqrt{t_c k_n}$ for short cycle times [Alpay and Scott, *Chem. Eng. Sci.*, **47**, 499 (1992)]. However, other results by Raghavan et al. [*Chem. Eng. Sci.*, **41**, 2787 (1986)] indicate that a limiting constant value of Ω (larger than 1) is obtained for very short cycles, when calculations are carried out for beds of finite length.

Determination of Controlling Rate Factor   The most important physical variables determining the controlling dispersion factor are particle size and structure, flow rate, fluid- and solid-phase diffusivities, partition ratio, and fluid viscosity. When multiple resistances and axial dispersion can potentially affect the rate, the spreading of a concentration wave in a fixed bed can be represented approximately

in terms of the single rate parameter k. In customary separation-process calculations, the height of an adsorption bed can be calculated approximately as the product of the number of transfer units times the height of one fluid-phase transfer unit (HTU). The HTU is related to the LDF rate parameters k_c and k_n by:

$$HTU = \frac{\varepsilon v}{\rho_b k_c} = \frac{\varepsilon v}{\Lambda k_n} \tag{16-92}$$

Figure 16-13 is a plot of the dimensionless HTU (htu = HTU/d_p) multiplied times the correction factor b_f (between 1 and 2) as a function of the dimensionless velocity $(Re)(Sc) = \varepsilon v d_p/D$ and a ratio of the controlling diffusivity to the fluid-phase diffusivity, generated on the basis of results of Vermeulen et al. (gen. ref.) using typical values of the individual physical factors likely to be found in adsorption beds. This figure can be used to determine the controlling rate factor from a knowledge of individual physical parameters. If fluid-side effects control, the dimensionless HTU is given by the bottom curve (dotted for gas and solid for liquid-phase systems). If particle-side diffusivities control, the dimensionless HTU is given by a point above the lower envelope on the appropriate diffusional contour (through the ψs, the contour value depends slightly on the separation factor R). If pore and solid diffusion occur in parallel, the reciprocal of the HTU is the sum of the reciprocals of the HTU values for the two mechanisms. Near the intersections of the diffusional contours with the envelope, the dimensionless HTU is the sum of the HTU values for fluid-side and particle-side resistances.

Example 7: Estimation of Rate Coefficient   An adsorption bed is used to remove methane from a methane-hydrogen mixture at 10 atm (abs.) (10.1 bar) and 25°C (298 K), containing 10 mol % methane. Activated carbon particles having a mean diameter $d_p = 0.17$ cm, a surface area $A = 1.1 \times 10^7$ cm²/g, a bulk density $\rho_b = 0.509$ g/cm³, a particle density $\rho_p = 0.777$ g/cm³, and a skeletal density $\rho_s = 2.178$ g/cm³ is used as the adsorbent. Based on data of Grant et al. [*AIChE J.*, **8**, 403 (1962)], adsorption equilibrium is represented by $n = 2.0 \times 10^{-3} K_A p_A/(1 + K_A p_A)$ mol/g adsorbent, with $K_A = 0.346$ atm⁻¹. Estimate the rate coefficient and determine the controlling rate factor for a superficial velocity of 30 cm/s.
    1.   The intraparticle void fraction is $\varepsilon_p = (0.777^{-1} - 2.178^{-1})/(0.777^{-1}) = 0.643$ and the extraparticle void fraction is $\varepsilon = (0.509^{-1} - 0.777^{-1})/(0.509^{-1}) = 0.345$. The pore radius is estimated from $r_p = 2\varepsilon_p/(A\rho_p) = 1.5 \times 10^{-7}$ cm.
    2.   The fluid phase diffusivity is $D = 0.0742$ cm²/s. The pore diffusivity is estimated from Eq. (16-66) with a tortuosity factor $\tau_p = 4$; thus, $D_p = 1.45 \times 10^{-3}$ cm²/s.
    3.   The fluid-side mass transfer coefficient is estimated from Fig. 16-10. For these conditions, $v = 0.108$ cm²/s, $Re = 30 \times 0.17/0.108 = 47$, and $Sc = 0.108/0.0742 = 1.5$. From Fig. 16-10 or equations in Table 16-9, $Sh \sim 13$.
    4.   The isotherm parameters based on the feed concentration are $R = 1/(1 + K_A p_A) = 0.4$ and $\Lambda = 0.509 \times 7.68 \times 10^{-4}/4.09 \times 10^{-5} = 9.56$. For pore diffusion, $\psi_p = 0.961$ from item 3A in Table 16-12. Thus, $(1 - \varepsilon)\psi_p\varepsilon_p D_p/D = (1 - 0.345) \times 0.961 \times 0.643 \times 1.45 \times 10^{-3}/0.0742 = 7.9 \times 10^{-3}$. From Fig. 16-13 at $ReSc = 69$, b htu ~ 150. b is found from Fig. 16-12. However, since the mechanism parameter Ψ is very small, $b \sim 1$. Thus, $k_n = \varepsilon v/(htu\ d_p\Lambda) = 0.12$ s⁻¹. This value applies to the driving force $n_i^e - \bar{n}_i$. Since pore diffusion is dominant, this value is very close to the value $k_n = 15(1 - \varepsilon)\psi_p\varepsilon_p D_p/(r_p^2\Lambda) = 0.13$ s⁻¹ obtained directly from Table 16-12. It should be noted that surface diffusion is neglected in this estimation. Its occurrence could significantly affect the overall mass transfer rate (see Suzuki, gen. refs., pp. 70–85).

Example 8: Estimation of Rate Coefficient   Estimate the rate coefficient for flow of a 0.01-M water solution of NaCl through a bed of cation exchange particles in hydrogen form with $\varepsilon = 0.4$. The superficial velocity is 0.2 cm/s and the temperature is 25°C. The particles are 600 μm in diameter, and the diffusion coefficient of sodium ion is 1.2×10^{-5} cm²/s in solution and 9.4×10^{-7} cm²/s inside the particles (cf. Table 16-8). The bulk density is 0.7 g dry resin/cm³ of bed, and the capacity of the resin is 4.9 mequiv/g dry resin. The mass action equilibrium constant is 1.5.
    1.   Estimate the fluid-side mass transfer coefficient; $Re = \varepsilon v d_p/v = 0.2 \times 0.06/0.00913 = 1.3$, $Sc = v/D = 0.00913/1.2 \times 10^{-5} = 761$. From Fig. 16-10 or Table 16-9, $Sh \sim 23$. Thus, $k_f = D\ Sh/d_p = 4.5 \times 10^{-3}$ cm/s.
    2.   From the equilibrium constant, $R = 1/K_{Na,\ H} = 0.67$. Thus, from Table 16-12, item 2A, $\psi_s = 0.979$. Using $n^{ref} = 4.9$ mequiv/g and $c^{ref} = 0.01$ mmole/cm³, $\Lambda = \rho_b n^{ref}/c^{ref} = 343$. Thus, $\psi_s D_s\Lambda/D = 26$ and the external mass-transfer resistance is controlling (cf. Fig. 16-13).
    3.   The rate coefficient for use with a fluid-phase driving force is $k_c = 3(1 - \varepsilon)k_f/(\rho_b r_p) = 0.39$ cm³/(g·s).
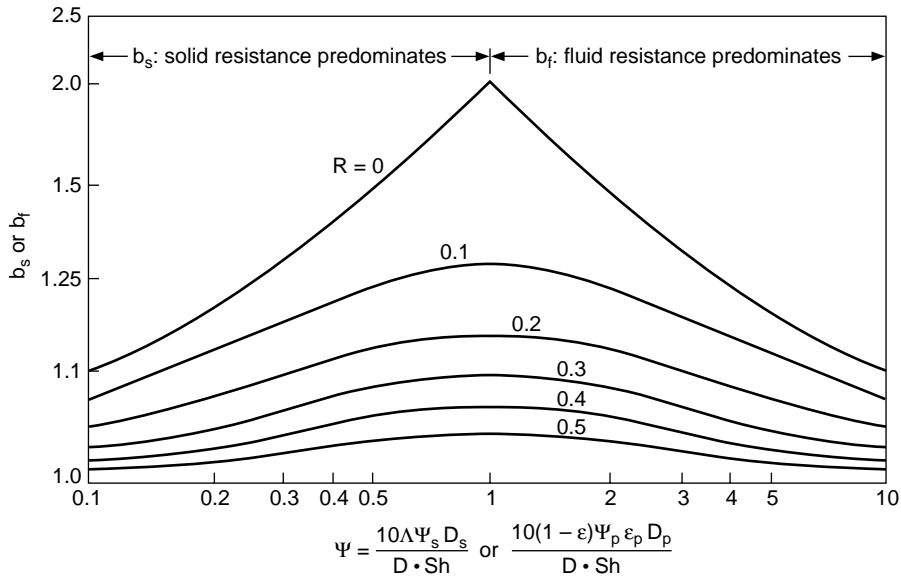
FIG. 16-12 Correction factors for addition of mass-transfer resistances, relative to effective overall solid phase or fluid phase rates, as a function of the mechanism parameter. Each curve corresponds to both b_s and b_f over its entire range.
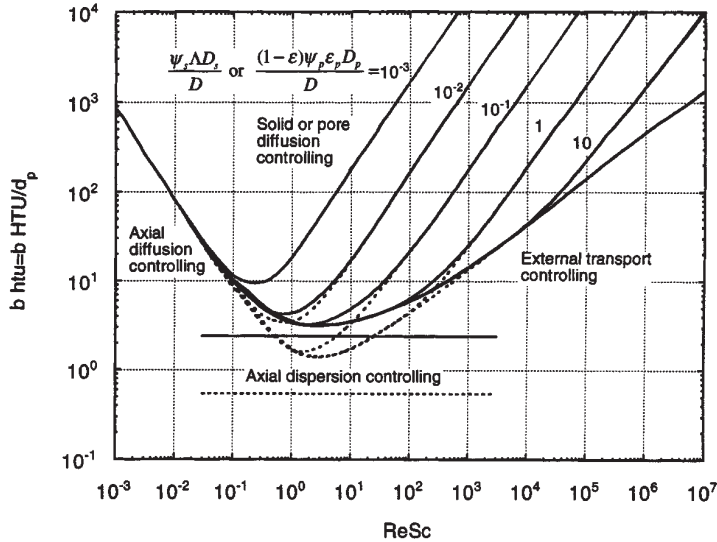

FIG. 16-13 Effect of $ReSc$ group, distribution ratio, and diffusivity ratio on height of a transfer unit. Dotted lines for gas and solid lines for liquid-phase systems.

BATCH ADSORPTION

In this section, we consider the transient adsorption of a solute from a dilute solution in a constant-volume, well-mixed batch system or, equivalently, adsorption of a pure gas. The solutions provided can approximate the response of a stirred vessel containing suspended adsorbent particles, or that of a very short adsorption bed. Uniform, spherical particles of radius r_p are assumed. These particles, initially of uniform adsorbate concentration, are assumed to be exposed to a step change in concentration of the external fluid.

In general, solutions are obtained by coupling the basic conservation equation for the batch system, Eq. (16-49) with the appropriate rate equation. Rate equations are summarized in Table 16-11 and 16-12 for different controlling mechanisms.

Solutions are provided for external mass-transfer control, intraparticle diffusion control, and mixed resistances for the case of constant V_f and $F_{v, in} = F_{v, out} = 0$. The results are in terms of the fractional approach to equilibrium $F = (\hat{n}_i - \hat{n}_i^{0'})/(\hat{n}_i^\infty - \hat{n}_i^{0'})$, where $\hat{n}_i^{0'}$ and $\hat{n}_i^\infty$ are

the initial and ultimate solute concentrations in the adsorbent. The solution concentration is related to the amount adsorbed by the material balance $c_i = c_i^0 - (\hat{n}_i - \hat{n}_i^{0'})M_s/V_f$.

Two general cases are considered: (1) adsorption under conditions of constant or nearly constant external solution concentration (equivalent to infinite fluid volume); and (2) adsorption in a batch with finite volume. In the latter case, the fluid concentration varies from c_i^0 to c_i^∞ when equilibrium is eventually attained. $\Lambda^\infty = (c_i^0 - c_i^\infty)/c_i^0 = M_s(\hat{n}_i^\infty - \hat{n}_i^0)/(V_f c_i^0)$ is a partition ratio that represents the fraction of adsorbate that is ultimately adsorbed. It determines which general case should be considered in the analysis of experimental systems. Generally, when $\Lambda^\infty \geq 0.1$, solutions for the second case are required.

EXTERNAL MASS-TRANSFER CONTROL

The intraparticle concentration is uniform, and the rate equation is given by column 1 in Table 16-12.

For a **Langmuir isotherm** with negligible solute accumulation in the particle pores, the solution for an infinite fluid volume:

$$(1-R)(1 - n_i^{0'}/n_i^0)F - R \ln (1-F) = (3k_f t/r_p)(c_i^0/\rho_p n_i^0) \quad (16\text{-}93)$$

where $n_i^0 = n_i^\infty = n_i^s K_i c_i^0/(1 + K_i c_i^0)$ is the adsorbate concentration in the particle at equilibrium with the fluid concentration. The predicted behavior is shown in Fig. 16-14 for $n_i^{0'} = 0$. In the **irreversible limit** $(R = 0)$, F increases linearly with time; and in the **linear limit** $(R = 1)$, $1 - F$ decreases exponentially with time.

For a finite fluid volume $(\Lambda^\infty > 0)$, the fractional approach to equilibrium is given by:

$$\left[1 - \frac{b'(1-R^\infty)}{2c'}\right]\frac{1}{q'} \ln \frac{(2c'F - b' - q')(-b' + q')}{(2c'F - b' + q')(-b' - q')}$$
$$- \frac{1-R^\infty}{2c'} \ln (1 - b'F + c'F^2) = \frac{3k_f t}{r_p} \frac{c_i^0}{\rho_p n_i^0} \quad (16\text{-}94)$$

where
$$b' = \frac{1-R^\infty}{1-R^0} + \Lambda^\infty \quad (16\text{-}95a)$$

$$c' = \Lambda^\infty(1-R^\infty) \quad (16\text{-}95b)$$

$$q' = (b'^2 - 4c')^{0.5} \quad (16\text{-}95c)$$

$$R^0 = \frac{1}{1 + K_i c_i^0} \quad (16\text{-}95d)$$

$$R^\infty = \frac{1}{1 + Kc_i^\infty} \quad (16\text{-}95e)$$

The predicted behavior is shown in Fig. 16-15 for $R^0 = 0.5$ with different values of Λ^∞.

SOLID DIFFUSION CONTROL

For a constant diffusivity and an infinite fluid volume the solution is:

$$F = 1 - \frac{6}{\pi^2} \sum_{n=1}^{\infty} \frac{1}{n^2} \exp\left(-\frac{n^2\pi^2 D_{si} t}{r_p^2}\right) \quad (16\text{-}96)$$

For short times, this equation does not converge rapidly. The following approximations can be used instead (Helfferich and Hwang, in Dorfner, gen. refs., pp. 1277–1309):

$$F = \frac{6}{r_p}\left(\frac{D_{si} t}{\pi}\right)^{0.5}, \qquad F < 0.2 \quad (16\text{-}97)$$

$$F = \frac{6}{r_p}\left(\frac{D_s t}{\pi}\right)^{0.5} - \frac{3D_{si} t}{r_p^2}, \qquad F < 0.8 \quad (16\text{-}98)$$

For values of $F > 0.8$, the first term $(n = 1)$ in Eq. (16-96) is generally sufficient. If the controlling resistance is diffusion in the subparticles of a bidispersed adsorbent, Eq. (16-96) applies with r_s, replacing r_p.

For a finite fluid volume the solution is:

$$F = 1 - 6 \sum_{n=1}^{\infty} \frac{\exp(-p_n^2 D_{si} t/r_p^2)}{9\Lambda^\infty/(1-\Lambda^\infty) + (1-\Lambda^\infty)p_n^2} \quad (16\text{-}99)$$

where the p_ns are the positive roots of

$$\frac{\tan p_n}{p_n} = \frac{3}{3 + (1/\Lambda^\infty - 1)p_n^2} \quad (16\text{-}100)$$

The predicted behavior is shown in Fig. 16-16. F is calculated from Eq. (16-96) for $\Lambda^\infty = 0$ and from Eq. (16-99) for $\Lambda^\infty > 0$. Significant deviations from the $\Lambda^\infty = 0$ curve exist for $\Lambda^\infty > 0.1$.

For nonconstant diffusivity, a numerical solution of the conservation equations is generally required. In molecular sieve zeolites, when equilibrium is described by the Langmuir isotherm, the concentration dependence of the intracrystalline diffusivity can often be approximated by Eq. (16-72). The relevant rate equation is:

$$\frac{\partial n_i}{\partial t} = \frac{D_{0i}}{r^2} \frac{\partial}{\partial r}\left(\frac{r^2}{1 - n_i/n_i^s} \frac{\partial n_i}{\partial r}\right) \quad (16\text{-}101)$$
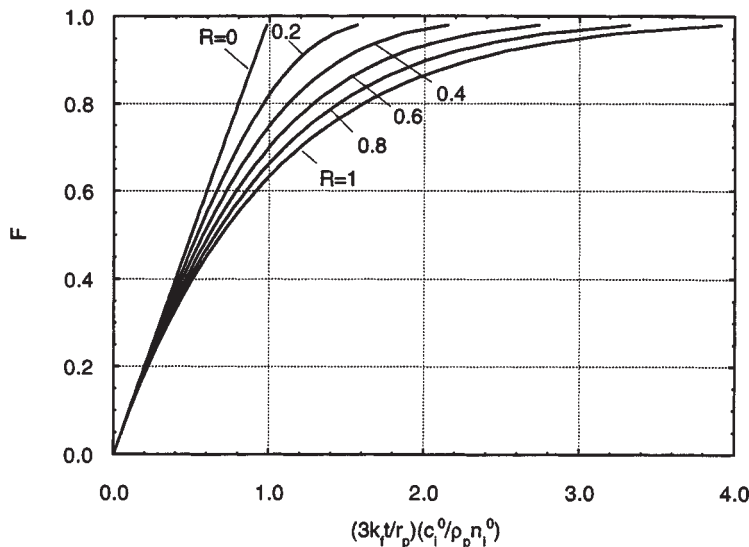
FIG. 16-14 Constant separation factor batch adsorption curves for external mass-transfer control with an infinite fluid volume and $n_i^0 = 0$.
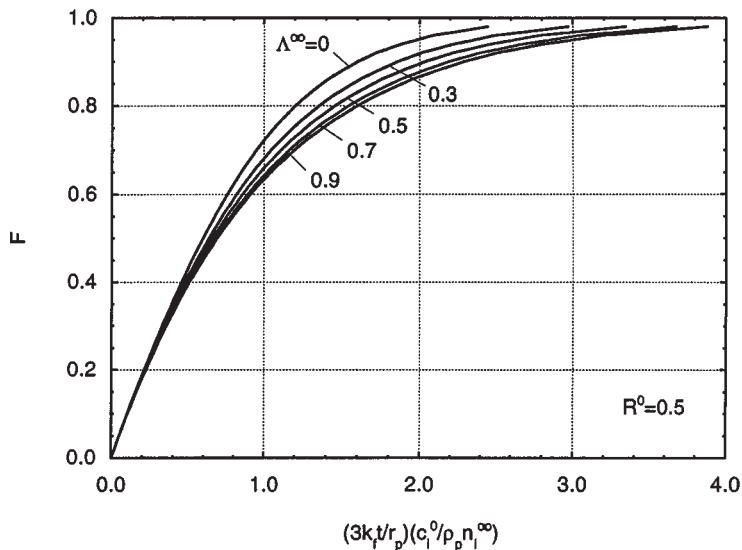
FIG. 16-15 Constant separation factor batch adsorption curves for external mass-transfer control with a finite fluid volume, $n_i^{0'} = 0$ and $R^0 = 0.5$.

A numerical solution of this equation for a constant surface concentration (infinite fluid volume) is given by Garg and Ruthven [*Chem. Eng. Sci.*, **27,** 417 (1972)]. The solution depends on the value of $\lambda = (n_i^0 - n_i^{0'})/(n_i^s - n_i^{0'})$. Because of the effect of adsorbate concentration on the effective diffusivity, for large concentration steps adsorption is faster than desorption, while for small concentration steps, when D_s can be taken to be essentially constant, adsorption and desorption curves are mirror images of each other as predicted by Eq. (16-96); see Ruthven, gen. refs., p. 175.

In binary ion-exchange, intraparticle mass transfer is described by Eq. (16-75) and is dependent on the ionic self diffusivities of the exchanging counterions. A numerical solution of the corresponding conservation equation for spherical particles with an infinite fluid volume is given by Helfferich and Plesset [*J. Chem. Phys.*, **66,** 28, 418

(1958)]. The numerical results for the case of two counterions of equal valence where a resin bead, initially partially saturated with A, is completely converted to the B form, is expressed by:

$$F = \{1 - \exp\left[\pi^2(f_1(\alpha')\tau_D + f_2(\alpha')\tau_D^2 + f_3(\alpha')\tau_D^3)\right]\}^{1/2} \quad (16\text{-}102)$$

with $f_1(\alpha') = -(0.570 + 0.430\alpha'^{0.775})^{-1}$ (16-103a)

$f_2(\alpha') = (0.260 + 0.782\alpha')^{-1}$ (16-103b)

$f_3(\alpha') = -(0.165 + 0.177\alpha')^{-1}$ (16-103c)

where $\tau_D = \overline{D}_A t/r_p^2$ and $\alpha' = 1 + (\overline{D}_A/\overline{D}_B - 1)n_A^{0'}/n^s$ for $0.1 \le \alpha' \le 10$. The predicted behavior is shown in Fig. 16-17. When $\alpha' = 1$ (equal ion diffusivities or $n_A^{0'} \sim 0$), the solution coincides with Eq. (16-96). For $\alpha' \ne 1$, the exchange rate is faster or slower depending on which coun-
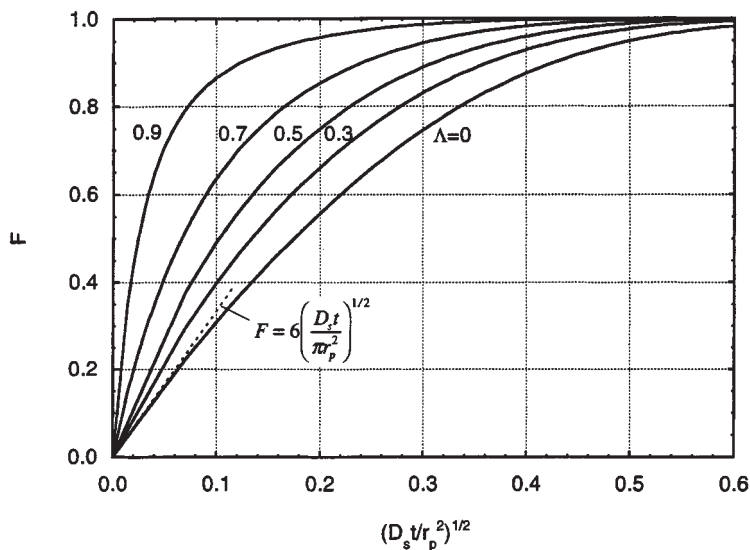
FIG. 16-16 Batch adsorption curves for solid diffusion control. The curve for $\Lambda^\infty = 0$ corresponds to an infinite fluid volume (adapted from Ruthven, gen. refs., with permission).
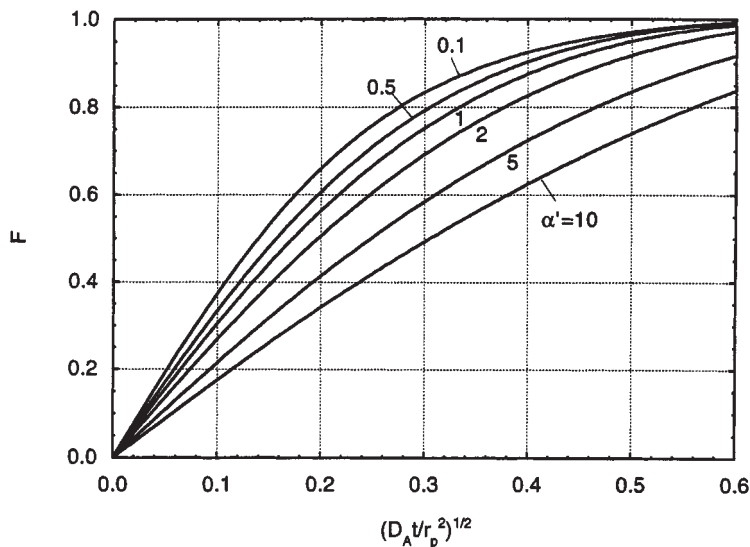
FIG. 16-17 Batch ion exchange for two equal-valence counterions. The exchanger is initially uniformly loaded with ion A in concentration $n_A^{0'}$ and is completely converted to the B form. $\alpha' = 1 + (\bar{D}_A/\bar{D}_B - 1)n_A^{0'}/n^s$.

terion is initially present in the ion exchanger and on the initial level of saturation.

For an initially fully saturated particle, the exchange rate is faster when the faster counterion is initially in the resin, with the difference in rate becoming more important as conversion from one form to the other progresses. Helfferich (gen. refs., pp. 270–271) gives explicit expressions for the exchange of ions of unequal valence.

PORE DIFFUSION CONTROL

The rate equation is given by item A in Table 16-11. With pore fluid and adsorbent at equilibrium at each point within the particle and for a constant diffusivity, the rate equation can be written as:

$$\frac{\partial c_{pi}}{\partial t} = \frac{\varepsilon_p D_{pi}}{\varepsilon_p + \rho_p \, dn_i^e/dc_i} \frac{1}{r^2} \frac{\partial}{\partial r}\left(r^2 \frac{\partial c_{pi}}{\partial r}\right) \quad (16\text{-}104)$$

For a **linear isotherm** ($n_i = K_i c_i$), this equation is identical to the conservation equation for solid diffusion, except that the solid diffusivity D_{si} is replaced by the equivalent diffusivity $D_{ei} = \varepsilon_p D_{pi}/(\varepsilon_p + \rho_p K_i)$. Thus, Eqs. (16-96) and (16-99) can be used for pore diffusion control with infinite and finite fluid volumes simply by replacing D_{si} with D_{ei}.

When the adsorption isotherm is nonlinear, a numerical solution is generally required. For a **Langmuir system** with negligible solute holdup in the pore fluid, item A in Table 16-11 gives:

$$\frac{\partial n_i}{\partial t} = \frac{\varepsilon_p D_{pi}}{\rho_p n_i^s K_i} \frac{1}{r^2} \frac{\partial}{\partial r}\left[\frac{r^2}{(1 - n_i/n_i^s)^2} \frac{\partial n_i}{\partial r}\right] \quad (16\text{-}105)$$

This equation has the same form of that obtained for solid diffusion control with D_{si} replaced by the equivalent concentration-dependent diffusivity $D_{ei} = \varepsilon_p D_{pi}/[\rho_p n_i^s K_i (1 - n_i/n_i^s)^2]$. Numerical results for the case of adsorption on an initially clean particle are given in Fig. 16-18 for different values of $\lambda = n_i^0/n_i^s = 1 - R$. The uptake curves become increasingly steeper, as the nonlinearity of the isotherm, measured by the parameter λ, increases. The desorption curve shown for a particle with $n_i^{0'}/n_i^s = 0.9$ shows that for the same step in concentration, adsorption occurs much more quickly than desorption. This difference, however, becomes smaller as the value of λ is reduced and in the linear region of the adsorption isotherm ($\lambda \to 0$), adsorption and desorption curves are mirror images. The solution in Fig. 16-18 is applicable to a nonzero initial adsorbent loading by redefining λ as $(n_i^0 - n_i^{0'})/(n_i^s - n_{0'}^{0'})$

and the dimensionless time variable as $[\varepsilon_p D_{pi} t/\rho_p (1 - n_i^{0'}/n_i^s)^2 n_i^s K_i r_p^2]^{1/2}$ (Ruthven, gen. refs.).

In the **irreversible limit** ($R < 0.1$), the adsorption front within the particle approaches a shock transition separating an inner core into which the adsorbate has not yet penetrated from an outer layer in which the adsorbed phase concentration is uniform at the saturation value. The dynamics of this process is described approximately by the shrinking-core model [Yagi and Kunii, *Chem. Eng. (Japan)*, **19**, 500 (1955)]. For an infinite fluid volume, the solution is:

$$\frac{\varepsilon_p D_{pi} t}{r_p^2} \frac{c_i^0}{\rho_p n_i^s} = \frac{1}{2} - \frac{1}{3} F - \frac{1}{2}(1 - F)^{2/3} \quad (16\text{-}106)$$

or, in explicit form [Brauch and Schlunder, *Chem. Eng. Sci.*, **30**, 540 (1975)]:

$$F = 1 - \left\{\frac{1}{2} + \cos\left[\frac{\pi}{3} + \frac{1}{3}\cos^{-1}\left(1 - \frac{12\varepsilon_p D_{pi} t}{r_p^2} \frac{c_i^0}{\rho_p n_i^s}\right)\right]\right\}^3 \quad (16\text{-}107)$$

For a finite fluid volume with $0 < \Lambda^\infty \le 1$, the solution is [Teo and Ruthven, *Ind. Eng. Chem. Process Des. Dev.*, **25**, 17 (1986)]:

$$\frac{\varepsilon_p D_{pi} t}{r_p^2} \frac{c_i^0}{\rho_p n_i^s} = I_2 - I_1 \quad (16\text{-}108)$$

where

$$I_1 = \frac{1}{\lambda'\Lambda^\infty\sqrt{3}}\left[\tan^{-1}\frac{2\eta - \lambda'}{\lambda'\sqrt{3}} - \tan^{-1}\frac{2 - \lambda'}{\lambda'\sqrt{3}}\right] + \frac{1}{6\lambda'\Lambda^\infty}\ln\left[\frac{\lambda'^3 + \eta^3}{\lambda'^3 + 1}\left(\frac{\lambda' + 1}{\lambda' + \eta}\right)^3\right]$$

$$(16\text{-}109a)$$

$$I_2 = \frac{1}{3\Lambda^\infty}\ln\frac{\lambda'^3 + \eta^3}{\lambda'^3 + 1} \quad (16\text{-}109b)$$

$$\eta = (1 - F)^{1/3} \quad (16\text{-}109c)$$

$$\lambda' = \left(\frac{1}{\Lambda^\infty} - 1\right)^{1/3} \quad (16\text{-}109d)$$

COMBINED RESISTANCES

In general, exact analytic solutions are available only for the linear ($R = 1$) and irreversible limits ($R \to 0$). Intermediate cases require
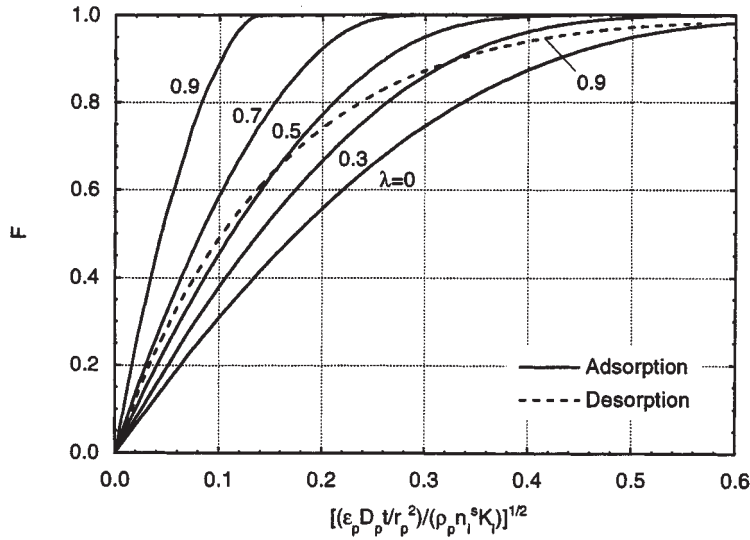
FIG. 16-18 Constant separation factor batch adsorption curves for pore diffusion control with an infinite fluid volume. λ is defined in the text.

numerical solution or use of approximate driving force expressions (see "Rate and Dispersion Factors").

Parallel Pore and Solid Diffusion Control With a **linear isotherm,** assuming equilibrium between the pore fluid and the solid adsorbent, batch adsorption can be represented in terms of an equivalent solid diffusivity $D_{ei} = (\varepsilon_p D_{pi} + \rho_p D_{si})/(\varepsilon_p + \rho_p K_i)$. Thus, Eqs. (16-96) and (16-99) can be used for this case with D_{si} replaced by D_{ei}.

External Mass Transfer and Intraparticle Diffusion Control With a **linear isotherm,** the solution for combined external mass transfer and pore diffusion control with an infinite fluid volume is (Crank, *Mathematics of Diffusion,* 2d ed., Clarendon Press, 1975):

$$F = 1 - \sum_{n=1}^{\infty} \frac{6Bi^2 \exp\left[-(p_n^2 \varepsilon_p D_{pi} t/r_p^2)/(\varepsilon_p + \rho_p K_i)\right]}{p_n^2 [p_n^2 + Bi(Bi-1)]} \quad (16\text{-}110)$$

where $Bi = k_f r_p / \varepsilon_p D_{pi}$ is the **Biot number** and the p_ns are the positive roots of

$$p_n \cot p_n = 1 - Bi \quad (16\text{-}111)$$

For a finite fluid volume the solution is:

$$F = 1 - 6\sum_{n=1}^{\infty} \frac{\exp\left[-(p_n^2 \varepsilon_p D_{pi} t/r_p^2)/(\varepsilon_p + \rho_p K_i)\right]}{\dfrac{9\Lambda^\infty}{1-\Lambda^\infty} + (1-\Lambda^\infty)p_n^2 - (5\Lambda^\infty + 1)\dfrac{p_n^2}{Bi} + (1-\Lambda^\infty)\dfrac{p_n^4}{Bi^2}}$$
$$(16\text{-}112)$$

where the p_ns are the positive roots of

$$\frac{\tan p_n}{p_n} = \frac{3 - \dfrac{1-\Lambda^\infty}{\Lambda^\infty}\dfrac{p_n^2}{Bi}}{3 + \dfrac{1-\Lambda^\infty}{\Lambda^\infty}\dfrac{(Bi-1)p_n^2}{Bi}} \quad (16\text{-}113)$$

These expressions can also be used for the case of external mass transfer and solid diffusion control by substituting D_{si} for $\varepsilon_p D_{pi}/(\varepsilon_p + \rho_p K_i)$ and $k_f r_p/(\rho_p K_i D_{si})$ for the Biot number.

In the **irreversible limit,** the solution for combined external resistance and pore diffusion with infinite fluid volume is (Yagi and Kunii):

$$\frac{\varepsilon_p D_{pi} t}{r_p^2} \frac{c_i^0}{\rho_p n_i^s} = \frac{1}{2} - \frac{1}{3}\left(1 - \frac{1}{Bi}\right)F - \frac{1}{2}(1-F)^{2/3} \quad (16\text{-}114)$$

For a finite fluid volume the solution is (Teo and Ruthen):

$$\frac{\varepsilon_p D_{pi} t}{r_p^2} \frac{c_i^0}{\rho_p n_i^s} = \left(1 - \frac{1}{Bi}\right)I_2 - I_1 \quad (16\text{-}115)$$

where I_1 and I_2 are given be Eqs. (16-109a) and (16-109b).

Bidispersed Particles For particles of radius r_p comprising adsorptive subparticles of radius r_s that define a macropore network, conservation equations are needed to describe transport both within the macropores and within the subparticles and are given in Table 16-11, item D. Detailed equations and solutions for a linear isotherm are given in Ruthven (gen. refs., p. 183) and Ruckenstein et al. [*Chem. Eng. Sci.,* **26,** 1306 (1971)]. The solution for a **linear isotherm** with no external resistance and an infinite fluid volume is:

$$F = 1 - \frac{18}{\beta + 3\alpha}\sum_{m=1}^{\infty}\sum_{n=1}^{\infty}\left(\frac{n^2\pi^2}{p_{n,m}^4}\right)$$
$$\times \frac{\exp(-p_{n,m}^2 D_{si} t/r_s^2)}{\alpha + \dfrac{\beta}{2}\left[1 + \dfrac{\cot p_{n,m}}{p_{n,m}}(p_{n,m}\cot p_{n,m} - 1)\right]} \quad (16\text{-}116)$$

where the $p_{n,m}$ values are the roots of the equation

$$\alpha p_{n,m}^2 - n^2\pi^2 = \beta(p_{n,m}\cot p_{n,m} - 1) \quad (16\text{-}117)$$

and

$$\alpha = \frac{D_{si}/r_s^2}{D_{pi}/r_p^2} \quad (16\text{-}118a)$$

$$\beta = \frac{3\alpha\rho_p K_i}{\varepsilon_p} \quad (16\text{-}118b)$$

In these equations, D_{si} is the diffusivity in the subparticles, and D_{pi} is the diffusivity in the pore network formed by the subparticles.

For large K_i values, the uptake curve depends only upon the value of the parameter β representing the ratio of characteristic time constants for diffusion in the pores and in the subparticles. For small β values, diffusion in the subparticles is controlling and the solution coincides with Eq. (16-96) with r_s replacing r_p. For large β values, pore diffusion is controlling, and the solution coincides with Eq. (16-96) with $\varepsilon_p D_{pi}/(\varepsilon_p + \rho_p K_i)$ replacing D_{si}.

Lee [*AIChE J.,* **24,** 531 (1978)] gives the solution for batch adsorption with bidispersed particles for the case of a finite fluid volume.

FIXED-BED TRANSITIONS

As discussed in "Design Concepts," a large fraction of adsorption and ion-exchange processes takes place in fixed beds. Two classical methods for analyzing fixed-bed transitions are described here. First, local equilibrium theory is presented. In this, all mass-transfer resistances are ignored to focus on the often dominating role of isotherm shape. Second, results of constant pattern analysis are presented. This gives the maximum breadth to which a mass-transfer zone will spread for various rate mechanisms. It is therefore conservative for design purposes. Both of these methods pertain to behavior in deep beds. For shallow beds, the equations given below must be solved for the particular case of interest.

DIMENSIONLESS SYSTEM

For the methods, we consider Eq. (16-52), the material balance for a fixed bed, written in the form

$$\rho_b \frac{\partial \bar{n}_i}{\partial t} + \varepsilon_b \frac{\partial c_i}{\partial t} + \varepsilon \frac{\partial (vc_i)}{\partial z} = \varepsilon D_L \frac{\partial}{\partial z}\left(c \frac{\partial y_i}{\partial z}\right) \quad (16\text{-}119)$$

where it has been assumed that D_L is constant and that $\hat{c}_i \approx c_i$ (or that the second term in the balance is small compared to the first—usually a good assumption).

Dimensionless variables can be defined for time, the axial coordinate, and velocity:

$$\tau = \frac{\varepsilon v^{\text{ref}} t}{L} \quad (16\text{-}120)$$

$$\zeta = \frac{z}{L} \quad (16\text{-}121)$$

$$v^\circ = \frac{v}{v^{\text{ref}}} \quad (16\text{-}122)$$

where L is bed length, v^{ref} is the interstitial velocity at the bed inlet, and τ is equal to the number of empty bed volumes of feed passed into the bed. The material balance becomes

$$\rho_b \frac{\partial \bar{n}_i}{\partial \tau} + \varepsilon_b \frac{\partial c_i}{\partial \tau} + \frac{\partial (v^\circ c_i)}{\partial \zeta} = \frac{1}{N_{Pe}}\frac{\partial}{\partial \zeta}\left(c \frac{\partial y_i}{\partial \zeta}\right) \quad (16\text{-}123)$$

where $N_{Pe} = \varepsilon v^{\text{ref}} L / D_L$ is a Peclet number for the bed or a **number of dispersion units.** Equation (16-123) or a similar equation is often the material balance used in nonisothermal problems, in problems involving adsorption of nontrace components, and in calculations of cycles.

For a trace, isothermal system, we have $v^\circ = 1$, and using the dimensionless system variables for concentrations [Eq. (16-10)], Eq. (16-123) becomes

$$\Lambda \frac{\partial \bar{n}_i^\circ}{\partial \tau} + \varepsilon_b \frac{\partial c_i^\circ}{\partial \tau} + \frac{\partial c_i^\circ}{\partial \zeta} = \frac{1}{N_{Pe}}\frac{\partial^2 c_i^\circ}{\partial \zeta^2} \quad (16\text{-}124)$$

where Λ is the **partition ratio** defined by

$$\Lambda = \frac{\rho_b n_i^{\text{ref}}}{c_i^{\text{ref}}} \quad (16\text{-}125)$$

This important dimensionless group is the volumetric capacity of the bed for the sorbable component divided by the concentration of the sorbable component in the feed. The stoichiometric capacity of the bed for solute is exactly equal to Λ empty bed volumes of feed (to saturate the sorbent at the feed concentration) plus a fraction of a bed volume of feed to fill the voids outside and inside the particles. Alternatively, we also obtain Eq. (16-124) using the dimensionless transition variables for concentrations [Eq. (16-11)], but now the partition ratio in the first term of Eq. (16-124) pertains to the transition and is given by

$$\Lambda = \rho_b \frac{n_i'' - n_i'}{c_i'' - c_i'} \quad (16\text{-}126)$$

Equation (16-124) is a commonly used form of material balance for a fixed-bed adsorber.

If the system under consideration involves use of the sorbent for only a single feed step or reuse after uniform regeneration, as in many applications with activated carbons and ion exchangers, then one of two paths is often followed at this point to simplify Eq. (16-124) further. The second term on the left-hand side of the equation is often assumed to be negligibly small (usually a good assumption), and time is redefined as

$$\tau_1 = \frac{\tau}{\Lambda} \quad (16\text{-}127)$$

to give

$$\frac{\partial \bar{n}_i^\circ}{\partial \tau_1} + \frac{\partial c_i^\circ}{\partial \zeta} = \frac{1}{N_{Pe}}\frac{\partial^2 c_i^\circ}{\partial \zeta^2} \quad (16\text{-}128)$$

Alternatively, in the absence of axial dispersion, a variable of the form

$$\tau_1 = \frac{\tau - \varepsilon_b \zeta}{\Lambda} \quad (16\text{-}129)$$

can be defined to reduce Eq. (16-124) directly to

$$\frac{\partial \bar{n}_i^\circ}{\partial \tau_1} + \frac{\partial c_i^\circ}{\partial \zeta} = 0 \quad (16\text{-}130)$$

The variable τ_1 defined by Eq. (16-127) or (16-129) is a **throughput parameter,** equal to unity (hence, the "1" subscript) at the time when the stoichiometric center of the concentration wave leaves the bed. This important group, in essence a dimensionless time variable, essentially determines the location of the stoichiometric center of the transition in the bed at any time.

LOCAL EQUILIBRIUM THEORY

In local equilibrium theory, fluid and sorbed phases are assumed to be in local equilibrium with one another at every axial position in the bed. Thus, because of uniform concentrations, the overbar on n_i° is not necessary and we have $\hat{c}_i \approx c_i$ [note Eqs. (16-52) and (16-119)].

Single Transition System For a system described by a single material balance, Eq. (16-130) gives

$$\frac{d\tau_1}{d\zeta} = -\frac{\partial c_i^\circ / \partial \zeta}{\partial c_i^\circ / \partial \tau_1} = \frac{dn_i^\circ}{dc_i^\circ} \quad (16\text{-}131)$$

where $d\tau_1/d\zeta$ is the reciprocal of a concentration velocity. Equation (16-131) is the equation for a **simple wave** (or gradual transition or proportionate pattern). If a bed is initially uniformly saturated, then $d\tau_1/d\zeta = \tau_1/\zeta$. Thus, for the dimensionless system, the reciprocal of the velocity of a concentration is equal to the slope of the isotherm at that concentration. Furthermore, from Eq. (16-131), the depth of penetration of a given concentration into the bed is directly proportional to time, so the breadth of a simple wave increases in direct proportion to the depth of its penetration into the bed (or to time). Thus, for the simple wave, the length of the MTZ is proportional to the depth of the bed through which the wave has passed. Consideration of isotherm shape indicates that a simple wave occurs for an unfavorable dimensionless isotherm $(d^2 n_i^\circ/dc_i^{\circ 2} > 0)$, for which low concentrations will go faster than high concentrations. Equation (16-131) also pertains to a linear isotherm, in which case the wave is called a **contact discontinuity,** because it has neither a tendency to spread nor sharpen. If mass-transfer resistance is added to the consideration of wave character for unfavorable isotherms, the wave will still asymptotically approach the simple wave result given by Eq. (16-131).

For a favorable isotherm $(d^2 n_i^\circ/dc_i^{\circ 2} < 0)$, Eq. (16-131) gives the impossible result that three concentrations can coexist at one point in the bed (see example below). The correct solution is a **shock** (or abrupt transition) and not a simple wave. Mathematical theory has been developed for this case to give "weak solutions" to conservation laws. The form of the solution is

$$\text{shock speed} = \frac{\text{change in flux}}{\text{change in accumulated quantity}}$$

where the changes are jump discontinuities across the shock. The reciprocal of this equation, using Eq. (16-130), is

$$\frac{d\tau_1}{d\zeta} = \frac{\Delta n_i^\circ}{\Delta c_i^\circ} \qquad (16\text{-}132)$$

where the differences are taken across the shock.

It is also possible to have a **combined wave,** which has both gradual and abrupt parts. The general rule for an isothermal, trace system is that in passing from the initial condition to the feed point in the isotherm plane, the slope of the path must not decrease. If it does, then a shock chord is taken for that part of the path. Referring to Fig. 16-19, for a transition from (0,0) to (1,1), the dashes indicate shock parts, which are connected by a simple wave part between points P_1 and P_2.

Example 9: Transition Types   For the constant separation-factor isotherm given by Eq. (16-31), determine breakthrough curves for $r = 2$ and $r = 0.5$ for transitions from $c_i^\circ = 0$ to $c_i^\circ = 1$.

Using Eq. (16-131), we obtain

$$\frac{\tau_1}{\zeta} = \frac{r}{[r + (1 - r)c_i^\circ]^2}$$

This equation, evaluated at $\zeta = 1$, is plotted for $r = 2$ and $r = 0.5$ in Fig. 16-20. Clearly, the solution for $r = 0.5$ is not physically correct. Equation (16-132), with $d\tau_1/d\zeta = \tau_1/\zeta$, is applied to this case to give the shock indicated by the dashed line. Alternatively, we could have obtained bed profiles by evaluating equations at $\tau_1 = $ const.

Multiple Transition System   Local equilibrium theory for multiple transitions begins with some combination of material and energy balances, written

$$\rho_b \frac{\partial n_i}{\partial \tau} + \varepsilon_b \frac{\partial c_i}{\partial \tau} + \frac{\partial (v^\circ c_i)}{\partial \zeta} = 0 \qquad (i = 1, 2, \dots) \quad (16\text{-}133)$$

$$\rho_b \frac{\partial u_s}{\partial \tau} + \varepsilon_b \frac{\partial (c u_f)}{\partial \tau} + \frac{\partial (v^\circ c h_f)}{\partial \zeta} = 0 \qquad (16\text{-}134)$$

which are Eq. (16-123) written with no dispersion and Eq. (16-55) written for an adiabatic bed.

For a simple wave, application of the method of characteristics (hodograph transformation) gives

$$\frac{d\tau}{d\zeta} = \frac{d(\rho_b n_1 + \varepsilon_b c_1)}{d(v^\circ c_1)} = \frac{d(\rho_b n_2 + \varepsilon_b c_2)}{d(v^\circ c_2)} = \dots = \frac{d(\rho_b u_s + \varepsilon_b c u_f)}{d(v^\circ c h_f)} \quad (16\text{-}135)$$

where the derivatives are taken along the path of a transition (i.e., directional derivatives).
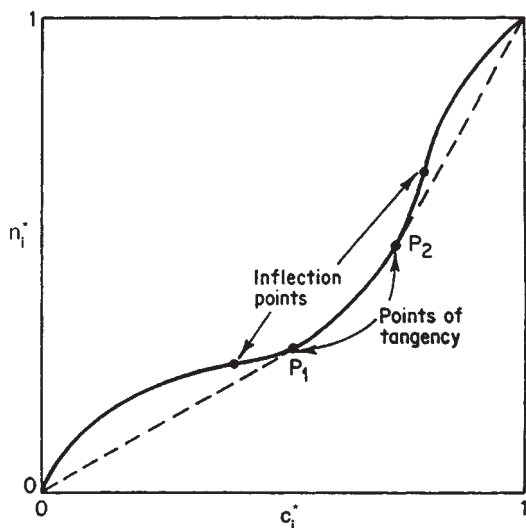
FIG. 16-19   Path in isotherm plane for a combined wave (After Tudge).
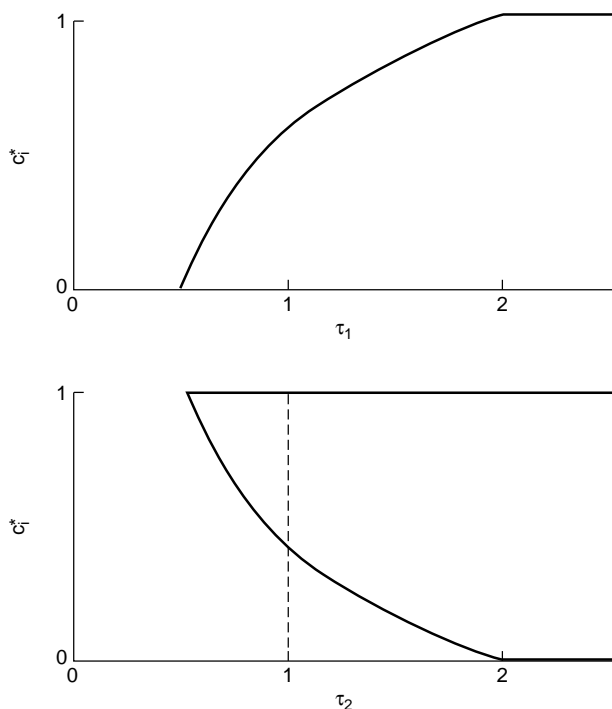
FIG. 16-20   Breakthrough curves for $r = 2$ (top) and $r = 0.5$ (bottom) for Example 9.

If a simple wave is not possible on physical grounds, then it (or part of it) is replaced by a shock, given by

$$\frac{d\tau}{d\zeta} = \frac{\Delta(\rho_b n_1 + \varepsilon_b c_1)}{\Delta(v^\circ c_1)} = \frac{\Delta(\rho_b n_2 + \varepsilon_b c_2)}{\Delta(v^\circ c_2)} = \dots = \frac{\Delta(\rho_b u_s + \varepsilon_b c u_f)}{\Delta(v^\circ c h_f)} \quad (16\text{-}136)$$

Extensions   When more than two conservation equations are to be solved simultaneously, matrix methods for eigenvalues and left eigenvectors are efficient [Jeffrey and Taniuti, *Nonlinear Wave Propagation,* Academic Press, New York, 1964; Jacob and Tondeur, *Chem. Eng. J.,* **22,** 187 (1981), **26,** 41 (1983); Davis and LeVan, *AIChE J.,* **33,** 470 (1987); Rhee et al., gen. refs.].

Nontrace isothermal systems give the "adsorption effect" (i.e., significant change in fluid velocity because of loss or gain of solute). Criteria for the existence of simple waves, contact discontinuities, and shocks are changed somewhat [Peterson and Helfferich, *J. Phys. Chem.,* **69,** 1283 (1965); LeVan et al., *AIChE J.,* **34,** 996 (1988); Frey, *AIChE J.,* **38,** 1649 (1992)].

Local equilibrium theory also pertains to adsorption with axial dispersion, since this mechanism does not disallow existence of equilibrium between stationary and fluid phases across the cross section of the bed [Rhee et al., *Chem. Eng. Sci.,* **26,** 1571 (1971)]. It is discussed below in further detail from the standpoint of the constant pattern.

Example 10: Two-Component Isothermal Adsorption   Two components present at low mole fractions are adsorbed isothermally from an inert fluid in an initially clean bed. The system is described by $\rho_b = 500$ kg/m^3, $\varepsilon_b = 0.7$, and the binary Langmuir isotherm

$$n_i = \frac{n_i^s K_i c_i}{1 + K_1 c_1 + K_2 c_2} \qquad (i = 1, 2)$$

with $n_1^s = n_2^s = 6$ mol/kg, $K_1 = 40$ m^3/mol, and $K_2 = 20$ m^3/mol. The feed is $c_1 = c_2 = 0.5$ mol/m^3. Find the bed profile.

Using the isotherm to calculate loadings in equilibrium with the feed gives $n_1 = 3.87$ mol/kg and $n_2 = 1.94$ mol/kg. An attempt to find a simple wave solution for this problem fails because of the favorable isotherms (see the next example for the general solution method). To obtain the two shocks, Eq. (16-136) is written

$$\frac{d\tau}{d\zeta} = \frac{\Delta(\rho_b n_1 + \varepsilon_b c_1)}{\Delta c_1} = \frac{\Delta(\rho_b n_2 + \varepsilon_b c_2)}{\Delta c_2}$$

The concentration of one of the components will drop to zero in the shock nearest the bed inlet. If it is component 1, then using feed values and the equation above, that shock would be at

$$\frac{\tau}{\zeta} = \frac{\rho_b n_1 + \varepsilon_b c_1}{c_1} \approx \frac{\rho_b n_1}{c_1} = 3870$$

Similarly, if the second component were to disappear in the first shock, we would have $\tau/\zeta = 1940$. Material balance considerations require that we accept the shorter distance, so component 1 disappears in the first shock.

The concentrations of component 2 on the plateau downstream of the first shock are then calculated from

$$\frac{\tau}{\zeta} = \frac{\Delta(\rho_b n_2 + \varepsilon_b c_2)}{\Delta c_2} \approx \frac{\rho_b \Delta n_2}{\Delta c_2} = 3870$$

and its pure component isotherm, giving $c_2 = 0.987$ mol/m^3 and $n_2 = 5.71$ mol/kg. The location of this shock is determined using these concentrations and

$$\frac{\tau}{\zeta} = \frac{\rho_b n_2 + \varepsilon_b c_2}{c_2} \approx \frac{\rho_b n_2}{c_2}$$

which gives $\tau/\zeta = 2890$. The bed profile is plotted in Fig. 16-21 using ζ/τ as the abissa. (This example can also be worked with the h-transformation described in this section under chromatography.)

Example 11: Adiabatic Adsorption and Thermal Regeneration
An initially clean activated carbon bed at 320 K is fed a vapor of benzene in nitrogen at a total pressure of 1 MPa. The concentration of benzene in the feed is 6 mol/m^3. After the bed is uniformly saturated with feed, it is regenerated using benzene-free nitrogen at 400 K and 1 MPa. Solve for both steps. For simplicity, neglect fluid-phase accumulation terms and assume constant mean heat capacities for stationary and fluid phases and a constant velocity. The system is described by

$$\rho_b n_1 = \frac{\rho_b n_1^s K_1 c_1}{1 + K_1 c_1}$$

$$\rho_b n_1^s = 2750 \text{ mol/m}^3$$

$$K_1 = 3.88 \times 10^{-8} \sqrt{T} \exp\left[q_1^{st}/(\Re T)\right] \text{ m}^3/(\text{mol K}^{1/2})$$

$$\rho_b C_{sm} = 850 \text{ kJ}/(\text{m}^3 \text{ K})$$

$$c C_{pfm} = 11.3 \text{ kJ}/(\text{m}^3 \text{ K})$$

$$q_1^{st} = 43.5 \text{ kJ/mol}$$

$$T^{\text{ref}} = 320 \text{ K}$$

Extensive analysis has been made of this system [Rhee et al., *Chem. Eng. J.*, **1**, 241 (1970) and gen. refs.; LeVan, in Rodrigues et al., gen. refs.].

To obtain the concentration and temperature profiles, the two transitions are first assumed to be gradual. Equation (16-135) is written in the form

$$\frac{\tau}{\zeta} = \rho_b \frac{dn_1}{dc_1} = \rho_b \frac{du_s}{d(ch_f)}$$

where, from Eqs. (16-56) to (16-60),

$$\rho_b u_s = \rho_b C_{sm}(T - T^{\text{ref}}) - \rho_b n_1 q_1^{st}$$

$$ch_f = cC_{pfm}(T - T^{\text{ref}})$$
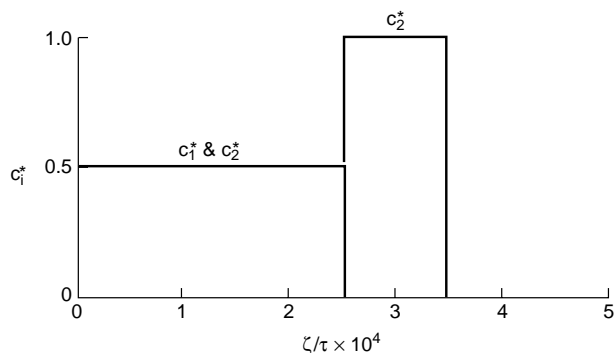
FIG. 16-21 Bed profiles for two-component isothermal adsorption, Example 10.

This equation is expanded in terms of c_1 and T to obtain

$$\frac{\tau}{\zeta} = \rho_b\left(\frac{\partial n_1}{\partial c_1} + \frac{\partial n_1}{\partial T}\frac{dT}{dc_1}\right) = \frac{\rho_b C_{sm}}{cC_{pfm}} - \frac{\rho_b q_1^{st}}{cC_{pfm}}\left(\frac{\partial n_1}{\partial T} + \frac{\partial n_1}{\partial c_1}\frac{dc_1}{dT}\right)$$

Solving the rightmost equality for the directional derivative using the quadratic formula gives

$$\frac{dc_1}{dT} = \frac{-b \pm \sqrt{b^2 - 4ad}}{2a}$$

with

$$a = \left[\frac{\rho_b q_1^{st}}{(cC_{pfm})}\right]\frac{\partial n_1}{\partial c_1}$$

$$b = \left[\frac{\rho_b q_1^{st}}{(cC_{pfm})}\right]\frac{\partial n_1}{\partial T} - \frac{\rho_b C_{sm}}{(cC_{pfm})} + \frac{\rho_b \partial n_1}{\partial c_1}$$

$$d = \frac{\rho_b \partial n_1}{\partial T}$$

The plus sign corresponds to the downstream transition and the minus sign to the upstream one. This equation is solved along each path beginning at the respective end points—the initial condition of the bed for the downstream transition and the feed condition for the upstream transition. If either path fails to evolve continuously in the expected direction, the difference form, from Eq. (16-136),

$$\frac{d\tau}{d\zeta} = \rho_b\frac{\Delta n_1}{\Delta c_1} = \rho_b\frac{\Delta u_s}{\Delta(ch_f)}$$

is used for that path (or part thereof, if appropriate); two solutions of this equation pass through each composition point, and care must be taken to ensure that the correct path is taken. The two correct paths found intersect to give the composition and temperature of an intermediate plateau region.

Letting $c_1^{\text{ref}} = 6$ mol/m^3, the isotherm gives $\rho_b n_1^{\text{ref}} = 2700$ mol/m^3, and the partition ratio is $\Lambda = 450$.

In the figures, $\Gamma(k)$ and $\Sigma(k)$ symbolize simple waves and shocks, respectively, with $k = 1$ downstream and $k = 2$ upstream.

Adiabatic Adsorption The construction is shown in Figs. 16-22 and 16-23. The first path begins at the initial condition, point A ($T = 320$ K, $c_1 = 0$ mol/m^3). Since $\partial n_1/\partial T = 0$ there, we obtain $dc_1/dT = 0$ and $\tau/\zeta = \rho_b C_{sm}/(cC_{pfm}) = 75.2$ (or $\tau/\Lambda = 0.167$ at $\zeta = 1$), corresponding to a pure thermal wave along the $c_1 = 0$ axis of Fig. 16-22. The second path begins at the feed condition, point B ($T = 320$ K, $c_1 = 6$ mol/m^3). A $\Sigma(2)$ fails, so a $\Sigma(2)$ is calculated and plotted in the two figures. The $\Gamma(1)$ and $\Sigma(2)$ intersect at point C ($T = 348$ K, $c_1 = 0$ mol/m^3) Breakthrough curves of temperature and concentration are shown in Fig. 16-24.

Thermal Regeneration The bed, initially at point B, is fed with pure nitrogen. The feed, at point D ($T = 400$ K, $c_1 = 0$ mol/m^3), provides a successful $\Gamma(2)$. The $\Gamma(1)$ from point B fails, so a $\Sigma(1)$, which differs imperceptibly from $\Gamma(1)$, is determined. The $\Sigma(1)$ and $\Gamma(2)$ meet at point E ($T = 320.8$ K, $c_1 = 8.93$ mol/m^3), where $\rho_b n_1 = 2716$ mol/m^3, greater than the initial loading, indicating "roll-up," a term attributed to Basmadjian et al. [*Ind. Eng. Chem. Process Des. Dev.*, **14**, 328 (1975)], of the adsorbed-phase concentration. Breakthrough curves are shown in Fig. 16-25. The $\Sigma(1)$ leaves the bed at $\tau/\Lambda = 0.011$. The $\Gamma(2)$ begins to emerge at $\tau/\Lambda = 0.169$, but regeneration is not complete until $\tau/\Lambda = 2.38$.

It is possible (with lower initial bed temperature, higher initial loading, or higher regeneration temperature or pressure) for the transition paths to contact the saturated vapor curve in Fig. 16-22 rather than intersect beneath it. For this case, liquid benzene condenses in the bed, and the effluent vapor is saturated during part of regeneration [Friday and LeVan, *AIChE J.*, **30**, 679 (1984)].

CONSTANT PATTERN BEHAVIOR FOR FAVORABLE ISOTHERMS

With a favorable isotherm and a mass-transfer resistance or axial dispersion, a transition approaches a **constant pattern,** which is an asymptotic shape beyond which the wave will not spread. The wave is said to be "self-sharpening." (If a wave is initially broader than the constant pattern, it will sharpen to approach the constant pattern.) Thus, for an initially uniformly loaded bed, the constant pattern gives the maximum breadth of the MTZ. As bed length is increased, the constant pattern will occupy an increasingly smaller fraction of the bed. (Square-root spreading for a linear isotherm gives this same qualitative result.)

The treatment here is restricted to the Langmuir or constant separation factor isotherm, single-component adsorption, dilute systems, isothermal behavior, and mass-transfer resistances acting alone. References to extensions are given below. Different isotherms have been considered, and the theory is well understood for general isotherms.
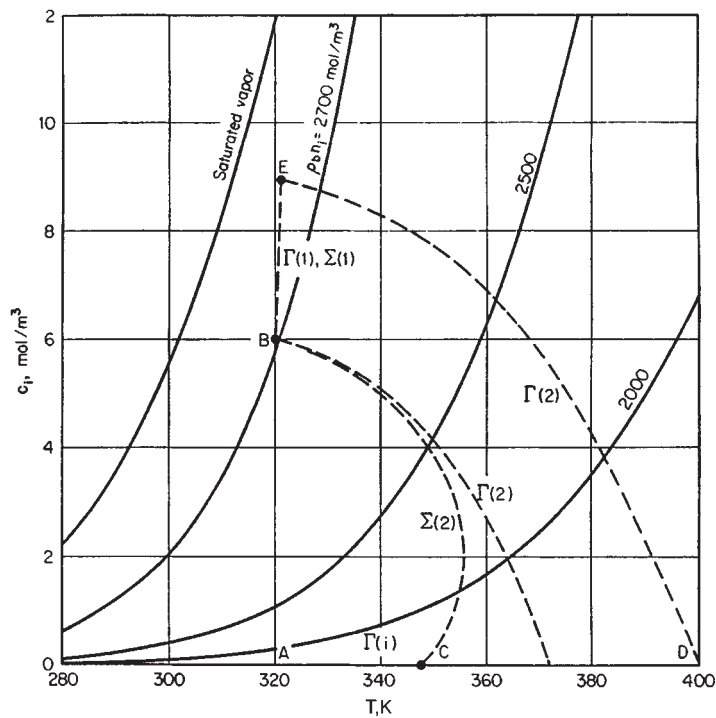
FIG. 16-22 Transition paths in c_1, T plane for adiabatic adsorption and thermal regeneration.
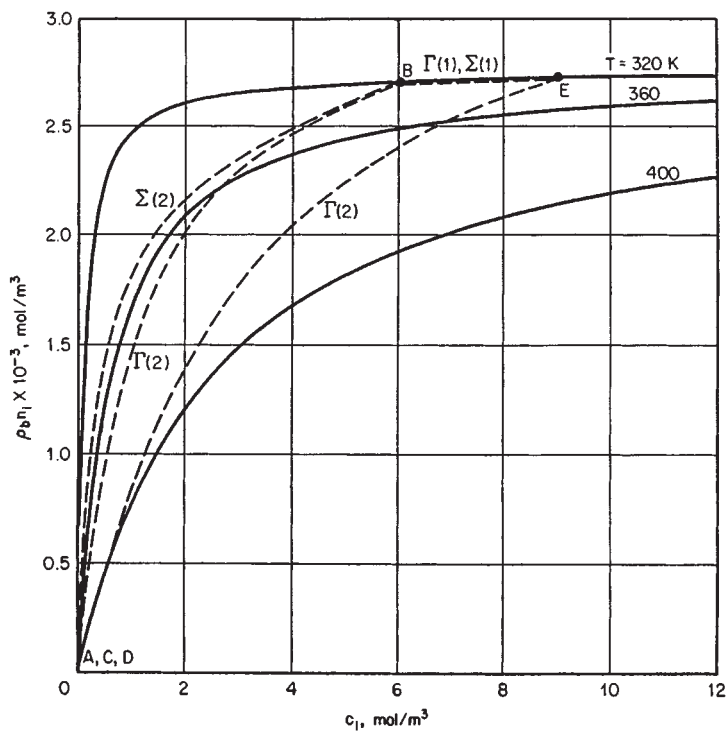

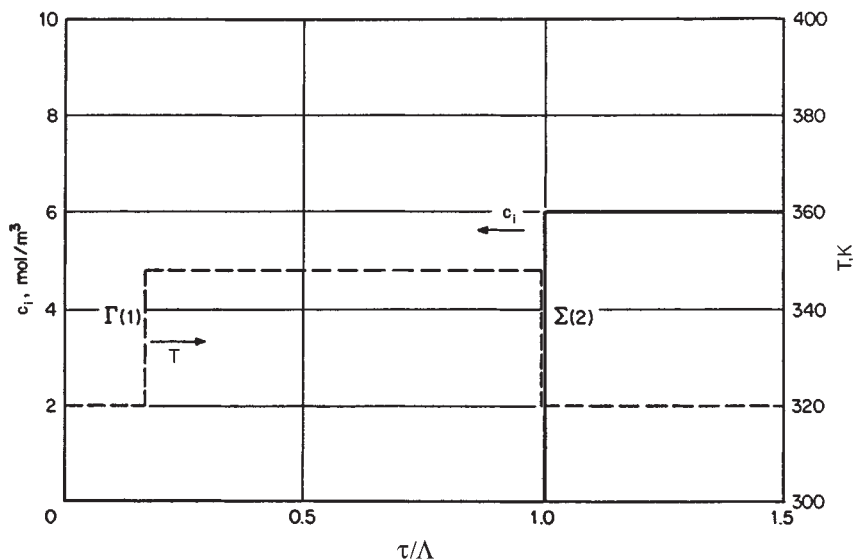**FIG. 16-23** Transition paths in isotherm plane for adiabatic adsorption and thermal regeneration.

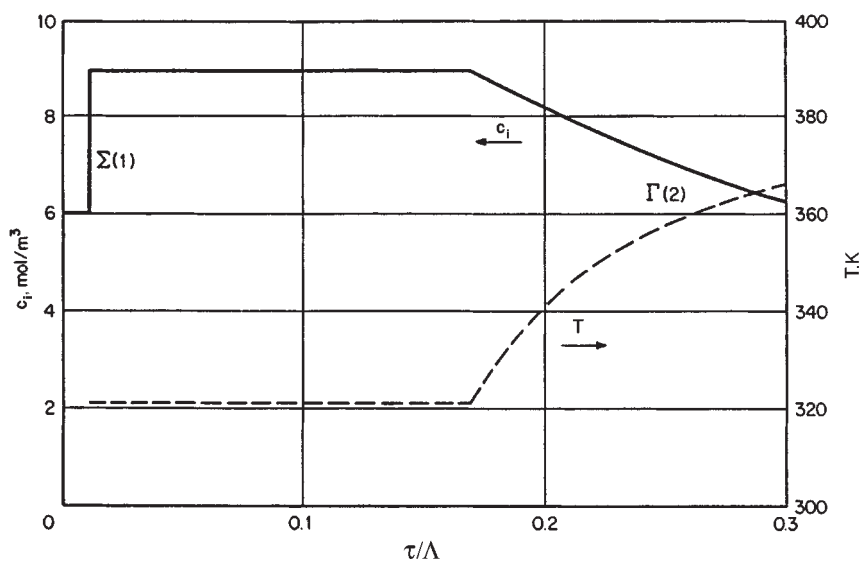**FIG. 16-24**   Breakthrough curves for adiabatic adsorption.

FIG. 16-25   Breakthrough curves for thermal regeneration.

Asymptotic Solution   Rate equations for the various mass-transfer mechanisms are written in dimensionless form in Table 16-13 in terms of a number of transfer units, $N = L/HTU$, for particle-scale mass-transfer resistances, a number of reaction units for the reaction kinetics mechanism, and a number of dispersion units, N_{Pe}, for axial dispersion. For pore and solid diffusion, $\xi = r/r_p$ is a dimensionless radial coordinate, where r_p is the radius of the particle. If a particle is bidisperse, then r_p can be replaced by r_s, the radius of a subparticle. For preliminary calculations, Fig. 16-13 can be used to estimate N for use with the LDF approximation when more than one resistance is important.

In constant pattern analysis, equations are transformed into a new coordinate system that moves with the wave. Variables are changed from (ζ, τ_1) to $(\zeta - \tau_1, \tau_1)$. The new variable $\zeta - \tau_1$ is equal to zero at the stoichiometric center of the wave. Equation (16-130) for a bed

with no axial dispersion, when transformed to the $(\zeta - \tau_1, \tau_1)$ coordinate system, becomes

$$-\frac{\partial \bar{n}_i^\circ}{\partial(\zeta - \tau_1)} + \frac{\partial \bar{n}_i^\circ}{\partial \tau_1} + \frac{\partial c_i^\circ}{\partial(\zeta - \tau_1)} = 0 \qquad (16\text{-}137)$$

The constant pattern is approached as the τ_1 dependence in this equation disappears. Thus, discarding the derivative with respect to τ_1 and integrating, using the condition that $\bar{n}_i^\circ$ and c_i° approach zero as $N(\zeta - \tau_1) \rightarrow \infty$ [or approach unity as $N(\zeta - \tau_1) \rightarrow -\infty$], gives simply

$$\bar{n}_i^\circ = c_i^\circ \qquad (16\text{-}138)$$

For adsorption with axial dispersion, the material balance transforms to

TABLE 16-13   Constant Pattern Solutions for Constant Separation Factor Isotherm (R < 1)

Mechanism	N	Dimensionless rate equation[1]	Constant pattern	Refs.
Pore diffusion	$\dfrac{15(1-\varepsilon)\varepsilon_p D_p L}{\varepsilon v^{\mathrm{ref}} R_p^2}$	$\dfrac{\partial n_i^\circ}{\partial \tau_1} = \dfrac{N}{15}\dfrac{1}{\xi^2}\dfrac{\partial}{\partial \xi}\left(\xi^2 \dfrac{\partial c_i^\circ}{\partial \xi}\right)$	Numerical	A
Solid diffusion	$\dfrac{15\Lambda D_s L}{\varepsilon v^{\mathrm{ref}} R_p^2}$	$\dfrac{\partial n_i^\circ}{\partial \tau_1} = \dfrac{N}{15}\dfrac{1}{\xi^2}\dfrac{\partial}{\partial \xi}\left(\xi^2 \dfrac{\partial n_i^\circ}{\partial \xi}\right)$	Numerical	B
External mass transfer	$\dfrac{k_f a L}{\varepsilon v^{\mathrm{ref}}}$	$\dfrac{\partial \bar{n}_i^\circ}{\partial \tau_1} = N\,(c_i^\circ - c_i^{e\circ})$	$\dfrac{1}{1-R}\ln\left[\dfrac{(1-c_i^\circ)^R}{c_i^\circ}\right] - 1 = N\,(\zeta - \tau_1)$	C
Linear driving force	$\dfrac{k_n \Lambda L}{\varepsilon v^{\mathrm{ref}}}$	$\dfrac{\partial \bar{n}_i^\circ}{\partial \tau_1} = N\,(n_i^{e\circ} - \bar{n}_i^\circ)$	$\dfrac{1}{1-R}\ln\left[\dfrac{1-c_i^\circ}{c_i^{\circ R}}\right] + 1 = N\,(\zeta - \tau_1)$	D
Reaction kinetics	$\dfrac{k_a c^{\mathrm{ref}}\Lambda L}{(1-R)\varepsilon v^{\mathrm{ref}}}$	$\dfrac{\partial \bar{n}_i^\circ}{\partial \tau_1} = N\,[(1-\bar{n}_i^\circ)c_i^\circ - R\bar{n}_i^\circ(1-c_i^\circ)]$	$\dfrac{1}{1-R}\ln\left[\dfrac{1-c_i^\circ}{c_i^\circ}\right] = N\,(\zeta - \tau_1)$	E
Axial dispersion	$\dfrac{v^{\mathrm{ref}}L}{D_L}$	Eq. (16-128)	$\dfrac{1}{1-R}\ln\left[\dfrac{1-c_i^\circ}{c_i^{\circ R}}\right] = N\,(\zeta - \tau_1)$	F

1: Dimensional rate equations are given in Table 16-11 and 16-12.
A: Hall et al., *Ind. Eng. Chem. Fundam.,* **5,** 212 (1966).
B: Hall et al., *Ind. Eng. Chem. Fundam.,* **5,** 212 (1966); Garg and Ruthven, *Chem. Eng. Sci.,* **28,** 791, 799 (1973).
C: Michaels, *Ind. Eng. Chem.,* **44,** 1922 (1952); Miura and Hashimoto, *J. Chem. Eng. Japan,* **10,** 490 (1977).
D: Glueckauf Coates, *J. Chem. Soc.,* **1947,** 1315 (1947); Vermeulen, *Advances in Chemical Engineering,* **2,** 147 (1958); Hall et al., *Ind. Eng. Chem. Fundam.,* **5,** 212 (1966); Miura and Hashimoto, *J. Chem. Eng. Japan,* **10,** 490 (1977).
E: Walter, *J. Chem. Phys.,* **13,** 229 (1945); Hiester and Vermeulen, *Chem. Eng. Progress,* **48,** 505 (1952).
F: Acrivos, *Chem. Eng. Sci.,* **13,** 1 (1960); Coppola and LeVan, *Chem. Eng. Sci.,* **36,** 967 (1981).

$$-\frac{\partial n_i^\circ}{\partial(\zeta - \tau_1)} + \frac{\partial n_i^\circ}{\partial \tau_1} + \frac{\partial c_i^\circ}{\partial(\zeta - \tau_1)} = \frac{1}{N_{Pe}}\frac{\partial^2 c_i^\circ}{\partial(\zeta - \tau_1)^2} \qquad (16\text{-}139)$$

The partial derivative with respect to τ_1 is discarded and the resulting equation integrated once to give

$$-n_i^\circ + c_i^\circ = \frac{1}{N_{Pe}}\frac{dc_i^\circ}{d(\zeta - \tau_1)} \qquad (16\text{-}140)$$

After eliminating n_i° or c_i° using the adsorption isotherm, Eq. (16-140) can be integrated directly to obtain the constant pattern.

For other mechanisms, the particle-scale equation must be integrated. Equation (16-140) is used to advantage. For example, for external mass transfer acting alone, the dimensionless rate equation in Table 16-13 would be transformed into the $(\zeta - \tau_1, \tau_1)$ coordinate system and derivatives with respect to τ_1 discarded. Equation (16-138) is then used to replace c_i° with $\bar{n}_i^\circ$ in the transformed equation. Furthermore, for this case there are assumed to be no gradients within the particles, so we have $\bar{n}_i^\circ = n_i^\circ$. After making this substitution, the transformed equation can be rearranged to

$$-\frac{dn_i^\circ}{n_i^\circ - c_i^\circ} = d(\zeta - \tau_1) \qquad (16\text{-}141)$$

Since n_i° and c_i° are related by the adsorption isotherm, Eq. (16-141) can be integrated.

The integration of Eq. (16-140) or (16-141) as an indefinite integral will give an integration constant that must be evaluated to center the transition properly. The material balance depicted in Fig. 16-26 is used. The two shaded regions must be of equal area if the stoichiometric center of the transition is located where the throughput parameter is unity. Thus, we have

$$\int_{-\infty}^{0}(1 - n_i^\circ)\,d(\zeta - \tau_1) = \int_0^\infty n_i^\circ\,d(\zeta - \tau_1) \qquad (16\text{-}142)$$

Integrating Eq. (16-142) by parts gives

$$\int_0^1 (N - NT)\,dn_i^\circ = 0 \qquad (16\text{-}143)$$

For all mechanisms except axial dispersion, the transition can be centered just as well using c_i°, because of Eq. (16-138). For axial dispersion, the transition should be centered using n_i°, provided the fluid-phase accumulation term in the material balance, Eq. (16-124),

can be neglected. If fluid-phase accumulation is important, then the transition for axial dispersion can be centered by taking into account the relative quantities of solute held in the fluid and adsorbed phases.

Constant pattern solutions for the individual mechanisms and constant separation factor isotherm are given in Table 16-13. The solutions all have the expected dependence on R—the more favorable the isotherm, the sharper the profile.

Figure 16-27 compares the various constant pattern solutions for $R = 0.5$. The curves are of a similar shape. The solution for reaction kinetics is perfectly symmetrical. The curves for the axial dispersion fluid-phase concentration profile and the linear driving force approximation are identical except that the latter occurs one transfer unit further down the bed. The curve for external mass transfer is exactly that for the linear driving force approximation turned upside down [i.e., rotated 180° about $c_i^\circ = n_i^\circ = 0.5$, $N(\zeta - \tau_1) = 0$]. The linear driving force approximation provides a good approximation for both pore diffusion and surface diffusion.

Because of the close similarity in shape of the profiles shown in Fig. 16-27 (as well as likely variations in parameters; e.g., concentration-dependent surface diffusion coefficient), a controlling mechanism cannot be reliably determined from transition shape. If reliable correlations are not available and rate parameters cannot be measured in independent experiments, then particle diameters, velocities, and other factors should be varied and the observed impact considered in relation to the definitions of the numbers of transfer units.
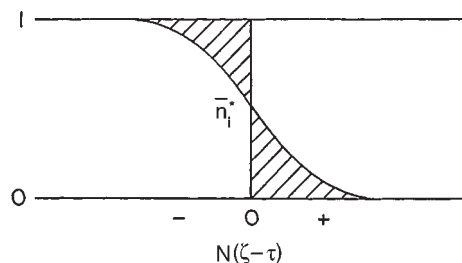

FIG. 16-26 Material balance for centering profile [*from LeVan in Rodrigues et al. (eds), Adsorption: Science and Technology, Kluwer Academic Publishers, Dordrecht, The Netherlands, 1989; reprinted with permission.*]
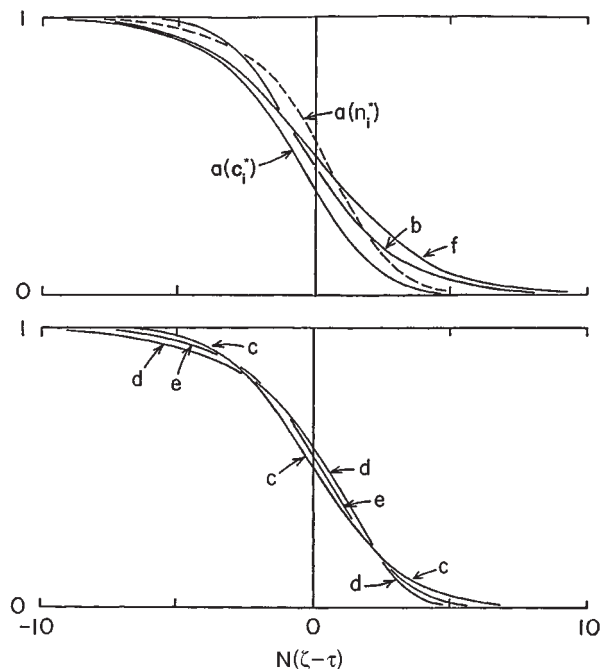
FIG. 16-27 Constant pattern solutions for $R = 0.5$. Ordinant is c_i° or n_i° except for axial dispersion for which individual curves are labeled: a, axial dispersion; b, external mass transfer; c, pore diffusion (spherical particles); d, surface diffusion (spherical particles); e, linear driving force approximation; f, reaction kinetics. [*from LeVan in Rodrigues et al. (eds.),* Adsorption: Science and Technology, *Kluwer Academic Publishers, Dordrecht, The Netherlands, 1989; reprinted with permission.*]

Breakthrough Behavior for Axial Dispersion Breakthrough behavior for adsorption with axial dispersion in a deep bed is not adequately described by the constant pattern profile for this mechanism. Equation (16-128), the partial differential equation of the second order Fickian model, requires two boundary conditions for its solution. The constant pattern pertains to a bed of infinite depth—in obtaining the solution we apply the downstream boundary condition $c_i^\circ \to 0$ as $N_{Pe}\zeta \to \infty$. Breakthrough behavior presumes the existence of a bed outlet, and a boundary condition must be applied there.

The full mathematical model for this problem is Eq. (16-128) with boundary conditions

$$c_i^\circ - \frac{1}{N_{Pe}} \frac{\partial c_i^\circ}{\partial \zeta} = 1 \qquad \text{at} \qquad \zeta = 0 \qquad (16\text{-}144)$$

$$\frac{\partial c_i^\circ}{\partial \zeta} = 0 \qquad \text{at} \qquad \zeta = 1 \qquad (16\text{-}145)$$

and an initial condition. Equation (16-144) specifies a constant flux at the bed inlet, and Eq. (16-145), the Danckwerts-type boundary condition at the bed outlet, is appropriate for fixed-bed adsorption, provided that the partition ratio is large.

The solution to this model for a deep bed indicates an increase in velocity of the fluid-phase concentration wave during breakthrough. This is most dramatic for the rectangular isotherm—the instant the bed becomes saturated, the fluid-phase profile jumps in velocity from that of the adsorption transition to that of the fluid, and a near shocklike breakthrough curve is observed [Coppola and LeVan, *Chem. Eng. Sci.,* **36,** 967 (1981)].

Extensions Existence, uniqueness, and stability criteria have been developed for the constant pattern [Cooney and Lightfoot, *Ind. Eng. Chem. Fundam.,* **4,** 233 (1965); Rhee et al., *Chem. Eng. Sci.,* **26,** 1571 (1971); Rhee and Amundson, *Chem. Eng. Sci.,* **26,** 1571 (1971), **27,** 199 (1972), **29,** 2049 (1974)].

The rectangular isotherm has received special attention. For this, many of the constant patterns are developed fully at the bed inlet, as shown for external mass transfer [Klotz, *Chem. Revs.,* **39,** 241 (1946); pore diffusion [Vermeulen, *Adv. Chem. Eng.,* **2,** 147 (1958); Hall et al., *Ind. Eng. Chem. Fundam.,* **5,** 212 (1966)], the linear driving force approximation [Cooper, *Ind. Eng. Chem. Fundam.,* **4,** 308 (1965)], reaction kinetics [Hiester and Vermeulen, *Chem. Eng. Progress,* **48,** 505 (1952); Bohart and Adams, *J. Amer. Chem. Soc.,* **42,** 523 (1920)], and axial dispersion [Coppola and LeVan, *Chem. Eng. Sci.,* **38,** 991 (1983)].

Multiple mass-transfer resistances have been considered in many studies [Vermeulen, *Adv. in Chem. Eng.,* **2,** 147 (1958); Vermeulen et al., Ruthven, gen. refs.; Fleck et al., *Ind. Eng. Chem. Fundam.,* **12,** 95 (1973); Yoshida et al., *Chem. Eng. Sci.,* **39,** 1489 (1984)].

Treatments of constant pattern behavior have been carried out for multicomponent adsorption [Vermeulen, *Adv. in Chem. Eng.,* **2,** 147 (1958); Vermeulen et al., Ruthven, gen. refs.; Rhee and Amundson, *Chem. Eng. Sci.,* **29,** 2049 (1974); Cooney and Lightfoot, *Ind. Eng. Chem. Fundam.,* **5,** 25 (1966); Cooney and Strusi, *Ind. Eng. Chem. Fundam.,* **11,** 123 (1972); Bradley and Sweed, *AIChE Symp. Ser. No. 152,* **71,** 59 (1975)]. The behavior is such that coexisting compositions advance through the bed together at a uniform rate; this is the *coherence* concept of Helfferich and coworkers [gen. refs.].

Nontrace systems have been considered [Sircar and Kumar, *Ind. Eng. Chem. Proc. Des. Dev.,* **22,** 271 (1983)].

Constant patterns have been developed for adiabatic adsorption [Pan and Basmadjian, *Chem. Eng. Sci.,* **22,** 285 (1967); Ruthven et al., *Chem. Eng. Sci.,* **30,** 803 (1975); Kaguei et al., *Chem. Eng. Sci.,* **42,** 2964 (1987)].

The constant pattern concept has also been extended to circumstances with nonplug flows, with various degrees of rigor, including flow profiles in tubes [Sartory, *Ind. Eng. Chem. Fundam.,* **17,** 97 (1978); Tereck et al., *Ind. Eng. Chem. Res.,* **26,** 1222 (1987)], wall effects [Vortmeyer and Michael, *Chem. Eng. Sci.,* **40,** 2135 (1985)], channeling [LeVan and Vermeulen in Myers and Belfort (eds.), *Fundamentals of Adsorption,* Engineering Foundation, New York (1984), pp. 305–314, *AIChE Symp. Ser. No. 233,* **80,** 34 (1984)], networks [Avilés and LeVan, *Chem. Eng. Sci.,* **46,** 1935 (1991)], and general structures of constant cross section [Rudisill and LeVan, *Ind. Eng. Chem. Res.,* **29,** 1054 (1991)].

SQUARE ROOT SPREADING FOR LINEAR ISOTHERMS

The simplest isotherm is $n_i^\circ = c_i^\circ$, corresponding to $R = 1$. For this isotherm, the rate equation for external mass transfer, the linear driving force approximation, or reaction kinetics, can be combined with Eq. (16-130) to obtain

$$\frac{\partial \overline{n}_i^\circ}{\partial \tau_1} = -\frac{\partial c_i^\circ}{\partial \zeta} = N(c_i^\circ - \overline{n}_i^\circ) \qquad (16\text{-}146)$$

The solution to this equation, with initial condition $n_i^\circ = 0$ at $\tau_1 = 0$ and boundary condition $c_i^\circ = 1$ at $\zeta = 0$, originally obtained for an analogous heat transfer case [Anzelius, *Z. Angew. Math. Mech.,* **6,** 291 (1926); Schumann, *J. Franklin Inst.,* **208,** 405 (1929)], is

$$c_i^\circ = J(N\zeta, N\tau_1) \qquad n_i^\circ = 1 - J(N\tau_1, N\zeta) \qquad (16\text{-}147)$$

where the J function is [Hiester and Vermeulen, *Chem. Eng. Prog.,* **48,** 505 (1952)]

$$J(s, t) = 1 - \int_0^s e^{-t-\xi} I_0(2\sqrt{t\xi}) \, d\xi \qquad (16\text{-}148)$$

where I_0 is the modified Bessel function of the first kind of order zero. This linear isotherm result can be generalized to remove the assumption that $\hat{c}_i^\circ \approx c_i^\circ$ if the throughput parameter is redefined as

$$\tau_1 = \frac{\tau - \varepsilon\zeta}{(1 - \varepsilon)(\rho_p K_i + \varepsilon_p)}$$

The J function is plotted in Fig. 16-28 and tables are available (e.g., Sherwood et al., *Mass Transfer,* McGraw-Hill, New York, 1975). Vermeulen et al. (gen. refs.) discuss several approximations of the J function. For large arguments it approaches
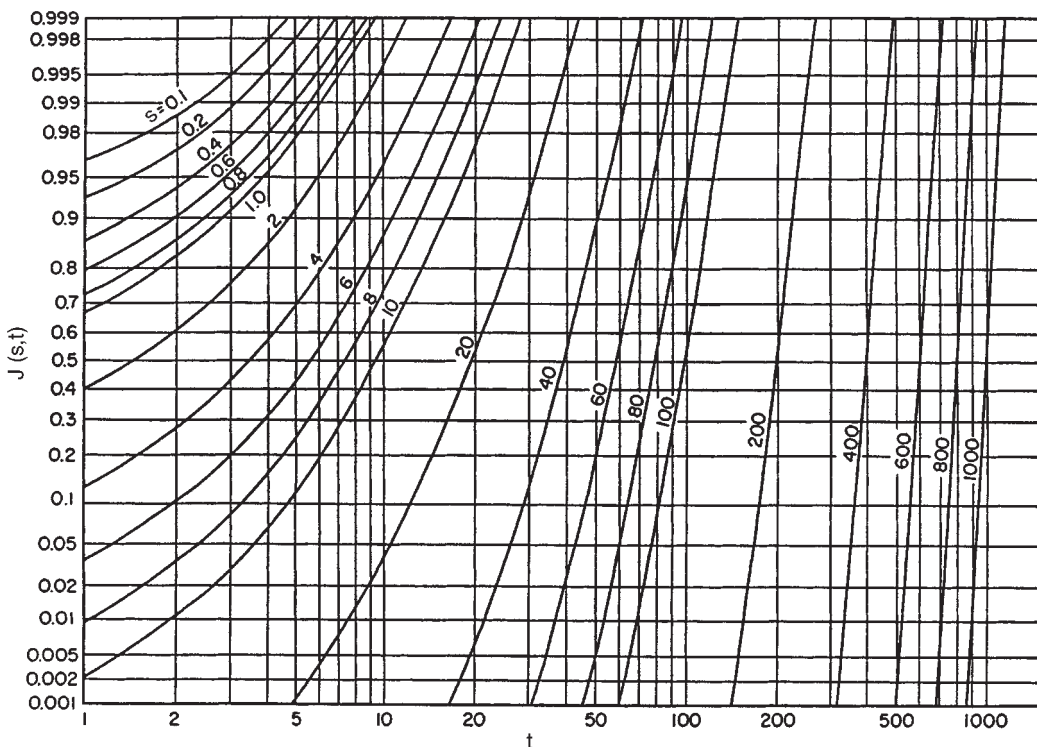
FIG. 16-28   Plot of the function $J(s, t)$ defined by Eq. (16-148).

$$J(s, t) = \frac{1}{2} \text{ erfc } [\sqrt{s} - \sqrt{t}] \qquad (16\text{-}149)$$

A derivation for particle-phase diffusion accompanied by fluid-side mass transfer has been carried out by Rosen [*J. Chem. Phys.*, **18**, 1587 (1950); ibid., **20**, 387 (1952); *Ind. Eng. Chem.*, **46**, 1590 (1954)] with a limiting form at $N > 50$ of

$$c_i^\circ = \frac{1}{2} \text{ erfc } \left[\frac{\sqrt{N}}{2} (\zeta - \tau_1) \right] \qquad (16\text{-}150)$$

For axial dispersion in a semi-infinite bed with a linear isotherm, the complete solution has been obtained for a constant flux inlet boundary condition [Lapidus and Amundson, *J. Phys. Chem.*, **56**, 984 (1952); Brenner, *Chem. Eng. Sci.*, **17**, 229 (1962); Coates and Smith, *Soc. Petrol. Engrs. J.*, **4**, 73 (1964)]. For large N, the leading term is

$$c_i^\circ = \frac{1}{2} \text{ erfc } \left[\frac{\sqrt{N}}{2\sqrt{\tau_1}} (\zeta - \tau_1) \right] \qquad (16\text{-}151)$$

All of these solutions are very similar and show, for large N, a wave with breadth proportional to the square root of the bed depth through which it has passed.

COMPLETE SOLUTION FOR REACTION KINETICS

In general, full time-dependent analytical solutions to differential equation-based models of the above mechanisms have not been found for nonlinear isotherms. Only for reaction kinetics with the constant separation factor isotherm has a full solution been found [Thomas, *J. Amer. Chem. Soc.*, **66**, 1664 (1944)]. Referred to as the *Thomas solution*, it has been extensively studied [Amundson, *J. Phys. Colloid Chem.*, **54**, 812 (1950); Hiester and Vermeulen, *Chem. Eng. Progress*, **48**, 505 (1952); Gilliland and Baddour, *Ind. Eng. Chem.*, **45**, 330 (1953); Vermeulen, *Adv. in Chem. Eng.*, **2**, 147 (1958)]. The solution to Eqs. (16-130) and (16-130) for the same boundary conditions as Eq. (16-146) is

$$c_i^\circ = \frac{J(RN\zeta, N\tau_1)}{J(RN\zeta, N\tau_1) + e^{-(R-1)N(\zeta - \tau_1)}[1 - J(N\zeta, RN\tau_1)]}$$

$$n_i^\circ = \frac{1 - J(N\tau_1, RN\zeta)}{J(RN\zeta, N\tau_1) + e^{-(R-1)N(\zeta - \tau_1)}[1 - J(N\zeta, RN\tau_1)]} \qquad (16\text{-}152)$$

The solution gives all of the expected asymptotic behaviors for large N—the proportionate pattern spreading of the simple wave if $R > 1$, the constant pattern if $R < 1$, and square root spreading for $R = 1$.

NUMERICAL METHODS AND CHARACTERIZATION OF WAVE SHAPE

For the solution of sophisticated mathematical models of adsorption cycles including complex multicomponent equilibrium and rate expressions, two numerical methods are popular. These are finite difference methods and orthogonal collocation. The former vary in the manner in which distance variables are discretized, ranging from simple backward difference stage models (akin to the plate theory of chromatography) to more involved schemes exhibiting little numerical dispersion. Collocation methods are often thought to be faster computationally, but oscillations in the polynomial trial function can be a problem. The choice of best method is often the preference of the user.

For both the finite difference and collocation methods a set of coupled ordinary differential equations results which are integrated forward in time using the method of lines. Various software packages implementing Gear's method are popular.

The development of mathematical models is described in several of the general references [Guiochon et al., Rhee et al., Ruthven, Ruthven et al., Suzuki, Tien, Wankat, and Yang]. See also Finlayson [*Numerical Methods for Problems with Moving Fronts,* Ravenna Park, Washington, 1992; Holland and Liapis, *Computer Methods for Solving Dynamic Separation Problems,* McGraw-Hill, New York, 1982; Villadsen and Michelsen, *Solution of Differential Equation Models by*

Polynomial Approximation, Prentice Hall, Englewood Cliffs, New Jersey, 1978].

For the characterization of wave shape and breakthrough curves, three methods are popular. The MTZ method [Michaels, *Ind. Eng. Chem.,* **44,** 1922 (1952)] measures the breadth of a wave between two chosen concentrations (e.g., $c_i^\circ = 0.05$ and 0.95 or $c_i^\circ = 0.01$ and 0.99). Outside of a laboratory, the measurement of full breakthrough curves is rare, so the breadth of the MTZ is often estimated from an independently determined stoichiometric capacity and a measured small concentration in the "toe" of the breakthrough curve. A second method for characterizing wave shape is by the slope of the breakthrough curve at its midheight (i.e., $c_i^\circ = 0.5$ [Vermeulen et al., gen. refs.]). The use of moments of the slope of breakthrough curves is a third means for characterization. They can often be used to extract numerical values for rate coefficients for linear systems [Ruthven, Suzuki, gen. refs.; Nauman and Buffham, *Mixing in Continuous Flow Systems,* Wiley-Interscience, New York, 1983]. The method of moments is discussed further in the following part of this section.

CHROMATOGRAPHY

CLASSIFICATION

Chromatography is a sorptive separation process where a portion of a solute mixture (feed) is introduced at the inlet of a column containing a selective adsorbent (stationary phase) and separated over the length of the column by the action of a carrier fluid (mobile phase) that is continually supplied to the column following introduction of the feed. The mobile phase is generally free of the feed components, but may contain various other species introduced to modulate the chromatographic separation. The separation occurs as a result of the different partitioning of the feed solutes between the stationary phase; the separated solutes are recovered at different times in the effluent from the column. Chromatography is used both in analysis of mixtures and in preparative and process-scale applications. It can be used for both trace-level and for bulk separations both in the gas and the liquid phase.

Modes of Operation The classical modes of operation of chromatography as enunciated by Tiselius [*Kolloid Z.,* **105,** 101 (1943)] are: elution chromatography, frontal analysis, and displacement development. Basic features of these techniques are illustrated in Fig. 16-29. Often, each of the different modes can be implemented with the same equipment and stationary phase. The results are, however, quite different in the three cases.

Elution Chromatography The components of the mobile phase supplied to the column after feed introduction have less affinity for the stationary phase than any of the feed solutes. Under trace conditions, the feed solutes travel through the column as bands or zones at different velocities that depend only on the composition of the mobile phase and the operating temperature and that exit from the column at different times.

Two variations of the technique exists: **isocratic elution,** when the mobile phase composition is kept constant, and **gradient elution,** when the mobile phase composition is varied during the separation. Isocratic elution is often the method of choice for analysis and in process applications when the retention characteristics of the solutes to be separated are similar and not dramatically sensitive to very small changes in operating conditions. Isocratic elution is also generally practical for systems where the equilibrium isotherm is linear or nearly linear. In all cases, isocratic elution results in a dilution of the separated products.
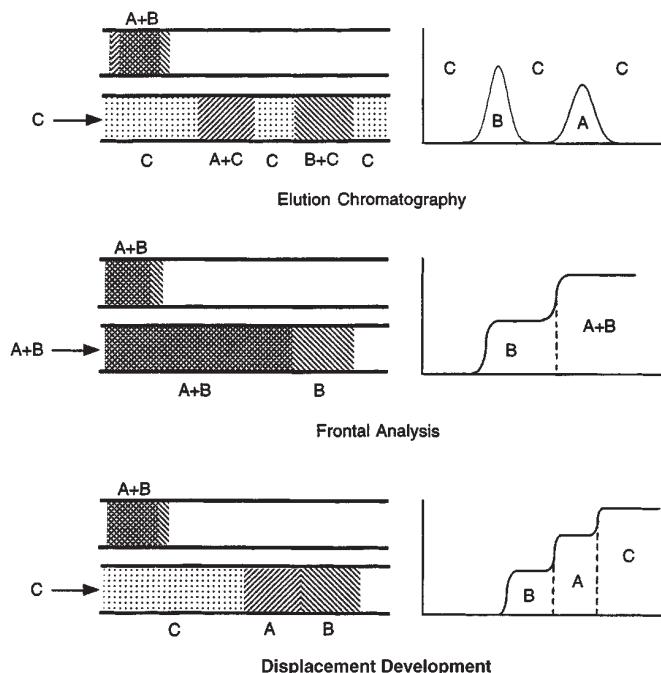

FIG. 16-29 Modes of operation of chromatography for the separation of a mixture of two components A and B. Figures on the left represent a schematic of the column with sample passing through it. Top diagrams show column at end of feed step. Figures on the right show the corresponding effluent concentrations. C is either the eluent or the displacer (adapted from Ettre, 1980).

In **gradient elution,** the eluting strength of the mobile phase is gradually increased after supplying the feed to the column. In liquid chromatography, this is accomplished by changing the mobile phase composition. The gradient in eluting strength of the mobile phase that is generated in the column is used to modulate the separation allowing control of the retention time of weakly and strongly retained components. A similar effect can be obtained in gas chromatography by modulating the column temperature. In either case, the column has to be brought back to the initial conditions before the next cycle is commenced.

Generally, gradient elution is best suited for the separation of complex mixtures that contain both species that interact weakly with the stationary phase and species that interact strongly. Since the eluting strength of the mobile phase is adjusted continuously, weakly retained components of a mixture are separated in the initial phase when the relative elution strength of the mobile phase is low, while strongly retained components are separated later in the gradient when the elution strength is high. In addition, the technique is used to obtain reproducible chromatographic separations when the solute retention characteristics are extremely sensitive to the operating conditions, as in the case of the chromatography of biopolymers, such as proteins. These molecules are often found to be very strongly retained in an extremely small range of mobile phase compositions and completely unretained elsewhere, making it practically impossible to obtain reproducible isocratic separations.

Frontal Analysis   The feed mixture to be separated is continuously supplied to the column where the mixture components are competitively retained by the stationary phase. These solutes are partially separated in a series of fronts, preceded downstream by the least strongly retained species forming a pure component band, and upstream by the feed mixture. The technique is best suited for the removal of strongly adsorbed impurities present in trace amounts from an unretained or weakly retained product of interest. In this case, a large amount of feed can be processed before the impurities begin to break through. When this point is reached, the bed is washed to remove any desired product from the interstitial voids, and the adsorbent is regenerated. The method can only provide a single component in pure form, but avoids product dilution completely. Multicomponent separations require a series of processing steps; either a series of frontal analysis separations, or a combination of elution and displacement separations. Example 10 illustrates bed concentration profiles for the frontal analysis separation of two components.

Displacement Development   The column is partially loaded with the feed mixture as in frontal analysis, usually for conditions where all solutes of interest are strongly and competitively retained by the stationary phase. The feed supply is then stopped and a mobile phase containing the **displacer,** a component that has an affinity for the stationary phase stronger than any of the feed components, is fed to the column. The advancement of the displacer front through the column causes desorption of the feed components and their competitive readsorption downstream of the displacer front. As in frontal chromatography, the less strongly retained species tends to migrate faster down the column concentrating in a band farthest from the displacer front, while the most strongly adsorbed solute tends to move more slowly concentrating in a band adjacent to the displacer front. If the column is sufficiently long, all feed components eventually become distributed into a pattern of adjacent pure component bands where each upstream component acts as a displacer for each downstream species located in the band immediately downstream. When this occurs, all bands in the displacement train move at the same velocity which is equal to the velocity of the displacer front and the bed concentration profile is called an **isotachic pattern.**

The various operational steps of a displacement development separation are shown in Fig. 16-30. Ideally, the separated species exit the column as adjacent rectangular bands in order of increasing affinity for the stationary phase as shown in this figure. In practice, dispersion effects result in a partial mixing of adjacent bands requiring recycling of portions of the effluent that do not meet purity requirements. Following separation, the displacer has to be removed from the column with a suitable regenerant and the initial conditions of the column restored before the next cycle. Column regeneration may consume a significant portion of the cycle, when removal of the displacer is difficult.

Displacement chromatography is suitable for the separation of multicomponent bulk mixtures. For dilute multicomponent mixtures it allows a simultaneous separation and concentration. Thus, it permits the separation of compounds with extremely low separation factors without the excessive dilution that would be obtained in elution techniques.
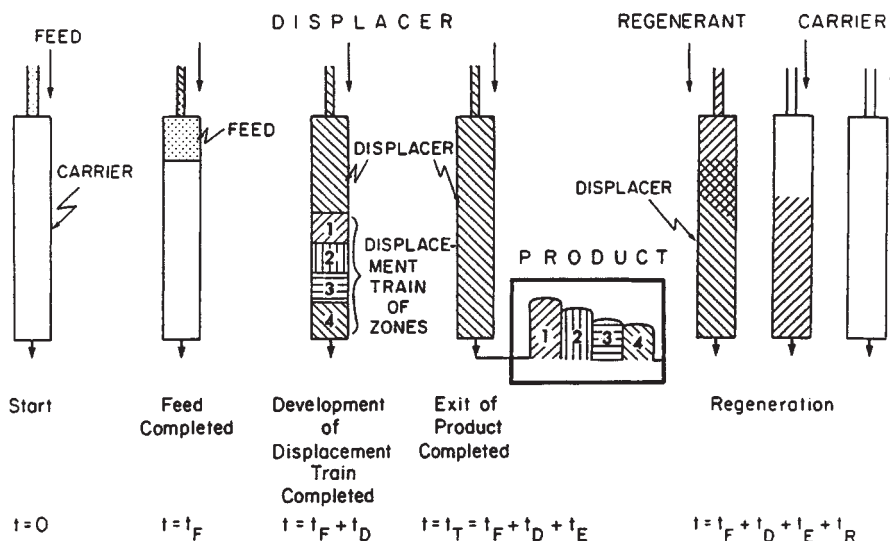

FIG. 16-30   Operational steps in displacement chromatography. The column, initially equilibrated with a carrier solvent at time 0, is loaded with feed until time t_F and supplied with displacer for a time $t_D + t_E$. Development of the displacement train occurs during the time t_D and elution of the separated products ends at time t_E. t_R is the time required to remove the displacer from the column and restore the initial conditions. Components are numbered in order of decreasing affinity for the stationary phase. [*Reference: Horvath et al.,* J. Chromatogr., **218,** 365 (1981). *Reprinted with permission of* J. Chromatogr.]

Other modes of operation, including recycle and flow reversal schemes and continuous chromatography, are discussed in Ganetsos and Barker (*Preparative and Production Scale Chromatography,* Marcel Dekker, New York, 1993).

CHARACTERIZATION OF EXPERIMENTAL CHROMATOGRAMS

Method of Moments   The first step in the analysis of chromatographic systems is often a characterization of the column response to small pulse injections of a solute under trace conditions in the Henry's law limit. For such conditions, the statistical moments of the response peak are used to characterize the chromatographic behavior. Such an approach is generally preferable to other descriptions of peak properties which are specific to Gaussian behavior, since the statistical moments are directly correlated to equilibrium and dispersion parameters. Useful references are Schneider and Smith [*AIChE J.,* **14,** 762 (1968)], Suzuki and Smith [*Chem. Eng. Sci.,* **26,** 221 (1971)], and Carbonell et al. [*Chem. Eng. Sci.,* **9,** 115 (1975); **16,** 221 (1978)].

The relevant moments are:

$$\mu_0 = \int_0^\infty c_i \, dt \tag{16-153}$$

$$\mu_1 = \frac{1}{\mu_0} \int_0^\infty c_i t \, dt \tag{16-154}$$

$$\sigma^2 = \frac{1}{\mu_0} \int_0^\infty c_i (t - \mu_1)^2 \, dt \tag{16-155}$$

where c_i is the peak profile. μ_0 represents the area, μ_1 the mean residence time, and σ^2 the variance of the response peak. Moments can be calculated by numerical integration of experimental profiles.

The **retention factor** is defined as a dimensionless peak locator as:

$$k_i' = \frac{\mu_1 - \mu_1^0}{\mu_1^0} \tag{16-156}$$

where μ_1^0 is the first moment obtained for an inert tracer which is excluded from the stationary phase. k_i' is a partition ratio representing the equilibrium ratio of the amount of solute in the stationary phase (including any pores) and the amount in the external mobile phase. Another commonly used definition of the retention factor uses as a reference the first moment of an inert that has access to all the pores.

The number of plates, N_p, and the height equivalent to a theoretical plate, HETP, are defined as measures of dispersion effects as:

$$N_p = \frac{L}{\text{HETP}} = \frac{\mu_1^2}{\sigma^2} \tag{16-157}$$

$$\text{HETP} = \frac{\sigma^2 L}{\mu_1^2} \tag{16-158}$$

A high number of plates and a low HETP indicate a high column efficiency.

Higher moments can also be computed and used to define the skewness of the response peak. However, difficulties often arise in such computations as a result of drifting of the detection system.

In practice, experimental peaks can be affected by extracolumn retention and dispersion factors associated with the injector, connections, and any detector. For linear chromatography conditions, the apparent response parameters are related to their corresponding true column value by

$$\mu_1^{app} = \mu_1 + \mu_1^{inj} + \mu_1^{conn} + \mu_1^{det} \tag{16-159}$$

$$\sigma^{2app} = \sigma^2 + \sigma^{2inj} + \sigma^{2conn} + \sigma^{2det} \tag{16-160}$$

Approximate Methods   For certain conditions, symmetrical, Gaussian-like peaks are obtained experimentally. Such peaks may be empirically described by:

$$c_i = \frac{Q_i/F_v}{\sigma\sqrt{2\pi}} \exp\left[-\left(\frac{t - t_{Ri}}{\sigma\sqrt{2}}\right)^2\right] = \frac{Q_i/F_v}{t_{Ri}} \sqrt{\frac{N_p}{2\pi}} \exp\left[-\frac{N_p}{2}\left(\frac{t}{t_{Ri}} - 1\right)^2\right] \tag{16-161}$$

where Q_i is the amount of solute injected, F_v is the volumetric flow rate, and t_{Ri} is the peak apex time. The relationships between the moments and other properties of such peaks are shown in Fig. 16-31. For such peaks, approximate calculations of the number of plates can be done with the following equations:

$$N_p = 5.54 \left(\frac{t_{Ri}}{\Delta}\right)^2 \tag{16-162}$$

$$N_p = 16 \left(\frac{t_{Ri}}{W}\right)^2 \tag{16-163}$$

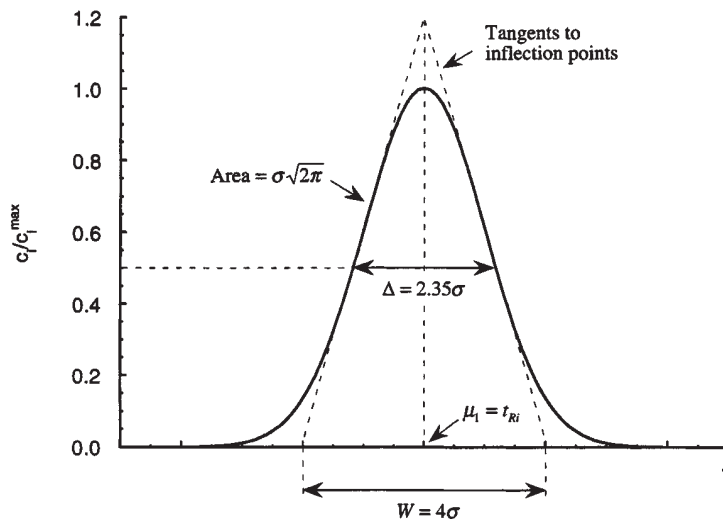$$N_p = 2\pi \left(\frac{c_i^{max} t_{Ri}}{\mu_0}\right)^2 \tag{16-164}$$

FIG. 16-31   Properties of a Gaussian peak. c_i^{max} is the peak height; t_{Ri}, the peak apex time; σ, the standard deviation; Δ, the peak width at midheight; and W, the distance between the baseline intercepts of the tangents to the peak.

where Δ is the peak width at half peak height and W is the distance between the baseline intercepts of the tangents to the inflection points of the peak.

In general, Gaussian behavior can be tested by plotting the cumulative fractional recovery $\int_0^t c_i \, dt/\mu_0$ versus time on probability-linear coordinates; if the plot is linear, Gaussian behavior is confirmed. For nearly Gaussian peaks, calculations of N_p based on Eqs. (16-162) to (16-164) provide results close to those obtained with a rigorous calculation of moments. When deviations from Gaussian behavior are significant, however, large errors can be obtained using these expressions.

Tailing Peaks   Tailing peaks can be obtained experimentally when the column efficiency is very low, when there are large extracolumn dispersion effects, when the stationary phase is heterogeneous (in the sense that it contains different adsorption sites), or when the adsorption equilibrium deviates from the Henry's law limit. Asymmetrical tailing peaks can some times be described empirically by an exponentially modified Gaussian (EMG) defined as the convolute integral of a Gaussian constituent with mean time t_G and standard deviation σ_G and an exponential decay with time constant τ_G [Grushka, *Anal. Chem.*, **44**, 1733 (1972)]:

$$c_i = \frac{Q_i/F_v}{\sigma_G \tau_G \sqrt{2\pi}} \int_0^\infty \exp\left[-\left(\frac{t - t_G - t'}{\sigma_G \sqrt{2}}\right)^2 - \frac{t'}{\tau_G}\right] dt' \quad (16\text{-}165)$$

Although a numerical integration is required to compute the peak profile, the moments are calculated directly as $\mu_1 = t_G + \tau_G$ and $\sigma^2 = \sigma_G^2 + \tau_G^2$ and the **peak skew** as:

$$\text{Peak skew} = \frac{1}{\mu_0 \sigma^3} \int_0^\infty c_i(t - \mu_1)^3 \, dt \sim \frac{2(\tau_G/\sigma_G)^3}{[1 + (\tau_G/\sigma_G)^2]^{3/2}} \quad (16\text{-}166)$$

For EMG peaks, peak skew increases with the ratio τ_G/σ_G. Figure 16-32 illustrates the characteristics of such a peak calculated for $\tau_G/\sigma_G = 1.5$. In general, with $\tau_G/\sigma_G > 1$ (peak skew > 0.7), a direct calculation of the moments is required to obtained a good approximation of the true value of N_p, since other methods give a large error (Yau et al., *Moderns Size-Exclusion Liquid Chromatography*, Wiley, New York, 1979). Alternatively, Eq. (16-165) can be fitted to experimental peaks to determine the optimum values of t_G, σ_G, and τ_G.

In practice, the calculation of peak skew for highly tailing peaks is rendered difficult by baseline errors in the calculation of third moments. The **peak asymmetry factor**, $A_s = b/a$, at 10 percent of peak height (see Fig. 16-32) is thus frequently used. An approximate relationship between peak skew and A_s for tailing peaks, based on data in Yau et al. is: Peak skew = $[0.51 + 0.19/(A_s - 1)]^{-1}$. Values of $A_s < 1.25$

(corresponding to peak skew < 0.7) are generally desirable for an efficient chromatographic separation.

Resolution   The chromatographic separation of two components, A and B, under trace conditions with small feed injections can be characterized in terms of the resolution, R_s. For nearly Gaussian peaks:

$$R_s = \frac{2(t_{R,A} - t_{R,B})}{W_A + W_B} \sim \frac{\Delta t_R}{4\sigma_{AB}} \quad (16\text{-}167)$$

where Δt_R is the difference in retention time of the two peaks and $\sigma_{AB} = (\sigma_A + \sigma_B)/2$ is the average of their standard deviations. When Eq. (16-161) is applicable, the resolution for two closely spaced peaks is approximated by:

$$R_s = \frac{1}{2} \frac{\alpha - 1}{\alpha + 1} \frac{\bar{k}_i'}{1 + \bar{k}_i'} \sqrt{N_p}$$

$$\sim \frac{\alpha - 1}{4} \frac{k_A'}{1 + k_A'} \sqrt{N_p}, \qquad \text{for } \alpha \sim 1 \quad (16\text{-}168)$$

where $\alpha = k_A'/k_B'$ and $\bar{k}' = (k_A' + k_B')/2$.

Equation (16-168) shows that the resolution is the result of independent effects of the separation selectivity (α), column efficiency (N_p), and capacity ($\bar{k}'$). Generally, peaks are essentially completely resolved when $R_s = 1.5$ (>99.5 percent separation). In practice, values of $R_s \sim 1$, corresponding to 98 percent separation, are often considered adequate.

The preceding equations are accurate to within about 10 percent for feed injections that do not exceed 40 percent of the final peak width. For large, rectangular feed injections, the baseline width of the response peak is approximated by:

$$W \sim 4\sigma + t_F \quad (16\text{-}169)$$

where 4σ is the baseline width obtained with a small pulse injection and t_F is the duration of feed injection. In this case, the resolution is defined as (see Ruthven, gen. refs., pp. 324–331):

$$R_s = \frac{t_{R,A} - t_{R,B} - t_F}{4\sigma_{AB}} \quad (16\text{-}170)$$

For strongly retained components ($\bar{k}' \gg 1$), the number of plates required to obtain a given resolution with a finite feed injection is approximated by:

$$N_p = 4R_s^2 \left(\frac{\alpha + 1}{\alpha - 1}\right)^2 \left(1 + \frac{t_F}{4\sigma_{AB}R_s}\right)^2 \quad (16\text{-}171)$$
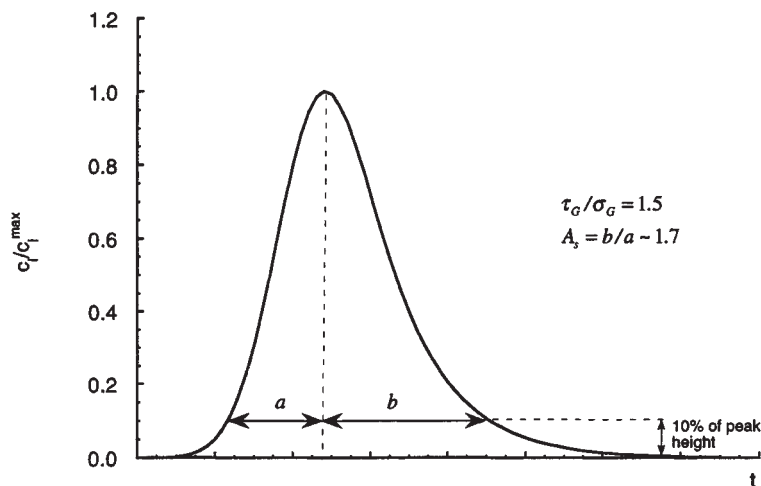

FIG. 16-32   Exponentially modified Gaussian peak with $\tau_G/\sigma_G = 1.5$. The graph also shows the definition of the peak asymmetry factor A_s at 10 percent of peak height.

PREDICTION OF CHROMATOGRAPHIC BEHAVIOR

The conservation equations and the rate models described in the "Rate and Dispersion Factors" can normally be used for a quantitative description of chromatographic separations. Alternatively, **plate models** can be used for an approximate prediction, lumping together all dispersion contributions into a single parameter, the HETP or the number of plates [Sherwood et al., *Mass Transfer,* McGraw-Hill, New York, 1975, p. 576; Dondi and Guiochon, *Theoretical Advancements in Chromatography and Related Techniques,* NATO-ASI, Series C: Mathematical and Physical Sciences, vol. 383, Kluwer, Dordrecht, 1992, pp. 1–61]. Exact analytic solutions are generally available for linear isocratic elution under trace conditions (see Dondi and Guiochon, ibid., Ruthven [gen. refs., pp. 324–335], Suzuki [gen. refs., pp. 224–243]). Other cases generally require numerical solution (see Guiochon et al., gen. refs.) or approximate treatments with simplified rate models.

Isocratic Elution   In the simplest case, feed with concentration c_i^F is applied to the column for a time t_F followed by the pure carrier fluid. Under trace conditions, for a linear isotherm with external mass-transfer control, the linear driving force approximation or reaction kinetics (see Table 16-12), solution of Eq. (16-146) gives the following expression for the dimensionless solute concentration at the column outlet:

$$c_i^\circ = J(N, N\tau_1) - J(N, N\tau_1') \qquad (16\text{-}172)$$

where N is the number of transfer units given in Table 16-13 and $\tau_1 = (\varepsilon v t/L - \varepsilon)/[(1 - \varepsilon)(\rho_p K_i + \varepsilon_p)]$ the throughput parameter (see "Square Root Spreading for Linear Isotherms" in "Fixed Bed Transitions"). τ_1' represents the value of τ_1 with time measured from the end of the feed step. Thus, the column effluent profile is obtained as the difference between a breakthrough profile for a feed started at $t = 0$ and another for a feed started at $t = t_F$.

The behavior predicted by this equation is illustrated in Fig. 16-33 with $N = 80$. $\tau_F = (\varepsilon v t_F/L)/[(1 - \varepsilon)(\rho_p K_i + \varepsilon_p)]$ is the dimensionless duration of the feed step and is equal to the amount of solute fed to the column divided by the sorption capacity. Thus, at $\tau_F = 1$, the column has been supplied with an amount of solute equal to the stationary phase capacity. The graph shows the transition from a case where complete saturation of the bed occurs before elution ($\tau_F = 1$) to incomplete saturation as τ_F is progressively reduced. The lower curves with $\tau_F \leq 0.4$ are seen to be nearly Gaussian and centered at a dimensionless time $\tau_m \sim (1 - \tau_F/2)$. Thus, as $\tau_F \to 0$, the response curve approaches a Gaussian centered at $\tau_1 = 1$.

When τ_F is small ($<<0.4$), the solution for a feed pulse represented by a Dirac's delta function at $\zeta = 0$ can be used in lieu of Eq. (16-172). In terms of the dimensionless concentration $c_i^\circ = c_i/c_i^F$ (Sherwood et al., ibid., pp. 571–577):

$$c_i^\circ = \frac{\tau_F N}{\sqrt{\tau_1}}\, e^{-N} e^{-N\tau_1} I_1(2N \sqrt{\tau_1}) \qquad (16\text{-}173)$$

where I_1 is the Bessel function of imaginary argument. When N is larger than 5, this equation is approximated by:

$$c_i^\circ = \frac{\tau_F}{2\sqrt{\pi}} \sqrt{\frac{N}{\tau_1}}\, \frac{\exp\left[-N(\sqrt{\tau_1} - 1)^2\right]}{(\tau_1)^{1/4}} \qquad (16\text{-}174)$$

The behavior predicted by Eq. (16-174) is shown in Fig. 16-34 as $c_i^\circ/(\tau_F \sqrt{N})$ versus τ_1 for different values of N. For $N > 50$, the response peak is symmetrical, the peak apex occurs at $\tau_1 = 1$, and the dimensionless peak height is $c_i^{\circ\,\max} = \tau_F \sqrt{N/4\pi}$. A comparison of this equation with Eq. (16-172) with $N = 80$ is shown in Fig. 16-33 for $\tau_F = 0.05$.

The moments of the response peak predicted by Eq. (16-173) are

$$\mu_1 = \frac{L}{v}\left[1 + \frac{1 - \varepsilon}{\varepsilon}(\varepsilon_p + \rho_p K_i)\right] = \frac{L}{v}(1 + k_i') \qquad (16\text{-}175)$$

$$\sigma^2 = \frac{2\mu_1^2}{N}\left(\frac{k_i'}{1 + k_i'}\right)^2 \qquad (16\text{-}176)$$

where $k_i' = (1 - \varepsilon)(\varepsilon_p + \rho_p K_i)/\varepsilon$. Correspondingly, the number of plates and the HETP are:

$$N_p = \frac{N}{2}\left(\frac{1 + k_i'}{k_i'}\right)^2 \qquad (16\text{-}177)$$

$$\text{HETP} = \frac{2L}{N}\left(\frac{k_i'}{1 + k_i'}\right)^2 \qquad (16\text{-}178)$$

Since the term $(1 + k_i')/k_i'$ approaches unity for large k'-value, the number of plates is equal to one half the number of transfer units for a strongly retained component. For these conditions, when $N_p = N/2$, Eq. (16-174) and Eq. (16-161) produce the same peak retention time, peak spreading, and predict essentially the same peak profile.

In the general case of axially dispersed plug flow with bidispersed particles, the first and second moment of the pulse response are [Haynes and Sarma, *AIChE J.,* **19,** 1043 (1973)]:

$$\mu_1 = \frac{L}{v}\left[1 + \frac{1 - \varepsilon}{\varepsilon}(\varepsilon_p + \rho_p K_i)\right] = \frac{L}{v}(1 + k_i') \qquad (16\text{-}179)$$
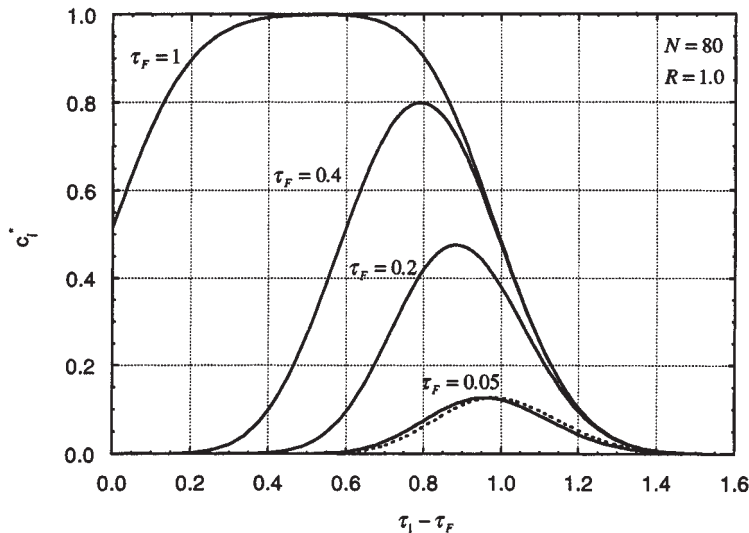

FIG. 16-33   Elution curves under trace linear equilibrium conditions for different feed loading periods and $N = 80$. Solid lines, Eq. (16-172); dashed line, Eq. (16-174) for $\tau_F = 0.05$.
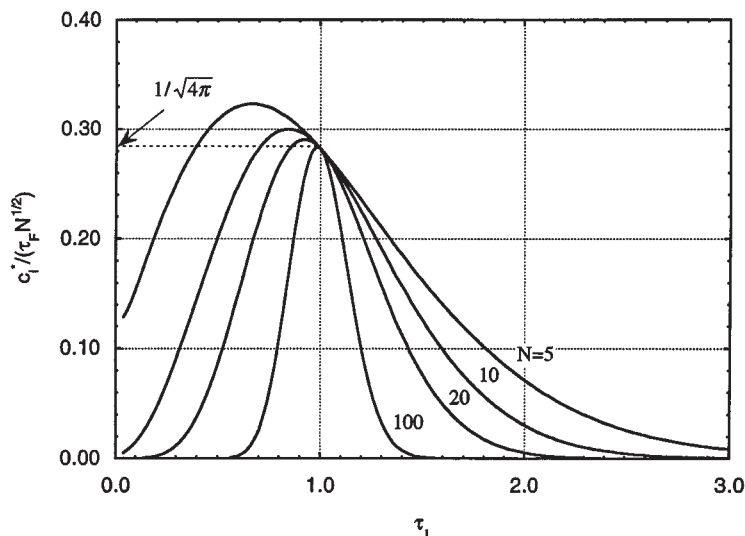
FIG. 16-34 Elution curves under trace linear equilibrium conditions with a pulse feed from Eq. (16-174).

$$\sigma^2 = \frac{2LD_L}{v^3}(1+k_i')^2$$

$$+2\frac{L}{v}\frac{\varepsilon k_i'^2}{1-\varepsilon}\left[\frac{r_p}{3k_f}+\frac{r_p^2}{15\varepsilon_p D_{pi}}+\frac{\rho_p K_i}{(\varepsilon_p+\rho_p K_i)^2}\frac{r_s^2}{15D_{si}}\right] \quad (16\text{-}180)$$

Correspondingly, the number of plates and the plate height are:

$$N_p = \left\{\frac{2D_L}{vL}+\frac{2\varepsilon}{1-\varepsilon}\frac{v}{L}\left(\frac{k_i'}{1+k_i'}\right)^2\right.$$

$$\left.\times\left[\frac{r_p}{3k_f}+\frac{r_p^2}{15\varepsilon_p D_{pi}}+\frac{\rho_p K_i}{(\varepsilon_p+\rho_p K_i)^2}\frac{r_s^2}{15D_{si}}\right]\right\}^{-1} \quad (16\text{-}181)$$

$$HETP = \frac{2D_L}{v}+\frac{2\varepsilon v}{1-\varepsilon}\left(\frac{k_i'}{1+k_i'}\right)^2$$

$$\times\left[\frac{r_p}{3k_f}+\frac{r_p^2}{15\varepsilon_p D_{pi}}+\frac{\rho_p K_i}{(\varepsilon_p+\rho_p K_i)^2}\frac{r_s^2}{15D_{si}}\right] \quad (16\text{-}182)$$

In dimensionless form, a **reduced HETP,** $h = HETP/d_p$, analogous to the reduced HTU (cf. Fig. 16-13), is obtained as a function of the dimensionless velocity $ReSc$:

$$h = \frac{b}{ReSc}+a+cReSc \quad (16\text{-}183)$$

where $b = 2\varepsilon\gamma_1$ $\quad\quad\quad\quad\quad\quad\quad\quad\quad\quad\quad\quad\quad\quad\quad\quad (16\text{-}184a)$

$a = 2\gamma_2$ $\quad\quad\quad\quad\quad\quad\quad\quad\quad\quad\quad\quad\quad\quad\quad\quad\quad (16\text{-}184b)$

$$c = \frac{1}{30}\frac{1}{1-\varepsilon}\left(\frac{k_i'}{1+k_i'}\right)^2\left[\frac{10}{Sh}+\frac{\tau_p}{\varepsilon_p}+\frac{\rho_p K_i}{(\varepsilon_p+\rho_p K_i)^2}\frac{r_s^2}{D_{si}}\frac{D_{pi}}{r_p^2}\right]$$

$$(16\text{-}184c)$$

Equation 16-183 is qualitatively the same as the **van Deemter equation** [van Deemter and Zuiderweg, *Chem. Eng. Sci.,* **5,** 271 (1956)] and is equivalent to other empirical reduced HETP expressions such as the **Knox equation** [Knox, *J. Chromatogr. Sci.,* **15,** 352 (1977)].

The Sherwood number, Sh, is estimated from Table 16-9, and the dispersion parameters γ_1 and γ_2 from Table 16-10 for well-packed columns. Typical values are $a = 1–4$ and $b = 0.5–1$. Since HETP ~ 2HTU, Fig. 16-13 can also be used for approximate calculations.

Concentration Profiles   In the general case but with a linear isotherm, the concentration profile can be found by numerical inversion of the Laplace-domain solution of Haynes and Sarma [see

Lenhoff, *J. Chromatogr.,* **384,** 285 (1987)] or by direct numerical solution of the conservation and rate equations. For the special case of no-axial dispersion with external mass transfer and pore diffusion, an explicit time-domain solution, useful for the case of time-periodic injections, is also available [Carta, *Chem. Eng. Sci.,* **43,** 2877 (1988)]. In most cases, however, when $N > 50$, use of Eq. (16-161), or (16-172) and (16-174) with $N = 2N_p$ calculated from Eq. (16-181) provides an approximation sufficiently accurate for most practical purposes.

When the adsorption equilibrium is nonlinear, skewed peaks are obtained, even when N is large. For a constant separation-factor isotherm with $R < 1$ (favorable), the leading edge of the chromatographic peak is steeper than the trailing edge. When $R > 1$ (unfavorable), the opposite is true.

Figure 16-35 portrays numerically calculated chromatographic peaks for a constant separation factor system showing the effect of feed loading on the elution profile with $R = 0.5$ ($\tau_1 - \tau_F = [\varepsilon v(t - t_F)/L - \varepsilon]/\Lambda$). When the dimensionless feed time $\tau_F = 1$, the elution curve comprises a sharp leading profile reaching the feed concentration followed by a gradual decline to zero. As τ_F is reduced, breakthrough of the leading edge occurs at later times, while the trailing edge, past the peak apex, continues to follow the same profile. As the amount of feed injected approaches zero, mass-transfer resistance reduces the solute concentration to values that fall in the Henry's law limit of the isotherm, and the peak retention time gradually approaches the value predicted in the infinite dilution limit for a linear isotherm.

For high feed loads, the shape of the diffuse trailing profile and the location of the leading front can be predicted from local equilibrium theory (see "Fixed Bed Transitions"). This is illustrated in Fig. 16-35 for $\tau_F = 0.4$. For the diffuse profile (a "simple wave"), Eq. (16-131) gives:

$$c_i^* = \frac{R}{1-R}\left[\left(\frac{1}{R(\tau_1-\tau_F)}\right)^{1/2}-1\right] \quad (16\text{-}185)$$

Thus, the effluent concentration becomes zero at $\tau_1 - \tau_F = 1/R$. The position of the leading edge (a "shock front") is determined from Eq. (16-132):

$$\tau_{1s} = \tau_F + \frac{1}{R}\left[1-\sqrt{(1-R)\tau_F}\right]^2 \quad (16\text{-}186)$$

and the peak highest concentration by [Golshan-Shirazi and Guiochon, *Anal. Chem.,* **60,** 2364 (1988)]:

$$c_i^{*\,max} = \frac{R}{1-R}\frac{\sqrt{(1-R)\tau_F}}{1-\sqrt{(1-R)\tau_F}} \quad (16\text{-}187)$$
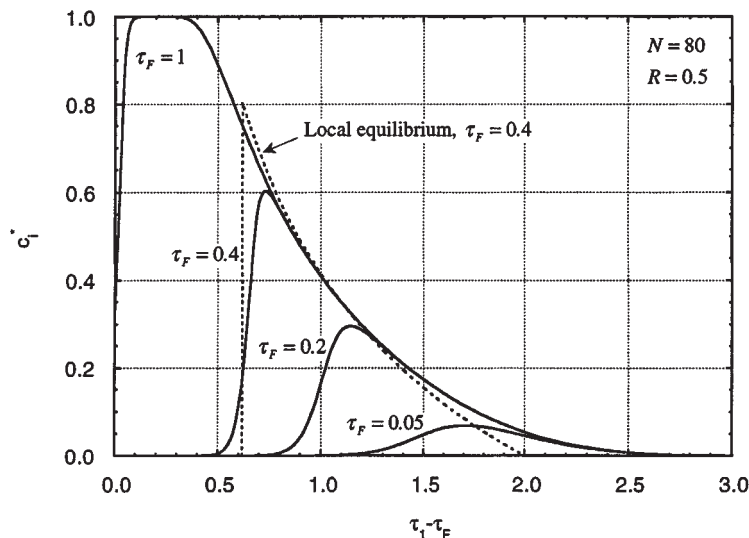
FIG. 16-35   Elution curves under trace conditions with a constant separation factor isotherm for different feed loadings and $N = 80$. Solid lines, rate model; dashed line, local equilibrium theory for $\tau_F = 0.4$.

The local equilibrium curve is in approximate agreement with the numerically calculated profiles except at very low concentrations when the isotherm becomes linear and near the peak apex. This occurs because band-spreading, in this case, is dominated by adsorption equilibrium, even if the number of transfer units is not very high. A similar treatment based on local equilibrium for a two-component mixture is given by Golshan-Shirazi and Guiochon [*J. Phys. Chem.,* **93,** 4143 (1989)].

Prediction of multicomponent nonlinear chromatography accounting for rate factors requires numerical solution (see Guiochon et al., gen. refs., and "Numerical Methods and Characterization of Wave Shape" in "Fixed Bed Transitions").

Linear Gradient Elution   Analytical solutions are available for special cases under trace conditions with a linear isotherm. Other situations normally require a numerical solution. General references are Snyder [in Horvath (ed.), *High Performance Liquid Chromatography: Advances and Perspectives,* vol. 1, Academic Press, 1980, p. 208], Antia and Horvath [*J. Chromatogr.,* **484,** 1 (1989)], Yamamoto et al. [*Ion Exchange Chromatography of Proteins,* Marcel Dekker, 1988], Guiochon et al. (gen. refs.).

The most commonly used gradients are linear gradients where the starting solvent is gradually mixed with a second gradient-forming solvent at the column entrance to yield a volume fraction φ of the mobile phase modulator that increases linearly with time:

$$\varphi = \varphi_0 + \beta t \tag{16-188}$$

When the mobile phase modulator is a dilute solute in a solvent, as when the modulator is a salt, φ indicates molar concentration.

Under *trace conditions,* the retention of the modulator in the column is independent of the presence of any solutes. The modulator concentration at the column exit is approximated by

$$\varphi = \varphi_0 + \beta \left[t - \frac{L}{v} (1 + k'_M) \right] \tag{16-189}$$

where k'_M is the retention factor of the modulator.

For a small feed injection, the modulator concentration φ_R at which a feed solute is eluted from the column is obtained from the following integral relationship

$$G(\varphi_R) = \frac{\beta L}{v} = \int_{\varphi_0}^{\varphi_R} \frac{d\varphi}{k'_i(\varphi) - k'_M} \tag{16-190}$$

where $k'_i(\varphi)$ is the solute retention factor as a function of the mobile

phase modulator concentration. Note that the solute retention time in the column is affected by the steepness of the gradient at the column entrance.

$k'_i(\varphi)$ can be obtained experimentally from isocratic elution experiments at different φ values, or from linear gradient elution experiments where the ratio $G = \beta L/v$ is varied. In the latter case, the retention factor is obtained by differentiation of Eq. (16-190) from $k'_i(\varphi_R) = k'_M + (dG/d\varphi_R)^{-1}$.

Table 16-14 gives explicit expressions for chromatographic peak properties in isocratic elution and linear gradient elution for two cases.

In **reversed-phase chromatography** (RPC), the mobile phase modulator is typically a water-miscible organic solvent, and the stationary phase is a hydrophobic adsorbent. In this case, the logarithm of solute retention factor is commonly found to be linearly related to the volume fraction of the organic solvent.

In **ion-exchange chromatography** (IEC), the mobile phase modulator is typically a salt in aqueous solution, and the stationary phase is an ion-exchanger. For dilute conditions, the solute retention factor is commonly found to be a power-law function of the salt normality [cf. Eq. (16-27) for ion-exchange equilibrium].

Band broadening is also affected by the gradient steepness. This effect is expressed in Table 16-14 by a **band compression factor** C, which is a function of the gradient steepness and of equilibrium parameters. Since $C < 1$, gradient elution yields peaks that are sharper than those that would be obtained in isocratic elution at $\varphi = \varphi_R$.

Other cases, involving an arbitrary relationship between the solute retention factor and the modulator concentration can be handled analytically using the approaches of Frey [*Biotechnol. Bioeng.,* **35,** 1055 (1990)] and Carta and Stringfield [*J. Chromatogr.,* **605,** 151 (1992)].

Displacement Development   A complete prediction of displacement chromatography accounting for rate factors requires a numerical solution since the adsorption equilibrium is nonlinear and intrinsically competitive. When the column efficiency is high, however, useful predictions can be obtained with the local equilibrium theory (see "Fixed Bed Transitions").

For constant-separation factor systems, the **h-transformation** of Helfferich and Klein (gen. refs.) or the method of Rhee et al. [*AIChE J.,* **28,** 423 (1982)] can be used [see also Helfferich, *Chem. Eng. Sci.,* **46,** 3320 (1991)]. The equations that follow are adapted from Frenz and Horvath [*AIChE J.,* **31,** 400 (1985)] and are based on the *h*-transformation. They refer to the separation of a mixture of $M - 1$

TABLE 16-14   Expressions for Predictions of Chromatographic Peak Properties in Linear Gradient Elution Chromatography under Trace Conditions with a Small Feed Injection and Inlet Gradient Described by $\varphi = \varphi_o + \beta t$ (Adapted from Refs. A and B).

Parameter	Isocratic	Gradient elution—RPC (Ref. A)	Gradient elution—IEC (Ref. B)
Dependence of retention factor on modulator concentration	—	$k' - k'_M = \alpha_s e^{-S\varphi}$	$k' - k'_M = \alpha_z \varphi^{-z}$
Retention time	$t_R = \dfrac{L}{v}(1 + k'_o)$	$t_R = \dfrac{L}{v}(1 + k'_M) + \dfrac{1}{S\beta}\ln\left[\dfrac{S\beta L}{v}(k'_o - k'_M) + 1\right]$	$t_R = \dfrac{L}{v}(1 + k'_M) + \dfrac{1}{\beta}\left[\dfrac{\alpha_z \beta L}{v}(Z+1) + \varphi_o^{Z+1}\right]^{1/(Z+1)} - \dfrac{\varphi_o}{\beta}$
Mobile phase composition at column exit	$\varphi_R = \varphi_o$	$\varphi_R = \varphi_o + \beta\left[t_R - \dfrac{L}{v}(1 + k'_M)\right]$	$\varphi_R = \varphi_o + \beta\left[t_R - \dfrac{L}{v}(1 + k'_M)\right]$
Retention factor at peak elution	$k'_R = k'_o$	$k'_R = \dfrac{k'_o + (k'_o - k'_M)S\beta L/v}{1 + (k'_o - k'_M)S\beta L/v}$	$k'_R = \alpha_z\left[\dfrac{\alpha_z \beta L}{v}(Z+1) + \varphi_o^{Z+1}\right]^{-Z/(Z+1)} + k'_M$
Peak standard deviation	$\sigma = \dfrac{L/v}{\sqrt{N_P}}(1 + k'_o)$	$\sigma = C\dfrac{L/v}{\sqrt{N_{pR}}}(1 + k'_R)$	$\sigma = C\dfrac{L/v}{\sqrt{N_{pR}}}(1 + k'_R)$
Band compression factor	—	$C = \dfrac{(1 + p + p^2/3)^{1/2}}{1 + p}$ $p = \dfrac{(k'_o - k'_M)(1 + k'_M)S\beta L/v}{1 + k'_o}$	$C = \begin{cases} \sqrt{M'} & \text{for } M' < 0.25 \\ \dfrac{3.22M'}{1 + 3.13M'} & \text{for } 0.25 < M' < 0.25 \\ 1 & \text{for } M' > 120.25 \end{cases}$ $M' = \dfrac{1}{2}\dfrac{1 + k'_R}{1 + k'_M}\dfrac{Z+1}{Z}$

References: A. Snyder in Horvath (ed.), *High Performance Liquid Chromatography: Advances and Perspectives*, vol. 1, Academic Press, 1980, p. 208.
B. Yamamoto, *Biotechnol. Bioeng.*, **48**, 444 (1995).
Solute equilibrium parameters: α_s, S for RPC and α_Z, Z for IEC
Solute retention factor for initial mobile phase: k'_o
Retention factor of mobile phase modulator: k'_M
Plate number obtained for $k' = k'_R$: N_{pR}

components with a displacer (component 1) that is more strongly adsorbed than any of the feed solutes. The **multicomponent Langmuir isotherm** [Eq. (16-39)] is assumed valid with equal monolayer capacities, and components are ranked numerically in order of decreasing affinity for the stationary phase (i.e., $K_1 > K_2 > \cdots K_M$).

The development of component bands is predicted by mapping the trajectories of the **h-function roots** h_i, which are obtained from the solution of

$$\sum_{i=1}^{M}\frac{K_i c_i}{h\alpha_{i,1} - 1} = 1 \tag{16-191}$$

where $\alpha_{i,j} = K_i/K_j$.

Trivial roots also exist for each component with zero concentration. In displacement chromatography, for each of the transitions at the column entrance, a new set of M roots is generated. These roots are given in Table 16-15. The change from the initial solvent (carrier) to feed changes $M - 1$ roots, generating $M - 1$ boundaries or transitions that move through the column. These boundaries are all self-sharpening, characterized by upstream h''_i values larger than the corresponding downstream h'_i values.

The switch from feed to displacer changes M roots, generating M boundaries. All of these boundaries are self-sharpening, except the boundary associated with the transition from h_{MF} to $\alpha_{1,M+1}$ that can be self-sharpening or diffuse depending on the relative value of these roots. Note that only one root changes value across a particular boundary.

The **adjusted propagation velocity** of each self-sharpening boundary is:

$$u_{si} = \frac{d\zeta}{d\tau_1} = h'_i h''_i P_i \tag{16-192}$$

$$P_i = \prod_{j=1}^{i-1} h'_j \prod_{j=i+1}^{M} h''_j \prod_{j=1}^{M+1} \alpha_{j,1} \tag{16-193}$$

and that of each diffuse boundary:

$$u_{hi} = h_i^2 P_i \tag{16-194}$$

where $\zeta = z/L$ and $\tau_1 = (\varepsilon vt/L - \varepsilon_b\zeta)/\Lambda$ with $\Lambda = \rho_b n_1^D/c_1^D$ equal to the partition ratio for the displacer.

The root trajectories are mapped as follows on the ζ-τ_1 plane:

1. The starting points are the beginning and end of the feed step. From these points trajectories are traced according to Eqs. (16-192) and (16-194).

2. At the points of intersection of trajectories, a change in boundary velocity occurs: When two boundaries associated with a change in the same root number intersect, they combine into a single boundary with velocity given by Eq. (16-192) or (16-194), intermediate in value between those of the intersecting trajectories. When two trajectories associated with different root numbers intersect, they both continue beyond the point of intersection with new velocities calculated from Eqs. (16-192) and (16-194), reflecting any change in root values.

3. After constructing the trajectories, the following equation is used to calculate the band profiles

$$c_j = \frac{\prod_{i=1}^{M}(h_i\alpha_{j,1} - 1)}{K_j\prod_{i=1}^{M}(\alpha_{j,i} - 1)} \tag{16-195}$$

TABLE 16-15   Concentrations and h-Function Roots for Displacement Chromatography of a Mixture of M-1 Components Numbered in Order of Decreasing Affinity for the Stationary Phase (Adapted from Frenz and Horvath, 1985).

Solution	$c_i = 0$		$c_i > 0$	
	i	h_i	i	h_i
Carrier	1, 2, ... M	$\alpha_{1,1}, ... \alpha_{1,M}$	—	—
Feed	1	$\alpha_{1,1}$	2, ... M	$h_{2F}, \cdots h_{MF}^{\circ}$
Displacer	2, 3, ... M	$\alpha_{1,2}, ... \alpha_{1,M}$	1	$\alpha_{1,M+1} = 1 + K_1 c_1^D$

*Roots calculated from the solution of Eq. (16-191).

Example 12: Calculation of Band Profiles in Displacement Chromatography An equimolar mixture of two components (concentrations $c_2^F = c_3^F = 1$ arbitrary unit) is separated with a displacer with concentration $c_1^F = 2$. The equilibrium isotherm is:

$$n_i = \frac{n^s K_i c_i}{1 + K_1 c_1 + K_2 c_2 + K_3 c_3} \qquad (i = 1, 2, 3)$$

with $K_1 = 2$, $K_2 = 1$, and $K_3 = 0.667$. The dimensionless feed time is $\tau_F = 0.2$. The separation factors used for calculating the trivial roots are $\alpha_{1,1} = 1$, $\alpha_{1,2} = 2$, $\alpha_{1,3} = 3$, $\alpha_{1,4} = 1 + K_1 c_1^D = 5$. The remaining h-function roots are calculated by solving Eq. (16-191) for the carrier, feed, and displacer concentrations. The results are summarized in Table 16-16.

TABLE 16-16   Values of h-Roots for Example 16-12

State	h_1	h_2	h_3
Carrier	1	2	3
Feed	1	2.44	6.56
Displacer	2	3	5

The switch from carrier to feed generates self-sharpening boundaries, since the h_i''s (upstream) are larger than the $h_i's$ (downstream). The switch from feed to displacer generates two self-sharpening boundaries (corresponding to h_1 and h_2) and a diffuse boundary (corresponding to h_3) since $h_3'' < h_3'$. The velocity of each boundary is calculated from Eq. (16-192) for self-sharpening boundaries and from Eq. (16-194) for diffuse boundaries. The root trajectories are shown in Fig. 16-36 (top). From one boundary to the next, the root values change one at a time from the values corresponding to the carrier to the values corresponding to the displacer. Concentration profiles calculated from Eq. (16-195) are shown in Fig. 16-36 (bottom) for two different values of ζ. The concentrations in the z and t coordinates are easily reconstructed from the definitions of τ_1 and ζ.

In general, for a constant separation factor system, complete separation is obtained when:

$$c_1^D > \frac{1}{K_1} (\alpha_{1,M} - 1) \qquad (16-196)$$

Then, band profiles eventually develop into the **isotachic pattern** of pure component bands moving at the velocity of the displacer front. In Example 12, this occurs at $\zeta = 0.765$.
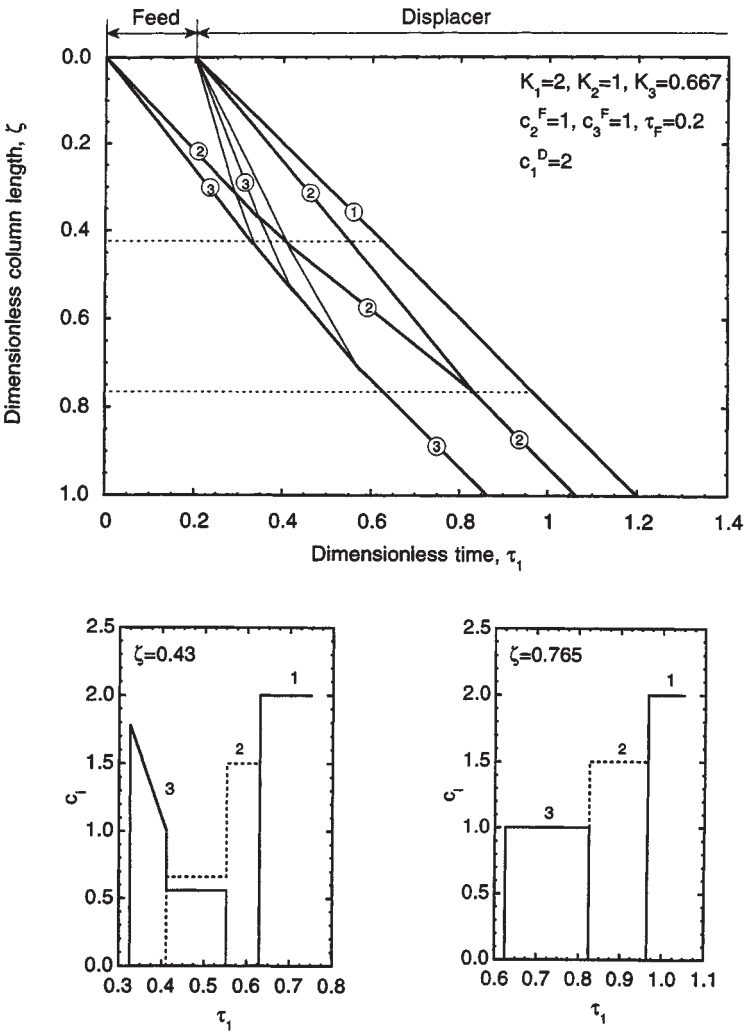
FIG. 16-36   Dimensionless time-distance plot for the displacement chromatography of a binary mixture. The darker lines indicate self-sharpening boundaries and the thinner lines diffuse boundaries. Circled numerals indicate the root number. Concentration profiles are shown at intermediate dimensionless column lengths $\zeta = 0.43$ and $\zeta = 0.765$. The profiles remain unchanged for longer column lengths.

The **isotachic concentrations** c_i^I in the fully developed train are calculated directly from the single component isotherms using:

$$\frac{n_1^e}{c_1^I} = \frac{n_2^e}{c_2^I} = \cdots = \frac{n_M^e}{c_M^I} \qquad (16\text{-}197)$$

or

$$c_j^I = c_1^D - \frac{1}{K_j}(1 - \alpha_{j,1}) \qquad (16\text{-}198)$$

The graphical interpretation of Eq. (16-197) is shown in Fig. 16-37 for the conditions of Example 12. An operating line is drawn from the origin to the point of the pure displacer isotherm at $c_1 = c_1^D$. For displacement to occur, the operating line must cross the pure component isotherms of the feed solutes. The product concentrations in the isotachic train are found where the operating line crosses the isotherms. When this condition is met, the feed concentrations do not affect the final product concentrations.

Analyses of displacement chromatography by the method of characteristics with non-Langmuirian systems is discussed by Antia and Horvath [*J. Chromatogr.,* **556,** 199 (1991)] and Carta and Dinerman [*AIChE J.,* **40,** 1618 (1994)]. Optimization studies and analyses by computer simulations are discussed by Jen and Pinto [*J. Chromatogr.,* **590,** 47 (1992)], Katti and Guiochon [*J. Chromatogr.,* **449,** 24 (1988)], and Phillips et al. [*J. Chromatogr.,* **54,** 1 (1988)].

DESIGN FOR TRACE SOLUTE SEPARATIONS

The design objectives of the analyst and the production line engineer are generally quite different. For analysis the primary concern is typically resolution. Hence operating conditions near the minimum value of the HETP or the HTU are desirable (see Fig. 16-13).

In preparative chromatography, however, it is generally desirable to reduce capital costs by maximizing the **productivity,** or the amount of feed processed per unit column volume, subject to specified purity requirements. This reduction, however, must be balanced against operating costs that are determined mainly by the mobile phase flow rate and the pressure drop. In practice, preparative chromatography is often carried out under **overload conditions,** i.e., in the nonlinear region of the adsorption isotherm. Optimization under these conditions is discussed in Guiochon et al. (gen. refs.). General guidelines for trace-level, isocratic binary separations, in the Henry's law limit of the isotherm are:

1. The stationary phase is selected to provide the maximum selectivity. Where possible, the retention factor is adjusted (by varying the mobile phase composition, temperature, or pressure) to an optimum value that generally falls between 2 and 10. Resolution is adversely affected when $k' \ll 2$, while product dilution and separation time

increase greatly when $k' \gg 10$. When this is not possible for all feed components and large differences exist among the k'-values of the different solutes, gradient elution should be considered.

2. The average feed mixture charging rate, molar or volumetric, is fixed by the raw material supply or the demand for finished product.

3. The value of N_p required to achieve a desired resolution is determined by Eq. (16-168) or (16-171). Since $N = L/\mathrm{HTU} \sim 2N_p = 2L/\mathrm{HETP}$, Fig. 16-13 or Eq. (16-183) can be used to determine the range of the dimensionless velocity $ReSc$ that maximizes N_p for a given particle diameter and column length.

4. The allowable pressure drop influences the choice of the particle size and helps determine the column length. Equations for estimating the pressure drop in packed beds are given in Section 6.

5. When only a few solutes are separated, they may occupy only a small portion of the total column volume at any given instant. In such cases, the productivity is improved by cyclic feed injections, timed so that the most strongly retained component from an injection elutes just before the least strongly retained component from the following injection (see Fig. 16-57). For a mixture of two components with $k' > 1$, when the same resolution is maintained between bands of the same injections and bands of successive injections, the cycle time t_C and the plate number requirement are:

$$t_C = 2(t_{R,A} - t_{R,B}) = \frac{2L}{v}(k_A' - k_B') \qquad (16\text{-}199)$$

$$N_p = 4R_s^2\left(\frac{\alpha+1}{\alpha-1}\right)^2(1-2\phi)^{-2} \qquad (16\text{-}200)$$

where $\phi = t_F/t_C$ is the fraction of the cycle time during which feed is supplied to the column. The productivity, P = volume of feed/(time × bed volume), is:

$$P = \frac{1}{4R_s^2}\left(\frac{\alpha-1}{\alpha+1}\right)^2\frac{\varepsilon v}{\mathrm{HETP}}\phi(1-2\phi)^2$$

$$= \frac{1}{4R_s^2}\left(\frac{\alpha-1}{\alpha+1}\right)^2\frac{D_i}{d_p^2}\left(\frac{ReSc}{b/ReSc+a+cReSc}\right)\phi(1-2\phi)^2 \qquad (16\text{-}201)$$

For a given resolution, P is maximized when $\phi = 1/6$ (i.e., feed is supplied for one sixth of the cycle time), and by the use of small particle sizes. The function $ReSc/(b/ReSc+a+cReSc)$ generally increases with $ReSc$, so that productivity generally increases with the mobile phase velocity. For typical columns, however, this function is within about 10 percent of its maximum value ($\sim 1/c$) when $ReSc$ is in the range 30–100. Thus, increasing the velocity above this range must be balanced against the costs associated with the higher pressure drop.
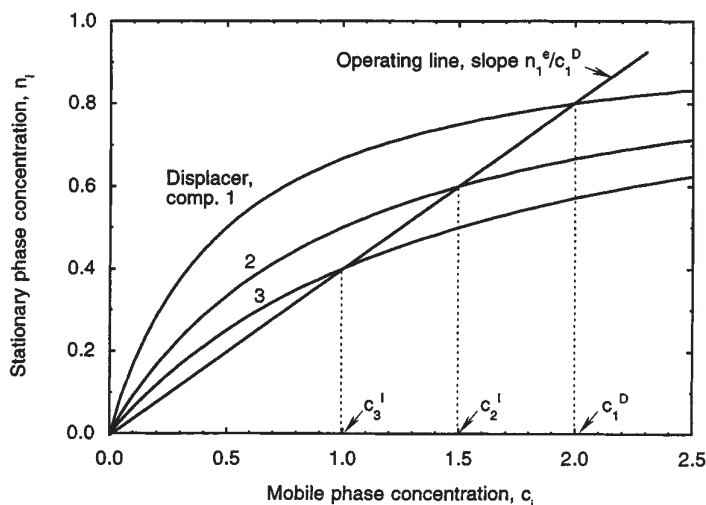

FIG. 16-37 Schematic showing the intersection of the operating line with the pure-component isotherms in displacement chromatography. Conditions are the same as in Fig. 16-36.

PROCESS CYCLES

GENERAL CONCEPTS

Some applications of adsorption and ion exchange can be achieved by sorbent-fluid contact in batch equipment. Batch methods are well adapted to laboratory use and have also been applied on a larger scale in several specific instances. In a batch run for either adsorption or ion exchange, a sorbent is added to a fluid, completely mixed, and subsequently separated. Batch treatment is adopted when the capacity and equilibrium of the sorbent are large enough to give nearly complete sorption in a single step, as in purifying and decoloration of laboratory preparations with carbons and clays. Batch runs are useful in the measurement of equilibrium isotherms and also of adsorptive diffusion rate. Batch tests or measurements are often conducted in portions of adsorbent or ion-exchange material intended for larger-scale use. For example, either the equilibrium sorption of a solid and/or its ultimate sorption capacity can be determined in this way. The solid is first equilibrated with a fluid at the concentration of interest; after separating the phases, gravimetric and chemical analyses can be used to determine the sorbed amount and composition.

Like the laboratory batch use, some commercial applications use the adsorbent on a throwaway basis. Reasons for using sorption non-regeneratively are usually: (1) low cost of the sorbent, (2) high value of the product, (3) very low dosage (sorbent-to-fluid ratio), and (4) difficulty in desorbing the sorbates. Magnesium perchlorate and barium oxide are used for drying, iron sponge (hydrated iron oxide on wood chips) is used to remove hydrogen sulfide, and sodium or potassium hydroxide is applied to removal of sulfur compounds or carbon dioxide. In wastewater treatment, powdered activated carbon (PAC) is added to enhance biological treatment but is not regenerated; instead, it remains with the sludge. Silica gel is used as a desiccant in packaging. Activated carbon is used in packaging and storage to adsorb other chemicals for preventing the tarnishing of silver, retarding the ripening or spoiling of fruits, "gettering" (scavenging) out-gassed solvents from electronic components, and removing odors. Synthetic zeolites, or blends of zeolites with silica gel, are used in dual-pane windows to adsorb water during initial dry-down and any in-leakage and to adsorb organic solvents emitted from the sealants during their cure; this prevents fogging between the sealed panes that could result from the condensation of water or the solvents [Ausikaitis, *Glass Digest*, **61**, 69–78 (1982)]. Activated carbon is used to treat recirculated air in office buildings, apartments, and manufacturing plants using thin filter-like frames to treat the large volumes of air with low pressure drop. On a smaller scale, activated carbon filters are in kitchen hoods, air conditioners, and electronic air purifiers. On the smallest scale, gas masks containing carbon or carbon impregnated with promoters are used to protect individual wearers from industrial odors, toxic chemicals, and gas-warfare chemicals. Activated carbon fibers have been formed into fabrics for clothing to protect against vesicant and percutaneous chemical vapors [Macnair and Arons in Cheremisinoff and Ellerbusch (eds.), gen. refs.].

Ion exchangers are sometimes used on a throwaway basis also. In the laboratory, ion exchangers are used to produce deionized water, purify reagents, and prepare inorganic sols. In medicine, they are used as antacid, for sodium reduction, for the sustained release of drugs, in skin-care preparations, and in toxin removal.

Although there are many practical applications for which the sorbent is discarded after one use, most applications of interest to chemical engineers involve the removal of adsorbates from the sorbent (i.e., regeneration). This allows the adsorbent to be reused and the adsorbates to be recovered.

The maximum efficiency that a cyclic adsorption process can approach for any given set of operating conditions is defined by the adsorptive loading in equilibrium with the feed fluid. There are several factors that reduce the practical (or "operating") adsorption: mass-transfer resistance (see above), deactivation (see above), and incomplete regeneration (or *desorption*). The severity of regeneration influences how closely the dynamic capacity of an adsorbent resembles that of fresh, virgin material. Regeneration, or reversal of the adsorption process, requires a reduction in the driving force for adsorption. This is accomplished by increasing the equilibrium driving force for the adsorbed species to desorb from the solid to the surrounding fluid.

TEMPERATURE SWING ADSORPTION

A temperature-swing, or thermal-swing, adsorption (TSA) process cycle is one in which desorption takes place at a temperature much higher than adsorption. The elevation of temperature is used to shift the adsorption equilibrium and affect regeneration of the adsorbent. Figure 16-38 depicts a simplified (and ideal) TSA cycle. The feed fluid containing an adsorbate at a partial pressure of p_1 is passed through an adsorbent at temperature T_1. This adsorption step continues until the equilibrium loading n_1 is achieved with p_1. Next the adsorbent temperature is raised to T_2 (heating step) so that the partial pressure in equilibrium with n_1 is increased to p_2, creating a partial pressure driving force for desorption into any fluid containing less than p_2 of the adsorbate. By means of passing a purge fluid across the adsorbent, adsorbate is swept away, and the equilibrium proceeds down the isotherm to some point such as p_1, n_2. (This point need not coincide with the feed partial pressure; it is selected for illustrative purposes. Also, in some applications, roll-up of the adsorbed-phase concentration can occur during heating such that in some regions of the bed p_2 reaches the condensation pressure of the component, causing a condensed liquid phase to form temporarily in particles [Friday and LeVan, *AIChE J.*, **31**, 1322 (1985)].) During a cooling step, the adsorbent temperature is returned to T_1. The new equilibrium p_3, n_2 represents the best-quality product that can be produced from the adsorbent at a regenerated loading of n_2 in the simplest cycle. The adsorption step is now repeated. The differential loading, $n_1 - n_2$, is the maximum loading that can be achieved for a TSA cycle operating between a feed containing p_1 at temperature T_1, regeneration at T_2, and a product containing a partial pressure p_3 of the adsorbate. The regeneration fluid will contain an average partial pressure between p_2 and p_1 and will therefore have accomplished a concentration of the adsorbate in the regenerant fluid. For liquid-phase adsorption, the partial pressure can be replaced by the fugacity of the adsorbate. Then, the entire discussion above is applicable whether the regeneration is by a fluid in the gas or liquid phase.

In a TSA cycle, the heating step must provide the thermal energy necessary to raise the adsorbate, adsorbent, and adsorber temperatures, to desorb the adsorbate, and to make up for heat losses. TSA regeneration is classified as (1) heating-limited (or stoichiometric-limited) when transfer of energy to the system is limiting, or (2) stripping-limited (or equilibrium-limited) when transferring adsorbate away is limiting. Heating is accomplished by either direct contact of the adsorbent by the heating medium (external heat exchange to a purge gas) or indirect means (heating elements, coils, or panels inside the adsorber). Direct heating is the most commonly used, especially for stripping-limited heating. Indirect heating can be considered for stripping-limited heating, but the complexity of indirect heating limits its practicality to heating-limited regeneration where purge gas is in short supply. Microwave fields [Benchanaa, Lallemant, Simonet-Grange, and Bertrand, *Thermochim. Acta,* **152,** 43–51 (1989)] and dielectric fields [Burkholder, Fanslow, and Bluhm, *Ind. Eng. Chem. Fundam.*, **25,** 414–416 (1986)] are also used to supply indirect heating.

Because high temperatures can be used, resulting in thorough desorption, TSA cycles are characterized by low residual loadings and thus high operating loadings. These high capacities at low concentrations allow long cycle times for reasonably sized adsorbers (hours to days). Long cycle time is needed because particles of adsorbent respond slowly to changes in gas temperature. Most applications of TSA are for systems in which adsorbates are present at low concentration (purification), such as drying, and in which species are strongly adsorbed, such as sweetening, CO_2 removal, and pollution control.
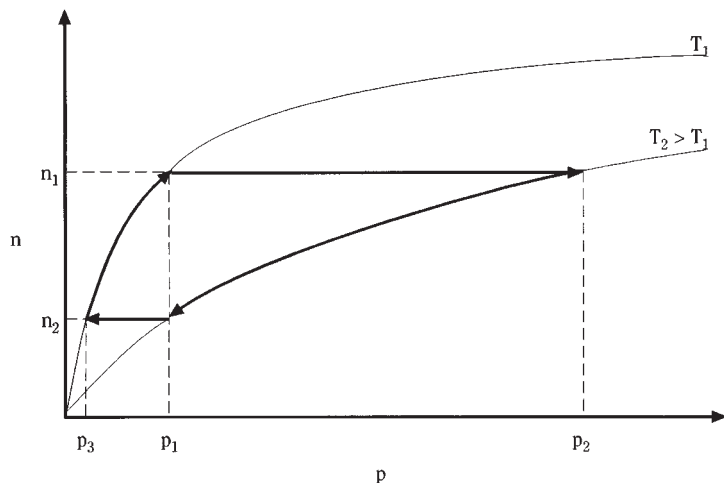
FIG. 16-38   Ideal temperature swing cycle. (*Reprinted with permission of UOP.*)

Other Cycle Steps   Besides the necessary adsorption and heating steps, TSA cycles may employ additional steps. A purge or sweep gas removes the thermally desorbed components from the adsorbent, and cooling returns it to adsorption temperature. Although the cooling is normally accomplished as a separate step after the heating, sometimes adsorption is started on a hot bed. If certain criteria are met [Basmadjian, *Can. J. Chem. Eng.,* **53,** 234–238 (1975)], the dynamic adsorption efficiency is not significantly affected by the lack of a cooling step.

For liquid-phase adsorption cycles when the unit is to treat a product of significant value, there must be a step to remove the liquid from the adsorbent and one to displace any liquid regenerant thoroughly before filling with the valuable fluid. Because adsorbents and ion exchangers are porous, some retention of the product is unavoidable but needs to be minimized to maximize recovery. When regeneration is by a gas, removal and recovery is accomplished by a drain (or pressure-assisted drain) step using the gas to help displace liquid from the sorbent before heating. When the regenerant is another liquid, the feed or product can be displaced out of the adsorbent. When heating and cooling are complete, liquid feed must be introduced again to the adsorbent with a corresponding displacement of the gas or liquid regenerant. In ion exchange, these steps for draining and filling are commonly referred to as "sweetening off" and "sweetening on," respectively.

Applications   Drying is the most common gas-phase application for TSA. The natural gas, chemical, and cryogenics industries all use adsorbents to dry streams. Zeolites, activated alumina, and silica gel are used for drying pipeline natural gas. Alumina and silica gel are used because they have higher equilibrium capacity and are more easily regenerated with waste-level heat [Crittenden, *Chem. Engr.,* **452,** 21–24 (1988); Goodboy and Fleming, *Chem. Eng. Progr.,* **80,** 63–68 (1984); Ruthven, *Chem. Eng. Progr.,* **84,** 42–50 (1988)]. The low dewpoint that can be achieved with zeolites is especially important when drying cryogenic-process feed-streams to prevent freeze-up. Zeolites dry natural gas before liquefaction to liquefied natural gas (LNG) and before ethane recovery utilizing the cryogenic turboexpander process [Anderson in Katzer (ed.), *Molecular Sieves—II, Am. Chem. Soc. Symp. Ser.,* **40,** 637–649 (1977); Brooking and Walton, *The Chem. Engr.,* **257,** 13–17 (1972)]. The feed air to be cryogenically separated into N_2, O_2, and argon is purified of both water and CO_2 with 13X zeolites using TSA cycles. Zeolites, silica gel, and activated alumina are used to dry synthesis gas, inert gas, hydrocracker gas, rare gases, and reformer recycle H_2. Because 3A and pore-closed 4A zeolites size-selectively adsorb water but exclude hydrocarbons, they are used extensively to dry reactive streams such as cracked gas in order to prevent coke formation on the adsorbent. This molecular sieving increases the recovery of hydrocarbons by reducing the coadsorption

that would otherwise cause them to be desorbed and lost with the water.

Another area of application for TSA processes is in sweetening. H_2S, mercaptans, organic sulfides and disulfides, and carbonyl sulfide all must be removed from natural gas, H_2, biogas, and refinery streams in order to prevent corrosion and catalyst poisoning. Natural gas feed to steam methane reforming is sweetened in order to protect the sulfur-sensitive, low-temperature shift catalyst. Well-head natural gas is treated by TSA to prevent pipeline corrosion using 4A zeolites to remove sulfur compounds without the coadsorption of CO_2 that would cause shrinkage. Sweetening and drying of refinery hydrogen streams are needed to prevent poisoning of reformer catalysts. Adsorption can be used to dry and sweeten these in the same unit operation.

TSA processes are applied to the removal of many inorganic pollutants. CO_2 is removed from base-load and peak-shaving natural-gas liquefaction facilities using 4A zeolite in a TSA cycle. The Sulfacid and Hitachi fixed-bed processes, the Sumitomo and BF moving-bed processes, and the Westvaco fluidized-bed process all use activated carbon adsorbents to remove SO_2 from flue gases and sulfuric acid plant tail gases [Juentgen, *Carbon,* **15,** 273–283 (1977)]. Activated carbon with a catalyst is used by the Unitaka process to remove NO_x by reacting with ammonia, and activated carbon has been used to convert NO to NO_2, which is removed by scrubbing. Mercury vapor from air and other gas streams is removed and recovered by activated carbon impregnated with elemental sulfur; the Hg is then recovered by thermal oxidation in a retort [Lovett and Cunniff, *Chem. Eng. Progr.,* **70,** 43–47 (1974)]. Applications for HCl removal from Cl_2, chlorinated hydrocarbons, and reformer catalyst gas streams use TSA with mordenite and clinoptilolite zeolites [Dyer, gen. refs., pp. 102–105]. Activated aluminas are also used for HCl adsorption as well as fluorine and boron-fluorine compounds from alkylation processes [Crittenden, ibid.].

PRESSURE-SWING ADSORPTION

A pressure-swing adsorption (PSA) process cycle is one in which desorption takes place at a pressure much lower than adsorption. Reduction of pressure is used to shift the adsorption equilibrium and affect regeneration of the adsorbent. Figure 16-39 depicts a simplified pressure-swing cycle. Feed fluid containing an adsorbate at a molar concentration of $y_1 = p_1/P_1$ is passed through an adsorbent at conditions T_1, P_1, and the adsorption step continues until the equilibrium loading n_1 is achieved with y_1. Next, the total pressure is reduced to P_2 during the depressurization (or blowdown) step. Now, although the partial pressure in equilibrium with n_1 is still p_1, there is a concentration driv-

ing force of $y_2 = p_1/P_2 > y_1$ for desorption into any fluid containing less than y_2. By passing a fluid across the adsorbent in a purge step, adsorbate is swept away, and the equilibrium proceeds down the isotherm to some point such as y_1, n_2. (The choice of y_1 is arbitrary and need not coincide with feed composition.) At this time, the adsorbent is repressurized to P_1. The new equilibrium y_3, n_2 represents the best quality product that can be produced from the adsorbent at a regenerated loading of n_2. The adsorption step is now repeated. The differential loading, $n_1 - n_2$, is the maximum loading that can be achieved for a pressure-swing cycle operating between a feed containing y_1 and a product containing a molar concentration y_3 of the adsorbate. The regeneration fluid will contain an average concentration between y_2 and y_1 and will therefore have accomplished a concentration of the adsorbate in the regenerant gas. There is no analog for a liquid-phase PSA process cycle.

Thus, in a PSA process cycle, regeneration is achieved by a depressurization that must reduce the partial pressure of the adsorbates to allow desorption. These cycles operate at constant temperature, requiring no heating or cooling steps. Rather, they use the exothermic heat of adsorption remaining in the adsorbent to supply the endothermic heat needed for desorption. Pressure-swing cycles are classified as: (1) PSA, which, although used broadly, usually swings between a high superatmospheric and a low superatmospheric pressure; (2) VSA (vacuum-swing adsorption), which swings from a superatmospheric pressure to a subatmospheric pressure; and (3) PSPP (pressure-swing parametric pumping) and RPSA (rapid pressure-swing adsorption), which operate at very fast cycle times such that significant pressure gradients develop in the adsorbent bed (see the subsection on parametric pumping). Otherwise, the broad principles remain the same.

Low pressure is not as effective in totally reversing adsorption as is temperature elevation unless very high feed to purge pressure ratios are applied (e.g., deep vacuum). Therefore, most PSA cycles are characterized by high residual loadings and thus low operating loadings. These low capacities at high concentrations require that cycle times be short for reasonably sized beds (seconds to minutes). These short cycle times are attainable because particles of adsorbent respond quickly to changes in pressure. Major uses for PSA processes include purification as well as applications where contaminants are present at high concentration (bulk separations).

Other Cycle Steps   A PSA cycle may have several other steps in addition to the basic adsorption, depressurization, and repressurization. Cocurrent depressurization, purge, and pressure-equalization steps are normally added to increase efficiency of separation and recovery of product. At the end of the adsorption step, the more weakly adsorbed species have been recovered as product, but there is still a significant amount held up in the bed in the inter- and intra-particle void spaces. A cocurrent depressurization step can be added before the blowdown step, which is countercurrent to adsorption. This increases the amount of product produced each cycle. In some applications, the purity of the more strongly adsorbed components has also been shown to be heavily dependent on the cocurrent depressurization step [Cen and Yang, *Ind. Eng. Chem. Fundam.*, **25**, 758–767 (1986)]. This cocurrent blowdown is optional because there is always a countercurrent one. Skarstrom developed criteria to determine when the use of both is justified [Skarstrom in Li, *Recent Developments in Separation Science*, vol. II, CRC Press, Boca Raton, pp. 95–106 (1975)].

Additional stripping of the adsorbates from the adsorbent and purging of them from the voids can be accomplished by the addition of a purge step. The purge can begin toward the end of the depressurization or immediately afterward. Purging is accomplished with a flow of product countercurrent to adsorption to provide a lower residual at the product effluent end of the bed.

The repressurization step that returns the adsorber to feed pressure and completes the steps of a PSA cycle should be completed with pressure equalization steps to conserve gas and compression energy. Portions of the effluent gas during depressurization, blowdown, and enrichment purge can be used for repressurization to reduce the quantity of feed or product gas needed to pressurize the beds. The most efficient cycle is one that most closely matches available pressures and adsorbate concentration to the appropriate portion of the bed at the proper point in the cycle.

Applications   PSA cycles are used primarily for purification of wet gases and of hydrogen. One of the earliest applications was the original Skarstrom two-bed cycle (adsorption, countercurrent blowdown, countercurrent purge, and cocurrent repressurization) to dry air stream to less than 1 ppm H_2O [Skarstrom, ibid.]. Instrument-air dryers still use a PSA cycle similar to Skarstrom's with activated alumina or silica gel [Armond, in Townsend, *The Properties and Applications of Zeolites*, The Chemical Society, London, pp. 92–102 (1980)].

The hydrocarbon exclusion by small-pore zeolites allows PSA to achieve a 10 to 30 K dewpoint depression in air-brake compressors, even at high discharge air temperatures in the presence of compressor oil [Ausikaitis, in Katzer, *Molecular Sieves—II, Am. Chem. Soc. Symp. Ser.*, **40**, pp. 681–695 (1977)]. The high-purity hydrogen employed in processes such as hydrogenation, hydrocracking, and ammonia and methanol production is produced by PSA cycles with adsorbent beds compounded of activated carbon, zeolites, and carbon molecular sieves [Martin, Gotzmann, Notaro, and Stewart, *Adv. Cryog. Eng.*, **31**, 1071–1086 (1986)]. The impurities to be removed include ammonia, carbon oxides, nitrogen, oxygen, methane, and heavier hydrocarbons. In order to be able to produce purities as high as 99.9999
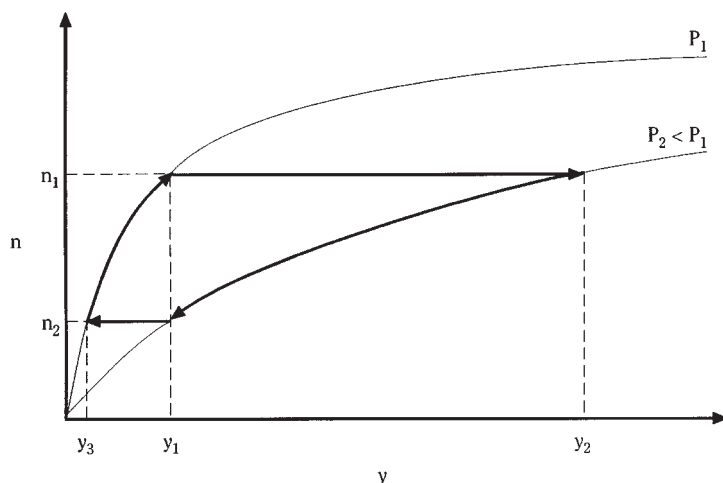

FIG. 16-39   Ideal pressure swing cycle. (*Reprinted with permission of UOP.*)

percent, systems such as a UOP™ Polybed™ separation unit use six to ten adsorbers with complex cycles (see below) [Fuderer and Rudelstorfer, U.S. Patent 3,986,849 (1976)].

Air separation, methane enrichment, and iso/normal separations are the major bulk separations utilizing PSA; recovery of CO and CO_2 are also growing uses. PSA process cycles are used to produce oxygen and/or nitrogen from air. Synthetic zeolites, clinoptilolite, mordenite, and carbon molecular sieves are all used in various PSA, VSA, and RPSA cycles. The 85 to 95 percent purity oxygen produced is employed for electric furnace steel, waste water treating, solid waste combustion, and kilns [Martin et al., ibid.]. Small PSA oxygen units are used for patients requiring inhalation therapy in the hospital and at home [Cassidy and Holmes, *AIChE Symp. Ser.,* **80** (1984), pp. 68–75] and for pilots on board aircraft [Tedor, Horch, and Dangieri, *SAFE J.,* **12,** 4–9 (1982)]. Lower purity oxygen (25 to 55 percent) can be produced to enhance combustion, chemical reactions, and ozone production [Sircar, in Rodrigues et al., gen. refs., pp. 285–321]. High purity nitrogen (up to 99.99 percent) for inert blanketing is produced in PSA and VSA processes using zeolites and carbon molecular sieves [Kawai and Kaneko, *Gas Sep. & Purif.,* **3,** 2–6 (1989); Ruthven, ibid.]. Methane is upgraded to natural gas pipeline quality by another PSA process. The methane is recovered from fermentation gases of landfills and wastewater purification plants and from poor-quality natural gas wells and tertiary oil recovery. Carbon dioxide is the major bulk contaminant but the gases contain water and other "garbage" components such as sulfur and halogen compounds, alkanes, and aromatics [Kumar and VanSloun, *Chem. Eng. Progr.,* **85,** 34–40 (1989)]. These impurities are removed by TSA using activated carbon or carbon molecular sieves and then the CO_2 is adsorbed using a PSA cycle. The cycle can use zeolites or silica gel in an equilibrium-selective separation or carbon molecular sieve in a rate-selective separation [Kapoor and Yang, *Chem. Eng. Sci.,* **44,** 1723–1733 (1989); Richter, Erdoel Kohle, Erdgas, *Petrochem.,* **40,** 432–438 (1987)]. The pore-size selectivity of zeolite 5A is employed to adsorb straight-chain molecules while excluding branched and cyclic species in the UOP IsoSiv[SM] process. This PSA process separates C_5 to C_9 range hydrocarbons into a normal-hydrocarbon fraction of better than 95 percent purity, and a higher-octane isomer fraction with less than 2 percent normals [Cassidy and Holmes, ibid.].

PURGE/CONCENTRATION SWING ADSORPTION

A purge-swing adsorption cycle is usually considered to be one in which desorption takes place at the same temperature and total pressure as adsorption. Desorption is accomplished either by partial-pressure reduction using an inert gas purge or by adsorbate displacement with another adsorbable component. Purge cycles operate adiabatically at nearly constant inlet temperature and require no heating or cooling steps. As with PSA, they utilize the heat of adsorption remaining in the adsorbent to supply the heat of desorption. Purge processes are classified as (1) inert or (2) displacement.

Inert Purge   In inert-purge desorption cycles, *inert* refers to the fact that the purge is not adsorbable at the cycle conditions. Inert purging desorbs the adsorbate solely by partial pressure reduction. Regeneration of the adsorbent can be achieved while maintaining the same temperature and pressure by the introduction of an inert purge fluid. Figure 16-40 depicts a simplified inert-purge swing cycle utilizing a nonadsorbing purge fluid. As before, the feed stream containing an adsorbate at a partial pressure of p_1 is passed through an adsorbent at temperature T_1, and the adsorption step continues until equilibrium n_1 is achieved. Next the nonadsorbing fluid is introduced to reduce the partial pressure below p_1 by dilution. Therefore, there is a partial pressure driving force for desorption into the purge fluid, and the equilibrium proceeds down the isotherm to the point p_2, n_2, where p_2 represents the best quality product that can be produced from the adsorbent at a regenerated loading of n_2. The adsorption step is now repeated, and the differential loading is $n_1 - n_2$. The regeneration fluid will contain an average partial pressure between p_2 and p_1, and the cycle will therefore not have accomplished a concentration of the adsorbate in the regenerant fluid. But it will have transferred the adsorbates to a fluid from which it may be more easily separated by means such as distillation.

Like PSA cycles, inert-purge processes are characterized by high residual loadings, low operating loadings, and short cycle times (minutes). Bulk separations of contaminants not easily separable at high concentration and of weakly adsorbed components are especially suited to inert-purge-swing adsorption. Another version of UOP's Iso-Siv process employs H_2 in an inert-purge cycle for separating C_5 to C_9 naphtha by adsorbing straight-chain molecules and excluding branched and cyclic species on size selective 5A zeolite [Cassidy and Holmes, ibid.]. Automobiles made in the United States have canisters of activated carbon to adsorb gasoline vapors lost from the carburetor or the gas tank during running, from the tank during diurnal cycling, and from carburetor hot-soak losses; the vapors are desorbed by an inert purge of air that is drawn into the carburetor as fuel when the engine is running [Clarke, Gerrard, Skarstrom, Vardi and Wade, *S.A.E. Trans.,* **76,** 824–842 (1968)]. UOP's Adsorptive Heat Recovery drying system has been commercialized for drying azeotropic ethanol to be blended with gasoline into gasohol; the process uses a closed loop of N_2 as the inert purge to desorb the water [Garg and Yon, *Chem. Eng. Progr.,* **82,** 54–60 (1986)].

Displacement Purge   Isothermal, isobaric regeneration of the
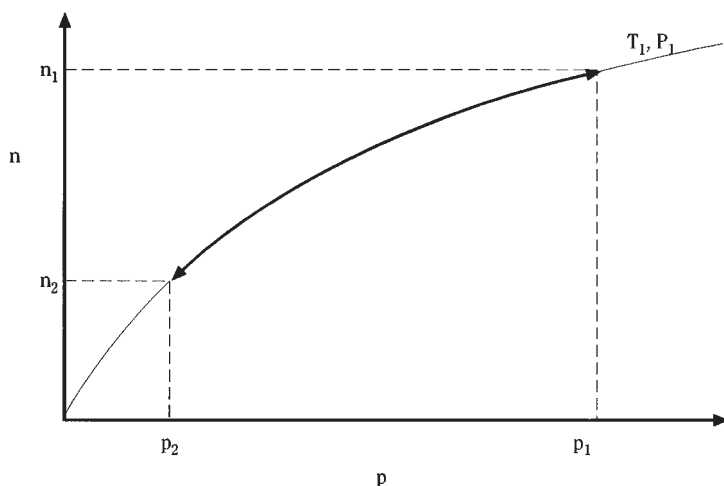

FIG. 16-40   Ideal inert-purge swing cycle. (*Reprinted with permission of UOP.*)

adsorbent can also be accomplished by using a purge fluid that can adsorb. In displacement-purge stripping, *displacement* refers to the displacing action of the purge fluid caused by its ability to adsorb at the cycle conditions. Figure 16-41 depicts a simplified displacement-purge swing cycle utilizing an adsorbable purge. Again, the feed stream containing an adsorbate at a partial pressure of p_1 is passed through an adsorbent at temperature T_1, and the adsorption step continues until equilibrium n_1 is achieved. Next the displacement fluid, B, is introduced. The presence of another adsorbable species reduces the adsorptivity of the key adsorbate, A. Therefore, there exists a partial pressure driving force for desorption into the purge fluid, and the equilibrium proceeds down the isotherm to some point such as p_1, n_2 (again arbitrary.) Next the adsorbent is recharged with a fluid that contains no component B, shifting the effective isotherm to that where the equilibrium of component A is p_3. The new equilibrium p_3, n_2 represents the best quality product that can be produced from the adsorbent at a regenerated loading of n_2. The adsorption step is now repeated. The differential loading $(n_1 - n_2)$ is the maximum loading that can be achieved for a pressure-swing cycle operating between a feed containing y_1 and a product containing a partial pressure p_3 of the adsorbate. The regeneration fluid will contain an average partial pressure between p_2 and p_1 and will therefore have accomplished a concentration of the adsorbate in the regenerant gas. Displacement-purge cycles are not as dependent on the heat of adsorption remaining on the adsorbent, because the adsorption of purge releases most or all of the energy needed to desorb the adsorbate. It is best if the adsorbate is more selectively adsorbed than the displacement purge, so that the adsorbates can easily desorb the purge fluid during adsorption. The displacement purge must be carefully selected, because it contaminates both the product stream and the recovered adsorbate, and requires separation for recovery (e.g., distillation).

Displacement-purge processes are more efficient for less selective adsorbate/adsorbent systems, while systems with high equilibrium loading of adsorbate will require more purging [Sircar and Kumar, *Ind. Eng. Chem. Proc. Des. Dev.*, **24**, 358–364 (1985)]. Several displacement-purge-swing processes have been commercialized for the separation of branched and cyclic C_{10}–C_{18} from normals using the molecular-size selectivity of 5A zeolite: Exxon's Ensorb, UOP's IsoSiv, Texaco Selective Finishing (TSF), Leuna Werke's Parex, and the Shell Process [Ruthven, ibid.]. All use a purge of normal paraffin or light naphtha with a carbon number of two to four less than the feed stream except for Ensorb, which uses ammonia [Yang, gen. refs.]. UOP has also developed a similar process, OlefinSiv, which separates isobutylene from normal butenes with displacement purge and a size-selective zeolite [Adler and Johnson, *Chem. Eng. Progr.*, **75**, 77–79

(1979)]. Solvent extraction to regenerate activated carbon is another example of a displacement-purge cycle; the adsorbent is then usually steamed to remove the purge fluid [Martin and Ng, *Water Res.*, **18**, 59–73 (1984)]. The best use of solvent regeneration is for water phase adsorption where the separation of water from carbon would use too much steam and where purge and water are easily separated; and for vapor-phase where the adsorbate is highly nonvolatile but soluble. Air Products has developed a process for separating ethanol/water on activated carbon using acetone as a displacement agent and adding a water rinse to improve the recovery of two products [Sircar, U.S. Patent 5,026,482 (1991)].

Displacement-purge forms the basis for most simulated continuous countercurrent systems (see hereafter) such as the UOP Sorbex^{SM} processes. UOP has licensed close to one hundred Sorbex units for its family of processes: Parex^{SM} to separate *p*-xylene from C_8 aromatics, Molex^{SM} for *n*-paraffin from branched and cyclic hydrocarbons, Olex^{SM} for olefins from paraffin, Sarex^{SM} for fructose from dextrose plus polysaccharides, Cymex^{SM} for *p*- or *m*-cymene from cymene isomers, and Cresex^{SM} for *p*- or *m*-cresol from cresol isomers. Toray Industries' Aromax^{SM} process is another for the production of *p*-xylene [Otani, *Chem. Eng.*, **80**(9), 106–107, (1973)]. Illinois Water Treatment [*Making Waves in Liquid Processing*, Illinois Water Treatment Company, IWT Adsep System, Rockford, IL, **6**(1), (1984)] and Mitsubishi [Ishikawa, Tanabe, and Usui, U.S. Patent 4,182,633 (1980)] have also commercialized displacement-purge processes for the separation of fructose from dextrose.

Chromatography   Chromatography is a sorptive separation technique that allows multicomponent separations in both gas and liquid phase. As a preparative tool, it is often used as a displacement-purge process, although many applications employ an inert-displacement mode, especially for use in analysis. General characteristics and operating modes are discussed in a separate part of this section.

ION EXCHANGE

Except in very small-scale applications, ion-exchangers are used in cyclic operations involving sorption and desorption steps. A typical ion-exchange cycle used in water-treatment applications involves (a) *backwash*—used to remove accumulated solids obtained by an upflow of water to expand (50–80 percent expansion is typical) and fluidize the exchanger bed; (b) *regeneration*—a regenerant is passed slowly through the used to restore the original ionic form of the exchanger; (c) *rinse*—water is passed through the bed to remove regenerant from the void volume and, in the case of porous exchangers, from the resin pores; (d) *loading*—the fresh solution to be treated is passed through
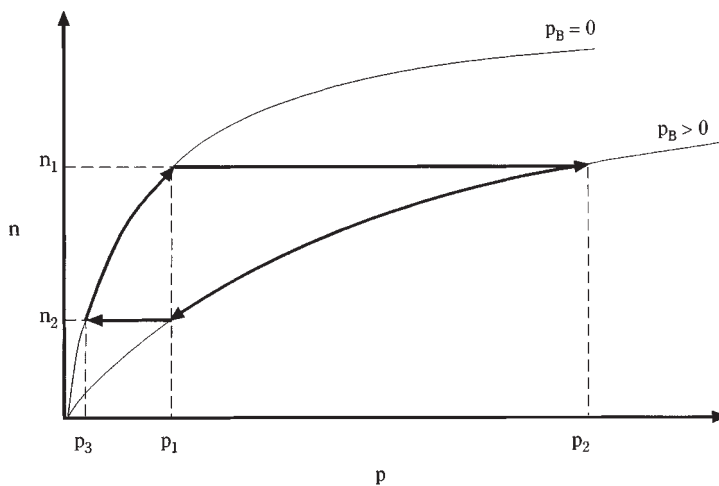

FIG. 16-41   Ideal displacement-purge swing cycle. (*Reprinted with permission of UOP.*)
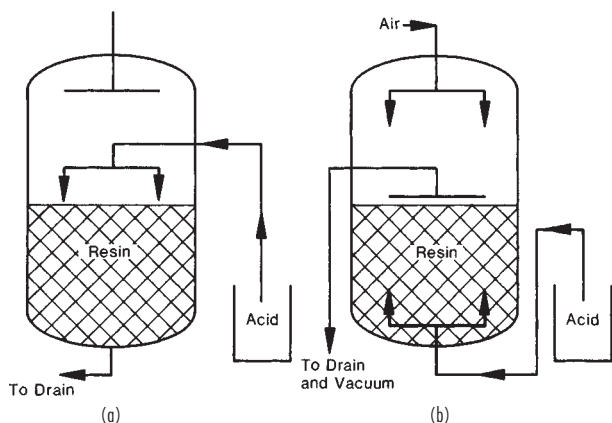
FIG. 16-42 Ion-exchanger regeneration. (*a*) Conventional. Acid is passed downflow through the cation-exchange resin bed. (*b*) Counterflow. Regenerant solution is introduced upflow with the resin bed held in place by a dry layer of resin.

the bed until leakage begins to occur. Water softening is practiced in this way with a cation exchange column in sodium form. At the low ionic strength used in the loading step, calcium and magnesium are strongly preferred over sodium, allowing nearly complete removal. Since the selectivity for divalent cations decreases sharply with ionic concentration, regeneration is carried out effectively with a concentrated sodium chloride solution. Removal of sulfates from boiler feed water is done by similar means with anion exchangers in chloride form.

Many ion-exchange columns operate downflow and are regenerated in the same direction (Fig. 16-42*a*). However, a better regeneration and lower leakage during loading can be achieved by passing the regenerant countercurrently to the loading flow. Specialized equipment is available to perform countercurrent regeneration (see "Equipment" in this section). One approach (Fig. 16-42*b*) is to apply a vacuum to remove the regenerant at the top of the bed.

Complete deionization with ion-exchange columns is the classical method of producing ultrapure water for boiler feed, in electronics manufacture, and for other general uses in the chemical and allied industries. Deionization requires use of two exchangers with opposite functionality to remove both cations and anions. These can be in separate columns, packed in adjacent layers in the same column, or, more frequently, in a mixed bed. In the latter case, the two exchangers are intimately mixed during the loading step. For regeneration, back-

washing separates the usually lighter anion exchanger from the usually denser cation exchanger. The column typically has a screened distributor at the interface between the two exchangers, so that they may be separately regenerated without removing them from the column. The most common cycle (Fig. 16-43) permits sequential regeneration of the two exchangers, first with alkali flowing downward through the anion exchanger to the interface distributor and then acid flowing downward from the interface distributor through the cation exchanger. After regeneration and rinsing, the exchangers are remixed by compressed air. To alleviate the problem of intermixing of the two different exchangers and chemical penetration through the wrong one, an inert material of intermediate density can be used to provide a buffer zone between layers of cation and anion exchangers.

When recovery of the sorbed solute is of interest, the cycle is modified to include a displacement step. In the manufacture of pharmaceuticals, ion-exchangers are used extensively in recovery and separation. Many of these compounds are amphoteric and are positively or negatively charged depending on the solution pH. Thus, using for example a cation exchanger, loading can be carried out at a low pH and displacement at a high pH. Differences in selectivity for different species can be used to carry out separations during the displacement [Carta et al., *AIChE Symp. Ser.*, **84**, 54–61 (1988)]. Multibed cycles are also used to facilitate integration with other chemical process operations. Fig. 16-44 shows a two-bed ion exchange system using both cation and anion exchangers to treat and recover chromate from rinse water in plating operations. The cation exchanger removes trivalent chromium, while the anion exchanger removes hexavalent chromium as an anion. Regeneration of the cation exchanger with sulfuric acid produces a concentrated solution of trivalent chromium as the sulfate salt. The hexavalent chromium is eluted from the anion exchanger with sodium hydroxide in a concentrated solution. This solution is recycled to the plating tank by passing it through a second cation exchange column in hydrogen form to convert the sodium chromate to a dilute chromic acid solution that is concentrated by evaporation.

PARAMETRIC PUMPING

The term *parametric pumping* was coined by Wilhelm et al. [Wilhelm, Rice, and Bendelius, *Ind. Eng. Chem. Fundam.*, **5**, 141–144 (1966)] to describe a liquid-phase adsorption process in which separation is achieved by periodically reversing not only flow but also an intensive thermodynamic property such as temperature, which influences adsorptivity. Moreover, they considered the concurrent cycling of pressure, pH, and electrical and magnetic fields. A lot of research and development has been conducted on thermal, pressure, and pH driven cycles, but to date only gas-phase pressure-swing parametric pumping has found much commercial acceptance.
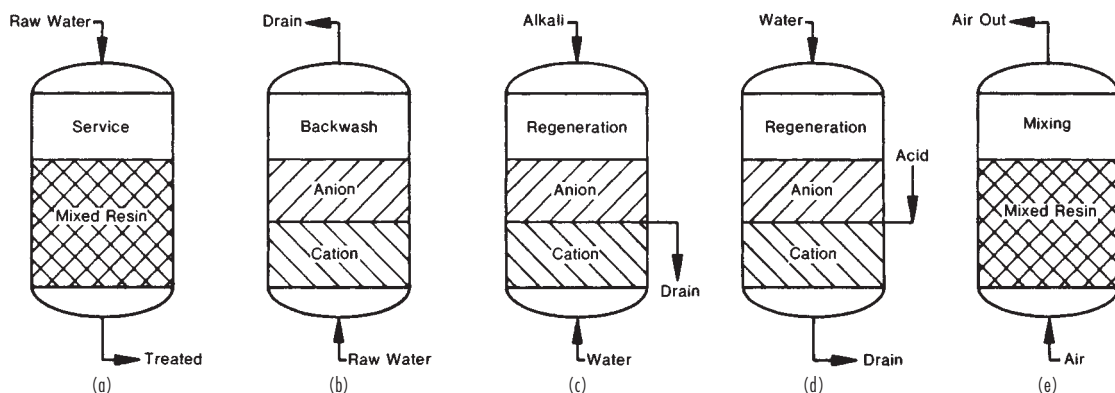

FIG. 16-43 Principles of mixed-bed ion exchange. (*a*) Service period (loading). (*b*) Backwash period. (*c*) Caustic regeneration. (*d*) Acid regeneration. (*e*) Resin mixing.
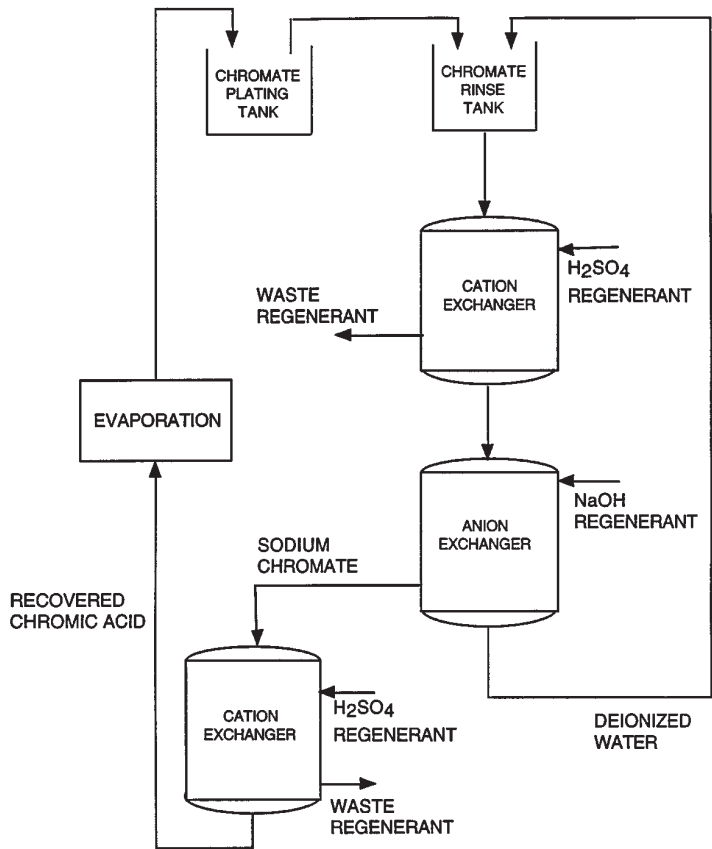
FIG. 16-44   Multicomponent ion-exchange process for chromate recovery from plating rinse water. (*Adapted from Rhom & Haas with permission.*)
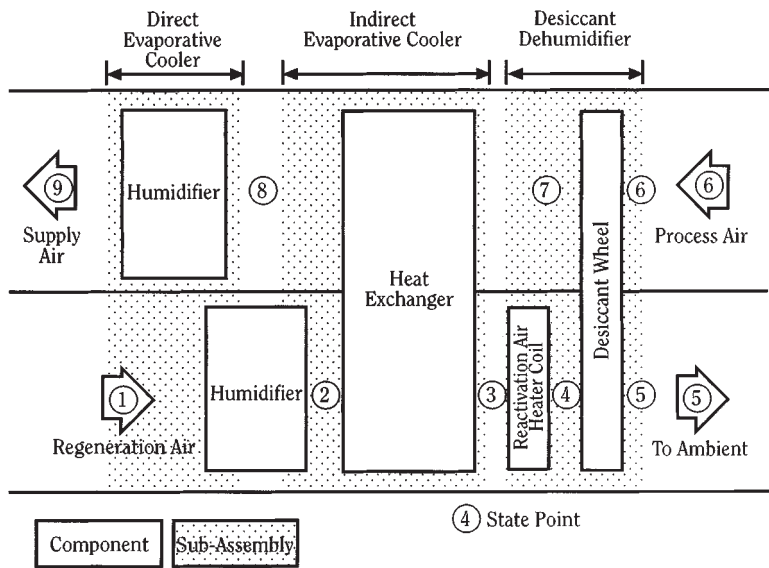

FIG. 16-45   Flow diagram of desiccant cooling cycle. [*Reprinted with permission of American Society of Heating, Refrigeration and Air Conditioning Engineers, Inc. (ASHRAE). Reference: Collier, Cohen, and Slosberg in Harrimam,* Desiccant Cooling and Dehumidification, *ASHRAE, Atlanta, 1992.*]

Temperature   Two modes of temperature parametric-pumping cycles have been defined—direct and recuperative. In direct mode, an adsorbent column is heated and cooled while the fluid feed is pumped forward and backward through the bed from reservoirs at each end. When the feed is a binary fluid, one component will concentrate in one reservoir and one in the other. In recuperative mode, the heating and cooling takes place outside the adsorbent column. Parametric pumping, thermal and pH modes, have been widely studied for separation of liquid mixtures. However, the primary success for separating gas mixtures in thermal mode has been the separation of propane/ethane on activated carbon [Jencziewski and Myers, *Ind. Eng. Chem. Fundam.,* **9,** 216–221 (1970)] and of air/SO$_2$ on silica gel [Patrick, Schrodt, and Kermode, *Sep. Sci.,* **7,** 331–343 (1972)]. The difficulty with applying the thermal mode to gas separation is that in a fixed-volume gas-pressure increases during the hot step, which defeats the desorption purpose of this step. No thermal parametric-pumping cycle has yet been practiced commercially.

Pressure   Another approach to parametric pumping is accomplished by pressure cycling of an adsorbent. An adsorbent bed is alternately pressurized with forward flow and depressurized with backward flow through the column from reservoirs at each end. Like TSA parametric pumping, one component concentrates in one reservoir and one in the other. The pressure mode of parametric pumping has been called pressure-swing parametric pumping (PSPP) and rapid pressure swing adsorption (RPSA). It was developed to minimize process complexity and investment at the expense of product recovery. RPSA is practiced in single-bed [Keller and Jones in Flank, *Adsorption and Ion Exchange with Synthetic Zeolites,* **135** (1980), pp. 275–286] and multiple-bed [Earls and Long, U.S. Patent number 4,194,892, 1980] implementations. Adsorbers are short (about 0.3 to 1.3 m), and particle sizes are very small (about 150 to 400 mm). The total cycle time including adsorption, dead time, countercurrent purge, and sometimes a second dead time, ranges from a few to about 30 seconds. The feature of RPSA that differentiates it from traditional PSA is the existence of axial pressure profiles throughout the cycle much as temperature gradients are present in TSA parametric-pumping. Whereas PSA processes have essentially constant pressure through the bed at any given time, the flow resistance of the very small adsorbent particles produce substantial pressure drops in the bed. These pressure dynamics are key to the attainment of separation performance. RPSA has been commercialized for the production of oxygen and for the recovery of ethylene and chlorocarbons (the selectively adsorbed species) in an ethylene-chlorination process while purging nitrogen (the less selectively adsorbed specie).

OTHER ADSORPTION CYCLES

Steam   When steam is used for regeneration of activated carbon, it is desorbing by a combination thermal swing and displacement purge (described earlier in this section). The exothermic heat released when the steam is adsorbed supplies the thermal energy much more efficiently than is possible with heated gas purging. Slightly super-heated steam at about 130°C is introduced into the bed countercurrent to adsorption; for adsorbates with high boiling points, the steam temperature must be higher. Adsorbates are desorbed and purged out of the bed with the steam. Steam and desorbates then go to a condenser for subsequent separation. The water phase can be further cleaned by air stripping, and the sorbate-laden air from that stripper can be recycled with the feed to the adsorption bed.

Steam regeneration is most commonly applied to activated carbon that has been used in the removal and/or recovery of solvents from gases. At volatile organic compound (VOC) concentration levels from 500 to 15,000 ppm, recovery of the VOC from the stream used for regeneration is economically justified. Below about 500 ppm, recovery is not economically justifiable, but environmental concerns often dictate adsorption followed by destruction. While activated carbon is also used to remove similar chemicals from water and wastewater, regeneration by steam is not usual. The reason is that the water-treatment carbon contains 1 to 5 kg of water per kg of adsorbent that must be removed by drying before regeneration or an excessive amount of superheated steam will be needed. In water treatment,

there can also be significant amounts of nonvolatile compounds that do not desorb during steam regeneration and that residual will reduce the adsorption working capacity. There is a growing use of reticulated styrene-type polymeric resins for VOC removal from air [Beckett, Wood, and Dixon, *Environ. Technol.,* **13,** 1129–1140 (1992); Heinegaard, *Chem.-Ing.-Tech.,* **60,** 907–908 (1988)]. LeVan and Schweiger [in Mersmann and Scholl (eds.), *Fundamentals of Adsorption,* United Engineering Trustees, New York (1991), pp. 487–496] tabulate reported steam utilizations (kg steam/kg adsorbate recovered) for a number of processes.

Energy Applications   Desiccant cooling is a means for more efficiently providing air conditioning for enclosures such as supermarkets, ice rinks, hotels, and hospitals. Adsorbers are integrated into evaporative and electric vapor compression cooling equipment into an overall air handling system. Air conditioning is comprised of two cooling loads, latent heat for water removal and sensible heat for temperature reduction. The energy savings derive from shifting the latent heat load from expensive compression cooling (chilling) to cooling tower load. Early desiccant cooling used adsorption wheels (see hereafter) impregnated with the hygroscopic salt, LiCl. More recently, these wheels are being fabricated with zeolite and/or silica gel. They are then incorporated into a system such as the example shown in Fig. 16-45 [Collier, Cohen, and Slosberg, in Harrimam, *Desiccant Cooling and Dehumidification,* ASHRAE, Atlanta (1992)]. Process air stream 6, to be conditioned, passes through the adsorbent wheel, where it is dried. This is a nonisothermal process due to the release of heat of adsorption and transfer of heat from a wheel that may be above ambient temperature. The dry but heated air (7) is cooled in a heat exchanger that can be a thermal wheel. This stream (8) is further cooled, and the humidity adjusted back up to a comfort range by direct contact evaporative cooling to provide supply air. Regeneration air stream 1, which can be ambient air or exhausted air, is evaporatively cooled to provide a heat sink for the hot, dry air. This warmed air (3) is heated to the desired temperature for regeneration of the adsorbent wheel and exhausted to the atmosphere. Many other combinations of drying and cooling are used to accomplish desiccant cooling [Belding, in *Proceedings of AFEAS Refrigeration and Air Conditioning Workshop,* Breckenridge, CO (June 23–25, 1993)].

Heat pumps are another developing application of adsorbents. Zeolite/water systems have been evaluated as a means for transferring heat from a low temperature to a higher, more valuable level. Both natural (chabazite and clinoptilolite) and synthetic (NaX and high silica NaY) zeolites have favorable properties for sorption heat pumps. Data have demonstrated that hydrothermally stable Na-mordenite and dealuminated NaY can be used with water in chemical heat pumps to upgrade 100°C heat sources by 50 to 80°C using a 20°C heat sink [Fujiwara, Suzuki, Shin, and Sato, *J. Chem. Eng. Japan,* **23,** 738–743 (1990)]. Other work has shown that integration of two adsorber beds can achieve heating coefficients of performance of 1.56 for the system NaX/water, upgrading 150°C heat to 200°C with a 50°C sink [Douss, Meunier, and Sun, *Ind. Eng. Chem. Res.,* **27,** 310–316 (1988)].

Energy Conservation Techniques   The major use of energy in an adsorption cycle is associated with the regeneration step, whether it is thermal energy for TSA or compression energy for PSA. Since the regeneration energy per pound of adsorbent tends to be constant, the first step in minimizing consumption is to maximize the operating loading. When the mass-transfer zone (MTZ) is a large portion of the adsorber relative to the equilibrium section, the fraction of the bed being fully utilized is small. Most fixed-bed adsorption systems have two adsorbers so that one is on stream while the other is being regenerated. One means of improving adsorbent utilization is to use a lead/trim (or cascade, or merry-go-round) cycle. Two (or more) adsorbent beds in series treat the feed. The feed enters the lead bed first and then the trim bed. The trim bed is the one that has most recently been regenerated. The MTZ is allowed to proceed through the lead beds but not to break through the trim bed. In this way the lead bed can be almost totally utilized before being regenerated. When a lead bed is taken out of service, the trim bed is placed in lead position, and a regenerated bed is placed in the trim position.

A thermal pulse cycle is a means of conserving thermal energy in

heating-limited desorption. A process cycle that is heat-limited needs only a very small time (dwell) at temperature to achieve satisfactory desorption. If the entire bed is heated before the cooling is begun, every part of the bed will dwell at temperature for the entire time it takes the cooling front to traverse the bed. Thus, much of the heat in the bed at the start of cooling would be swept from the bed. Instead, cooling is begun before any heat front has exited the bed, creating a thermal pulse that moves through the bed. The pulse expends its thermal energy for desorption so that only a small temperature peak remains at the end of the regeneration and no excess heat has been wasted. If the heating step is stripping-limited, a thermal pulse is not applicable.

A series cool/heat cycle is another way in which the heat that is purged from the bed during cooling can be conserved. Sometimes the outlet fluid is passed to a heat sink where energy is stored to be reused to preheat heating fluid, or cross exchanged against the purge fluid to recover energy. However, there is also a process cycle that accomplishes the same effect. Three adsorbers are used, with one on adsorption, one on heating, and one on cooling. The regeneration fluid flows in series, first to cool the bed just heated and then to heat the bed to be desorbed. Thus all of the heat swept from the adsorber during heating can be reused to reduce the heating requirement. Unlike thermal pulse, this cycle is applicable to both heat- and stripping-limited heating.

Process Selection   The preceding sections present many process cycles and their variations. It is important to have some guidelines for design engineers to narrow their choice of cycles to the most economical for a particular separation. Keller and coworkers [Keller et al., gen. refs.] have presented a method for choosing appropriate adsorp-

TABLE 16-17   Process Descriptors

Number	Statement
1	Feed is a vaporized liquid or a gas.
2	Feed is a liquid that can be fully vaporized at less than about 200°C.
3	Feed is a liquid that cannot be fully vaporized at 200°C.
4	Adsorbate concentration in the feed is less than about 3 wt %.
5	Adsorbate concentration in the feed is between about 3 and 10 wt %.
6	Adsorbate concentration in the feed is greater than about 10 wt %.
7	Adsorbate must be recovered in high purity (> than 90–99% rejection of nonadsorbed material).
8	Adsorbate can be desorbed by thermal regeneration.
9	Practical purge or displacement agents cannot be easily separated from the adsorbate.

Keller, Anderson, and Yon in Rousseau (ed.), *Handbook of Separation Process Technology,* John Wiley & Sons, Inc., New York, 1987; reprinted with permission.

tion processes. Their procedure considers the economics of capital, energy, labor, and other costs. Although these costs can vary from site to site, the procedure is robust enough to include most scenarios. In Table 16-17, nine statements are made about the character of the separation being considered. The numbers of the statements that are true (i.e., applicable) are used in the matrix in Table 16-18. A "no" for any true statement under a given process should remove that process from further consideration. Any process having all "yes" answers for true statements deserves strong consideration. Entries other than "yes" or "no" provide a means of prioritizing processes when more than one cycle is satisfactory.

TABLE 16-18   Process Selection Matrix

Statement number, Table 16-17	Gas- or vapor-phase processes					Liquid-phase processes		
	Temperature swing	Inert purge	Displacement purge	Pressure swing	Chromatography	Temperature swing°	Simulated moving bed	Chromatography
1	Yes	Yes	Yes	Yes	Yes	No	No	No
2	Not likely	Yes	Yes	Yes	Yes	Yes	Yes	Yes
3	No	No	No	No	No	Yes	Yes	Yes
4	Yes	Yes	Not likely	Not likely	Not likely	Yes	Not likely	Maybe
5	Yes	Yes	Yes	Yes	Yes	No	Yes	Yes
6	No	Yes	Yes	Yes	Yes	No	Yes	Yes
7	Yes	Yes	Yes	Maybe†	Yes	Yes	Yes	Yes
8	Yes	No	No	No	No	Yes‡	No	No
9	Maybe§	Not likely	Not likely	N/A	Not likely	Maybe§	Not likely	Not likely

°Includes powdered, fixed-bed, and moving-bed processes.
†Very high ratio of feed to desorption pressure (>10:1) will be required. Vacuum desorption will probably be necessary.
‡If adsorbate concentration in the feed is very low, it may be practical to discard the loaded adsorbent or reprocess off-site.
§If it is not necessary to recover the adsorbate, these processes are satisfactory.
Keller, Anderson, and Yon in Rousseau (ed.), *Handbook of Separation Process Technology,* John Wiley & Sons, Inc., New York, 1987; reprinted with permission.

EQUIPMENT

ADSORPTION

General Design   Adsorbents are used in adsorbers with fixed inventory, with intermittent solids flow, or with continuous-moving solids flow. The most common are fixed beds operating as batch units or as beds of adsorbent through which the feed fluid passes, with periodic interruption for regeneration. Total systems consist of pressure vessels or open tanks along with the associated piping, valves, controls, and auxiliary equipment needed to accomplish regeneration of the adsorbent. Gas treating equipment includes blowers or compressors with a multiplicity of paths to prevent dead-heading. Liquid treating equipment includes pumps with surge vessels as needed to assure continuous flow.

Adsorber Vessel   The most frequently used method of fluid-solid contact for adsorption operations is in cylindrical, vertical vessels, with

the adsorbent particles in a fixed and closely but randomly packed arrangement. The adsorbers must be designed with consideration for pressure drop and must contain a means of supporting the adsorbent and a means of assuring that the incoming fluid is evenly distributed to the face of the bed. There are additional design considerations for adsorbers when the streams are liquid and for high-performance separation applications using very small particles (<0.05 mm) such as in HPLC.

For most large-scale processes, adsorbent particle size varies from 0.06 to 6 mm (0.0025 to 0.25 in), but the adsorbent packed in a fixed bed will have a fairly narrow particle size range. Pressure drop in adsorbers can be changed by changing the diameter to bed depth ratio and by changing the particle size (see Sec. 5). Adsorbent size also determines separation performance of adsorbent columns—increasing efficiency with decreasing particle size. In liquid-phase process-

ing, total cost of the adsorption step can sometimes be reduced by designing for overall pressure drops as large as 300 to 600 kPa (45 to 90 psi) because pumping is not the major utility cost. In special, high-resolution applications (HPLC), pressure drops as high as 5000–25,000 kPa (800–4000 psi) are sometimes used requiring special pumping and column hardware [Colin in Ganetsos and Barker, *Preparative and Production Scale Chromatography*, Marcel Dekker, New York, 1993, pp. 11–45]. However, the cost of compressing gases is significant. Since blowers are limited to about 5 kPa (20 in wc) of lift, atmospheric gas applications are typically designed with adsorbent pressure drops of 1 to 4 kPa (4 to 16 in wc). To keep compression ratio low, compressed gas adsorption pressure drops are 5 to 100 kPa (0.7 to 15 psi) depending on the pressure level.

Besides influencing how much pressure drop is allowable, the operating pressure determines other design features. When adsorption and/or regeneration is to be performed at pressures above atmospheric, the adsorber vessels are designed like process pressure vessels (Fig. 16-46 [EPA, gen. refs.]). Their flow distributors can consume more gas momentum at higher pressure. On the other hand, for applications near atmospheric pressure, any pressure drop can be costly, and most design choices are made in the direction of minimizing head loss. Beds have large face areas and shallow depth. Many times, the choice is to fabricate a horizontal (horizontal axis) vessel where flows are radial rather than axial as in conventional vertical beds. Figure 16-47 [Leatherdale in Cheremisinoff and Ellerbusch, gen. refs.] depicts how a rectangular, shallow adsorber bed is oriented in a horizontal vessel. Flow distributors, especially for large units, are often elaborate in order to evenly divide the flow rather than consume precious head.

There are two types of support systems used for fixed beds of adsorbent. The first is a progressive series of grid- and screen-layers. In this system, each higher layer screen has successively smaller openings, with the last small enough to prevent particles from passing through. Each lower layer has greater strength. A series of I-beams can be used to support a layer of subway grating that, in turn, supports several layers of screening. In other cases, special support grills such as John-son™ screens may rest on the I-beams or on clips at the vessel wall and thus directly support the adsorbent. The topmost screen must retain the original size particles and some reasonable size of broken particles. The second type of support is a graded system of particles such as ceramic balls or gravel that rests directly on the bottom of the adsorber. A typical system might consist of 100 mm (4 in) of 50 mm (2 in) diameter material, covered by succeeding layers of 25, 12, and 6 mm (1, ½, ¼ in) of support material for a 3 mm (⅛ in) adsorbent. In water treatment, the support may actually start with filter blocks and have an upper layer of sand (see Fig. 16-48 [EPA, gen. refs.]).

If flow is not evenly distributed throughout the bed of adsorbent, there will be less than maximum utilization of the adsorbent during adsorption and of the desorption fluid during regeneration. Incoming fluids from the nozzles is at a much higher velocity than the average through the bed and may have asymmetric momentum components due to the piping manifold. The simplest means of allowing flow to redistribute across the face of the bed is to employ ample plenum space above and below the fixed bed. A much more cost-effective
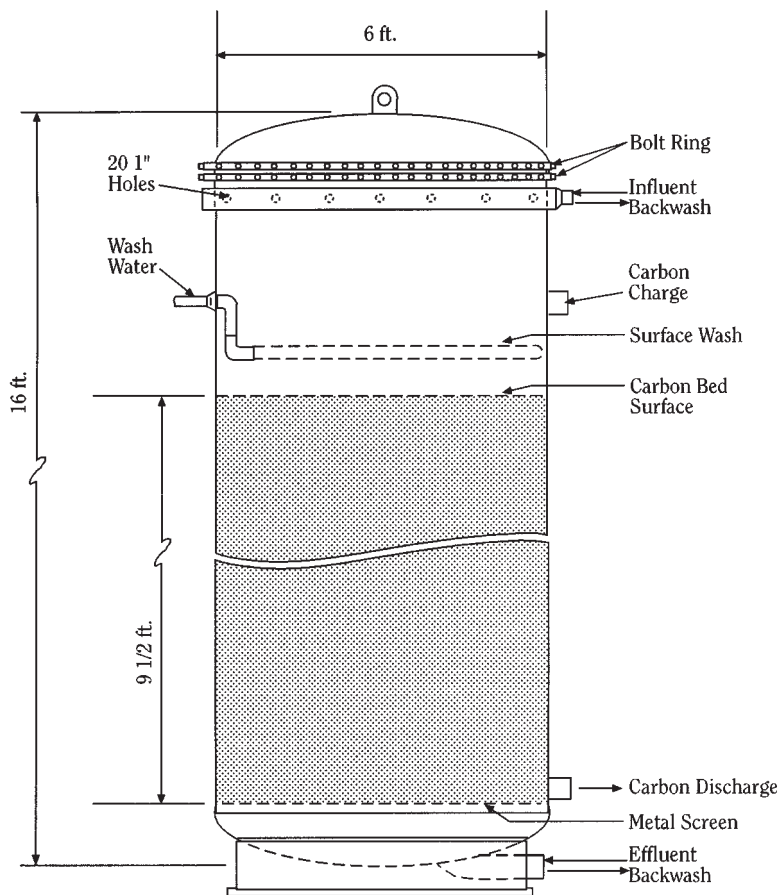

FIG. 16-46 Pressurized adsorber vessel. (*Reprinted with permission of EPA. Reference: EPA, Process Design Manual for Carbon Adsorption, U.S. Envir. Protect. Agency., Cincinnati, 1973.*)
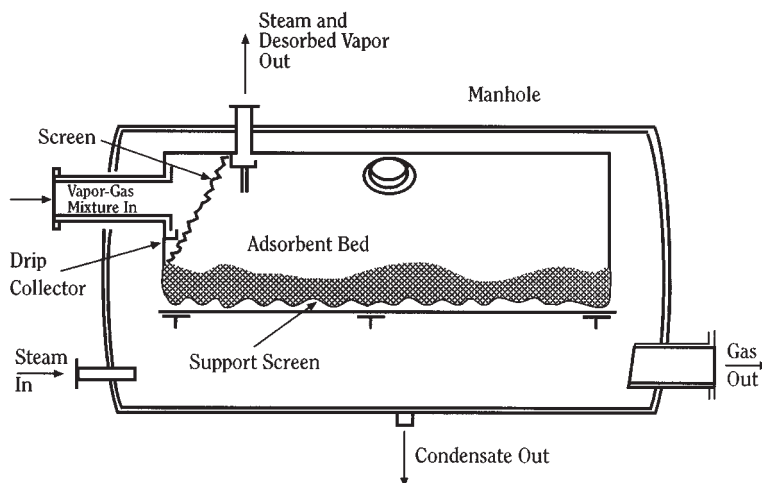
FIG. 16-47 Ambient pressure adsorber vessel. (*Reprinted with permission of Ann Arbor Science. Reference: Leatherdale in Cheremisinoff and Ellerbusch,* Carbon Adsorption Handbook, *Ann Arbor Science, Ann Arbor, 1978.*)

method is to install simple baffle plates with symmetrically placed inlet and outlet nozzles. The solid, or perforated, baffles are designed to break the momentum of the incoming fluid and redistribute it to prevent direct impingement on the adsorbent. When graded bed support is installed at the bottom, the baffles should be covered by screening to restrain the particles. An alternative to screened baffles is slotted metal or Johnson™ screen distributors. Shallow horizontal beds often have such a large flow area that multiple inlet and outlet nozzles are required. These nozzle headers must be carefully designed to assure balanced flow to each nozzle. In liquid systems, a single inlet may enter the vessel and branch into several pipes that are often perforated along their length (Fig. 16-46). Such "spiders" and "Christmas trees" often have holes that are not uniformly spaced and sized but are distributed to provide equal flow per bed area.

Although allowable pressure loss with liquids is not a restricting factor, there are special considerations for liquid treating systems. Activated carbon adsorbers used in water and wastewater treatment are designed and constructed using the same considerations used for turbidity removal by sand or multilayer filters. A typical carbon bed is shown in Fig. 16-48. Such contactors for liquids at ambient pressure are often nothing more than open tanks or concrete basins with flow distribution simply an overflow weir. In liquid treating, the adsorbers must be designed with a means for liquid draining and filling occasionally or during every cycle when a gas is used for regeneration. Draining is by gravity, sometimes assisted by a 70–140 kPa (10–20 psig) pressure pad. Even with time to drain, there will be significant liquid holdup to recover. As much as 40 cc of liquid per 100 g of adsorbent is retained in the micro- and macropores and bridged between particles. When drain is cocurrent to adsorption, the drained liquid can be recovered as treated product. When drain is countercurrent, drained fluid must be returned to feed surge. Minimizing other holdup in dead volume is especially important for liquid separation processes such as chromatography, because it adversely affects product recovery and regeneration efficiency. In filling an adsorber, there must be sufficient time for any gas trapped in the pores to escape. The fill step is preferably upflow to sweep the vapor out and to prevent gas pockets that could cause product contamination, bed lifting, or flow maldistribution. In liquid upflow, the buoyancy force of the liquid plus the pressure drop must not exceed the gravitational forces if bed lifting is to be prevented. Because there is very little increase in pressure drop beyond the lifting (or fluidization) velocity, some liquid systems are designed with bed expansion to limit pressure drop. Upflow-adsorption expanded-beds are also preferred when the liquid contains any suspended solids, so that the bed does not act as a filter and

become plugged. Since increased expansion causes the adsorbent to become increasingly well mixed, with accompanying drop in removal efficiency, expansion is usually limited to about 10 percent. Higher velocities also tend to cause too much particle turbulence, abrasion, attrition, and erosion.

Regeneration Equipment Sometimes it is economically justified to remove the adsorbent from the adsorber when it is exhausted and have an outside contractor regenerate it rather than install on-site regeneration equipment. This is feasible only if the adsorbent can treat feed for weeks or months rather than only hours or days. In other cases, the process conditions during regeneration are so much more severe than those for adsorption that a single regenerator with materials of construction capable of handling the conditions is more cost-effective than to make all adsorbers the expensive material. This is
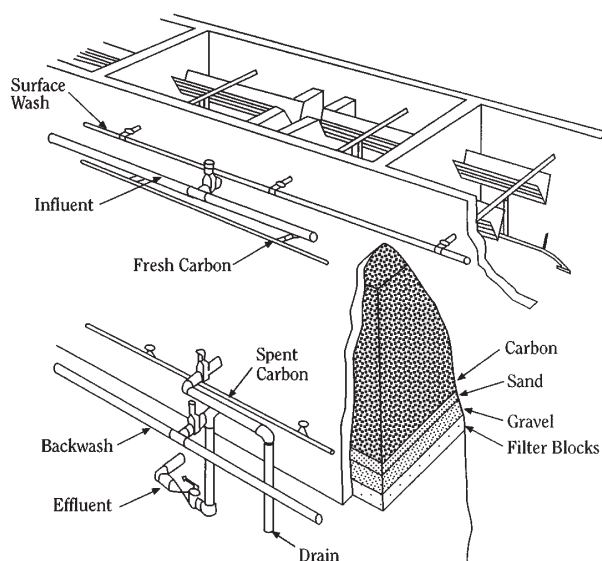

FIG. 16-48 Adsorber vessel with graded support system. (*Reprinted with permission of EPA. Reference: EPA,* Process Design Manual for Carbon Adsorption, *U.S. Envir. Protect. Agency., Cincinnati, 1973.*)
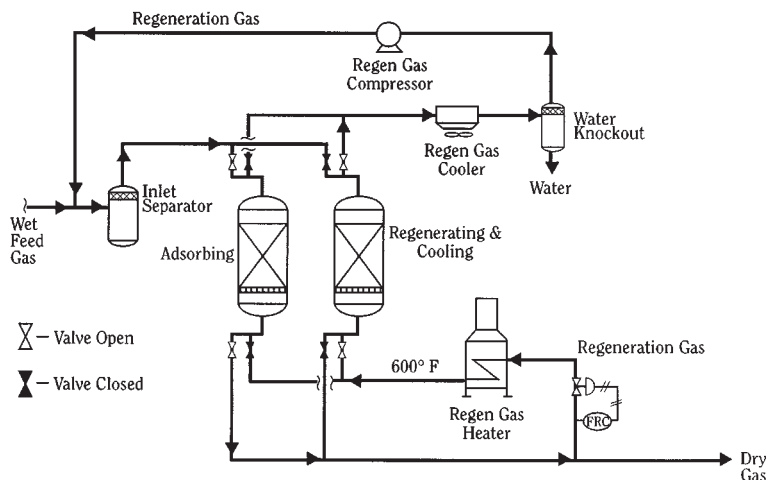
FIG. 16-49   Two-bed TSA system with regeneration equipment. (*Reprinted with permission of GPSA. Reference:* Engineering Data Book, *10th ed., Gas Processors Suppliers Association, Tulsa, 1988, Sec. 20, p. 22.*)

true for most water and wastewater treatment with thermally reactivated carbon. Otherwise, desorption is conducted in situ with any additional equipment connected to the adsorbers.

Figure 16-49 [*Engineering Data Book*, 10th ed., Gas Processors Suppliers Association, Tulsa, 1988, Sec. 20, p. 22] depicts the flow scheme for a typical two-bed TSA dryer system showing the auxiliary equipment associated with regeneration. Some of the dry product gas is externally heated and used countercurrently to heat and desorb water from the adsorber not currently drying feed. The wet, spent regeneration gas is cooled; the water is condensed out; and the gas is recycled to feed for recovery.

The thermal reactivation of spent activated carbon may require the same high temperatures and reaction conditions used for its manufacture. Although the exact conditions to be used for reactivation depend on the type of carbon and the adsorbates to be removed, the objective is to remove the adsorbed material without altering the carbon structure. This occurs in four stages: (a) drying, (b) desorption, (c) pyrolysis and carbonization, and (d) burnoff. Each of these steps is associated with a particular temperature range and is carried out in a multiple hearth furnace such as that depicted in Fig. 16-50. This six-hearth system is a typical configuration for water treatment carbons. The gas temperature ranges from 100°C on the top hearth to 950°C at the bottom. The rotating rabble arms rake the carbon from hearth to hearth. Wet, spent carbon is fed to the top, where it is dried by the top two hearths. Pyrolysis (desorption and decomposition) is accomplished on the next hearth. The bottom four hearths are for reactivation. Varying amounts of air, steam, and/or fuel are added to the different hearths to maintain the conditions established for the particular reactivation. A hearth area requirement of 0.1 m²/kg/hr (0.5 ft²/lb/hr) is adequate for cost estimating, but there are also detailed design procedures available [von Dreusche in Cheremisinoff and Ellerbusch, gen. refs.].

In addition to the multiple-hearth furnace, the reactivation system is comprised of additional equipment to transport, store, dewater, and quench the carbon.

A typical two-bed PSA dryer process flow scheme is very similar to Fig. 16-49 without the regeneration gas heater. A portion of the dry product gas is used countercurrently to purge the water from the adsorber not currently drying feed. Again, the wet, spent purge gas is cooled, and the water is condensed out and recycled to feed for recovery. If the cycle is VSA, then instead of the regeneration gas compressor, there is a vacuum compressor at the purge outlet upstream of the regeneration cooler. Some PSA cycles such as in air-brake dryers operate with one adsorber, a surge volume, and a three-way valve to

switch between pressurizing and countercurrent blowdown. The other extreme of complexity is demonstrated by the UOP nine-bed Polybed PSA H_2 unit shown in Fig. 16-51 [Fuderer and Rudelstorfer, U.S. Patent number 3,986,849, 1976]. This cycle requires nine adsorbers sequenced by fifty-five valves to maximize purity and recovery.

Cycle Control   Valves are the heart of cycle control for cyclic adsorption systems. These on/off valves switch flows among beds so
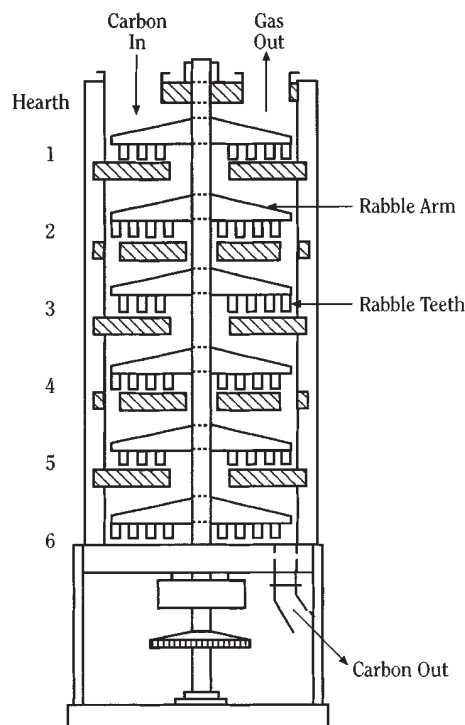

FIG. 16-50   Multiple hearth furnace for carbon reactivation. (*Reprinted with permission of EPA. Reference: EPA,* Process Design Manual for Carbon Adsorption, *U.S. Envir. Protect. Agency., Cincinnati, 1973.*)
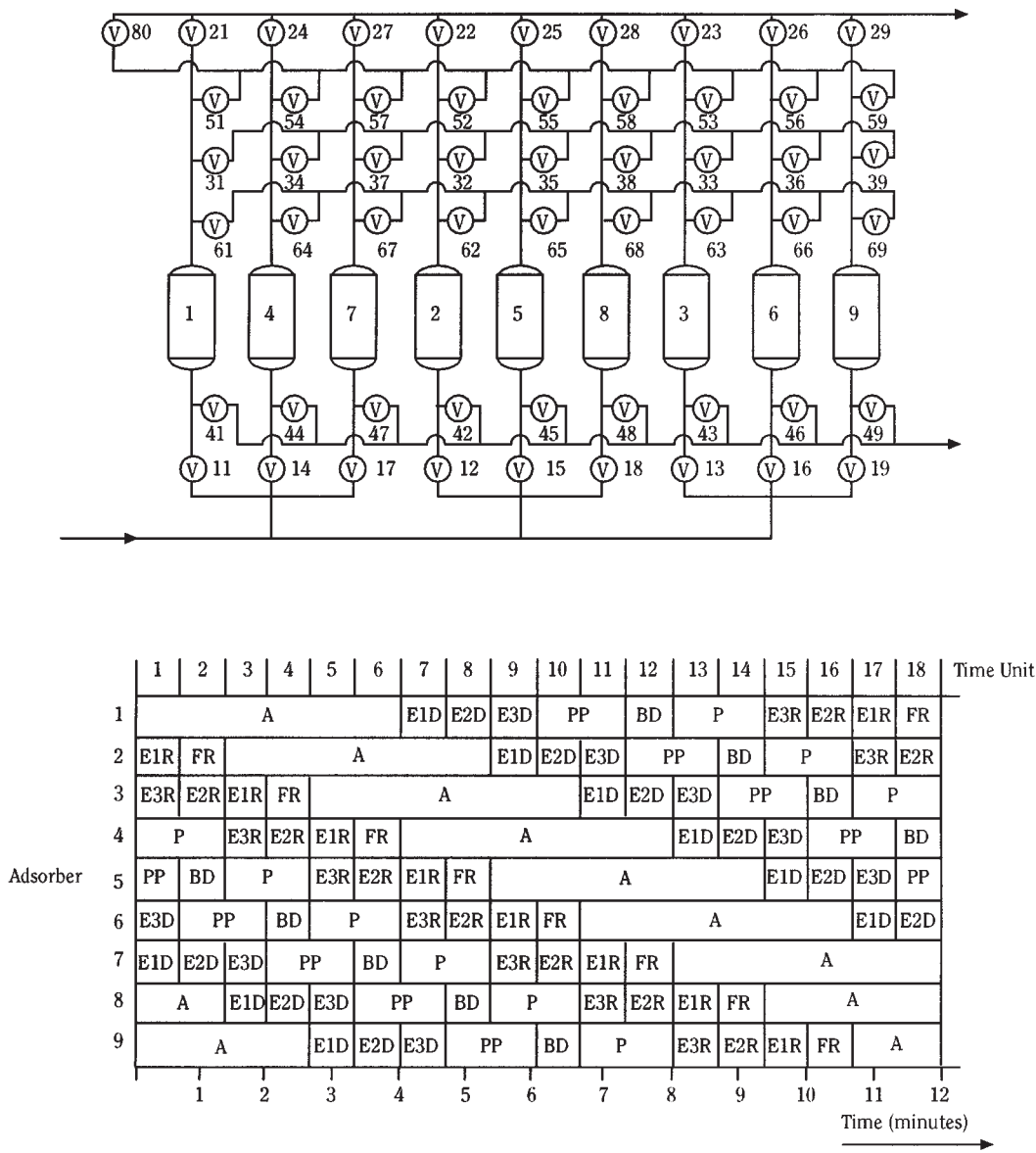
FIG. 16-51 UOP nine-bed polybed PSA H_2 unit: (*a*) flow scheme; (*b*) cycle diagram. (*Reference: Fuderer and Rudelstorfer, U.S. Patent number 3,986,849, 1976.*)

Cycle diagram (b):

Adsorber	1	2	3	4	5	6	7	8	9	10	11	12	13	14	15	16	17	18	Time Unit
1	A	A	A	A	A	A	E1D	E2D	E3D	PP	PP	BD	P	P	E3R	E2R	E1R	FR	
2	E1R	FR	A	A	A	A	A	A	E1D	E2D	E3D	PP	PP	BD	P	P	E3R	E2R	
3	E3R	E2R	E1R	FR	A	A	A	A	A	A	E1D	E2D	E3D	PP	PP	BD	P	P	
4	P	P	E3R	E2R	E1R	FR	A	A	A	A	A	A	E1D	E2D	E3D	PP	PP	BD	
5	PP	BD	P	P	E3R	E2R	E1R	FR	A	A	A	A	A	A	E1D	E2D	E3D	PP	
6	E3D	PP	PP	BD	P	P	E3R	E2R	E1R	FR	A	A	A	A	A	A	E1D	E2D	
7	E1D	E2D	E3D	PP	PP	BD	P	E3R	E2R	E1R	FR	A	A	A	A	A	A	A	
8	A	A	E1D	E2D	E3D	PP	PP	BD	P	E3R	E2R	E1R	FR	A	A	A	A	A	
9	A	A	A	E1D	E2D	E3D	PP	PP	BD	P	E3R	E2R	E1R	FR	A	A	A	A	

Time (minutes): 1 2 3 4 5 6 7 8 9 10 11 12

that external to the system it appears as if operation is continuous. In general, one valve is needed for each bed at each end for each step that is performed (e.g., for a two-bed system with an adsorption step plus heating and cooling step [carried out in the same direction and during the same step], only $2 \times 2 \times 2 = 8$ valves would be needed [see Fig. 16-49]). In some cycles such as pressure-swing systems, it may be possible to use valves for more than one function (e.g., repressurization with feed gas using the same manifold as adsorption feed). Without multiple use, the cycle in Fig. 16-51 would need $9 \times 2 \times 5 = 90$ valves instead of 55 to accommodate the five steps of adsorption, purge to product, blowdown, purge, and feed repressurization (even without the equalization). For some applications, 3- and 4-way valves can replace two and four valves, respectively. The ultimate integration of switching valves is the UOP rotary valve discussed below. For long step times (8 hours or more) it is possible for the valves to be manually switched by operators. For most systems, it is advantageous for the opening and closing of the valves be controlled by automatic timers. The same controller can be responsible for maintaining flows and pressure, logic for proceeding only on completion of events, and safety bypass or shutdown. Automatic control can provide for a period of parallel flow paths to assure transitions. In some applications, process analyzers can interface with the controller to initiate bed-switching when adsorbate is detected breaking through into the effluent.

Continuous Countercurrent Systems Most adsorption systems use fixed-bed adsorbers. However, if the fluid to be separated and that used for desorption can be countercurrently contacted by a moving bed of the adsorbent, there are significant efficiencies to be realized. Because the adsorbent leaves the adsorption section essentially in equilibrium with the feed composition, the inefficiency of the

mass-transfer zone is eliminated. The adsorption section only needs to contain a MTZ length of adsorbent compared to a MTZ plus an equilibrium section in a fixed bed. Likewise, countercurrent regeneration is more efficient. Since the adsorbent is moved from an adsorption chamber to another chamber for regeneration, only the regeneration section is designed for the often more severe conditions. Countercurrent adsorption can take advantage of an exceptionally favorable equilibrium in water softening; and the regeneration step can be made favorable by the use of relatively concentrated elutent. Continuous units generally require more headroom but much less footprint. The foremost problems to be overcome in the design and operation of continuous countercurrent sorption operations are the mechanical complexity of equipment and the attrition of the sorbent.

An early example of a commercial countercurrent adsorption processes is the hypersorption process developed by Union Oil Company for the recovery of propane and heavier components from natural gas [Berg, *Chem. Eng. Progr.,* **47,** 585–590 (1951)]. Hypersorption used an activated carbon adsorbent moving as a dense bed continuously downward through a rising gas stream (Fig. 16-52 [Berg, ibid.]). However, this process proved to be less economical than cryogenic distillation and had excessive carbon losses resulting from attrition. The commercialization by Kureha Chemical Co. of Japan of a new, highly attrition-resistant, activated-carbon adsorbent, allowed development of a process employing fluidized-bed adsorption and moving bed desorption for removal of VOC compounds from air. The process has been marketed as GASTAK[SM] in Japan and as PuraSiv[SM] HR (Fig. 16-53 [Anon., *Chem. Eng.,* **84**(18), 39–40 (1977)]) in the United States, and now as SOLDACS by Daikin Industries, Ltd. A
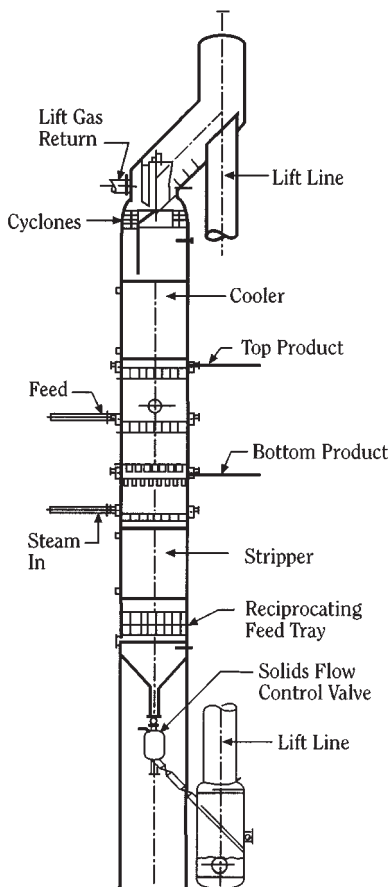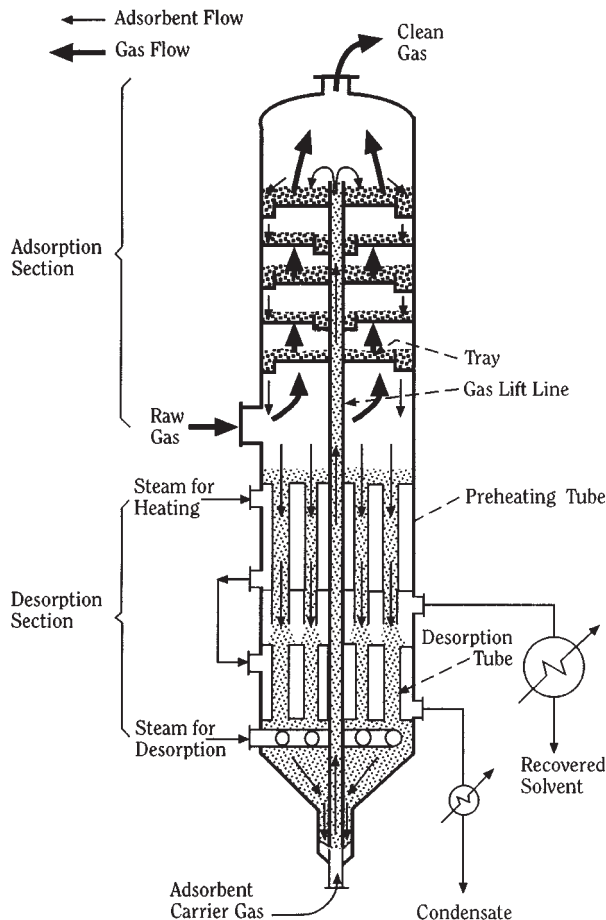

FIG. 16-53   PuraSiv HR adsorber vessel. [*Reprinted with permission of Chemical Engineering. Reference: Anon.,* Chem. Eng., **84***(18), 39–40 (1977).*]

similar process using beaded polymeric resin is offered by Chematur [Heinegaard, *Chem.-Ing.-Tech.,* **60,** 907–908 (1988)]. The recent discovery [Acharya and BeVier, U.S. Patent number 4,526,877, 1985] that the graphite coating of zeolites can dramatically improve attrition resistance without significantly impairing adsorption performance could allow the extension of moving-bed technology to other separations. A good review of continuous ion-exchange applications is presented by Wankat [gen. refs.].

Continuous Cross-Flow Systems   There are at least three implementations of moving-bed adsorption that are cross flow rather than fixed beds or countercurrent flow: (1) panel beds, (2) adsorbent wheels, and (3) rotating annular beds. By *cross flow* is meant that the adsorbent is moving in a direction perpendicular to the fluid flow. All of these employ moving adsorbent—the first, a down-flowing solid; and the others, a constrained solid. Panel beds of activated carbon like those depicted in Fig. 16-54 [Lovett and Cunniff, *Chem. Eng. Progr.,* **70**(5), 43–47 (1974)] have been applied to odor control [Lovett and Cunniff, ibid.] and to the desulfurization of waste gas [Richter, Knoblauch, and Juntgen, *Verfahrenstechnik (Mainz),* **14,** 338–342 (1980)]. The spent solid falls from the bottom panel into a load-out bin, and fresh regenerated carbon is added to the top; gas flows through as shown.

The heart of an adsorbent wheel system is a rotating cylinder containing the adsorbent. Figure 16-55 illustrates two types: horizontal and vertical. In some adsorbent wheels, the adsorbent particles are placed in basket segments (a multitude of fixed beds) to form a hori-
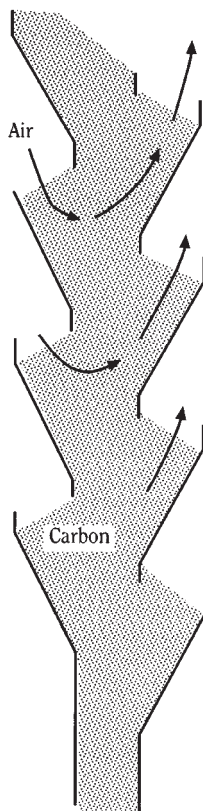

FIG. 16-52   Hypersorption adsorber vessel [*Reprinted with permission of AIChE. Reference: Berg,* Chem. Eng. Progr., **47,** 585–590 (1951).]

FIG. 16-54 Cross-flow panel-bed adsorber. [*Reprinted with permission of AIChE. Reference: Lovett and Cunniff,* Chem. Eng. Progr., **70**(5), 43–47 (1974).]

zontal wheel that rotates around a vertical axis. In other instances, the adsorbent is integral to the monolithic wheel or coated onto a metal, paper, or ceramic honeycomb substrate. These monolithic or honeycomb structures rotate around either a vertical or a horizontal axis. The gas to be treated usually flows through the wheel parallel to the axis of rotation, although some implementations use radial flow con-

figurations. Most of the wheel is removing adsorbates. The remaining (smaller) portion of the wheel is undergoing thermal regeneration—usually countercurrently. The wheel constantly rotates to provide a continuous treated stream and a steady concentrated stream. Adsorbent wheels are most often used to treat ambient air because they have very low pressure drop. One application of wheels is the removal of VOC where the regeneration stream is usually sent to an incinerator for destruction of VOC. Another use is in desiccant cooling (see previously). They do suffer from low efficiency due to the short contact time, mechanical leakage at seals, and the tendency to allow the wheel to exceed breakthrough in order to get better adsorbent utilization. Some adsorbent wheels are operated in an intermittent manner such that the wheel periodically indexes to a new position; this is particularly true of radial flow wheels.

The rotating annular bed system for liquid chromatographic separation (two-dimensional chromatography) is analogous to the horizontal adsorbent wheel for gases. Feed to be separated flows to a portion of the top face of an annular bed of sorbent. A displacement purge in the form of a solvent or carrier gas flows to the rest of the annulus. The less strongly adsorbed components travel downward through the sorbent at a higher rate. Thus, they will exit at the bottom of the annulus at a smaller angular distance from the feed sector. The more strongly adsorbed species will exit at a greater angle. The mechanical and packing complexities of such an apparatus have been overcome for a pressurized system by workers at the Oak Ridge National Laboratory shown in Fig. 16-56 [Canon, Begovich, and Sisson, *Sep. Sci. Technol.*, **15**, 655–678 (1980)]. Several potential applications are reviewed by Carta and Byers [*Chromatographic and Membrane Processes in Biotechnology*, NATO ASI Proceeding, Kluwer, 1991].

Simulated Continuous Countercurrent Systems Because of the problems associated with moving adsorbent in true continuous countercurrent mode, most commercial application of continuous countercurrent processes has been accomplished by using flow schemes that simulates the flow of adsorbent and process fluid. There are at least four types of implementation: (1) units designed to intermittently move the adsorbent rather than continuously, (2) continuously operating chromatographic columns to which the feed is periodically pulsed, (3) enhancement of the chromatographic separation by dividing the column and using recycles, and (4) moving the point of introduction of the feed and regeneration point along a series of beds.

Pulsed beds of activated carbon are used in water and wastewater treatment systems. The adsorber tank is usually a vertical cylindrical pressure vessel, with fluid distributors at top and bottom, similar to the arrangement of an ion exchanger. The column is filled with granular carbon. Fluid flow is upward, and carbon is intermittently dis-
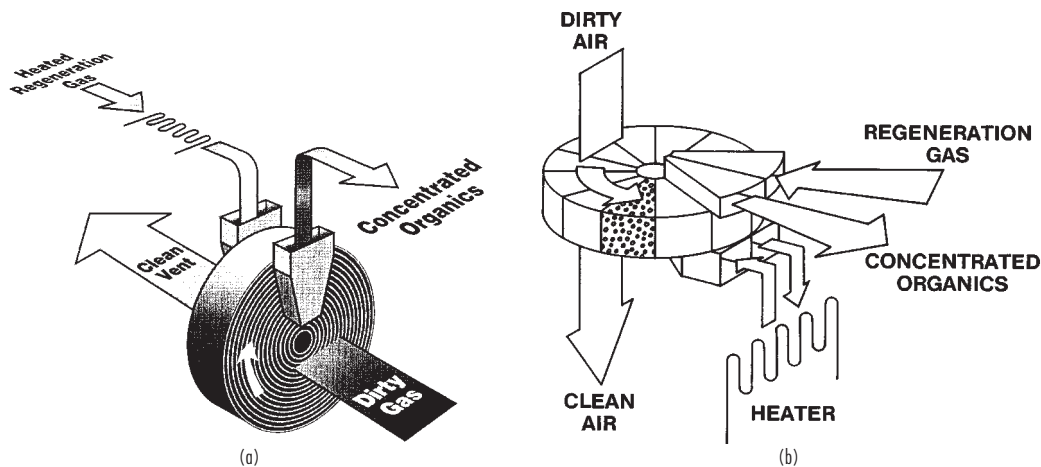

FIG. 16-55 Adsorbent wheels for gas separation: (*a*) horizontal with fixed beds; (*b*) vertical monolith. (*Reprinted with permission of UOP.*)
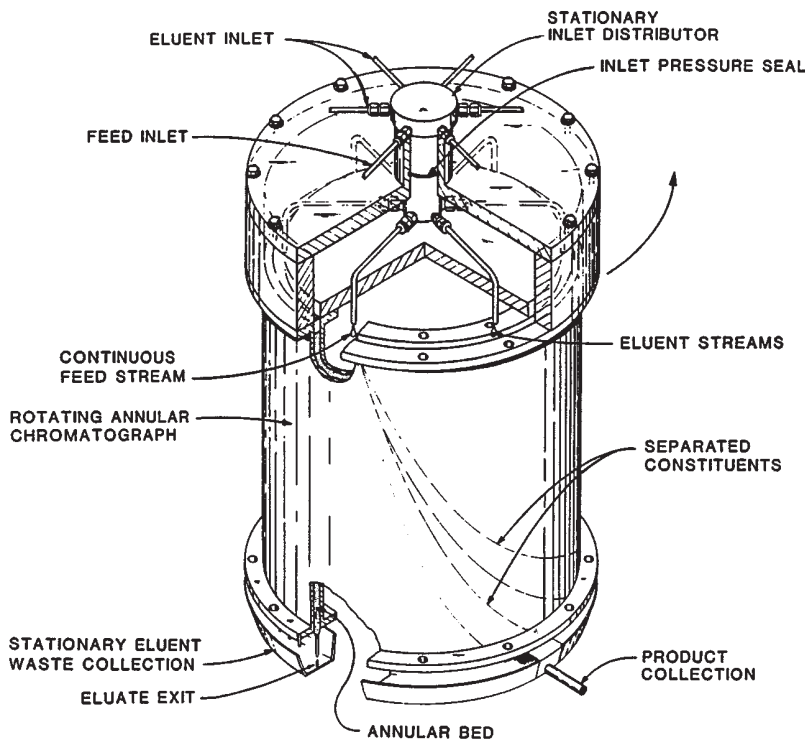
FIG. 16-56   Annular bed for liquid separation. [*Reprinted with permission of* Marcel Dekker. *Reference: Canon, Begovich, and Sisson,* Sep. Sci. Technol., **15,** 655–678 (1980).]

placed downward by opening a valve at the bottom and injecting a measured slug of carbon into the top of the vessel. The exhausted slug (a small fraction of the total charge in order to approximate fully countercurrent operation very closely) is transferred to the sweeten-off tank, where residual product is displaced. It next is dewatered and fed to the regeneration furnace. The carbon is eventually returned to the adsorber where fluid flow is interrupted briefly to permit carbon transfer in, as in continuous ion exchanger systems.

Liquid chromatography has been used commercially to separate glucose from fructose and other sugar isomers, for recovery of nucleic acids, and other uses. A patent to Sanmatsu Kogyo Co., Ltd [Yoritomi, Kezuka, and Moriya, U.S. Patent number 4,267,054, 1981] presents an improved chromatographic process that is simpler to build and operate than simulated moving-bed processes. Figure 16-57 [Keller et al., gen. refs.] diagrams its use for a binary separation. It is a displacement-purge cycle where pure component cuts are recovered, while cuts that contain both components are recycled to the feed end of the column.

The UOP Cyclesorb^SM is another adsorptive separation process with semicontinuous recycle. It utilizes a series of chromatographic columns to separate fructose from glucose. A series of internal recycle streams of impure and dilute portions of the chromatograph are used to improve the efficiency [Gerhold, U.S. Patent numbers 4,402,832, 1983; and 4,478,721, 1984]. A schematic diagram of a six-vessel UOP Cyclesorb process is shown in Fig. 16-58 [Gembicki et al., gen. refs., p. 595]. The process has four external streams and four internal recycles: Dilute raffinate and impure extract are like displacement steps; and impure raffinate and dilute extract are recycled from the bottom of an adsorber to its top. Feed and desorbent are fed to the top of each column in a predetermined sequence. The switching of the feed and desorbent are accomplished by the same rotary valve used for Sorbex switching (see hereafter). A chromatographic profile is established in each column that is moving from top to bottom, and all portions of an adsorber are performing a useful function at any time.

The concept of a simulated moving bed (SMB) was originally used in a process developed and licensed under the name UOP Sorbex process [Broughton, Bieser, and Anderson, *Pet. Int. (Milan), ***23**(3), p. 91 (1976); Broughton, Bieser, and Persak, *Pet. Int. (Milan), ***23**(5), p. 36 (1976)]. The following discussion is based on that process, but the concepts can be generally applied. In a moving-bed system for continuous countercurrent effect, solids move continuously in a closed loop past fixed points of introduction and withdrawal of feed and regenerant. The same effect can be achieved by holding the bed stationary and periodically moving the points of introduction and withdrawal of the various streams. Shifting those points in the direction of fluid flow simulates the movement of solid in the opposite direction. Since moving the positions continuously is impractical, a finite number of access lines are provided to a limited series of adsorbent beds. The Sorbex commercial application of this concept is portrayed in Fig. 16-59, which shows the adsorbent as a stationary bed and the auxiliary distillation columns needed to separate the desorbent from raffinate and extract so that it can be recycled to the process. In this example, feed flows through the three beds of Zone 1, where the most strongly adsorbed component A is adsorbed and depleted from the raffinate. Desorbent flows through the three beds of Zone 3 to displace component A into the extract. The less strongly adsorbed component B is adsorbed slightly in the two beds of Zone 4 between raffinate outlet and desorbent, inlet to prevent it from contaminating extract in Zone 3. Component B is desorbed in the four beds of Zone 2 between the extract outlet and the feed inlet and most leaves with the raffinate. A pump draws liquid from the bottom outlet to the top inlet of the adsorbent chamber. All flows in the beds are downward, simulating an upward flow of solid. The four active port positions are likewise moved downward by the selection of the rotary valve. The rotary valve functions in the same manner as a multiport stopcock or chromatography valve, sequencing the four streams on the right to the lines connected to the inlet/outlet nozzles on the adsorber. The next position of the rotary valve will direct desorbent to
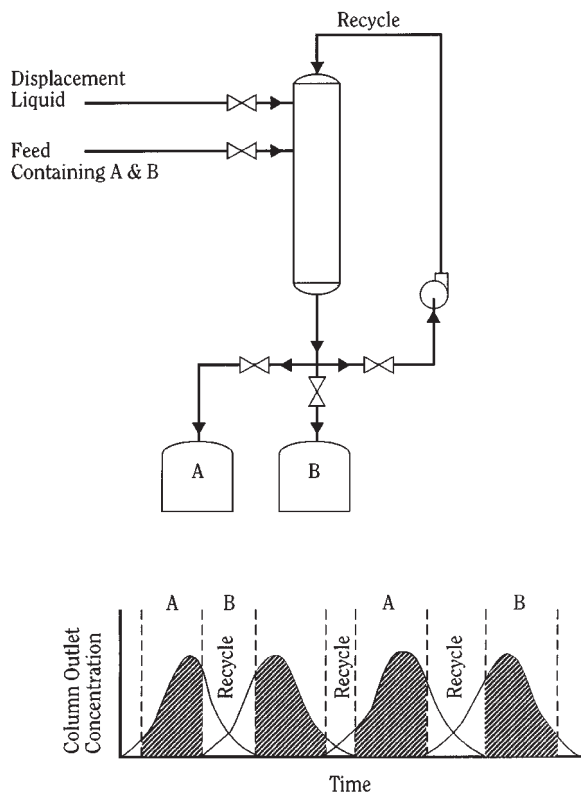
FIG. 16-57   Sanmatsu Kogyo chromatographic process. (*Reprinted with permission of Wiley. Reference: Keller, Anderson, and Yon, Chap. 12 in Rousseau, Handbook of Separation Process Technology, John Wiley & Sons, Inc., New York, 1987.*)

line 3, extract from 6, and feed to 10; and raffinate moves to the top of the column at line 1. The liquid flow rate in each of the four zones is different because of the addition or withdrawal of the various streams and is controlled by the circulating pump. The circulating pump must be programmed to pump at four different rates in order to keep the flow in each zone constant. The variables available for fine tuning performance are the cycle time, measured as the time required for one rotation of the rotary valve, and the liquid flow rate in Zones 2, 3, and 4. Chemical analyses at the liquid circulating pump can trace the performance of the entire bed and are used for changing operating conditions. Other versions of the SMB system have been used commercially by Toray Industries, Illinois Water Treatment and Mitsubishi (see "Displacement Purge").

ION EXCHANGE

A typical fixed-bed ion exchanger consists of a vertical cylindrical vessel of lined steel or stainless steel. Linings are usually of natural or synthetic rubber. Spargers are provided at the top and bottom, and frequently a separate distributor is used for the regenerant solution. The resin bed, consisting of a meter or more of ion-exchange particles, is supported by the screen of the bottom distributor. Externally, the unit is provided with a valve manifold to permit downflow loading, upflow backwash, regeneration, and rinsing. For deionization, a two-exchanger assembly comprising a cation and an anion exchanger, is a common configuration (Fig. 16-60).

Column hardware designed to allow countercurrent, upflow regeneration of ion-exchange resins is available. An example is given in Fig. 16-61. During upflow of the regenerant, bed expansion is prevented by withdrawing the effluent through the application of vacuum. A layer of drained particles is formed at the top of the bed while the rest of the column functions in the usual way.

Typical design data for fixed-bed ion-exchange columns are given in Table 16-19. These should be used for preliminary evaluation purposes only. Characteristic design calculations are presented and illustrated by Applebaum [*Demineralization by Ion Exchange*, Academic, New York, 1968]. Large amounts of data are available in published literature and in bulletins of manufacturers of ion exchangers. In general, however, laboratory testing and pilot-plant work is advisable to determine usable exchanger capacities, regenerant quantities,
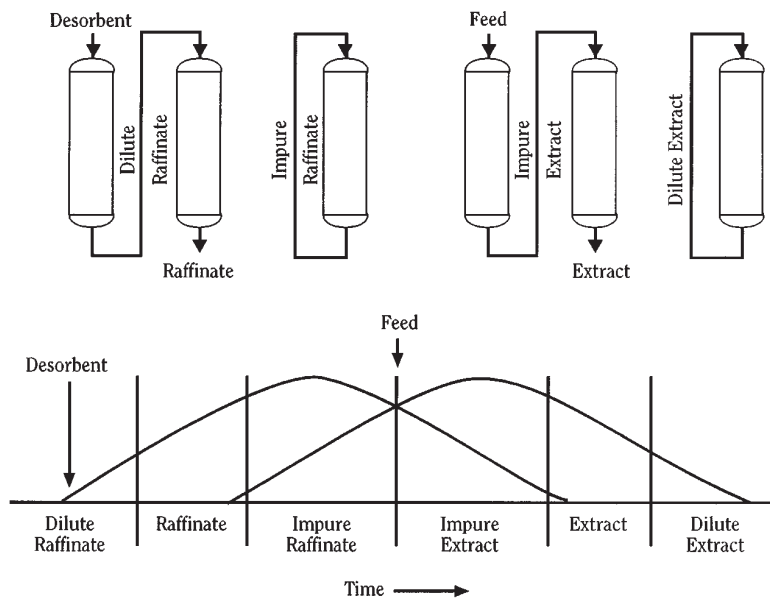

FIG. 16-58   UOP Cyclesorb process. (*Reprinted with permission of John Wiley & Sons, Inc. Reference: Gembicki, Oroskar, and Johnson, "Adsorption, Liquid Separation," in* Kirk-Othmer Encyclopedia of Chemical Technology, 4th ed., Wiley, New York, 1991.)
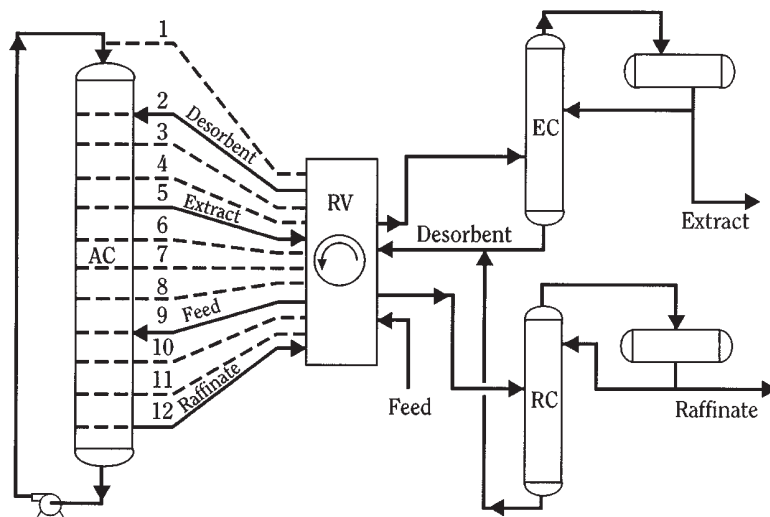
FIG. 16-59 UOP Sorbex process. (*Reprinted with permission of John Wiley & Sons, Inc. Reference: Gembicki, Oroskar, and Johnson, "Adsorption, Liquid Separation," in Kirk-Othmer Encyclopedia of Chemical Technology, 4th ed., John Wiley & Sons, Inc., New York, 1991.*)

exchanger life, and quality of product for any application not already thoroughly proven in other plants for similar conditions. Firms that manufacture ion exchangers and ion-exchange equipment will often cooperate in such tests.

For larger-scale applications, a number of continuous or semicontinuous ion-exchange units are also available. The Higgins contactor (Fig. 16-62) was originally developed to recover uranium from leach slurries at the Oak Ridge National Laboratory. More recently, it has been adapted to a wide variety of applications, including large-volume water softening.

The Asahi process (Fig. 16-63) is used principally for high-volume water treatment. The liquid to be treated is passed upward through a resin bed in the adsorption tank. The upward flow at 30–40 m/h [12–16 gal/(min ft²)] keeps the bed packed against the top. After a preset time, 10 to 60 min, the flow is interrupted for about 30 s, allowing the entire bed to drop. A small portion (10 percent or less) of the ion-exchange resin is removed from the bottom of the adsorption tank and transferred hydraulically to the hopper feeding the regeneration tank.
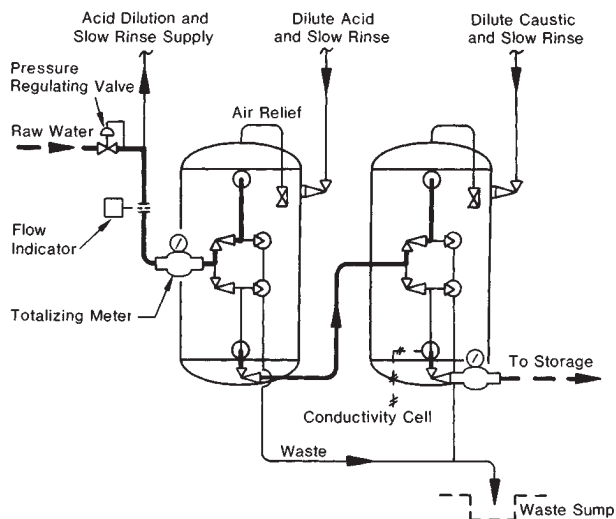
The process is then resumed. Meanwhile, regeneration is occurring by a similar flow system in the regeneration tank, from which the regenerated ion exchanger is transferred periodically to the hopper above the water-rinse tank. In the latter, the resin particles are fluidized to flush away fines and accumulated foreign matter before the resin is returned to the adsorption tank.

Another continuous ion-exchange system is described by Himsley and Farkas (see Fig. 16-64). Such a system is used to treat 1590 m³/h (7000 gal/min) of uranium-bearing copper leach liquor using fiberglass-construction columns 3.7 m (12 ft) in diameter. The adsorption column is divided vertically into stages. Continuous transfer of batches of resin occurs from stage to stage without any interruption of flow. This is accomplished by pumping solution from one stage (A) to the stage (B) immediately above by means of external pumping in such a
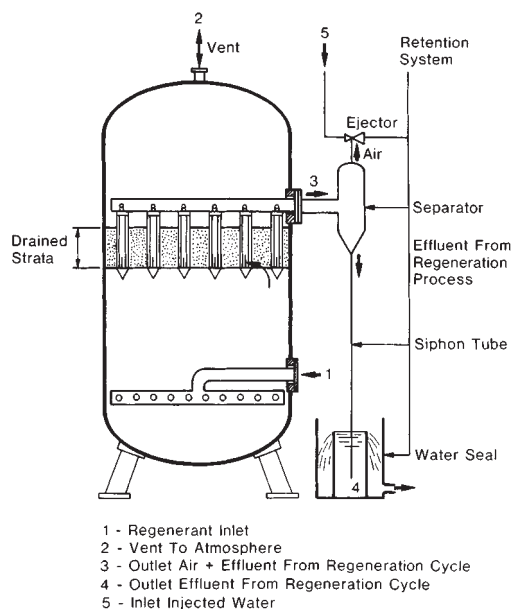

FIG. 16-60 Typical two-bed deionizing system. (*Infilco Degremont Inc.*)

1 - Regenerant Inlet
2 - Vent To Atmosphere
3 - Outlet Air + Effluent From Regeneration Cycle
4 - Outlet Effluent From Regeneration Cycle
5 - Inlet Injected Water

FIG. 16-61 Internals of an upflow regenerated unit. (*Infilco Degremont Inc.*)

TABLE 16-19 Design Data for Fixed-Bed Ion Exchanger*

Type of resin	Maximum and minimum flow, m/h [gal/(min·ft²)]	Minimum bed depth, m (in)	Maximum operating temperatures, °C (°F)	Usable capacity, g-equivalent/L†	Regenerant, g/L resin‡
Weak acid cation	20 max. (8) 3 min. (1)	0.6 (24)	120 (248)	0.5–2.0	110% theoretical (HCl or H₂SO₄)
Strong acid cation	30 max. (12) 3 min. (1)	0.6 (24)	120 (248)	0.8–1.5 0.5–1.0 0.7–1.4	80–250 NaCl 35–200 66° Bé. H₂SO₄ 80–500 20° Bé. HCl
Weak and intermediate base anions	17 max. (7) 3 min. (1)	0.75 (30)	40 (104)	0.8–1.4	35–70 NaOH
Strong-base anions	17 max. (7) 3 min. (1)	0.75 (30)	50 (122)	0.35–0.7	70–140 NaOH
Mixed cation and strong-base anion (chemical-equivalent mixture)	40 max. (16)	1.2 (47)	50 (122)	0.2–0.35 (based on mixture)	Same as cation and anion individually

*These figures represent the usual ranges of design for water-treatment applications. For chemical-process applications, allowable flow rates are generally somewhat lower than the maximums shown, and bed depths are usually somewhat greater.
†To convert to capacity in terms of kilograins of CaCO₃ per cubic foot of resin, multiply by 21.8.
‡To convert to pounds of regenerant per cubic foot of resin, multiply by 0.0625.
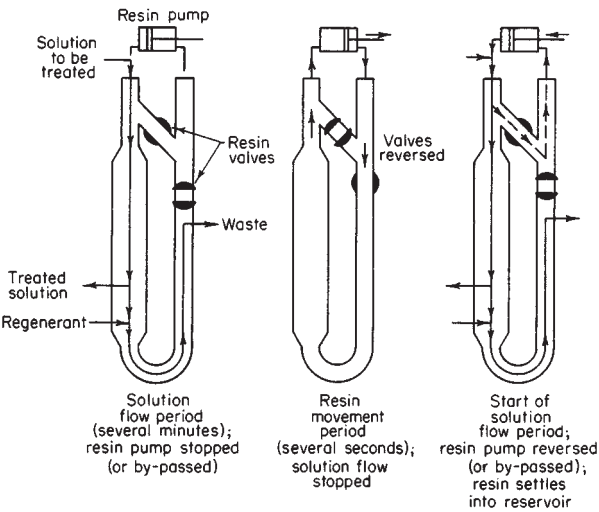

FIG. 16-62 Mode of operation of the Higgins contractor. (*ORNL-LR-Dwg. 27857R.*)
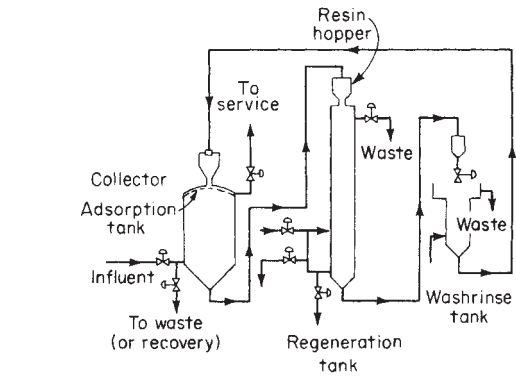

FIG. 16-63 Asahi countercurrent ion-exchange process. [*Gilwood,* Chem. Eng., **74**(26), 86 (1967); copyright 1967 by McGraw-Hill, Inc., New York. *Excerpted with special permission of McGraw-Hill.*]

manner that the net flow through stage B is downward, carrying with it all of the resin in that stage B. When transfer of the ion exchanger is complete, the resin in stage C above is transferred downward in a similar manner. The process continues until the last stage (F) is empty. The regenerated resin is then transferred from the elution column to the empty stage (F). Elution of the sorbed product is carried out in the elution column in a moving packed bed mode. The countercurrent contact achieved in this column yields a concentrated eluate with a minimum consumption of regenerant.

Disadvantages of these continuous countercurrent systems are associated primarily with the complexity of the equipment required and with the attrition resulting from the transport of the ion exchanger. An effective alternative for intermediate scale processes is the use of merry-go-round systems and SMB units employing only packed-beds with no movement of the ion-exchanger.
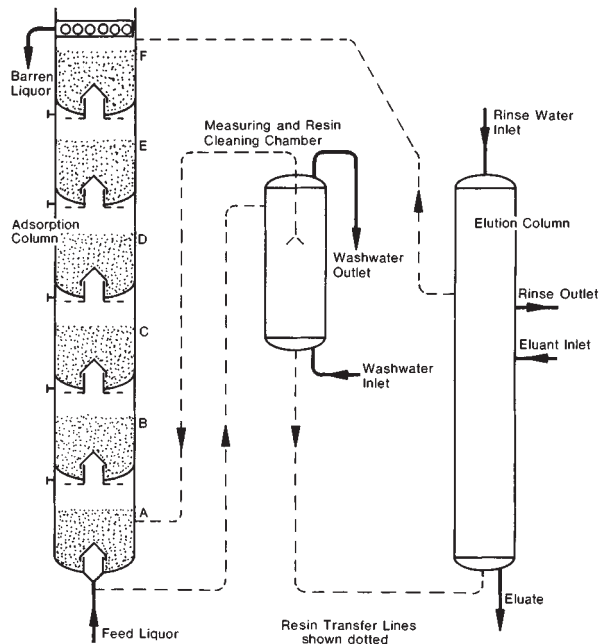

FIG. 16-64 Himsley continuous ion-exchange system. (*Himsley and Farkas,* "Operating and Design Details of a Truly Continuous Ion Exchange System," Soc. Chem. Ind. Conf., *Cambridge, England, July 1976. Used by permission of the Society of Chemical Industry.*)